Quantum mechanical systems with holographic duals

Alexey Milekhin

A Dissertation
Presented to the Faculty
of Princeton University
in Candidacy for the Degree
of Doctor of Philosophy

Recommended for Acceptance
by the Department of
Physics
Adviser: Professor Juan Maldacena

September 2020

Abstract

This thesis is devoted to studying quantum mechanical systems with gravity duals. It is interesting to study holographic correspondence for quantum mechanical systems since we have much more theoretical control over them compared to quantum field theories. At the same time, gravity duals to quantum mechanical systems are quite rich as they can include black holes and wormholes.

Chapter 2 is based on work [1] with J. Maldacena and studies aspects of gauge symmetry in Banks-Fishler-Shenker-Susskind(BFSS) model. In the original formulation it includes gauged $SU(N)$ symmetry. However, we argued that non-singlet states are separated by a finite gap from the ground state. Therefore, gauging $SU(N)$ symmetry is not important at low energies.

Chapter 3 is based on paper [2] with A. Almheiri and B. Swingle. It is dedicated to studying thermalization dynamics of systems with gravity duals. We argued that average null energy condition(ANEC) in the bulk leads to a universal bound on the total amount of energy exchange between two quantum systems. We study this bound perturbatively and in Sachdev-Ye-Kitaev(SYK) model at arbitrary coupling. As a byproduct, we studied the non-equilibrium dynamics of SYK, both analytically and numerically.

Chapter 4 is based on paper [3] with J. Maldacena. We study wormhole formation in SYK model in real time. We start from a high temperature state, let it cool by coupling to a cold bath and numerically solve for the large N dynamics. Our main result is that the system forms a wormhole by going through a region with negative specific heat, taking time that is independent of N.

Chapter 5 is based on paper [4] with I. Klebanov, F. Popov and G. Tarnopolsky. This paper is dedicated to studying various spectral properties of large N melonic tensor models. They have the same large N limit as SYK model, but unlike SYK they do not include disorder average. We find the exact expression for the number of singlet states and derive various bounds on energies.

Acknowledgements

Chapter 3 of this thesis was presented at the program Universality and ergodicity in quantum many-body systems in Stony Brook University. Chapter 4 was presented at Quantum matter/Quantum field theory seminar in Harvard University.

First of all, I am indebted to my adviser, Juan Maldacena, for his constant guidance and patience through many different research projects and topics and also for sharing his incredible physical intuition with me. I am especially grateful to Igor Klebanov for a long-term collaboration, his creativity and open-mindedness and his willingness to be in the thesis committee. I must also mention my undergraduate adviser, Alexander Gorsky, for introducing me to quantum field theory, a lot of scientific discussions and his continual support for almost ten years.

Also I am grateful to my co-authors throughout my graduate years: Ahmed Almheiri, Ksenia Bulycheva, Bruno Le Floch, Sergei Nechaev, Fedor Popov, Nikita Sopenko, Brian Swingle, Grigory Tarnopolsky and Wenli Zhao. All of them have their unique approach to physics and research in general, and I feel that each of these collaborations have made me better as a scientist.

I am thankful to Simone Giombi for being the second reader of the thesis and Lyman Page for being in the thesis committee.

I would like to thank all the people I have had discussions with for their ideas, encouragement, criticism, comments and time: Alexander Abanov, Semeon Artamonov, Alexander Avdoshkin, Ilya Belopolski, Damon Binder, Yiming Chen, Raffaele D'Agnolo, Nikolay Dedushenko, Xi Dong, Yale Fan, Hrant Gharibyan, Akash Goel, Luca Iliesiu, Christian Jepsen, Ziming Ji, Jiaqi Jiang, Alex Kamenev, Dmitri Kharzeev, Sergey Khilkov, Vladimir Kirilin, Zohar Komargodski, Ho Tat Lam, Henry Lin, Mariangela Lisanti, Donald Marolf, Victor Mikhaylov, Baur Mukhametzhanov, Nikita Nekrasov, Silviu Pufu, Boris Runov, Andrey Sadofyev, Stephen Shenker, Douglas Stanford, Nikolay Sukhov, Joaquin Turiaci, Jacobus Verbaarschot, Herman Verlinde, Zhenbin Yang, Przemek Witaszczyk, Wenli Zhao and Yunqin Zheng.

I would like to give special thanks to my friends: Ksenia Bulycheva, Ivan Danilenko, Maria Danilenko, Antonio Alfieri and Fedor Popov for their constant support throughout my

PhD years. I am sure without them I would not have been able to carry through. I am grateful to my girlfriend, Courtney King, for her support, patience, creativity and proofreading.

Last, but not least, I want to thank my friends: Vasyl Alba, Lev Arzamasskiy, Levon Avanesyan, Tyler Boyd-Meredith, David Buniatyan, Erin Ellis, Himanshu Khanchandani, Misha Ivanov, Natasha Klimova, Roman Kolevatov, Artem Kotelskiy, Alexey Lavrov, Steven Li, Maksim Litskevich, Elizaveta Mankovskaya, Vadim Munirov, Congling Qiu, Sergey Ryabichko, Elvira Sayfutyarova, Charlie Stibitz, Alina Tokmakova, Eva Troje, Yury Ustinovskiy, Anibal Velozo and Andrei Zeleneev for making Princeton feel like home.

To my mother.

Contents

Chapter 1

Introduction

1.1 An overview

By now holographic correspondence [5] is a well-established tool in many different areas of physics, such as quantum gravity, high energy physics and condensed matter physics. Originally formulated for $\mathcal{N} = 4$ super Yang–Mills theory and IIB supergravity in $AdS_5 \times S^5$, it has led to a plethora of impressive results in this theory [6]. However, it was quickly realized that it also implies other deep and sometimes unexpected results, such as the bound for a ratio of shear viscosity to entropy density [7] at large N and the bound on Liapunov exponent in chaotic systems [8]. However, the most exciting and challenging opportunity it provides is the study of quantum gravity. Recently there was a huge progress in understanding the properties of entanglement entropy in systems coupled to gravity which allowed to reproduce the Page curve for an evaporating black hole [9, 10, 11]. Naturally, if we want to understand quantum gravity in the bulk better, it would be instructive to find an example of holographic duality with a simple theory on the boundary. The most simple quantum systems are, of course, quantum mechanical systems.

Banks–Fishler–Shenker–Susskind(BFSS) model is a dimensional reduction of $SU(N)$ $\mathcal{N} = 4$ super Yang–Mills from four down to one dimension. Despite being a quantum mechanical model its bulk is ten-dimensional [12]. It provides one of the strongest evidences for the holographic

correspondence, as the gravity predictions from black hole thermodynamics, including stringy α' corrections, have been matched with numerical Monte–Carlo simulation of this model [13, 14, 15].

One of the most prominent advances in holographic correspondence is the discovery of Sachdev–Ye–Kitaev model(SYK) [16, 17]. Unlike $\mathcal{N} = 4$ super Yang–Mills its formulation is exceptionally simple: it involves a random quartic interaction of N Majorana fermions. SYK model is very interesting to both high-energy physics and condensed matter physics: on one hand it provides UV completion to two-dimensional Jackiw–Teitelboim gravity, on the other hand it is a soluble example of a non-Fermi liquid. Moreover, at both large N and finite N many properties of this system can be easily analyzed numerically.

However, SYK model is not a genuine quantum mechanical system, as it involves quenched disorder average. Its large N expansion is dominated by the so-called melonic diagrams. It was realized [18, 19, 20] that there are quantum mechanical models involving rank 3 tensor fields which are dominated by the same class of diagrams. However, they have unusually high symmetry groups($O(N)^3$ or $O(N)^5$) and have subleading $1/N$ corrections which involve additional contributions compared to SYK model. Despite the fact that they have approximate conformal symmetry in the IR, it remains an open question if they correspond to any quantum gravity models.

The present thesis is devoted to studying these three holographic systems: BFSS model, SYK model and melonic tensor models. In the rest of the Introduction we will give a very brief overview of the basic properties of these models.

1.2 The D0 brane matrix model

In this section we review the D0 brane matrix model and its gravity dual. Readers familiar with this material can jump directly to the next section.

1.2.1 The matrix model

The D0 matrix model [21], or BFSS matrix model [22], has the action

$$S = \frac{1}{g^2}\int dt\,\mathrm{Tr}\left(\frac{1}{2}(D_t X^I)^2 + \frac{1}{2}\psi_\alpha D_t\psi_\alpha + \frac{1}{4}[X^I, X^J]^2 + \frac{1}{2}i\psi_\alpha\gamma^I_{\alpha\beta}[\psi_\beta, X^I]\right) \tag{1.2.1}$$

where all indices are summed over. $I, J = 1, \cdots, 9$, $\alpha, \beta = 1, \cdots 16$. where γ^I are nine dimensional gamma matrices which are real, symmetric and traceless[1]. ψ_α are hermitian $N \times N$ matrices, which can be expanded as $\psi_\alpha = \psi^r_\alpha T^r$ where the T^r are a complete set of hermitian $N \times N$ matrices, and we can think of the r index as a real index of the adjoint representation of $U(N)$. Then ψ^r_α are Majorana fermions. We have $16 \times N^2$ Majorana fermions. This model is invariant under 16 supersymmetries and also under an $SO(9)$ R-symmetry.

The model has a $U(N)$ gauge symmetry and the derivative is defined as $D_t B = \partial_t B + i[A_t, B]$ where A_t is the gauge field.

We could choose the gauge where $A_t = 0$ and then we have to impose Gauss's law:

$$G = \frac{i}{2g^2}\left(2[D_t X^I, X^I] + [\psi_\alpha, \psi_\alpha]\right) = 0 \tag{1.2.2}$$

It restricts all states to be singlets under the $U(N)$ symmetry.

Classical zero energy configurations correspond to simultaneously diagonal matrices X^I. Quantum mechanically, the model has a zero energy bound state. At finite temperature it is expected (from the gravity picture) to have a metastable bound state.

It is interesting to ask what the typical size of the matrices X^I is in the ground state or in a thermal state. This was estimated [23] by setting a lower bound for $\frac{1}{N}\mathrm{Tr}[X^2]$, using virial theorem ideas. That lead to

$$\sqrt{\langle\frac{1}{N}\mathrm{Tr}[X^2]\rangle} \sim \lambda^{1/3}\,, \qquad \lambda \equiv g^2 N \tag{1.2.3}$$

[1] We can view them as coming from the ten dimensional Majorana Weyl representation $\gamma^I = \Gamma^0\Gamma^I$.

In a heuristic way, this can also be obtained by dimensional analysis and large N counting if one assumes that λ is the only relevant scale (and not the temperature). This result will be particularly useful when we analyze the gravity solution.

There is a variant of this model where we add mass terms that break $SO(9) \to SO(3) \times SO(6)$ [24]. The additional terms in the action are

$$S_{BMN} = S_{[\text{from (1.2.1)}]} + S_\mu \ , \tag{1.2.4}$$

$$S_\mu = -\frac{1}{g^2}\int dt\, \mathrm{Tr}\left(\frac{1}{2}\left(\frac{\mu}{3}\right)^2 \sum_{a=1}^{3}(X^a)^2 + \frac{1}{2}\left(\frac{\mu}{6}\right)^2 \sum_{i=4}^{9}(X^i)^2 + \frac{\mu}{8}\psi\gamma_{123}\psi + \right.$$
$$\left. + i\frac{\mu}{3}\sum_{a,b,c=1}^{3} X^a X^b X^c \epsilon_{abc}\right) \tag{1.2.5}$$

It also preserves 16 supercharges but with a different supersymmetry algebra, $SU(2|4)$. We can view view (1.2.4) as a collection of harmonic oscillators and Majorana fermions with some particular interactions.

The mass terms remove the flat directions in the potential. Apart from the simplest vacuum with $X^I = 0$, the BMN model also has additional vacua [25, 26, 27], characterized by non-zero $X^a,\ a = 1, 2, 3$ such that:

$$i\epsilon_{abc}X^b X^c = \frac{\mu}{3}X^a \tag{1.2.6}$$

This equation is solved by $X^a = \frac{\mu}{3}J^a$, where J^a are $SU(2)$ algebra generators in an N-dimensional representation, not necessarily irreducible. Such solutions represent a collection of fuzzy spheres. Although this vacuum breaks $SU(N)$ symmetry, there are no physical Goldstone bosons because of the gauge symmetry. We will return to $SU(N)$ Goldstone bosons later in Section 2.2 when we discuss the ungauged model.

1.2.2 The gravity dual

We will be mostly discussing the gravity dual at finite temperature. The geometry is a solution of ten dimensional type IIA supergravity closely related to the near horizon geometry of a charged

black hole in ten dimensions [28]. It is given by [12]

$$\begin{aligned}
\frac{ds^2}{\alpha'} &= -\frac{f_0(r) r^{7/2}}{\sqrt{\lambda d_0}} dt^2 + \sqrt{\frac{\lambda d_0}{r^3}} \left(\frac{1}{f_0(r) r^2} dr^2 + d\Omega_8^2 \right) \\
e^{\phi} &= \frac{(2\pi)^2}{d_0} \frac{1}{N} \left(\frac{\lambda d_0}{r^3} \right)^{7/4} \\
\tilde{A}_t &= \frac{N}{(2\pi)^2} \frac{r^7}{\lambda^2 d_0} \\
f_0(r) &= 1 - \frac{r_0^7}{r^7}, \qquad d_0 \equiv 240\pi^5, \qquad \lambda \equiv g^2 N,
\end{aligned} \tag{1.2.7}$$

where r_0 and the inverse temperature $\beta = 1/T$ are related by[2]

$$\frac{1}{T} = \beta = \frac{4}{7} \pi \sqrt{\lambda d_0} r_0^{-5/2} \tag{1.2.8}$$

This geometry has an effective radius of curvature given by the radius of S^8

$$\frac{R_{eff}^2}{\alpha'} = \sqrt{\frac{\lambda d_0}{r^3}} \tag{1.2.9}$$

which is a function of the radial direction. For this reason we can trust (1.2.7) only in some region of the geometry, namely $r \lesssim \lambda^{1/3}$. Note that r has units of energy. At larger values of r, when $\lambda^{1/3} \lesssim r$, the curvature is high and we cannot trust the gravity solution. The large r region is where the boundary is and it corresponds to the UV of the boundary theory. In this region the matrix model is weakly coupled and we can trust perturbation theory.

The geometry at the horizon of the black hole will be weakly curved as long as

$$1 \ll \lambda \beta^3 \tag{1.2.10}$$

There is an additional N dependent constraint $\lambda \beta^3 \ll N^{10/7}$ on the validity of this IIA supergravity solution that arises when we also demand that the dilaton is not too large at the horizon.

[2] We can think of the relation between β and r_0 as a way to translate between time scales in the matrix model (β) and radial position in the bulk (r_0) [29].

In this thesis, we will imagine that we are in the 't Hooft limit where N is taken to be very large compared to other quantities, such as λ or β, or more precisely $\lambda\beta^3$. So we do not have to worry about this second constraint.

Using the Bekenstein–Hawking formula one can easily find the entropy and free energy[3]

$$S = N^2 4^{13/5} 15^{2/5} (\pi/7)^{14/5} \left(\frac{T}{\lambda^{1/3}}\right)^{9/5} \approx 11.5 N^2 \left(\frac{T}{\lambda^{1/3}}\right)^{9/5} \tag{1.2.11}$$

$$F = N^2 \lambda^{1/3} \frac{5}{14} 4^{13/5} 15^{2/5} (\pi/7)^{14/5} \left(\frac{T}{\lambda^{1/3}}\right)^{14/5} \approx 7.4 N^2 \lambda^{1/3} \left(\frac{T}{\lambda^{1/3}}\right)^{14/5} \tag{1.2.12}$$

These predictions were checked in an increasingly sophisticated set of numerical computations [13, 30, 14, 31, 32, 33] culminating in [15], where also the leading α' corrections were computed[4].

The gravity dual for the BMN case is a bit more complicated, it has some gapped states described in [34] and a black hole thermal state which looks like a deformation of (1.2.7) [35]. The magnitude of the deformation involves μ/T and it is very small if μ/T is small.

1.3 A brief review of Sachdev–Ye–Kitaev model

In this section we will study the conventional SYK model [17, 36]. Let us briefly summarize the relevant results about the conformal limit, Dyson–Schwinger and Kadanoff–Baym equations and also introduce our notations.

SYK is a model of N Majorana fermions ψ_i with the all-to-all interactions and a quench disorder governed by the Hamiltonian:

$$H_S = i^{q_S/2} \sum_{1 \le i_1 < \cdots < i_{q_S} \le N} J_{i_1 \ldots i_{q_S}} \psi_{i_1} \ldots \psi_{i_{q_S}} \tag{1.3.13}$$

[3] The temperature dependence can be recovered from the properties of (1.2.7) under rescalings. Namely sending $t \to \eta t$ and $r \to \eta^{-2/5} r$ the metric gets rescaled by an overall factor and the action by $S \to \eta^{-9/5} S$, which is also the scaling of the entropy. See Appendix A.3.

[4] It is an interesting challenge to match the first correction by computing the full tree level α'^3 corrections to the tree level IIA supergravity in the effective action.

Coefficients J are real and Gauss-random with variance:

$$\langle J^2_{i_1 \ldots i_{q_S}} \rangle = \frac{J_S^2 (q_S - 1)!}{N^{q_S - 1}} \quad \text{(no sum)} \tag{1.3.14}$$

Below we will use the symbol $\{i\}$ to denote sums like $1 \leq i_1 < \cdots < i_{q_S} \leq N$

Since we are dealing with the quench disorder we have to introduce replicas in the path integral. However, in the large N limit the interaction between the replicas is suppressed and in the replica-diagonal phase (non-spin glass state) the *Euclidean* effective action reads:

$$\frac{S[\Sigma_S, G_S]}{N} = \log \mathrm{Pf}\,(\partial_\tau - \Sigma_S) + \frac{1}{2} \int d\tau_1 d\tau_2 \ \left(-\Sigma_S(\tau_1, \tau_2) G_S(\tau_1, \tau_2) + \frac{J_S^2}{q} G_S(\tau_1, \tau_2)^q \right) \tag{1.3.15}$$

The auxiliary variables Σ_S, G_S have physical meaning: G_S is the Euclidean time-ordered fermion two-point function,

$$G_S(\tau_1, \tau_2) = \frac{1}{N} \sum_{i=1}^{N} \langle T \psi_i(\tau_1) \psi_i(\tau_2) \rangle, \tag{1.3.16}$$

and Σ_S is the fermion self-energy. The large N Euclidean saddle-point equations are identical to the Dyson–Schwinger equations:

$$\begin{aligned} \Sigma_S(\tau) &= J_S^2 G_S(\tau)^{q_S} \\ (-i\omega - \Sigma_S(\omega)) G_S(\omega) &= 1. \end{aligned} \tag{1.3.17}$$

For later use, note that the energy is

$$E_S = \langle H_S \rangle = -\frac{J_S^2}{q_S} \int_0^\beta d\tau \ G_S(\tau)^{q_S}. \tag{1.3.18}$$

At low temperatures the system develops an approximate conformal symmetry and the Green's function can be found explicitly:

$$G_S(\tau) = b \, \mathrm{sgn}(\tau) \left(\frac{\pi}{\beta J_S \sin\left(\frac{\pi |\tau|}{\beta} \right)} \right)^{2/q} \tag{1.3.19}$$

The coefficient b is just a numerical constant. It is determined by

$$b^{q_S}\pi = \left(\frac{1}{2} - \frac{1}{q_S}\right)\tan\frac{\pi}{q_S}, \tag{1.3.20}$$

and for $q_S = 4$, $b = 1/(4\pi)^{1/4}$.

Having reviewed the Euclidean properties, let us turn to the Lorentzian (real time) physics. It is be convenient to work with the Keldysh contour right away, so we will assume that the reader is familiar with this technique.

One central object is the Wightman (or "greater") Green's function:

$$G_S^{>}(t_1, t_2) = G_S(t_1^-, t_2^+) = -i\frac{1}{N}\sum_i \langle \psi_i(t_1^-)\psi_i(t_2^+)\rangle \tag{1.3.21}$$

Please note that we have $-i$ in our definition. Because of the Majorana commutation relations, the greater Green's function reduces to $-i/2$ at coincident points:

$$G_S^{>}(t_1, t_1) = -\frac{i}{2}. \tag{1.3.22}$$

The "lesser" function $G^{<}$ for Majorana fermions is directly related to $G^{>}$:

$$G_S^{<}(t_1, t_2) = G_S(t_1^+, t_2^-) = -G_S^{>}(t_2, t_1) \tag{1.3.23}$$

Two final pieces are the retarded and advanced functions:

$$\begin{aligned} G_S^R(t_1, t_2) &= \theta(t_1 - t_2)\left(G_S^{>}(t_1, t_2) - G_S^{<}(t_1, t_2)\right) \\ G_S^A(t_1, t_2) &= \theta(t_2 - t_1)\left(G_S^{<}(t_1, t_2) - G_S^{>}(t_1, t_2)\right) \end{aligned} \tag{1.3.24}$$

Now we can finally write down the Lorentzian form of the Dyson–Schwinger equations (4.2.8). The analytic continuation of the time-ordered Euclidean Green's function from imaginary time to real time yields the Wightman function, and because the self-energy equation is naturally

formulated in real time, one gets

$$\Sigma_S^>(t_1,t_2) = -i^{q_S} J_S^2 \left(G_S^>(t_1,t_2)\right)^{q_S} . \tag{1.3.25}$$

However, the continuation in frequency space (from the upper-half plane) yields the retarded function, therefore the second equation in (4.2.8) transforms into:

$$G_S^R(\omega)(\omega - \Sigma^R(\omega)) = 1 \tag{1.3.26}$$

We need a relation between G^R and $G^>$ in order to close the system of equations. If the system is in a thermal state, this relation is provided by the fluctuation-dissipation theorem (FDT):

$$G_S^>(\omega) = 2i \,\mathrm{Im}\, G_S^R(\omega) \frac{1}{e^{-\beta\omega}+1}. \tag{1.3.27}$$

This system of equations can be solved by an iterative procedure to obtain the real time correlation functions [36, 37].

There is another away we can treat the second DS equation in (4.2.8). We can rewrite it in the time-domain using the convolution:

$$\partial_\tau G_S(\tau) = \delta(\tau) + \int_0^\beta d\tau' \; \Sigma_S(\tau-\tau')G_S(\tau'). \tag{1.3.28}$$

Upon the analytic continuation this yields the so-called Kadanoff–Baym equations[5]:

$$\begin{aligned} i\partial_{t_1} G_S^>(t_1,t_2) &= \int_{-\infty}^{+\infty} dt' \;\left(\Sigma^R(t_1,t')G_S^>(t',t_2) + \Sigma^>(t_1,t')G^A(t',t_2)\right) \\ -i\partial_{t_2} G^>(t_1,t_2) &= \int_{-\infty}^{+\infty} dt' \;\left(G^R(t_1,t')\Sigma^>(t',t_2) + G^>(t_1,t')\Sigma^A(t',t_2)\right). \end{aligned} \tag{1.3.29}$$

[5]The integral on the right hand side is simply the convolution along the Keldysh contour of $\Sigma_S(t_1^+,\cdot) * G_S(\cdot,t_2^-)$. The precise result for the integral is known as Langreth rule in condensed matter literature [38].

Note that these equations are causal due to the retarded and advanced propagators in the integrand. A more straightforward way to obtain these equations is to write down the large N effective action (1.3.15) on the Keldysh contour and find the classical equations of motion.[6]

These equations can be used in non-equilibrium situations. They also have a very generic form that simply encodes the relation between the Green's function and the self-energy. So, the actual non-trivial piece of information is the relation (1.3.25). When we couple the system to a bath the integral equations (1.3.29) will stay exactly the same, whereas the answer for the self-energy (1.3.25) will change. Appendix B.1 describes our approach to solving the KB equations (1.3.25).

To conclude this subsection, let us write down the expression for the energy:

$$E_S(t) = \langle H_S(t) \rangle = -i^{q_S+1} \frac{J_S^2}{q_S} \int_{-\infty}^{t} dt' \, \left(G_S(t,t')^{q_S} - G_S(t',t)^{q_S} \right) \tag{1.3.30}$$

Using the equations of motion (1.3.29), it follows that

$$E_S(t) = \frac{1}{q_S} \partial_t G_S(t,t). \tag{1.3.31}$$

This is not a general expression; it holds because the SYK Hamiltonian only contains terms with q_S identical fermions.

1.4 Klebanov–Tarnopolsky tensor model

Let us consider the quantum mechanical model of a real anticommuting 3-tensor ψ^{abc} with the action [20]

$$S = \int dt \Big(\frac{i}{2} \psi^{abc} \partial_t \psi^{abc} + \frac{1}{4} g \psi^{a_1 b_1 c_1} \psi^{a_1 b_2 c_2} \psi^{a_2 b_1 c_2} \psi^{a_2 b_2 c_1} \Big) . \tag{1.4.32}$$

[6] Strictly speaking, for a thermal initial state the right hand side contains the integral over the imaginary axis running from $-i\beta$ to 0. However we can imagine that all non-equilibrium processes happen at large positive Lorentzian times so this piece is essentially zero if correlators decay with time. This is the reason why the integration over t' starts at $-\infty$.

The three indices, each of which runs from 1 to N, are treated as distinguishable, and the Majorana fermions satisfy the anti-commutation relations

$$\{\psi^{abc}, \psi^{a'b'c'}\} = \delta^{aa'}\delta^{bb'}\delta^{cc'} \ . \tag{1.4.33}$$

This model is a somewhat simplified version of the $O(N)^6$ symmetric Gurau-Witten model [19]. Both are in the class of 3-tensor models which possess a "melonic" large N limit where $J = gN^{3/2}$ is held fixed [39, 18, 40, 41, 42, 43, 44, 45, 46, 47, 48]. The large N model is nearly conformal in the IR [16, 17]; for example, the two-point function is

$$\langle T(\psi^{abc}(t_1)\psi^{a'b'c'}(t_2))\rangle = -\delta^{aa'}\delta^{bb'}\delta^{cc'}\Big(\frac{1}{4\pi g^2 N^3}\Big)^{1/4}\ \frac{\mathrm{sgn}(t_1-t_2)}{|t_1-t_2|^{1/2}}\,. \tag{1.4.34}$$

The model (1.4.32) has the $O(N)_1 \times O(N)_2 \times O(N)_3$ symmetry under the replacement[7]

$$\psi^{abc} \to M_1^{aa'} M_2^{bb'} M_3^{cc'} \psi^{a'b'c'}, \tag{1.4.35}$$

$$M_1 \in O(N)_1, \quad M_2 \in O(N)_2, \quad M_3 \in O(N)_3\,. \tag{1.4.36}$$

As far as the group $O(N)_1$ is concerned, we may think of b and c as flavor indices; therefore ψ^{abc} produces N^2 flavors of real fermions in the fundamental of $O(N)_1$. An analogous picture applies to $O(N)_2$ and $O(N)_3$. The three sets of $SO(N)$ symmetry charges are

$$Q_1^{a_1a_2} = \frac{i}{2}[\psi^{a_1bc}, \psi^{a_2bc}]\ , \quad Q_2^{b_1b_2} = \frac{i}{2}[\psi^{ab_1c}, \psi^{ab_2c}]\ , \quad Q_3^{c_1c_2} = \frac{i}{2}[\psi^{abc_1}, \psi^{abc_2}]\,. \tag{1.4.37}$$

The gauging of $SO(N)_1 \times SO(N)_2 \times SO(N)_3$ sets these charges to zero; this restricts the operators to the invariant ones, where all the indices are contracted. In the ungauged model (1.4.32) a more general class of operators is allowed, and they can be classified according to representations of the $SO(N)_1 \times SO(N)_2 \times SO(N)_3$.

[7] More generally, we could consider a model with $O(N_1) \times O(N_2) \times O(N_3)$ symmetry, where a runs from 1 to N_1, b from 1 to N_2, and c from 1 to N_3. This may be thought of as a model of a large number N_2 of $N_1 \times N_3$ matrices [49].

Each $O(N)$ group includes parity transformations (axis reflections) P_{a_0}: for a given a_0, P_{a_0} sends $\psi^{a_0 bc} \to -\psi^{a_0 bc}$ for all b, c and leaves all $\psi^{a_1 bc}, a_1 \neq a_0$ invariant. In a physical language, these are "big" gauge transformations and operators should be invariant under them. Therefore we can build operators using ψ^{abc} and the delta symbol $\delta^{aa'}$ only. In the case of $SO(N)$ gauge group one can use the fully antisymmetric tensor $\epsilon_{a_1 \dots a_N}$ as well; it is invariant under $SO(N)$, but changes its sign under the parity transformations. Because of this, there are additional "long" operators containing at least N fields, like

$$O_{\text{long}} = \epsilon_{a_1 \dots a_N} \epsilon_{b_1 \dots b_N} \epsilon_{c_1 \dots c_N} \prod_{j=1}^{N} \psi^{a_j b_j c_j} \ . \tag{1.4.38}$$

The difference between gauging $O(N)$ and $SO(N)$ becomes negligible in the large N limit.

Let us define three operations which permute pairs of the $O(N)$ symmetry groups (and thus interchange indices in the tensor field), while also reversing the direction of time,

$$s_{ab} : \psi^{abc} \to \psi^{bac}, \qquad t \to -t; \tag{1.4.39}$$

$$s_{bc} : \psi^{abc} \to \psi^{acb}, \qquad t \to -t; \tag{1.4.40}$$

$$s_{ac} : \psi^{abc} \to \psi^{cba}, \qquad t \to -t\,. \tag{1.4.41}$$

Each of these transformations preserves the equations of motion for the ψ^{abc} field,

$$\dot{\psi}^{abc} = ig(\psi^3)^{abc}\,, \quad (\psi^3)^{abc} \equiv \psi^{ab_1c_1}\psi^{a_1bc_1}\psi^{a_1b_1c}\ . \tag{1.4.42}$$

The Hamiltonian, including a quantum shift due to (1.4.33),

$$H = -\frac{1}{4} g \psi^{a_1 b_1 c_1} \psi^{a_1 b_2 c_2} \psi^{a_2 b_1 c_2} \psi^{a_2 b_2 c_1} + \frac{gN^4}{16} = -\frac{1}{4} g [\psi^{a_1 b_1 c_1}, \psi^{a_1 b_2 c_2}][\psi^{a_2 b_1 c_2}, \psi^{a_2 b_2 c_1}]\ , \tag{1.4.43}$$

changes sign under each of the transformations s_{ab}, s_{bc}, s_{ac}. This means that these transformations are unitary: they preserve e^{iHt}. In contrast, the usual time reversal transformation is anti-unitary because it also requires complex conjugation $i \to -i$.

The $O(N)^3$ invariant operators form representations under the permutation group S_3, which acts on the three $O(N)$ symmetry groups (it contains the elements s_{ab}, s_{bc} and s_{ac}). For example, H is in the degree 1 "sign representation" of S_3: it changes sign under any pair interchange, but preserves its sign under a cyclic permutation.

It is also interesting to study the spectrum of eigenstates of the Hamiltonian for small values of N; first steps on this were made in [50, 51, 52]. When gauging the $O(N)^3$ symmetry one needs to worry about the Z_2 anomaly, which affects the gauged $O(N)$ quantum mechanics with an odd number of flavors of real fermions in the fundamental representation [53, 54]. Since for each of the three $O(N)$ groups we find N^2 flavors of fundamental fermions, the gauged model is consistent for even N, but is anomalous for odd N.[8] This means that, for odd N, the spectrum does not contain states which are invariant under $O(N)^3$ (for $N = 3$ this can be seen via an explicit diagonalization of the Hamiltonian (1.4.43) [50]).

[8] We are grateful to E. Witten for pointing this out to us.

Chapter 2

To gauge or not to gauge?

2.1 Introduction

Many examples of the holographic correspondence involve very strongly coupled large N gauge theories which are dual to a bulk Einstein gravity theory [5, 55, 56]. In such theories, the gauge symmetry leads to a reduction in the naive number of low dimension operators from N^2 to an order one number. The D0 brane matrix model [21], also known as BFSS model [22], is an example of such gauge/gravity duality [12]. In a 0+1 dimensional theory, the only role of the gauge symmetry is to impose an $SU(N)$ singlet constraint. Therefore, we can consider an alternative model where we set $A_t = 0$. The theory now has a global $SU(N)$ symmetry. If we impose a "Gauss Law" constraint restricting to $SU(N)$ singlets, then we recover the gauged model. In this work we study the properties of the model where we *do not* impose this singlet constraint.

At first sight, one might think that not imposing this constraint leads to many more states, of order N^2 of them. The presence of these new states could modify the properties of the system substantially. This is indeed correct in the weakly coupled regime. However, we will argue that in the strongly coupled regime we have essentially the same gravity dual description as for the gauged model.

In this matrix model, the coupling constant, g^2, has dimensions of (mass)^3. Therefore it is weakly coupled at high energies and strongly coupled at low energies. Correspondingly, the gravity dual has a curvature that depends on the radial position. Near the boundary it is highly curved, but away from the boundary we have a low curvature region where we can trust Einstein gravity. See Figure 2.1. This low curvature region corresponds to the energy scales where the matrix model is strongly coupled.

We will argue/conjecture that the gravity picture of the non-singlet states is the following. The non-singlet states have an energy of order the order $\lambda^{1/3} = (g^2 N)^{1/3}$ and are located in the high curvature region, away from the region that is described by Einstein gravity, see Figure 2.1. In the planar approximation, we also have states corresponding to additional excitations of these non-singlet states which can be represented as folded strings with their ends stuck to the highly curved region near the boundary. At finite temperature we can further have non-singlet states that correspond to black holes with strings that come in from the boundary and end on the black hole, see Figure 2.2 (b,c).

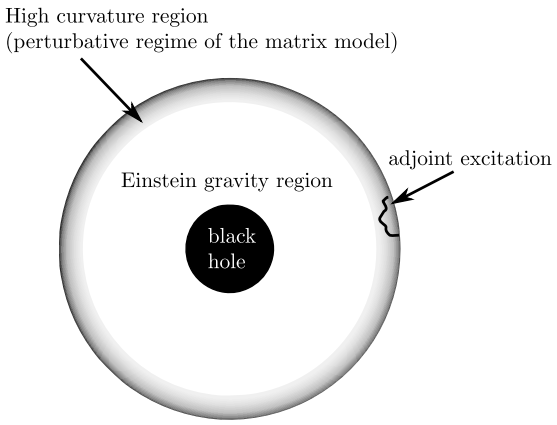

Figure 2.1: Sketch of the gravity solution at finite temperature. The shaded region near the boundary is highly curved. Moving further inwards we find a region of lower curvature that can be described by Einstein gravity. We will argue that the lowest energy non-singlet excitations live purely in the shaded region and have an energy that roughly corresponds to that of a massive string state located in the interface between the two.

We have not derived this picture rigorously, we will simply present some plausibility arguments and consistency checks. In [57], Berkowitz, Hanada, Rinaldi and Vranas present more evidence supporting this picture by performing a direct numerical simulation of the ungauged model[1].

In [58], a similar conclusion was reached for the "double scaling" limit of a single matrix quantum mechanics for low enough temperatures See also [59, 60, 61, 62, 63] for further discussion of non-singlets in that model.

We were motivated to ask the question in the title by the Gurau-Witten tensor models [18, 19]. There one has the choice of either imposing or not imposing a singlet constraint. It is sometimes thought that the models with a singlet constraint would be more likely to have a gravity or string dual. Our main message is that the existence of a local gravity dual is independent of whether we do or do not impose this constraint. Einstein-like gravity is associated to very strong interactions but not to the presence or absence of the boundary theory gauge symmetry (or gauge redundancies).

When we consider the ungauged model we break supersymmetry, since in the original model the algebra only closes up to gauge transformations. Nevertheless the modified algebra can be used to argue that the energy is positive, even for non-singlet states. Of course, singlet states are the same as those of the gauged model. For non-singlet states, the lowest energy state appears to be when all branes are separated by a large amount (namely, the matrices get large diagonal expectation values). In this regime, the non-zero $SU(N)$ charges lead to a kind of angular potential going like $1/X^2$ for diagonal matrices of typical magnitude X. This potential leads to even larger expectation values for the matrices. Nevertheless, for finite temperatures, we expect to have a metastable state where the expectation values of the matrices are relatively small (or the branes are together), since this state has more entropy. This state can be viewed as a black hole. Our previous remarks on the equality of the gravity configurations applied for these metastable black hole configurations.

We are arguing that non-singlets are energetically disfavored at low energies. This seems to contradict the picture proposed in [64, 65] for the deconfinement/black hole transition that is

[1] We thank the authors of [57] for detailed explanations on their computations and for ongoing discussions.

based on the idea that the Polyakov loop gets an expectation value. If the only states contributing were singlets we would get no potential for the eigenvalues of the Polyakov loop. We will discuss how the two pictures are consistent. We are lead to a picture where the values of the holonomy indeed break the center symmetry but only by a very small amplitude "wave" in the eigenvalue distribution.

This chapter is organized as follows. In Section 2.2 we describe how one can remove the singlet constraint and obtain the deformation of the supersymmetry algebra. We also relate it to the insertion of Wilson loops in the gauged model. Section 2.3 is devoted to non-singlets. We first look at the lowest energy excitations of the thermal background. We then consider the region where all branes are far away. We also use perturbation theory to find the shifts to the spectrum in the weakly coupled region. We also discuss the thermodynamic properties of the ungauged model. We discuss further aspects of the Polyakov loop and thermal phase transitions in section 2.4. After making some further comments we present some conclusions.

2.2 The ungauged model

In this chapter we will consider the situation where we set $A_t = 0$ and we *do not* impose the $SU(N)$-singlet constraint[2]. This amounts to treating the $SU(N)$ symmetry as a global symmetry rather than as a gauge symmetry. In higher dimensions, gauging a symmetry introduces extra degrees of freedom. In quantum mechanics it does not. The theory with $A_t = 0$ is a perfectly well defined theory, with global $SU(N)$ symmetry, and we can consider it in its own right. This theory has a singlet subsector where it identical to the usual one in Section 1.2, but it also has non-singlet states whose interpretation in the gravity dual we want to elucidate.

It is sometimes said that gauging the $SU(N)$ symmetry reduces the number of operators drastically and that this is important for the gravity solution to work. We will see that the gravity solution can be valid whether we gauge the $SU(N)$ symmetry or not.

[2] We could also say that we have a $U(N)$ gauge symmetry. However, since there are no fields charged under the overall $U(1)$, it does not matter whether we gauge or do not gauge the overall $U(1)$.

2.2.1 The size of the matrix versus the size of the Einstein gravity region

It is interesting to translate (1.2.3) to the gravity side. On the gravity side we can consider D0 brane probes that sit at particular values of r. A string stretching from this brane probe to $r = 0$, or the horizon, has an energy of the order of r. Now, if we consider the mass of an off-diagonal mode of a matrix in the diagonal background $m \sim X_{diag}$ we expect to get the same energy. It means that the radial direction is related to matrix elements as $r \sim X$. Using this procedure to translate between radial positions and matrix eigenvalues, we now ask: What value of r would the scale (1.2.3) correspond to? Interestingly, it corresponds to a scale $r \sim \lambda^{1/3}$, which is the scale at which the supergravity solution breaks down!This important point was emphasized in [23], and we are repeating it because we think it is not widely appreciated. In fact, some papers in the literature seem to suggest that the typical size of the matrices in the thermal state would be $X \sim r_0$. Note that $r_0 \ll \lambda^{1/3}$ in the region where we can trust gravity.

This means that the whole Einstein gravity region of Figure 2.1 corresponds to a highly quantum region of the wave function for the matrix model. The matrices have large fluctuations. However, these fluctuations are highly correlated. Indeed, via supersymmetric localization, [66, 67] computed $\frac{1}{N}\langle \mathrm{Tr}[(X^1 + iX^9)^{2k}]\rangle$. They found a much smaller answer agreeing with naive bulk expectations. Due to the i, in this expectation values there are interesting cancellations.

2.2.2 Lack of supersymmetry

Let us define the hamiltonian of the ungauged model to be simply the one obtained from eq. (1.2.1) by setting $A_t = 0$. We can then wonder whether the resulting theory is supersymmetric. We certainly continue to have the operators Q_a that were generating the SUSY transformations before:

$$Q\epsilon = -\frac{1}{g^2}\,\mathrm{Tr}\left(\dot{X}^I \psi\gamma^I\epsilon + i\frac{1}{2}[X^K, X^L]\psi\gamma^{KL}\epsilon\right) \tag{2.2.1}$$

where $\gamma^{KL} = \frac{1}{2}\left(\gamma^K\gamma^L - \gamma^L\gamma^K\right)$. We can now ask whether these operators commute with the Hamiltonian. We find

$$[Q_\alpha, H] = -\,\mathrm{Tr}\,(\psi_\alpha G) \tag{2.2.2}$$

We see that the right hand side can be written in terms of the $SU(N)$ symmetry generators, G in (1.2.2). This means that, while (2.2.2) vanishes when it acts on singlet states, it will be non-vanishing acting on non-singlet states. Therefore we expect that non-singlets will not come in supersymmetry multiplets. We can also compute the anticommutators

$$\{Q_\alpha, Q_\beta\} = 2H\delta_{\alpha\beta} + 2\,\mathrm{Tr}\left(GX^I\right)\gamma^I_{\alpha\beta} \tag{2.2.3}$$

We see that we get non-zero answers in the right hand side because the supersymmetry transformations only close up to $SU(N)$ transformations. In the gauged model these are gauge transformations. But in the ungauged model we get a non-zero right hand side. Nonetheless, we can still infer some information from this algebra.

Let us note first, that even for non-singlet states the energy is non-negative. Indeed, since the supercharges are self-adjoint $Q^\dagger_\alpha = Q_\alpha$ and gamma matrices are traceless, summing over the spinor indices leads to

$$32H = \sum_{\alpha=1}^{16}\{Q_\alpha, Q_\alpha\} = \sum_{\alpha=1}^{16}\{Q^\dagger_\alpha, Q_\alpha\} \geq 0 \tag{2.2.4}$$

2.2.3 Supersymmetric version of the ungauged model

In principle, we could modify the definition of the supercharges so as to have a supersymmetric theory. We do not think that is possible. Nevertheless, if we are willing to also redefine the Hamiltonian, then it is possible to preserve some of the supersymmetry. This can be achieved by adding a new term to the Hamiltonian:

$$H_{\mathrm{susy}} = H - \mathrm{Tr}\left(X^1 G\right) \tag{2.2.5}$$

This breaks the $SO(9)$ symmetry to $SO(8)$, and it preserves half of the supersymmetry, those whose spinorial parameter obeys

$$(\gamma^1 + \mathbf{1})\epsilon = 0 \tag{2.2.6}$$

Moreover, now we have the standard supersymmetry algebra:

$$\{Q.\epsilon, Q.\epsilon'\} = 2H_{\text{susy}}\epsilon.\epsilon' \tag{2.2.7}$$

This might seem surprising at first sight, but there is a simple explanation for the existence of this Hamiltonian. In this chapter we will concentrate on the model with the original Hamiltonian.

2.2.4 Relation to Wilson loop insertions

There is a physical situation that arises in the gauged model which is very closely connected to the ungauged model. We can have the original gauged theory and add an external quark in some representation $\bar{R}$, by coupling it through a Wilson line operator in representation $\bar{R}$. This is very closely related to the ungauged theory restricted to the representation R [3]. The only difference is that in the thermal partition function, restricted to representation R, we would include a factor of the dimension of the representation in the ungauged case but not in the gauged case with a Wilson loop.

The simplest Wilson loop operators we can consider are $\text{Tr}_{\bar{\text{R}}}\, Pe^{i\int A_t dt}$. These break supersymmetry. Another commonly considered operator preserves half of the supersymmetries and has the form $\text{Tr}_{\bar{\text{R}}}\, Pe^{i\int dt(A_t+X^1)}$, where we have picked one of the scalar fields [68, 69]. The extra term corresponds to the extra term in the Hamiltonian (2.2.5). When we add the supersymmetric Wilson loop in the adjoint representation, in the gravity dual we get a string coming in from the boundary at $X^1 = \infty$ and a string going to $X^1 = -\infty$. Equivalently, we can say we have a string anti-string pair with the string pinned on the north pole of the S^8 and the anti-string on the south pole of S^8. See Figure 2.2 (a).

In conclusion, we can translate many of the statements in this chapter to statements about insertions of Wilson lines for the original, gauged, model.

[3] We can only consider representations transform trivially under the Z_N center of $SU(N)$, which are the ones we can get from products of adjoints.

2.3 Gravity duals of non-singlets

Let us consider first the gravity dual of the adjoint states, states in the adjoint representation of $SU(N)$. They are described by the gravity dual of the non-supersymmetric Wilson loop $e^{i\int A_t dt}$. As pointed out in [70] (see also [71]), the gravity dual of these Wilson loops differs from the supersymmetric Wilson loops only through the fact that the strings are not pinned at a particular point on the sphere, but they can move to any point on the sphere. See Figure 2.2(b,c). In other words, on the boundary of the bulk they obey Neumann, rather than Dirichlet, boundary conditions in the sphere directions. If we have an adjoint, this means that the string and the anti-string could lower their energy by coming closer together on the sphere. If they coincide on the sphere, then we have a folded string whose energy can be lowered by moving the tip further and further to the boundary, see Figure 2.2(c).

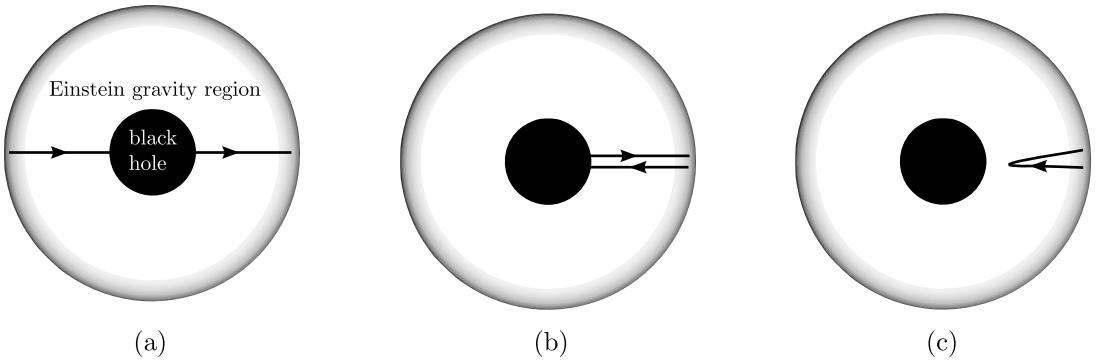

Figure 2.2: (a): The string configuration corresponding to a supersymmetric Wilson line in the adjoint representation. (b): The string and anti-string configuration representing a non-supersymmetric adjoint. We get it from (a) by moving the left string segment to the right side of the figure . (c): We further lower the energy configuration of (b) by moving the tip away from the horizon. The idea is that the end point of this motion is a configuration as in Figure 2.1.

According to the gravity solution, the energy of folded stretched string (at $\beta = \infty$), with its tip momentarily at rest, is given by

$$E = \frac{2}{2\pi}\int_{r_{tip}}^{r_\infty} dr = \frac{1}{\pi}\left(r_\infty - r_{tip}\right) \tag{2.3.8}$$

This computation, valid in the gravity regime, would suggest that we can lower the energy to zero by moving $r_{tip} \to r_\infty$, where r_∞ is some large r cutoff. However, at very large r we cannot trust the gravity computation. In other words, the fact that as $r_{tip} \to r_\infty$ the energy goes to zero cannot be trusted when both of these quantities are in the highly curved region. Therefore, it could be that even the lowest energy configuration has a non-zero energy. What would be a natural value for this energy? One natural possibility would be to think that $r_\infty \propto \lambda^{1/3}$ which is the value of r where the curvature becomes of the order of the string scale. Furthermore, we can also assume that naive cancellation between r_{tip} and r_∞ does not happen and that we get an energy that is the typical energy of a massive string state at the location given by $r \sim \lambda^{1/3}$. From (1.2.7) we find that this is an energy of the order of $\lambda^{1/3}$. We get the same answer if we use dimensional analysis and assume that it will be of the order of the 't Hooft coupling. In both cases we get

$$E_{\min} = C\lambda^{1/3} \tag{2.3.9}$$

where C is an unknown numerical constant. In the next subsection we will present an argument saying that $C > 0$. Note that C cannot be negative because we have argued near (2.2.4) that the energy should be positive. The fact that C is positive is also suggested by the numerical computation in [57].

We can speculate about the temperature corrections to the estimate (2.3.9). We expect these to come from the fact that at finite temperature the metric at the transition region, at $r \sim \lambda^{1/3}$, will be changed due to the r_0 dependent terms in (1.2.7). We expect this to produce an extra factor of $(1 + a_1 \frac{r_0^7}{r^7})$, where $r \sim \lambda^{1/3}$. Using (1.2.8) we find then that

$$E = C\lambda^{1/3}\left(1 + \tilde{a}_1 \left(\frac{T^3}{\lambda}\right)^{\frac{14}{15}} + \cdots\right) \tag{2.3.10}$$

where $\tilde{a}_1$ is an unknown numerical constant. The main point is that it is small for $T \ll \lambda^{1/3}$.

2.3.1 Exploring the large X region

In the above discussion we have assumed that the model starts in a state with $X \sim 0$ and then we add the adjoint as a perturbation. This is particularly reasonable if the branes are trapped near the origin by thermal effects.

On the other hand, we can set the temperature to zero and consider a situation where all branes are separated from each other. In this case, we can ask about the energy of the adjoint state. First we should note that if we do not gauge the symmetry, then we have a manifold of Goldstone modes coming from applying the $SU(N)$ transformations to the original configurations. This manifold has an $SU(N)$ symmetry and we can consider a wave function which is in the adjoint representation under this global $SU(N)$ symmetry. We can think of this as a configuration which has an $SU(N)$ "angular momentum" along this manifold. The typical radius of this manifold is given by the distance between the branes, call it X. Then we get an energy which goes like

$$V \sim +\frac{\lambda}{X^2} \tag{2.3.11}$$

We discuss and derive this in more detail in Appendix A.1.2. One can view this final formula as analogous to the angular momentum potentials we get when a particle moves in three dimensions in a spherically symmetric potential and with some angular momentum. It makes sense to first freeze X and then calculate the potential (2.3.11) for the following reason. The effective mass of the X variables is of order $1/g^2 \sim \frac{N}{\lambda}$, which is large in the 't Hooft limit. Therefore, the motion in the X directions produced by (2.3.11) will be relatively slow. This is like the Born-Oppenheimer approximation. We can trust (2.3.11) when $|X|$ is large enough that we can use perturbation theory in the matrix model. This means that $\lambda/X^3 \ll 1$. If we extend this to the boundary of its regime of validity, namely to $X^3 \sim \lambda$, then we find that the energy becomes $\sim \lambda^{1/3}$, in agreement with the estimate (2.3.9). Figure 2.3 shows the form of the potential when we separate the branes and we are in an adjoint state. The reason we get a constant when $|X| \lesssim \lambda^{1/3}$ is the picture we suggested in Figure 2.1 where the adjoint is localized in the transition region. When the branes

are located within the Einstein gravity region they have shed their adjoint charge, leaving it as a string with endpoints in the high curvature region.

Note that this transition happens at a value of r that coincides with the size of the ground state wave function (1.2.3). This also suggests that when the X have an expectation value of this size there will be other degrees of freedom that can carry the adjoint quantum numbers.

Note that the presence of the potential in Figure (2.3) suggests that the adjoint state with $X \sim 0$ is unstable and the system is driven to $X \sim \infty$. We think that this is the ultimate fate of adjoint states. On the other hand, at finite temperature the gravity solution shows that thermal effects will trap the branes at $X \sim 0$, leading to a metastable minimum. As we will recall near (2.3.23), this metastable state is very long lived in the 't Hooft limit, so that we only need to worry about this decay mode at very low temperatures.

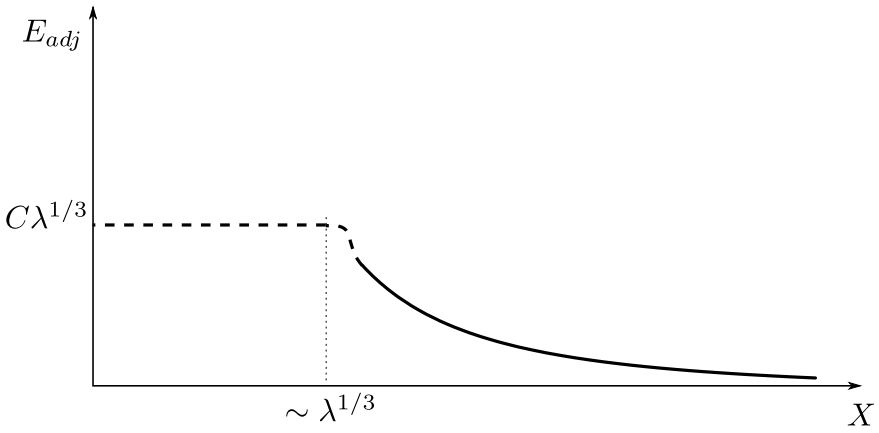

Figure 2.3: Energy of an adjoint state where we explore the flat directions of the potential in (1.2.1), which correspond to mutually diagonal matrices X^I. The solid line denotes the potential computed in the region where we can trust perturbation theory in the matrix model side, which is $\lambda^{1/3} \lesssim |X|$. The details depend on the particular form of the diagonal matrices X. In this region, the energy comes from the angular momentum along the $SU(N)$ directions in the moduli space of vacua of the ungauged model. The horizontal doted line corresponds to the energy of a massive string state in the transition region, as in Figure (2.1). We expect a smooth transition region in between. We have not included here the effects of the thermal potential which produces a large dip near $X \sim 0$, or $r \sim r_0$, (for $T \ll \lambda^{1/3}$) because it is common to the gauged and ungauged models.

2.3.2 Adjoint energies at weak coupling in the BMN matrix model

The BFSS matrix model is always strongly coupled at low energies. On the other hand, the BMN matrix model has another scale, given by the mass μ. If we take $\lambda \ll \mu^3$, we can trust perturbative computations even around the simplest, $X = 0$, vacuum. The expansion parameter is λ/μ^3. In the simplest vacuum we have a collection of bosonic and fermionic harmonic oscillators. The lightest sector with matrix creation–annihilation operators $a_i^\dagger, a_i,\ i = 1, \ldots, 6$ corresponds to $SO(6)$ operators $X^i = i,\ i = 1, \ldots, 6$, see Appendix A.1.1 for details. Each oscillator $a_i^\dagger$ has energy $\mu/6$. In the gauged $SU(N)$ model we cannot act with a single creation operator because it would be in the adjoint of $SU(N)$. The first singlet appears for a pair of operators $\mathrm{Tr}[a_i^\dagger a_j^\dagger]|0\rangle$, where the trace is over the $SU(N)$ indices r, s: $\mathrm{Tr}[a_i^\dagger a_j^\dagger] = (a_i^\dagger)_r{}^s (a_j^\dagger)_s{}^r$. On the other hand, in the ungauged model we can have a state of the form $a_i^\dagger|0\rangle$. This state has energy $\mu/6$ at zero coupling. One can compute the first perturbative correction and we find that it is given by (see Appendix A.1.1)

$$E_{\text{adjoint}} = \frac{\mu}{6} + \frac{9}{2}\frac{\lambda}{\mu^2} + \cdots \tag{2.3.12}$$

where the dots are higher order terms in the λ/μ^3 expansion. The idea is that if we were to sum all the corrections and continue the answer to strong coupling we would get that $E_{\text{adj}} \sim C\lambda^{1/3}$ for $\lambda/\mu^3 \gg 1$.

It is interesting that one can obtain a relatively simple answer for this one loop shift for the energy of more general adjoint states. This can be done using the general expression for the one loop Hamiltonian in [27] and observing that it contains an additional piece for non-singlets in representation R

$$\Delta\hat{H}_{\text{1-loop}} = \Delta\hat{H}_{\text{gauged, 1-loop}} + \frac{9g^2}{2\mu^2} C_2(R) \tag{2.3.13}$$

The explicit expressions for $\Delta\hat{H}_{\text{1-loop}}$ and $\Delta\hat{H}_{\text{gauged, 1-loop}}$ are given in eq. (A.1.14).

In general one should be careful with translating (2.3.13) to the energy shifts, since $\Delta\hat{H}_{\text{gauged, 1-loop}}$ may act differently on non-singlets. This point deserves some clarifications. Since the trace is cyclic, operators $a_i^\dagger$, forming a single-trace singlet operator $\mathrm{Tr}[a_i^\dagger a_j^\dagger \ldots]$ are placed on "a circle". From this point of view, non-singlets have "boundaries". So, generically,

singlets and non-singlets have quite different Hilbert spaces and $\Delta\hat{H}_{\text{gauged, 1-loop}}$ may have completely different eigenvalues.

For example, in the gauged model on level two we have BPS states $\text{Tr}[a_i^\dagger a_j^\dagger],\ i \neq j$. However, in the adjoint sector of the ungauged model operators $a_i^\dagger a_j^\dagger$ and $a_j^\dagger a_i^\dagger$ are different if $i \neq j$. One can check explicitly using eq. (A.1.14) that the state corresponding $a_i^\dagger a_j^\dagger + a_j^\dagger a_i^\dagger$ still does not receive corrections from $\Delta\hat{H}_{\text{gauged, 1-loop}}$, whereas antisymmetric combination $a_i^\dagger a_j^\dagger - a_j^\dagger a_i^\dagger$ receives an additional shift of $4g^2\left(\frac{3}{\mu}\right)^2$. Nonetheless, both symmetric and anti-symmetric combinations get contribution from $\frac{9g^2}{2\mu^2}C_2(\text{adj}) = \frac{9g^2N}{2\mu^2}$. The reason the symmetric combination is still protected against $\Delta\hat{H}_{\text{gauged, 1-loop}}$ is that symmetrization restores the cyclic symmetry. It is natural to conjecture that cyclic-symmetric non-singlets receive the same contribution from $\Delta\hat{H}_{\text{gauged, 1-loop}}$ as singlets.

So far we have discussed the vacuum with $X = 0$. One can also consider a fuzzy sphere vacuum (1.2.6) with $X^a = \frac{\mu}{3}J^a,\ a = 1, 2, 3$. In this case, one also expects $SU(N)$ Goldstone bosons. As in the discussion in section 2.3.1, we could calculate the energy of states with non-trivial $SU(N)$ quantum numbers by considering states with $SU(N)$ angular momentum along the manifold spanned by the Goldstone bosons. We discuss this in more detail in Appendix A.1.3 where we found a simple lower bound on the energy of the adjoint of the form

$$\frac{g^2N}{R^2} = \frac{\lambda}{R^2} \lesssim E_{\text{adjoint}}\ , \qquad \text{for} \quad \mu^3 \gg \lambda \tag{2.3.14}$$

where $R^2 = \frac{1}{3N}\frac{\mu^2}{9}\,\text{Tr}\left(J_1^2 + J_2^2 + J_3^2\right)$ is the average radius of the fuzzy spheres. This is consisent with the expectations based on (2.3.11).

2.3.3 Spectrum above the minimum

We now return to strong coupling. Around the thermal background we have argued that the minimum energy for the adjoint state is given in (2.3.9). We would now like to discuss excitations above these states. In the planar limit these excitations will be single strings of operators with a fundamental index at one end and an antifundamental at the other end, combined so that we

an adjoint index in total. We expect that these states would be strings whose ends are located in the high curvature region.

Of course, when we quantize the string we expect a large number of modes. So we expect a number of energy eigenstates above the minimum given by (2.3.9). The first few are expected to be separated from the minimum by gaps which are of the same order of magnitude as the lowest energy itself (2.3.9). In general, it seems complicated to determine this spectrum because it depends both on what is happening in the high curvature region as well as in the low curvature region. As the string gets more excited it can dip further into the region described by Einstein gravity. An example of an excitation would be a stretched folded string that goes from the high curvature region to some radial position $r_{\rm min}$. If $r_{\rm min}$ is within the weakly coupled region, then its motion could be as indicated in Figure A.1, namely the tip of the string goes into the weakly coupled region, it is slowed down by the string that pulls it from the boundary and it bounces back to the high curvature region[4]. After it goes back into the high curvature region it could come back out with other worldsheet excitations, depending on the physics in the high curvature region. The full spectrum cannot be obtained unless we can solve both parts of the motion, namely the one in the low curvature region as well as the one in the high curvature region. In Appendix A.2 we discuss a toy problem where we assume that the string tip is reflected from the high curvature region without any further excitation, thought this is probably not what happens in reality.

When the excitation energy is large enough that the string can reach all the way to the horizon, something new happens. The string falls into the horizon and we end up with a string and an anti-string pair, each ending on the horizon. The minimum energy when this happens is given by the energy of a folded string that stretches all the way from the high curvature region to the horizon,

$$E_{\rm dec} = \frac{1}{\pi}\int_{r_0}^{r_{\rm high}\sim\lambda^{1/3}} dr = \tilde{C}\lambda^{1/3} - \frac{r_0}{\pi} = \lambda^{1/3}\left[\tilde{C} - \frac{1}{\pi}\left(\frac{T4\pi\sqrt{d_0}}{7\lambda^{1/3}}\right)^{\frac{2}{5}}\right] \tag{2.3.15}$$

[4] We compute the phase shift for this motion in Appendix A.2. A similar computation for the single matrix model in the double scaling limit was done in [62, 63] and matched to the matrix model.

where we expect that $\tilde{C}$ is an order one quantity bigger than C in (2.3.9).

We will call this the "deconfinement" energy, because above this energy the adjoint is effectively behaving as two independent excitations, a quark and an anti-quark, corresponding to the string and antistring segments ending on the horizon. Furthermore, when a string ends on the horizon, there is an additional factor N in the effective number of states. This arises as follows. When a string wraps the Euclidean black hole it has a disk topology, which produces and additional factor of $1/g_s \propto N$. This is *in addition* to the factor of N that we get from all the possible values of the fundamental index at the boundary. This new factor is present for both the gauged and ungauged models and it is related to the physics at the horizon.

When the string is not reaching the black hole horizon we can effectively think of the large N Hilbert space as factorizing into the black hole part which lives in the singlet Hilbert space and non-singlet excitations that live close to the boundary.

$$\mathcal{H}_{\text{non}-\text{singlets}} \sim \mathcal{H}_{\text{singlets}} \otimes \mathcal{H}_{\text{boundary string Fock space}} \tag{2.3.16}$$

Furthermore there is a Fock space of boundary excitations, generated by the adjoint excitations which appear as strings with ends in the large curvature region, as in Figure 2.1. Each generator has the degeneracy of an adjoint, or a factor of N^2. [5]

The strings that end on the horizon can be qualitatively viewed as extra tensor factors, one for the quarks and one for the anti-quarks (or strings or anti-strings), see Figure 2.2(b). Each of these generates a Fock space. The string ending on the horizon is expected to have minimum energy $\tilde{C}\lambda^{1/3}/2$. The same is true for the anti-string. This is because the folded string whose tip is at the horizon has energy $\tilde{C}\lambda^{1/3}$ by definition. And this is becoming the string/anti-string pair. The degeneracy of each generator also is proportional to N^2 but with a temperature dependent factor that can be computed by considering a string wrapping the black hole, which has an extra free energy given by (2.3.15) plus a logarithm of N, related to the factor of $1/g_s$ in the partition function mentioned above. This extra degeneracy is not exact, it simply reflects an increase in

[5] We are idenfiying $N^2 - 1 \sim N^2$ since we are only discussing the leading N effects.

the entropy of the combined black hole and string system, but we do not expect to be able to separate it cleanly into a black hole part and a string part. We get the following *schematic* decomposition of the Hilbert space

$$\mathcal{H}_{\text{non-singlets}} \sim \mathcal{H}_{\text{singlets}} \otimes \mathcal{H}_{\text{boundary string Fock}} \otimes \mathcal{H}_{\text{horizon string Fock}} \otimes \mathcal{H}_{\text{horizon antistring Fock}} \quad (2.3.17)$$

2.3.4 The free energy

In this subsection we consider the free energy of the ungauged theory. Because gauging is removing of order N^2 degrees of freedom, and given that the free energy is of order N^2, one might worry that the free energy of the gauged model would be very different than that of the ungauged one.

In fact, large N counting tells us that

$$-\beta F_{\text{ungauged}} - \beta F_{\text{gauged}} = N^2 f(\lambda^{1/3}\beta) \quad (2.3.18)$$

For simplicity we could start considering the BMN model at weak coupling. In this case, in the ungauged theory we basically have $9N^2$ bosonic harmonic oscillators, while in the gauged theory we have $8N^2$ bosonic oscillators since the gauge constraint is essentially removing one matrix (the one we can diagonalize). The fermions give a subleading contribution in this high temperature limit. Therefore, in this case we get

$$f \sim -\log(\mu\beta) \ , \qquad \lambda\beta^3 \ll 1 \ , \qquad \frac{\lambda}{\mu^3} \ll 1 \quad (2.3.19)$$

On the other hand, at strong coupling, $\lambda\beta^3 \gg 1 \gg \beta\mu$, where we can trust the black hole solution, we have a different picture. The idea is that non-singlets are extra adjoint particles living near the boundary of the gravity solution. Because of the factorization (2.3.17) they contribute with extra factors of the form

$$(1 + N^2 d_{Adj} e^{-\beta\lambda^{1/3}C}) \quad (2.3.20)$$

in the partition function. This is the contribution of just the lowest energy adjoint state and d_{Adj} is its degeneracy. We expect it to be of order one. The factor of N^2 comes from the dimension of the adjoint representation. Therefore we expect that the leading energy difference is

$$\beta F_{\text{gauged}} - \beta F_{\text{ungauged}} = N^2 d_{Adj} e^{-\beta\lambda^{1/3}C} , \qquad \lambda\beta^3 \gg 1 \tag{2.3.21}$$

This shows that F_{gauged} and F_{ungauged} are exponentially close in the strongly coupled limit, while they are different at weak coupling (2.3.19).

Let us emphasize that at strong coupling we have a reduction in the naively expected number of states in both theories. For that reason one might have thought that the gauging or not gauging would have a large impact. However, we see that this is is not what is happening, both theories have a common low energy description.

Using the factorized from of the Hilbert space, we can write a more precise form for the free energy difference

$$f \sim \sum_n -(-1)^F \log\left[1 - (-1)^F e^{-\beta E_n}\right] \tag{2.3.22}$$

where n runs over all the adjoint states which can be bosons or fermions. This follows from standard large N counting.

We can further improve the discussion by including strings ending at the horizon. These contributions are most clear in Euclidean space. They still give contributions to f that are exponentially suppressed $\propto e^{-\beta\lambda^{1/3}\tilde{C}}$. These are smaller than (2.3.21) because $C < \tilde{C}$.

We have mentioned in the introduction that both ungauged and gauged models are unstable at very low temperatures. Here we will review more precise estimates for the decay rates (see eg. [72]). Let us start from the gauged model. Emitting a single D0 brane to infinity will lower the Bekenstein–Hawking entropy (1.2.11). Therefore such process is suppressed by:

$$P \sim \exp\left(-\frac{\partial S}{\partial N}\right) = \exp\left(-2\frac{S}{N}\right) \tag{2.3.23}$$

where S is given in (1.2.11). The instability is unsuppressed when

$$T_c \sim \frac{\lambda^{1/3}}{N^{5/9}} \tag{2.3.24}$$

Formally, at this temperature the dilaton becomes large at the horizon and one has to lift the gravity solution (1.2.7) to 11d M-theory black string [12]. Generically, black strings suffer from the Gregory–Laflamme instability [73], which, in this case, also occurs at the temperature (2.3.24).

The contribution from the lowest adjoint (2.3.21) will enhance (2.3.23) by $\sim e^{-\beta\lambda^{1/3}C}$. However at T_c this factor is extremely small $e^{-N^{5/9}}$. Therefore the instability in the ungauged model occurs at the same temperature. Indeed, as we have mentioned before, this instability is the instability of the black hole *itself*, so excitations near the boundary should not affect it.

2.4 Deconfinement and the eigenvalues Polyakov loop holonomy

The main point of this work is that in theories with gravity duals all non-singlets have high energies and are not dynamically important at low energies. On the other hand, the arguments in [64, 65] seem to suggest that non-singlets are important for modifying the eigenvalue distribution of the Polyakov loop. Furthermore, the fact that this distribution is not uniform is viewed as a signal of a black hole formation in the bulk.

This seems to be in contradiction with what we are saying, since we are emphasizing that the non-singlets are dynamically unimportant at low energies and strong coupling. We will here show why there is no contradiction.

To start, let us suppose that we are studying the gauged model. Then the partition function includes the integral over the gauge field holonomy, which we can take to diagonal $U = \text{diag}\left(e^{i\theta_1}, \ldots, e^{i\theta_N}\right)$. In the large N limit it is convenient to introduce the normalized density function $\rho(\theta)$

$$\int_{-\pi}^{\pi} d\theta\ \rho(\theta) = 1 \tag{2.4.25}$$

and the corresponding moments $\rho_n = \int_{-\pi}^{\pi} d\theta \ e^{in\theta}\rho(\theta)$. The moments ρ_n measure the non-homogeneity of the density function.

Since we only have adjoint fields in the matrix model, the energy can depend only on the relative distance between the eigenvalues $\theta_i - \theta_j$. There is a constant repulsion of order one among eigenvalues θ_i due to the group measure. Integrating out the matter fields leads to an attraction of eigenvalues. At very low temperatures the repulsions dominates and the density function is uniform (in the BMN model). As the temperature increases, the attraction becomes stronger and stronger until the density function jumps to a non-uniform distribution. In other words, eigenvalues from a cluster [65]. However, since the energy depends on the relative distance only, the absolute position of the cluster is not fixed, and one has to integrate over this zero mode. This is the reason why the Polyakov loop in the fundamental representation is still zero after the transition.

This resembles the gravity computation of the Polyakov loop in the fundamental [64]: one can have a single string stretched between the horizon and infinity. Such a string has a finite action and one could expect that the Polyakov loop will not be zero. However, in the black hole background one has a normalizable mode of the 2-form $B_{\mu\nu}$, which couples to the string as

$$\exp(ib) \ , \qquad b \equiv \int B \tag{2.4.26}$$

And after the integration over b one gets zero.

If we have just a single adjoint particle of mass $C\lambda^{1/3}$ and degeneracy d_{Adj}, then the partition function reads as (see [65] for the derivation):

$$Z = \int d\rho_1 \ \exp\left(-N^2|\rho_1|^2\left[1 - d_{Adj}e^{-\beta C\lambda^{1/3}}\right]\right) \tag{2.4.27}$$

where in the exponent we have ignored the small terms proportional to $e^{-2\beta C\lambda^{1/3}}, e^{-3\beta C\lambda^{1/3}}$ and so on. The first term in brackets, the one, comes from the $SU(N)$ measure, whereas the second term comes from the matter contribution, where $|\rho_1|^2$ is the contribution of the trace of the holonomy in the adjoint representation.

Assuming that d_{Adj} and C are of order 1 and $\beta\lambda^{1/3} \gg 1$, the integral is dominated by $\rho_1 = 0$. Then, the density is uniform and we expect no black hole!This would be the right conclusion if the only states we had were the ones corresponding to strings with both ends at the high curvature region. For example, these are the only non-singlets around the gapped vacua of the BMN model in the strong coupling region.

However, apart from those strings, we can also have strings ending on the black hole. These strings effectively behave as quarks and antiquarks, with an overall constraint that there is an equal number of quarks and anti-quarks. We can view the integral over b in (2.4.26) as enforcing this constraint. Therefore we can now write a partition function of the form

$$Z = \int d^2\rho_1 db \ \exp\left(-N^2\left[|\rho_1|^2 - d' e^{-\beta\lambda^{1/3}\tilde{C}/2}(e^{ib}\rho_1 + e^{-ib}\bar{\rho}_1)\right]\right) \tag{2.4.28}$$

where d' is a temperature dependent quantity that is less important than the exponential factor we are explicitly writing. We will discuss the origin of d' below. We now see that, before integrating over b, the integral does have a non-trivial saddle point for ρ_1

$$\rho_1^s = e^{-ib} d' e^{-\beta\lambda^{1/3}\tilde{C}/2} \tag{2.4.29}$$

Higher $\rho_n,\ n \geq 2$ are suppressed by factors of $(e^{-\beta\lambda^{1/3}\tilde{C}/2})^n$. It means that the density $\rho(\theta)$ has a bump determined by the cosine function, see Figure 2.4. Of course, in this discussion we used the gravity solution to say what answer to expect on the matrix model side. We have not derived this directly from the matrix model side!We are simply spelling out what answer we expect.

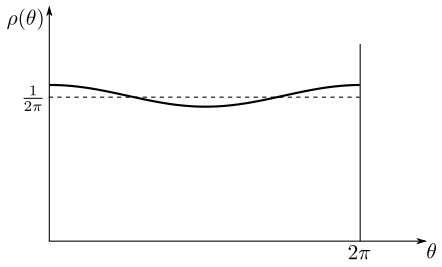

Figure 2.4: The eigenvalue density of the Polyakov loop at strong coupling. It is only slightly non-uniform.

We have a non-zero VEV of the Polyakov loop in the adjoint representation:

$$\langle W_{\rm adj}\rangle = \langle {\rm Tr}_{\rm adj}\, P e^{i\int A}\rangle = N^2|\rho_1^s|^2 \propto N^2 e^{-\beta\lambda^{1/3}\tilde{C}} \tag{2.4.30}$$

In other words, the large energy required to stretch a string from the boundary to the horizon implies that the expectation value of this Wilson loop is very small. Of course, the Polyakov loop in the fundamental is still zero since we have an integral over b.

Let us say a few words about the pre-exponent factor d'. The combination $d'e^{-\beta\lambda^{1/3}\tilde{C}/2}$ in eq. (2.4.28) comes from a single string stretched between the boundary at $r=\tilde{r}_\infty$ and the horizon at $r=r_0$. Therefore,

$$d'\exp\left(-\beta\lambda^{1/3}\tilde{C}/2\right) = \mathcal{D}\exp\left(-\beta\frac{\tilde{r}_\infty - r_0}{2\pi}\right) \tag{2.4.31}$$

The prefactor $\mathcal{D}$ arises from the one loop integral around the classical string configuration, which is a string that wraps the radial and Euclidean time directions. Due to the scaling properties of the solution (1.2.7), it can only give a power law term in the temperature. The exponential term $\beta\frac{\tilde{r}_\infty - r_0}{2\pi}$ arises from the classical string action. As before, we expect that $\tilde{r}_\infty$ is a cutoff dependent quantity that is independent of the temperature, which we write as $\tilde{r}_\infty/\pi = \tilde{C}\lambda^{1/3}$. This constant is expected to be larger that C in (2.3.9) since a string/anti-string pair ending on the horizon can decay into the massive string modes that live at the high curvature regions, which have the energy (2.3.9). On the other hand the r_0 term gives a temperature dependent term in the exponent

$$\frac{\beta r_0}{2\pi} = \frac{\beta^{3/5}}{2\pi}\left(\frac{4\pi\sqrt{\lambda d_0}}{7}\right)^{2/5} \tag{2.4.32}$$

where we have used eq. (1.2.8) to find r_0 in terms of β.

The adjoint particles that live near the high curvature region (see Figure 2.1) contribute as $e^{-\beta\lambda^{1/3}C}$ to the expectation value in (2.4.30), which is suppressed by $1/N^2$ compared to (2.4.30), but the exponential suppression is smaller, since $C<\tilde{C}$. So the full expectation value in the

adjoint is

$$\langle W_{\rm adj}\rangle \propto N^2 e^{-\beta\lambda^{1/3}\tilde{C}} + e^{-\beta\lambda^{1/3}C} + \cdots \tag{2.4.33}$$

where the dots refer to other contributions described by strings that are not ending at the horizon. The order N^0 contribution can be viewed as arising from doing the Gaussian integral in (2.4.27). In matrix model vacua with no black holes (such as the $X = 0$ vacuum of the BMN matrix model) we only get the second term in (2.4.33).

2.5 Further comments

2.5.1 Is there a bulk $SU(N)$ gauge field associated to the $SU(N)$ global symmetry of the ungauged model?

The ungauged model has a global $SU(N)$ symmetry. According to the usual expectations, this should correspond to an $SU(N)$ gauge symmetry in the bulk. On the other hand, we have argued that the bulk theory, at least in the Einstein gravity region, is essentially the same as that of the gauged model. In our case, the states charged under $SU(N)$ are localized near the boundary of the geometry. The fact that a global symmetry might not extend over the full bulk is not at all surprising and it happens in other situations. For example if we add N_f massive fundamental fields, all with the same mass, to an $SU(N)$ gauge theory, then we have an $SU(N_f)$ flavor symmetry. In the gravity dual, this is realized as a brane that reaches up to a finite distance $r_{\rm min}$ in the bulk [74]. The larger the mass, the larger $r_{\rm min}$. For low energies, we explore the bulk only in the region where $r < r_{\rm min}$ and we do not encounter states charged under the global flavor symmetry.

Here something similar is happening, the bulk $SU(N)$ gauge symmetry, if present, is located only in the highly curved region, so it is not visible in the gravity region. And all bulk states that carry $SU(N)$ charge, have some excitations located in that highly curved region. We can say that the $SU(N)$ gauge symmetry we expected is "confined" in the bulk gravity region, but it is present in the highly curved region.

2.5.2 Are there gauge fields on brane probes?

Let us consider the ungauged model. Let us say that we have a probe D0 brane located in the region of the geometry described by Einstein gravity. Does this brane probe have a gauge field on its worldvolume? Naively, one would say no, since we are dealing with the ungauged model. On the other hand, we have argued that the bulk gravity region should be essentially the same for the gauged and ungauged models, so that we would expect a gauge field on the probe worldvolume.

We think that the right answer is the second, namely that there is a gauge field on the brane probes if the probes are in the Einstein gravity region, the region where $r < \lambda^{1/3}$. This seems to be the only reasonable answer since these are the only kinds of D0 branes that we have in the ten dimensional string theory. This gauge field imposes a constraint saying that the number of strings ending on the D0 brane should be equal to the number coming out. From the matrix model point of view, the degrees of freedom on the brane probe are effective low energy degrees of freedom that describe a complicated bound state where the matrices have large fluctuations. Recall the discussion in section 2.2.1. For this reason they reflect more the dynamics of these degrees of freedom than the properties of the precise UV definition of the model.

On the other hand, if we consider a D0 brane probe in the highly curved region, which is described in perturbation theory, then we do not expect to have a gauge field on the brane probe, since we do not have it in the ungauged model.

It would be interesting to understand what kind of transmutation the brane probe undergoes so that this happens as it crosses from the weakly curved bulk region to the strongly curved one.

2.5.3 The ungauged model and M-theory

In [22] the BFSS model was introduced as a tool to extract the S-matrix for 11 dimensional M-theory. In contrast to the discussion in most of this chapter, the BFSS proposal is to consider a very low energy limit of this matrix model. In this very low energy limit we go very deep inside the bulk, where the 11th dimension becomes large compared to other quantities and the physics is expected to reproduce the 11d one. It seems that the difference between the gauged and the

ungauged model is really lost when we go to such low energies, $E \propto 1/N$, so that we could have as well started from the ungauged model also.

2.5.4 Physical realizations

It seems that the remarks in this work suggest that if we wanted to build a quantum computer that simulates this problem we could start with a set of harmonic oscillators and Majorana fermions and then fine tune the interactions so that we get the ungauged model. This seems simpler than producing the gauged model where the $SU(N)$ gauge redundancy should emerge from some other further model. In other words, it seems simpler to try to arrange for a model having an approximate $SU(N)$ global symmetry than having to produce one with the $SU(N)$ gauge symmetry. Because the energy of the non-singlets is higher than that of singlets we would expect that small perturbations that break the $SU(N)$ global symmetry should not be important in the IR. Still, it is important not to generate terms that lead to relevant perturbations of the model. But the number of those to fine tune seems smaller than those of all possible couplings.

2.6 Conclusions

We have seen that the Einstein gravity region can be present in both the gauged and ungauged versions of the model. The extra degrees of freedom of the ungauged model reside in the highly curved region of the geometry. We can say that both the gauged and ungauged models flow to the same theory in the infrared. Or that the ungauged model flows to the gauged model in the IR. Of course, it is not surprising that they have something in common, since the singlet sector is common to both theories. What we wanted to highlight here was that the non-singlets do not modify the gravity solution in the region where the gravity approximation is valid.

A very similar story was found in the single matrix quantum mechanics in [58]. There the two models coincided as long as the temperature was low enough. In that case, at temperatures higher than a critical temperature the ungauged model would undergo a phase transition, somewhat reminiscent of the deconfinement transitions. See also [61] for a relation between that phase

and black holes. In our case, the black hole phase is present both for the gauged and ungauged models.

We should emphasize that many of our statements can be rephrased in terms of expectations values of Wilson loops in the gauged model. We mainly talked about the non-supersymmetric Wilson loop. For example, a Wilson loop in the adjoint representation computed by a string like the one displayed in Figure 2.1 (and extended along the time direction). This same loop has higher energy excitations where the string looks like the ones in Figure 2.2(b,c).

We have noted that the fact that the string has high tension implies that the eigenvalue distribution of the thermal holonomy, or Polyakov loop operator, has only a very small inhomogeneity when we have black hole present, see Figure 2.4. One might have expected that the black hole formation would result in a stronger eigenvalue localization for the Polyakov loop. This is the Polyakov loop of the full model, the UV theory, which is the only one we know how to define precisely in this theory.

In the Gurau-Witten tensor models, in a sense, the opposite from what we said here happens. In such models, in the leading large N approximation the basic field behaves as a conformal field with low scaling dimension. Therefore we *do not have* an energy gap to the non-singlets as we had in the D0 brane matrix model. In those cases the ungauged model seems a better starting point to describe the physics.

Chapter 3

SYK thermalization and universal constraints on energy flow

3.1 Introduction

Motivated by numerous recent experiments probing the out-of-equilibrium dynamics of reasonably well isolated quantum many-body systems, e.g. [75, 76, 77], and by long-standing theoretical questions concerning the nature of information processing in complex quantum systems, there has been a recent surge of interest in the physics of thermalization. In general, the phenomenon of thermalization is complex, involving many physical processes, including local relaxation of disturbances, diffusion of charge and energy, global spreading or scrambling of quantum information [78, 79, 80], and much more. This makes the subject complicated and rich.

Given this complexity, one natural starting point is to search for fundamental bounds on quantum dynamics. For example, in the context of strongly interacting many-body systems, physicists have speculated about a 'Planckian' limit to scattering that might shed light on various material properties, e.g. [81, 7, 82, 83, 84, 85, 86, 87].[1] In the context of quantum chaos, a similar kind of Planckian bound has been derived for the growth as chaos as diagnosed by so-called out-

[1] 'Planckian' because the scattering time estimate uses only Planck's constant and the thermal scale: $\frac{\hbar}{k_B T}$

of-time-order correlators [8]. One may wonder if such Planckian bounds can also be found for other aspects of thermalization.

In addition to general bounds, simple solvable models provide another powerful approach to understand quantum thermalization. Whereas bounds control the shape of the space of possibilities, solvable models give us archetypal behaviors or fixed points to which general models can be compared. In this context, considerable recent attention has been paid to the Sachdev-Ye-Kitaev (SYK) model [16, 88, 89, 17, 90, 36, 91, 92] and its variants [93, 94, 95, 96, 97, 98, 99, 100, 101] as tractable models of chaotic, thermalizing systems.

In this work, we study the equilibration of a system suddenly coupled to a large bath. The key object in our analysis is the energy curve: the time-dependence of the system energy after the system-bath coupling is suddenly turned on at zero time. At a schematic level, our results are as follows. First, we show that the energy curve has generic early time feature in which the system energy first increases with time even when the bath is cooler than the system. This initial increase is shown to obey a universal Planckian bound which constrains the shape of the early time energy bump. Second, we setup and analyze in detail a simple model of system-bath thermalization in which both system and bath are SYK models and the bath size is much greater than the system size. We are able to numerically compute the energy curve in this setup, including the early time energy rise and subsequent crossover to energy loss, the intermediate time draining of energy from the system, and the late time approach to equilibrium. In the low temperature limit, we also derive various analytical results, for example, the case of energy loss into a zero-temperature bath (Sec. 3.3.7).

Our results are related to the physics of black hole evaporation in AdS [102, 103, 104]. One precise connection can be made via the SYK model, which at low temperatures exhibits a dynamical sector that is identical to a form a quantum gravity in a two-dimensional nearly AdS spacetime. In this context, we show that our universal bound on the early time bump in the energy curve is equivalent to an instance of the averaged null energy condition. The latter is an important constraint on energy flow that is often assumed in general relativity. Moreover, our

coupled SYK system-bath setup reproduces and generalizes simple phenomenological models of black hole evaporation in which absorbing boundary conditions were used to extract the radiation.

The rest of the chapter is structured as follows. In the remainder of the Introduction we summarize our results in more detail. In Section 3.2 we setup and prove a rigorous bound on early time energy dynamics and demonstrate its relation to the averaged null energy condition in quantum gravity. In Section 3.3 we setup the coupled SYK cluster model. We analyse its equilibrium properties and use a Schwinger-Keldysh approach to analyse the system out-of-equilibrium. We report both numerical studies as well as comprehensive analytical results in various limits. In particular, Section 3.3.7 is dedicated to studying total evaporation into a zero-temperature bath. The description of the exact numerical setup and detailed calculations can be found in Appendices. Section 3.4 contains a brief discussion of our results and possible future directions.

3.1.1 Summary of results

This section describes the setting for our results and summarizes again the main points in more technical language. We consider the interaction of a system S with a bath B which is much larger than the system. This allows one to ignore the backreaction of the system on the bath. The system and bath have Hamiltonians H_S and H_B, respectively, and at time zero they are coupled via gH_{SB}. The goal is to understand how the system energy changes as a function of time due to this coupling.

Just before the coupling is turned on, the system and bath are in independent thermal states at inverse temperatures $\beta_S^{(0)}$ and $\beta_B^{(0)}$, respectively. The time evolution of the system-bath composite is

$$\rho_{SB}(t) = e^{-iHt}\left(\frac{e^{-\beta_S^{(0)}H_S}}{Z_S}\otimes\frac{e^{-\beta_B^{(0)}H_B}}{Z_B}\right)e^{iHt} \tag{3.1.1}$$

where

$$H = H_S + H_B + gH_{SB} \tag{3.1.2}$$

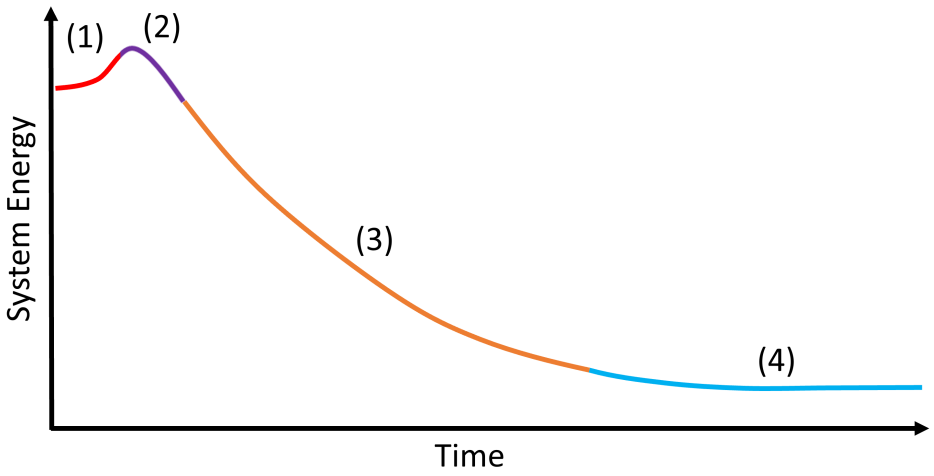

Figure 3.1: Typical behavior of system energy as a function of time for a large bath at lower temperature. We distinguish four dynamical regimes, labeled (1), (2), (3), and (4), which are discussed in detail in the text. Roughly they correspond to the early time energy rise, the subsequent turnover to energy loss, a sustained period of energy loss, and the final approach to global equilibrium.

and

$$H_{SB} = O_S O_B \tag{3.1.3}$$

is a product of two Hermitian operators. We also present some numerical calculations (Section 3.3.9) where the system and bath are initialized into pure states.

The primary observable of interest is the energy curve of the system,

$$E_S(t) = \mathrm{tr}[H_S \rho_{SB}(t)]. \tag{3.1.4}$$

A typical energy curve is sketched in Figure 3.1. Assuming the bath is cooler than the system, there are four key pieces of the energy curve: (1) the very early time energy increase, (2) the subsequent turnover to energy loss, (3) a sustained period of quasi-steady-state energy loss, and (4) a final approach to true system-bath equilibrium.

The first main result is a general bound on the energy curve whenever the system-bath interaction is a single product of operators. For simplicity, consider a limit where the system-bath coupling g is small, so that the system temperature is approximately constant on the time-scale

of the inherent system dynamics. Define the integrated energy flux by

$$F_\kappa = \int_0^\infty dt e^{-\kappa t} \dot{E}_S. \tag{3.1.5}$$

We show that this quantity is guaranteed to be positive for sufficiently large κ:

$$\kappa \geq 2/\beta_S \implies F_\kappa \geq 0. \tag{3.1.6}$$

This result is proven for any system and any bath to leading order in perturbation theory in g. In the context of SYK, we show that it holds more generally (Section 3.3.8). The constant κ sets the time-scale; reintroducing Planck's constant $\hbar$ and Boltzmann's constant k_B, the boundary value of κ is

$$\frac{2}{\beta_S} = \frac{2\hbar}{T_S k_B} = 2.6 \times 10^{-14}\ s \text{ at } T_S = 293\ K \tag{3.1.7}$$

The other main results are obtained in a particular model in which both system and bath are SYK clusters. We consider two SYK models, a system composed of N fermions with q_S-body interactions and a bath composed of M fermions with q_B-body interactions. The system and bath are coupled via a random term involving f_S system fermions and f_B bath fermions. We take $M \gg N$ so that the bath is unaffected by the coupling to the system. See Section 1.3 for more details and Ref. [105] for another study of two coupled SYK clusters.

We derive the full large N, large M Schwinger-Keldysh equations of motion for this system and numerically solve them following the technique in Refs. [37, 106]. This allows us to compute the entire energy curve for this system-bath model as a function of the initial system temperature, the initial bath temperature, and all the other parameters of the model.

Moreover, in the the low temperature limit we are able to solve the Kadanoff-Baym equation analytically to determine properties of the initial energy bump, the rate of energy loss, and the approach to final equilibrium.

Finally, using the gravitational description of the low energy dynamics of SYK, we argue that our general bound on energy flux is equivalent to one instance of a bulk energy bound called

the average null energy condition. Specifically, we show that the positivity of the energy flux for $\kappa \geq 2\pi/\beta_S$ implies the ANEC in the bulk integrated over the black hole horizon. Curiously, the condition $\kappa \geq 2\pi/\beta_S$ is actually weaker than the most general condition proven in perturbation theory, which is $F_\kappa \geq 0$ for all $\kappa \geq 2/\beta_S$.

3.2 Bounds on energy dynamics

In this section we discuss the general positivity bound on the integrated energy flux introduced above. This bound holds perturbatively in the system-bath coupling whenever the system-bath interaction is a simple product form, $H_{SB} = O_S O_B$. In subsequent subsections, we discuss the general situation with multiple operator couplings and the relation to energy conditions in holography.

3.2.1 Perturbative bound

Recall that the integrated energy flux is defined by

$$F_\kappa = \int_0^\infty dt e^{-\kappa t} \dot{E}_S. \tag{3.2.8}$$

In Appendix B.5 we prove that

$$F_\kappa \geq 0 \text{ for } \kappa \geq \frac{2}{\beta_S} \tag{3.2.9}$$

in the weak coupling limit, $g \to 0$, for any system and bath Hamiltonians.

The proof proceeds by explicitly computing the integrated flux F_κ in terms of spectral functions associated with the system operator O_S and the bath operator O_B. The positivity of the spectral functions can then be used to constrain the integrated flux. Making no other assumptions about the system and bath spectral functions, one can show that $F_\kappa \geq 0$ for all $\kappa \geq 2/\beta_S$. With further assumptions on the system or bath, it might be possible to strengthen this result.

The details are in Appendix B.5, but a few key formulas are reproduced here. To begin, we define the spectral function for an operator O via the response function,

$$X^R(t) = -i\theta(t)\langle[O(t), O(0)]\rangle_\beta. \tag{3.2.10}$$

The Fourier transform is denoted $X^R(\omega)$, and the spectral function $A(\nu)$ is then

$$X^R(\omega) = \int \frac{d\nu}{2\pi} \frac{A(\nu)}{\omega + i0^+ - \nu}. \tag{3.2.11}$$

We may further decompose the spectral function $A(\nu)$ into two positive definite pieces,

$$A(\nu) = A_+(\nu) - A_-(\nu), \tag{3.2.12}$$

defined by

$$A_\pm(\nu) = 2\pi \sum_{n,m} p_n |\langle n|O|m\rangle|^2 \delta(\nu \mp [E_m - E_n]) \tag{3.2.13}$$

where $p_n = e^{-\beta E_n}/Z$ is the thermal probability.

The integrated flux in terms of the spectral functions A_{S+} and A_{B+} is

$$F_\kappa = 2g^2 \int \frac{d\omega}{2\pi} \frac{d\omega'}{2\pi} \frac{\omega A_{S+}(\omega) A_{B+}(\omega')}{(\omega + \omega')^2 + \kappa^2}. \tag{3.2.14}$$

The short-time limit, corresponding the initial rise of energy [part (1) of Figure 3.1], can be accessed by taking $\kappa \to \infty$ to give

$$F_{\kappa\to\infty} \to 2\frac{g^2}{\kappa^2} \int \frac{d\omega}{2\pi} \frac{d\omega'}{2\pi} \omega A_{S+}(\omega) A_{B+}(\omega'). \tag{3.2.15}$$

Using

$$\int d\omega\omega A_+(\omega) = \frac{1}{2}\int d\omega\omega A(\omega) = \int_{\omega\geq 0} d\omega\omega A(\omega) \geq 0, \tag{3.2.16}$$

it follows that

$$F_{\kappa\to\infty} \geq 0 \tag{3.2.17}$$

in agreement with results in [104].

The long-time limit, corresponding to the steady loss of energy [part (3) of Figure 3.1], can be accessed by taking $\kappa \to 0$ to give

$$F_{\kappa\to 0} \to -\frac{g^2}{\kappa}\int_{\omega\geq 0}\frac{d\omega}{2\pi}\omega\frac{\sinh\frac{(\beta_B-\beta_S)\omega}{2}A_S(\omega)A_B(\omega)}{2\sinh\frac{\beta_S\omega}{2}\sinh\frac{\beta_B\omega}{2}}. \tag{3.2.18}$$

This expression shows that energy always flows from hot to cold on these timescales. Note that we are not accessing the final approach to equilibrium since the coupling g is being treated perturbatively and we are not yet studying the time-dependence of the system temperature.

3.2.2 Multi-operator couplings

It is natural to ask if the bound if the bound can be extended to include more general system-bath couplings. Consider a coupling of the form

$$H_{SB} = \sum_\alpha O_S^\alpha O_B^\alpha. \tag{3.2.19}$$

In this case, a more general expression for the integrated flux can be derived which involves mixed correlators of O^α with O^β. We have not recorded this expression here because, as we show by example shortly, the integrated flux in this case does not obey a general positivity condition.[2]

If the correlations between O^α and O^β are diagonal, then the positivity result continues to hold. This is because the diagonal terms reduce to the single product of operators case considered above. Although this is a special case, it is not an uncommon situation; for example, in the SYK model, different fermions are approximately decorrelated to leading order in N.

However, for a generic multi-operator coupling the energy may go down initially. For example, consider a single-qubit system s interacting with a bath qubit b. The unperturbed Hamiltonian reads as:

$$H_S + H_B = \omega_0 s^\dagger s + \Omega b^\dagger b \tag{3.2.20}$$

[2]We thank Daniel Ranard for discussions on multi-operator couplings.

where s and b are lowering operators in a two-level system. We switch on the following quadratic interaction at time $t = 0$:

$$H_{SB} = V(s^\dagger b + b^\dagger s) \tag{3.2.21}$$

It is easy to solve this quadratic theory exactly. If the initial density matrices are diagonal,

$$\rho_{S(B)}(t = 0) = \text{diag}(1 - n_{S(B)}, n_{S(B)}), \tag{3.2.22}$$

then the expression for the system's energy at early times is given by:

$$E_S(t) = \omega_0 \langle s^\dagger s \rangle(t) = \omega_0 n_S + \omega_0 V^2 t^2 (n_B - n_S) + \dots . \tag{3.2.23}$$

From this expression it is obvious that the system energy may go down initially.

3.2.3 Relation to energy conditions in holography

The motivation for the bound discussed above originates from considering evaporating black holes in AdS [104]. Take the two sided eternal AdS black hole or the wormhole connecting two asymptotically AdS regions. In the context of AdS/CFT, this geometry can be understood as the holographic dual of a pair of decoupled but entangled CFTs prepared in the thermofield double state. We will label these two boundary CFTs as L (left) and R (right), see figure 3.2.

The decoupling of the two CFTs should be manifested in the bulk dual as the absence of causal signaling between the two boundaries through the AdS wormhole spacetime. This translates to the wormhole being non-traversable. Traversability is precluded by the so-called average null energy condition [107, 108, 109, 110] on the matter stress energy tensor T_{ab} along the horizon of the black hole

$$\text{ANEC}: \quad \int T_{ab} k^a k^b d\lambda \geq 0 \tag{3.2.24}$$

where k^a is the null tangent vector along the horizon of the black hole and λ is an affine parameter along the null ray. The eternal black hole with matter in the Hartle-Hawking vacuum has

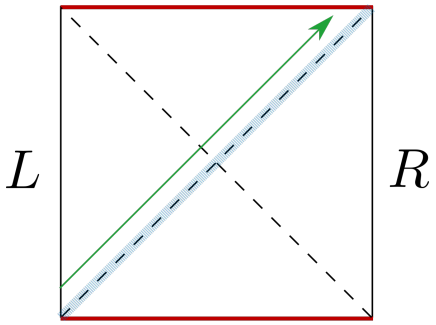

Figure 3.2: Geometry of the AdS wormhole dual to two entangled CFTs living on the boundaries. The ANEC along the horizon (shaded blue) guarantees that a signal sent from the left boundary (green arrow) does not traverse the wormhole and crashes into the singularity.

vanishing stress tensor along its horizons making it only marginally non-traversable. In fact, there is a simple protocol that makes the wormhole traversable by coupling the two boundaries [111].

We will now consider a setting in which this ANEC places a bound on the energy flux of the boundary system. We will consider the eternal black hole in a 1+1 dimensional setting and allow it to evaporate by imposing absorbing boundary conditions at the boundary. This is a model for starting with two entangled holographic quantum systems dual to the eternal black hole and where one of systems, say the right system, is coupled to an external bath allowing energy to flow between the two.

Consider the Jackiw-Teitelboim (JT) model [112, 113, 114] coupled to matter given by the action

$$I = I_{JT}[\phi, g] + I_{\text{matter}} \tag{3.2.25}$$

$$I_{JT}[\phi, g] = \frac{1}{16\pi G_N}\int d^2x\ \phi\,(R+2) + \frac{\phi_b}{8\pi G_N}\int_\partial K \tag{3.2.26}$$

where ϕ is the dilaton and g is the two dimensional metric.[3] This model has been studied recently in [115, 116, 103]. Along with this action this theory comes with a pair of boundary conditions

[3]Note we are disregarding a topological term $\phi_0 \int d^2x R$ in the action which is not important for questions we are interested in regarding dynamics.

on the metric and dilaton

$$g_{uu} \sim \frac{1}{\epsilon^2}, \quad \phi = \phi_b \sim \frac{\phi_r}{\epsilon} \tag{3.2.27}$$

where u is the time along the boundary and ϵ is the radial coordinate distance away from the boundary. u is sometimes called the physical boundary time. Integrating over the dilaton along an imaginary contour fixes the metric to be that of AdS_2, in which it is convenient to work in Poincare coordinates

$$ds^2 = \frac{-dt^2 + dz^2}{z^2} = \frac{-4dx^+dx^-}{(x^+ - x^-)^2}, \quad x^\pm = t \pm z. \tag{3.2.28}$$

The gravitational constraints of this theory imply that the only dynamical gravitational degree of freedom lives on the boundary of the spacetime, and is given by the reparameterization between the Poincare time t and physical boundary time u, $t(u)$.

The ADM energy of the spacetime, or the energy as measured on the boundary, is given by

$$E = \frac{\phi_r}{G_N}\{t(u), u\} \tag{3.2.29}$$

The equation of motion of this theory comes from balancing the fluxes of energy of the gravitational sector and the matter.

$$\dot{E} = \dot{t}^2(u) \left[T_{x^-x^-} - T_{x^+x^+}\right] \Big|_{\text{boundary}} \tag{3.2.30}$$

where on the right hand of the equation we have the expectation value of the stress tensors evaluated on the boundary of the spacetime.

The eternal black hole is a vacuum solution of this model with

$$T_{x^+x^+} = T_{x^-x^-} = 0 \tag{3.2.31}$$

This fixes the reparameterization, up to an SL2(R) transformation, to be

$$t(u) = \frac{\beta}{\pi} \tanh\left[\frac{\pi}{\beta} u\right] \tag{3.2.32}$$

Now lets imagine coupling the right boundary to a large external system in the vacuum to allow the black hole to evaporate. This will only modify the left moving stress $T_{x^-x^-}$. The equation of motion will therefore be

$$\dot{E} = \dot{t}^2(u) T_{x^-x^-}\big|_{\text{boundary}} \tag{3.2.33}$$

We want to use this expression to find the stress tensor on the horizon. In general, the relation between the stress tensor near the boundary and the one at the horizon is very complicated in the presence of massive matter or graybody factors. We specialize to the case with matter where these complications are absent, for example by considering conformal matter in the bulk on the background metric g, with no coupling to the dilaton. Due to holomorphic factorization, we can write

$$T_{x^-x^-}(x^-) = T_{x^-x^-}(x^-)\big|_{\text{boundary}} = \dot{t}^{-2}(u)\dot{E}(u) \tag{3.2.34}$$

where we used that $x^- = t$ at the boundary. The first equality follows because there is no dependence on x^+ and the stress energy flows on null lines.

We need to plug this into the average null energy along the future horizon on the right exterior. It is important here that we are working to leading order in the gravitational coupling $\kappa_g \equiv \beta G_N/\phi_r$, so that the reparameterization $t(u)$ is still given by the unperturbed form (3.2.32). Therefore, the horizon along which we want to evaluate the ANEC is still at $x^+ = \beta/\pi$. Using the affine parameterization along the horizon given by

$$x^-(\lambda) = \frac{\beta}{\pi} - \frac{1}{\lambda},\ x^+ = \frac{\beta}{\pi} \tag{3.2.35}$$

$$k^- = \frac{dx^-}{d\lambda},\ k^+ = 0 \tag{3.2.36}$$

we have

$$\int T_{ab}k^a k^b d\lambda = \int T_{x^-x^-}\left(\frac{dx^-}{d\lambda}\right)^2 d\lambda \tag{3.2.37}$$

$$= \int_0^\infty \dot{E}\, e^{-\frac{2\pi u}{\beta}} du \tag{3.2.38}$$

Therefore in this case, the ANEC can be recast as a bound on the integrated energy flux,

$$\text{ANEC} \implies \int_0^\infty \dot{E}\, e^{-\frac{2\pi u}{\beta}} du \geq 0. \tag{3.2.39}$$

We see that the ANEC translates to a weighted integral of the energy flux at the boundary. This weighting factor is what allows the initial positive energy excitation to overwhelm the subsequent negative energy flux from the black hole losing energy to the external bath. It is interesting that this condition is implied by the general perturbative bound Eq. (3.1.5).

3.3 Thermalization in SYK

3.3.1 Coupling to a bath

Suppose that one system fermion ψ couples to an external bath operator $\mathcal{O}_B$,

$$S_{\text{int}} = iV \int_{\mathcal{C}} du \psi \mathcal{O}_B. \tag{3.3.40}$$

If the interaction is weak enough, we can use the 1-loop approximation to the interaction term:

$$S_{\text{int}} \to \frac{V^2}{2} \int_{\mathcal{C}} du_1 du_2 \; X_B(u_1, u_2), G_S(u_1, u_2) \tag{3.3.41}$$

where the function X_B is simply the two-point function of the bath operator $X_B(t_1, t_2) = \langle \mathcal{O}_B(t_1)\mathcal{O}_B(t_2)\rangle_B$. Moreover, if the bath is large, we can neglect the back reaction on the bath and take X_B to be fixed. This logic can be made precise if we couple a large-N SYK to another

large-M SYK with $M \gg N$. Consider a general interaction of the form[4]

$$V_{i_1,\ldots,i_{f_S}}^{j_1,\ldots,j_{f_B}} \psi_{i_1} \ldots \psi_{i_{f_S}} \chi_{i_1} \cdots \chi_{i_{f_B}}, \tag{3.3.42}$$

where $\chi_j,\ j = 1, \ldots, M$ are the M Majorana fermions of the bath and $V_{i_1,\ldots,i_{f_S}}^{j_1,\ldots,j_{f_B}}$ is a random Gaussian variable with variance

$$\langle \left(V_{i_1,\ldots,i_{f_S}}^{j_1,\ldots,j_{f_B}} \right)^2 \rangle = \frac{V^2 (f_S - 1)! f_B!}{N^{f_S - 1} M^{f_B}} \quad \text{(no sum)}. \tag{3.3.43}$$

Note that this expression allows for a quite general coupling between f_S system fermions and f_B bath fermions. Based on it, we can derive an effective action similar to (1.3.15). The Euclidean action has the form:

$$\begin{aligned} S = & \sum_{i=1}^{N} \psi_i \partial_\tau \psi_i - i^{q_S/2} \sum_{\{i\}} J_S^{\{i\}} \psi_{i_1} \ldots \psi_{i_{q_S}} \\ & + \sum_{j=1}^{M} \chi_j \partial_\tau \chi_j - i^{q_B/2} \sum_{\{j\}} J_B^{\{j\}} \chi_{j_1} \cdots \chi_{j_{q_B}} \\ & - i^{\gamma} \sum_{\{i\},\{j\}} V_{\{i\}}^{\{j\}} \psi_{i_1} \ldots \psi_{i_{f_S}} \chi_{i_1} \cdots \chi_{i_{f_S}}, \end{aligned} \tag{3.3.44}$$

where

$$\gamma = f_S f_B + f_S (f_S - 1)/2 + f_B (f_B - 1)/2. \tag{3.3.45}$$

The powers of i are needed to make the action real.

[4] A similar interaction was independently studied in [105, 117]

It is convenient to introduce the Green's functions by adding Lagrange multipliers Σ_S, Σ_B (which we integrate over the imaginary axis):

$$\begin{aligned}\Delta S = &\frac{1}{2}\Sigma_S \left(\sum_i \psi_i(\tau_1)\psi_i(\tau_2) - NG_S(\tau_1,\tau_2)\right) \\ &+ \frac{1}{2}\Sigma_B \left(\sum_j \chi_i(\tau_1)\chi_i(\tau_2) - MG_B(\tau_1,\tau_2)\right)\end{aligned} \tag{3.3.46}$$

If we assume no replica symmetry breaking, we can treat J_S, J_B, V as conventional integration variables in the path integral. After integrating them out, we can replace fermionic bilinears with $G_{S/B}$. Then the action becomes quadratic in ψ and χ and they can be integrated out as well. The result is the following effective action:

$$\begin{aligned}S = &N \log \mathrm{Pf}\left(\partial_\tau - \Sigma_S\right) + M \log \mathrm{Pf}\left(\partial_\tau - \Sigma_B\right) \\ &+ \frac{1}{2}\int d\tau_1 d\tau_2 \ \left(-N\Sigma_S G_S - M\Sigma_B G_B + \frac{N}{q_S}G_S^{q_S} + \frac{M}{q_B}G_B^{q_B}\right) \\ &+ \frac{V^2 N}{2f_S}\int d\tau_1 d\tau_2 \ G_S^{f_S} G_B^{f_B}.\end{aligned} \tag{3.3.47}$$

Hence, the equations of motion for the bath variables G_B, Σ_B will be corrected by a term of order N/M which is suppressed for $M \gg N$. However, there is a non-vanishing correction the the system's self-energy:

$$\begin{aligned}\Sigma_S &= J_S^2 G_S^{q_S - 1} + \Delta\Sigma_S \\ \Delta\Sigma_S &= V^2 G_S^{f_S - 1} G_B^{f_B}.\end{aligned} \tag{3.3.48}$$

The same computation can be performed in Lorentzian time with the following result for $\Delta\Sigma_S^>$:

$$\Delta\Sigma_S^>(t_1,t_2) = -i^{f_S+f_B}\left(G_S^>(t_1,t_2)\right)^{f_S-1}\left(G_B^>(t_1,t_2)\right)^{f_B}. \tag{3.3.49}$$

Computations in SYK simplify a lot when we take the large q limit. Now we have additional parameters $f_{S/B}$ which we can take to infinity along with $q_{S/B}$. For example, consider large q_B.

Then the Euclidean Green's function has the following expansion:

$$G_B(\tau) = \frac{1}{2}\,\mathrm{sgn}(\tau)\left(1 + \frac{g_B}{q_B}\right) \tag{3.3.50}$$

By taking $q_B \to +\infty, f_B \to +\infty$ we get the following term in the interaction:

$$G_B^{f_B} = \text{const}\ \exp\left(\frac{f_B}{q} g_B\right), \tag{3.3.51}$$

where f_B/q can be any rational number. Recall that at zero temperature and large q_B one has [36]:

$$e^{g_B} = \frac{1}{(J_B|\tau| + 1)^2}. \tag{3.3.52}$$

This provides an example when we know the bath Green's function explicitly for all times.

3.3.2 Equilibrium

Let us first study the equilibrium Dyson–Schwinger equation in presence of a bath. It happens that they can be solved in the IR regime. With the above setup, the Euclidean self-energy reads:

$$\Sigma_S = J_S^2 G_S^{q_S - 1} + V^2 G_S^{f_S - 1} G_B^{f_B}. \tag{3.3.53}$$

In equilibrium, the system and bath will have the same temperature. Thus, we make an ansatz for G_S which is an SYK Green function with certain effective parameters $\tilde{q_S}, \tilde{J_S}$.

Suppose first that we try to retain the same q_S, so $\tilde{q_S} = q_S$. Remember that the SYK Green functions decay for large Lorentzian times as $G_S \sim 1/\sinh(\pi t/\beta)^{2/q_S}$. Thus, there are three possible situations:

- The system term ($G_S^{q_S - 1}$) dominates in the IR. Then the interaction with the bath is irrelevant and in the IR we recover the decoupled system physics.

- The bath term ($G_S^{f_S-1}G_B^{f_B}$) dominates. This means G_S with $\tilde{q_S} = q_S, \tilde{J_S} = J_S$ is not a solution. The interaction is relevant and the system now has an effective $\tilde{q_S} < q_S$. The solution can be found by assuming that for a given $\tilde{q_S}$ the second term is dominant.

- Both terms are of the same order, so the interaction is marginal. This means that $\tilde{q_S} = q_S$, but J can be renormalized.

Let us study the particular example of a marginal deformation of $q_S = 4$, where the bath is also a $q_B = 4$ SYK. Take $f_S + f_B = 4$. In Euclidean time the full DS equation reads:

$$\Sigma = J_S^2 G_S^3 + V^2 G_S^{f_S-1} G_b^{4-f_S}, \tag{3.3.54}$$

and in the low energy limit,

$$\Sigma * G_S = \delta(t_1 - t_2). \tag{3.3.55}$$

Recall also that G_B satisfies the following equation in the IR:

$$J_B^2 G_B^3 * G_B = \delta(t_1 - t_2) \tag{3.3.56}$$

The ansatz is then $G_S = \frac{\sqrt{J_B}}{\sqrt{\tilde{J}_S}} G_B$. Remembering that in the IR the only dependence on the coupling is $G_B \sim 1/\sqrt{J_B}$, this ansatz can be understood as a renormalization of the quartic SYK coupling.

From this ansatz it follows that $\tilde{J}$ is determined by,

$$\frac{J_S^2}{\tilde{J_S}^2} + V^2 \frac{J_B^{f_S/2-2}}{\tilde{J_S}^{f_S/2}} = 1. \tag{3.3.57}$$

This corresponds to an increase in the effective coupling $\tilde{J_S}$ relative to J_S. We have also confirmed this equation in our numerical results.

3.3.3 Energy flux

We now derive an equation for the rate of change of the system energy within the non-equilibrium formalism. Suppose we have a generic quantum system with a Hamiltonian H_S, which we couple to a bath with Hamiltonian H_B and the interaction term is $V\mathcal{O}_B\mathcal{O}_S$, which we turn on at time $t = 0$. The total Hamiltonian is

$$H = H_S + H_B + V\theta(t)\mathcal{O}_S\mathcal{O}_B \tag{3.3.58}$$

The time derivative of the system's energy is not zero for $t > 0$:

$$E'_S = \frac{d}{dt}H_S = -i[H, H_S] = V\partial_t\mathcal{O}_S\mathcal{O}_B, \tag{3.3.59}$$

where the $\partial_t\mathcal{O}_S$ indicates the time derivative of this operator with respect to unperturbed equations of motion for the system. If the bath is large, we completely ignore the back-reaction on the bath. Moreover, if V is small, we can find the right hand side in perturbation theory in V:

$$E'_S = -i(-1)^F \int_{\mathcal{C}} dt' \partial_t \langle V^2 \mathcal{O}_S(t)\mathcal{O}_S(t')\rangle_S \langle \mathcal{O}_B(t)\mathcal{O}_B(t')\rangle_B, \tag{3.3.60}$$

where the integral over t' goes along the Keldysh contour from 0 to t and the correlators are taken in the unperturbed systems. F is the fermion number of the operator $\mathcal{O}_S$. For the SYK model with a random interaction (3.3.42) this equation leads to

$$E'_S = iV^2 \int_{-t}^{t} du G_B^{>}(u - i\epsilon)^{f_B} \partial_u G_S^{>}(u - i\epsilon)^{f_S}. \tag{3.3.61}$$

In this specific case, this equation can also be derived directly from the Kadanoff–Baym equations (Appendix B.2) or from Schwarzian (Section 3.3.6).

3.3.4 Very early time

At very early times, $t \ll 1/J_S, 1/J_B$, we can assume that G_B and $\partial_u G_S$ are just constants. Then we can use the relation (1.3.22) for G_B and Eq. (1.3.31) to connect the derivative with system's energy. Collecting the factors of i, we obtain:

$$E_S' = -tV^2 E_S(0) \frac{1}{2^{f_S+f_B-2}}. \tag{3.3.62}$$

Since for SYK $E < 0$ in thermal equilibrium, we see that the energy initially increases. This is an illustration of the general statement we discussed in Section 3.2. In the case of SYK, the initial energy growth rate is proportional to the initial energy. This result is very general for SYK and an arbitrary bath of Majorana fermions. This is valid for SYK at any coupling $J_S\beta$.

3.3.5 Early time

At early times, the state of the system has not changed much, so we can use the initial G_S in Eq. (3.3.61). Put another way, Eq. (3.3.61) is already the leading term in V^2, so V-corrections to G_S are smaller. We can trust this approximation as long as change in β is of order V. Below we will argue that we can use the conformal approximation for G_S, so we must restrict ourselves to times $t \gtrsim 1/J_S$.

Also, from now on we assume that the system is $q_S = 4$ SYK and there is only one system fermion in the interaction, $f_S = 1$. By going to the conformal limit, we will arrange the situation so that an analytical calculation of various parts of the energy curve is possible. This is also the limit of interest for the black hole evaporation problem. Since the bath temperature is set to zero, we now denote β_S by just β.

For finite q SYK we know the Green's function analytically only in the conformal regime, when $u \gg 1/J_B$. If we try to use the conformal answer for G_B we will encounter a divergence at $u = 0$ for $f_B \geq 2$, since at short times $G_B \sim 1/\sqrt{u}$. The physically interesting cases of marginal and irrelevant deformations correspond to $f_B \geq 3$ so we need to find another approximation to G_B. One way around this is to couple the system to large-q SYK. For simplicity we will study

the case of zero temperature bath. As we have shown in Section 3.3.1, we can adjust the number of bath fermions in the interaction such that

$$G_B^{f_B} = \left(\frac{i}{2} \frac{1}{(iJ_B u + 1)^{1/2}} \right)^p \tag{3.3.63}$$

for any rational number p. Then $p = 3$ corresponds to a marginal deformation, whereas $p > 3$ produces an irrelevant interaction.

With this setup, the relevant integrals converge. However, the question of whether we can use the conformal approximation for G_S is still open. One obvious constraint is that the system is at strong coupling, so we require

$$J_S \beta \gg 1 \tag{3.3.64}$$

From the integral in Eq. (3.3.61) it follows that the bath probes the system Green's function at times of order $1/J_B$. In order to use the conformal approximation for G_S, this time should be large compared to $1/J_S$. So we should restrict ourselves to

$$J_S \gg J_B. \tag{3.3.65}$$

In the conformal approximation,

$$G_S = b \left(i \frac{\pi}{\beta J_S \sinh(\pi u/\beta)} \right)^{1/2}, \tag{3.3.66}$$

so $\partial_u G_S$ contains a $1/u^{3/2}$ term at small u which generates divergences in integrals. However, we can integrate by parts to give,

$$E_S' = -iV^2 \left(G_B^{f_B}(t) G_S(t) - G_B(-t)^{f_B} G_S(-t) - \int_{-t}^{t} du \; \partial_u G_B(u)^{f_B} G_S(u - i\epsilon) \right). \tag{3.3.67}$$

Using the fact that for Majorana fermions the Green's function obeys

$$G_{S,B}(-t) = -G_{S,B}^*(t), \tag{3.3.68}$$

we can rewrite the flux as

$$E_S' = 2V^2 \ \mathrm{Im}\left(G_B^{f_B}(t)G_S(t) - \int_0^t du\ \partial_u G_B(u)^{f_B} G_S(u - i\epsilon)\right). \tag{3.3.69}$$

A comparison between this result and the exact numerical integration for the marginal case $p = 3$ is presented in Figure 3.3. Notice that the two curves do not quite match at very early times. Because of the form of the conformal propagator, the flux behaves as $1/\sqrt{t}$, which is not physical. Had we taken the exact system two-point function we would have reproduced the numerical answer perfectly even at very early times. Slight deviations occur later because the system's temperature is finally changing. These discrepancies decreases with decreasing the system-bath coupling.

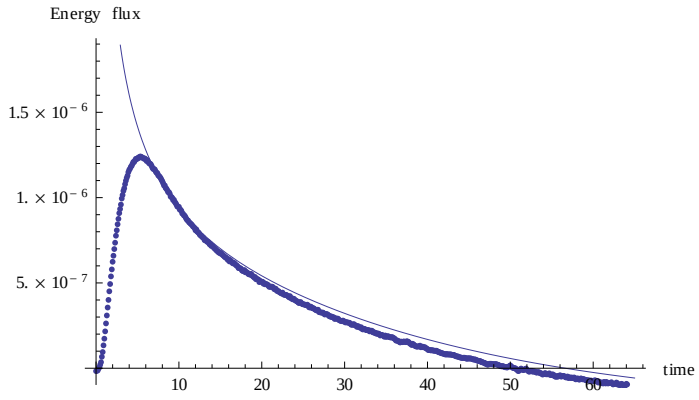

Figure 3.3: Early time energy flux as function of time. The solid curve is the analytic result (3.3.67), and the dots show the direct numerical integration. The parameters used are $V^2 = 2.5 \times 10^{-5}, J_S = 0.5, J_B = 0.005, \beta_{\text{init}} = 50, dt = 0.1$. The conformal approximation is responsible for the disagreement at early time while the slight change in temperature is responsible for the disagreement at late time.

We have studied the analytic expression for the marginal case $p = 3$ in two limits, $J_B\beta \ll 1$ and $J_B\beta \gg 1$, in Appendix B.3. The parameter βJ_B tells us how "fast" the bath degrees of freedom are compared to the thermal scale of the system. For a "slow bath" with $J_B\beta \ll 1$, the peak occurs at times logarithmically bigger than β:

$$t_{\text{peak}} \sim \beta \log\left(\frac{1}{J_B\beta}\right), J_B\beta \ll 1. \tag{3.3.70}$$

In the opposite limit of a "fast bath" with $J_B\beta \ll 1$, we find that the peak time is much less than β:

$$t_{\text{peak}} \sim \frac{\beta}{(\beta J_B)^{1/3}}, J_B\beta \gg 1. \tag{3.3.71}$$

3.3.6 Intermediate time

At finite temperature the Green's functions in Eq. (3.3.61) decay exponentially with time. Assuming that the bath is at a lower temperature than the system, the integral saturates at times $t \gtrsim \beta$. After this the energy flow comes to a steady state, meaning that it is not sensitive to when exactly the interaction was switched on.

We can patch this regime with the previous discussion if the coupling is small enough. Namely the change in temperature over thermal time scale is much less than temperature:

$$\beta\partial_u\beta \ll \beta \to \partial_u\beta \ll 1. \tag{3.3.72}$$

But this requirement is equivalent to saying that at each point in time the system is in quasi-equilibrium and has a definite temperature.

We expect that in this regime the system's dynamics can be described by the Schwarzian. In this approximation, the system's Lagrangian is equal to the Schwarzian derivative:

$$S_{\text{kin}} = -\frac{\alpha_S}{\mathcal{J}_S}\int_{\mathcal{C}} du\ \text{Sch}(t,u) = \frac{\alpha_S\sqrt{2}}{2J_S}\int_{\mathcal{C}} du\ \left(\frac{t'''}{t'} - \frac{3}{2}\left(\frac{t''}{t'}\right)^2\right). \tag{3.3.73}$$

Since for $q = 4$, $\mathcal{J}_S = J_S/\sqrt{2}$ and the coefficient in front of the Schwarzian is $\alpha_S = 0.007$. The system's energy is given by,

$$E = E_0 + \frac{\alpha_S\sqrt{2}}{J_S}\,\text{Sch}(t[u],u) = E_0 + \frac{2\pi^2\sqrt{2}\alpha_S}{J_S\beta^2}, \tag{3.3.74}$$

where E_0 is the ground state energy.

The interaction with the bath comes from reparametrizations of G_S in the action term (3.3.41):

$$S_{\rm pot} = i\frac{V^2}{2}\int_{\mathcal{C}} du_1 du_2 X_B(u_1,u_2) G_S(u_1,u_2) = \tag{3.3.75}$$
$$= i\sqrt{ib}\frac{V^2}{2J_S^{1/2}}\int_{\mathcal{C}} du_1 du_2 \left(\frac{t'[u_1]t'[u_2]}{(t[u_1]-t[u_2])^2}\right)^{1/4} X_B(u_1-u_2).$$

With this normalization of V^2, one has the following extra term in the Dyson–Schwinger equation (compare with Eq. (3.3.49)):

$$\Delta\Sigma_S^{>} = -V^2 X_B^{>}. \tag{3.3.76}$$

Note that the above action is written on the Keldysh contour, so we have two functions $t_+[u], t_-[u]$. The semiclassical equations of motion are obtained by varying with respect to $t_q = t_+ - t_-$ and putting $t_+ = t_-$ [118]. This way the equations of motion are causal.

During the approach to equilibrium we expect that the solution has the form

$$t[u] = \tanh\left(\frac{\pi u}{\beta[u]}\right), \tag{3.3.77}$$

where $\beta[u]$ is a slowly varying function of u. As discussed, the difference between the times u_1, u_2 in $G_S(u_1,u_2)$ should be less than the characteristic scale at which β changes: $\beta/\beta' \gg |u_1-u_2|$.

We go through the derivation of the equations of motion in Appendix B.4. The result is:

$$\frac{4\pi^2\sqrt{2}\alpha_S}{J_S\beta^3}\beta' = \frac{i\sqrt{ib}V^2\pi^{3/2}}{2(J_S\beta)^{1/2}}\int_{-\infty}^{+\infty} du\; X_B(\beta(u-i\epsilon))\frac{\cosh\pi(u-i\epsilon)}{\sinh^{3/2}\pi(u-i\epsilon)}. \tag{3.3.78}$$

This result coincides with the general answer (3.3.61) when the system Green's function is approximated by the conformal expression and the energy of the system is given by Schwarzian result (3.3.74).

There is one subtlety here.[5] In the Schwarzian approximation the energy above the vacuum is proportional to $-\,\mathrm{Sch}(t[u],u)$. For a thermal state this is equal to $2\pi^2/\beta^2$. Correspondingly

[5]We are grateful to Juan Maldacena for a discussion on this point.

we expect that the energy flux is proportional to $-4\pi^2\beta'/\beta^3$. This is how (3.3.78) was obtained (see Eq. (B.4.18) in Appendix B.4). However, if we formally evaluate the Schwarzian on the configuration (3.3.77) we will get an extra term,

$$-\operatorname{Sch}(t[u],u) = \frac{2\pi^2}{\beta^2} - \frac{4\pi^2 u\beta'}{\beta^3}. \tag{3.3.79}$$

And after differentiating with respect to time u, we get an expression $-8\pi^2\beta'/\beta^3$, which is twice as big as it should be.

The resolution of this problem is that the expression (3.3.77) is not an actual solution if $\beta[u]$ is not constant. The argument of tanh should include an additional term proportional to β' in order to cancel the extra derivative term in Eq. (3.3.79). The true solution is easily found,

$$t[u] = \tanh\left(\frac{\pi u}{\beta[u]} + \frac{\pi u^2\beta[u]'}{2\beta[u]^2}\right). \tag{3.3.80}$$

Now we specialize again to the case of a $q_B = 4$ bath and study both marginal and irrelevant interactions. We also assume that the bath is at strong coupling. And by this we mean that it is strongly coupled by itself,

$$J_B\beta_{\text{bath}} \gg 1, \tag{3.3.81}$$

and it is strongly coupled on the thermal time scale of the system,

$$J_B\beta \gg 1. \tag{3.3.82}$$

Otherwise, the ϵ-prescriptions in integrals should be replaced by the actual UV cut-off $\sim 1/(\beta J_{S/B})$.

In the subsequent sections we are going to compare Schwarzian results with numerical computations. Our timestep will be $dt = 0.1$ and $J_S = 0.5$, so all the numerical answers should come with $\sim Jdt = 0.05 = 5\%$ uncertainty. Later when we check the bound we will estimate the uncertainties more carefully.

Marginal deformation: bath at zero temperature

For a marginal deformation with $f_B = 3$ and when the bath is at zero temperature, the function X_B is given by

$$X_B = G_B^3 = i^{3/2} \left(\frac{b}{\sqrt{J_B t}} \right)^3, \tag{3.3.83}$$

and the integral over x evaluates to,

$$\int_{-\infty}^{+\infty} dx \; \frac{1}{(x - i\epsilon)^{3/2}} \frac{\cosh \pi (x - i\epsilon)}{\sinh^{3/2} \pi (x - i\epsilon)} = i \frac{\pi^{3/2}}{4}. \tag{3.3.84}$$

The time-dependence of the temperature is therefore

$$\beta' = \beta \frac{\pi V^2 b^4 \sqrt{J_S}}{32\sqrt{2} \alpha_S J_B^{3/2}}, \quad \text{marginal.} \tag{3.3.85}$$

For $J_S = J_B$ we have verified this numerically as shown in Figure 3.4. The above equation yields $\beta' = 0.0028\beta$ for $V^2 = 0.002, J = 0.5$, whereas the best fit from numerics is $\beta' = 0.0029\beta$.

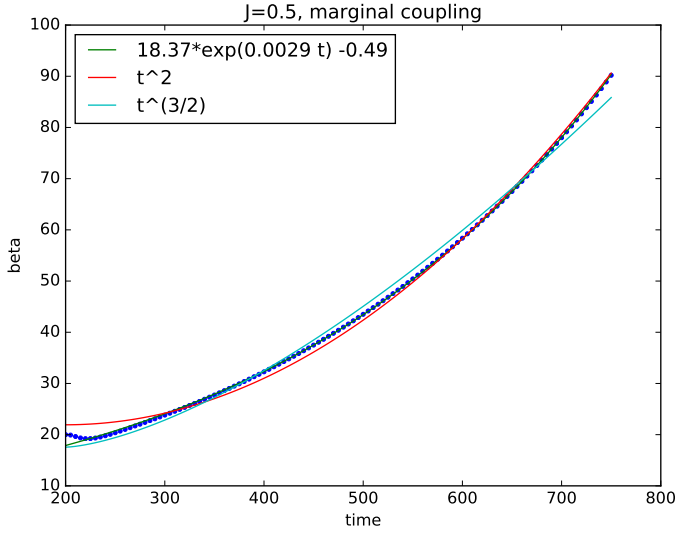

Figure 3.4: β as a function of time for a marginal coupling. Blue circles are data points, and the green curve is an exponential fit. The fit almost coincides with data points. Fits for other powers are shown for comparison.

Marginal deformation: bath at finite temperature

In this case, we take the conformal SYK answer for the bath Green's function:

$$X_B = G_B^3 = i^{3/2} \left(\frac{b\sqrt{\pi}}{\sqrt{\beta_B J_B \sinh\left(\frac{\pi u}{\beta_B}\right)}} \right)^3 . \tag{3.3.86}$$

If $\beta_B \sim \beta$, then we can expand the integral in powers of $\beta_B - \beta$:

$$\begin{aligned} \int_{-\infty}^{+\infty} dx \ \frac{\pi^{3/2}\beta^{3/2}}{\beta_B^{3/2} \sinh^{3/2}\left(\pi(x-i\epsilon)\frac{\beta}{\beta_B}\right)} \frac{\cosh \pi\,(x-i\epsilon)}{\sinh^{3/2} \pi\,(x-i\epsilon)} = \\ = -\frac{3}{2}\pi^{5/2}\left(\frac{\beta}{\beta_B}-1\right) \int_{-\infty}^{+\infty} dx \ \frac{(x-i\epsilon)\cosh^2 \pi\,(x-i\epsilon)}{\sinh^4(\pi(x-i\epsilon))} = \\ = -i\frac{\pi^{3/2}}{2}\frac{\beta-\beta_B}{\beta_B}. \end{aligned} \tag{3.3.87}$$

The approach to the bath temperature is exponential. Explicitly, we have

$$\beta' = (\beta_B - \beta)\frac{\pi b^4}{32\sqrt{2}\alpha_S}\frac{V^2\sqrt{J_S}}{J_B^{3/2}}, \quad \text{marginal.} \tag{3.3.88}$$

Again, this matches perfectly with the numerics as shown in Figure 3.5.

Irrelevant deformation: bath at zero temperature

For an irrelevant deformation with $f_B = 5$ we have

$$X_B = -G_B^5 \tag{3.3.89}$$

and the integral is

$$\int_{-\infty}^{+\infty} dx \ \frac{1}{(x-i\epsilon)^{5/2}} \frac{\cosh \pi\,(x-i\epsilon)}{\sinh^{3/2} \pi\,(x-i\epsilon)} = -1.98. \tag{3.3.90}$$

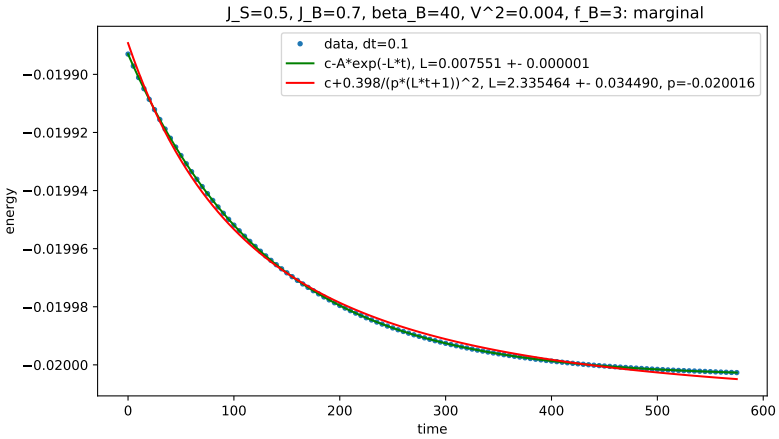

Figure 3.5: Energy as a function of time for $\beta_{\text{init}} = 35$ and $\beta_B = 40$. Only the late time behavior is shown. The green line is an exponential fit. For comparison we also included fits with $E \sim 1/t^2$. The analytical answer for the rate is 0.0075 from Eq. (3.3.88).

Hence, the temperature obeys

$$\beta' = 1.98 \frac{V^2 b^6 \sqrt{J_S}}{J_B^{5/2} \alpha_S 8\sqrt{2\pi}}, \quad \text{irrelevant, } f_B = 5. \tag{3.3.91}$$

Again we have very good agreement with the numerics, see Figure 3.6.

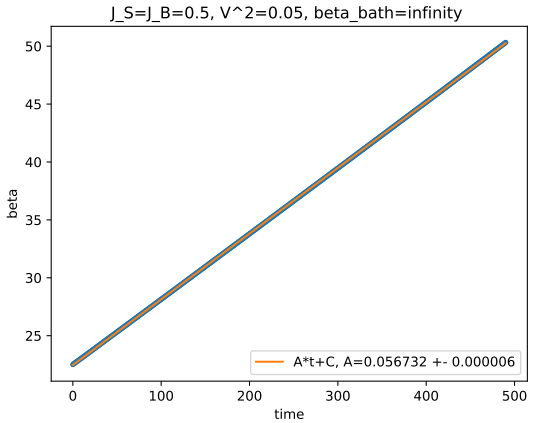

Figure 3.6: Energy and β for the irrelevant coupling $q_B = 4, f_B = 5, J_S = J_B = 0.5$. The dense blue points are numerical data. The analytical answer for the slope is 0.063 from Eq. (3.3.91).

Irrelevant deformation: bath at finite temperature

On physical grounds, we expect that if the system and the bath have close temperatures then the flux will be proportional to the temperature difference. Indeed, if $\beta_B \sim \beta$ we again get exponential approach:

$$\int_{-\infty}^{+\infty} dx \, \frac{\pi^{5/2}\beta^{5/2}}{\beta_B^{5/2}\sinh^{5/2}\left(\pi(x-i\epsilon)\frac{\beta}{\beta_B}\right)} \frac{\cosh \pi\,(x-i\epsilon)}{\sinh^{3/2}\pi\,(x-i\epsilon)} = \tag{3.3.92}$$
$$= -\frac{5}{2}\pi^{7/2}\left(\frac{\beta}{\beta_B}-1\right)\int_{-\infty}^{+\infty} dx \, \frac{(x-i\epsilon)\cosh^2\pi\,(x-i\epsilon)}{\left(\sinh^2(\pi(x-i\epsilon))\right)^{10/4}} =$$
$$= 8.57\frac{\beta-\beta_B}{\beta_B}.$$

Hence, the temperature obeys

$$\beta' = 8.57(\beta_B-\beta)\frac{V^2 b^6\sqrt{J_S}}{8\sqrt{2\pi}J_B^{5/2}\beta_B}, \quad \text{irrelevant, } f_B = 5. \tag{3.3.93}$$

For $J_S = 0.5, J_B = 0.7$ the agreement is again very good as shown in Figure 3.7.

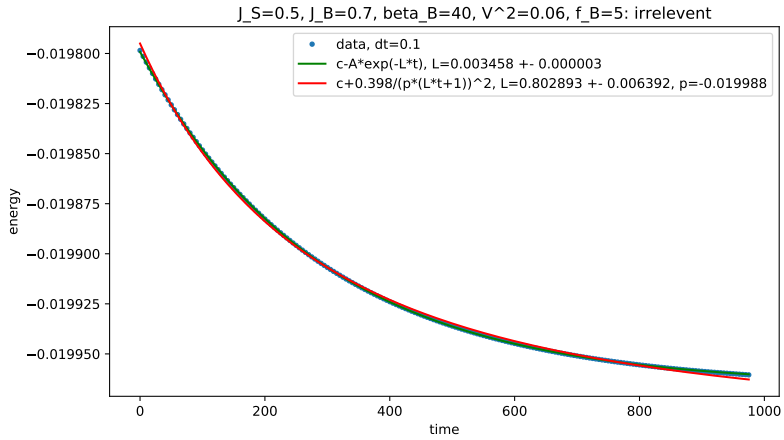

Figure 3.7: Energy as a function of time for $\beta_{\text{init}} = 35$ and $\beta_B = 40$. Only the late time behavior is shown. The green line is an exponential fit. For comparison we also included a fit with $E \sim 1/t^2$. The analytical answer for the rate is 0.0034 from Eq. (3.3.93).

3.3.7 Late time: approach to equilibrium and black hole evaporation

We have seen that the late time approach to true equilibrium is in many cases exponential. This agrees with our physical expectations since the heat flux should be proportional to the temperature difference.

Obviously, this process of energy flow cannot last forever. At the very least, the temperature has thermodynamic fluctuations,

$$\langle (\Delta T)^2 \rangle = \frac{T^2}{C_v}, \tag{3.3.94}$$

where C_v is the heat capacity, which is of order N for SYK if the temperatures is not too low. These fluctuations imply that once the difference $T_S - T_{\text{bath}}$ becomes of order $\Delta T \sim 1/\sqrt{N}$, we have effectively reached true equilibrium. In the situations studied so far, this will take a time of order $\log N$.

However, one important point is the way V^2 scales with N. For an evaporating black hole in which the energy transfer is accomplished by a small number of light fields, the energy loss rate should be of order N^0 instead of order N^1. This can be modeled by taking V^2 to scale with N as N^{-1} instead of as N^0, e.g.

$$V^2 \sim \frac{V_0^2}{N},\ V_0^2 \sim N^0. \tag{3.3.95}$$

Our analysis is still valid in this case, because we can use the classical Schwarzian description until $\beta \sim N$ and it is not important that the perturbation has $1/N$ suppression. Hence, the evaporation time becomes $N \log N$.

However, this estimate is somewhat imprecise. As we just said, we can trust our classical computation in the previous subsection as long as $\beta \ll N/J_S$. Once β becomes of order N we have to quantize the Schwarzian. This is quite complicated given the non-local term (3.3.75) in the action. Hence, it appears challenging to derive an analogue of Eq. (3.3.78) directly from the Schwarzian.

As an aside, notice that the problem does simplify when $V^2 \sim 1/N$ because when β reaches N/J_S, the integration range in Eq. (3.3.61) is already $N \log N$ (instead of $\log N$ when V^2 is order N^0), so we do not need to worry about the boundary term.

Fortunately, we do not need to carry out the full quantization procedure.[6] Recall that we derived Eq. (3.3.61) for any Majorana system interacting with a Majorana bath. It happens that Eq. (3.3.78) follows from it if we use the classical Schwarzian expression for the energy and the conformal approximation for the Green's functions. We will employ the same strategy in the quantum case. The exact expression for Schwarzian free energy is

$$F = -\frac{2\pi^2 \alpha_S}{\mathcal{J}_S \beta^2} + \frac{3}{2N\beta} \log \beta, \tag{3.3.96}$$

and the energy is

$$E = F + \beta \frac{dF}{d\beta} = \frac{2\pi^2 \alpha_S}{\mathcal{J}_S^2 \beta^2} + \frac{3}{2N\beta}. \tag{3.3.97}$$

In particular, when $\beta \sim N$ the last term dominates.

The behavior of SYK Green's function strongly depends on the relation between t, β and C where $C = N\alpha_S/\mathcal{J}_S$ is the coefficient in front of the Schwarzian term. As long as $t, \beta \ll C$ we have the classical result:

$$G_S \sim \frac{1}{\sqrt{J\beta \sinh\left(\frac{\pi t}{\beta}\right)}}. \tag{3.3.98}$$

Here and below we will suppress the numerical coefficients, but keep the factors of β and N explicit. A generic answer for G_S was obtained in [119, 91]:

$$G_S \sim \frac{1}{\sqrt{J_S C}} e^{-\frac{2\pi C}{\beta}} \left(\frac{\beta}{C}\right)^{3/2} \int_{-\infty}^{+\infty} d\mu(k_1) d\mu(k_2)\ \gamma(k_1, k_2)^2 \times \\ \times \exp\left(-\frac{1}{2c}\left(-itk_1^2 - (\beta - it)k_2^2 - \epsilon k_1^2 - \epsilon k_2^2\right)\right), \tag{3.3.99}$$

$$\gamma(k_1, k_2)^2 = \frac{1}{\Gamma(1/2)} \Gamma(1/4 + i(k_1 + k_2)) \Gamma(1/4 - i(k_1 + k_2)) \times \\ \times \Gamma(1/4 + i(k_1 - k_2)) \Gamma(1/4 - i(k_1 - k_2)) \tag{3.3.100}$$

$$d\mu(k) = \sinh(2\pi k) k dk. \tag{3.3.101}$$

[6] We are grateful to Alex Kamenev, Juan Maldacena and Luca Iliesiu for discussions about the following computation.

Suppose that $\beta \gg C$ is large in the above expression. Then we can use the saddle-point approximation for k_2 with the following result:

$$G_S \sim \frac{\beta^{3/2}}{\sqrt{J_S C}(t+i\beta)^{3/2}} \int_{-\infty}^{\infty} d\mu(k_1)\; e^{-\frac{1}{2c}\left(-itk_1^2-\epsilon k_1^2\right)} \Gamma(1/4+ik_1)^2 \Gamma(1/4-ik_1)^2. \tag{3.3.102}$$

If $t \ll C$, then the integral is dominated by large k_1, so expanding the Gamma functions for large k_1 yields

$$G_S \sim \frac{1}{\sqrt{J_S(t-i\epsilon)}},\; t \ll C \ll \beta, \tag{3.3.103}$$

which is the expected result for zero-temperature case. However, if $t \gg C$ we can use the saddle point approximation again, this time for k_2 [119, 91]:

$$G_S \sim \frac{N\beta^{3/2}}{J_S^{3/2}(t+i\beta)^{3/2}(t-i\epsilon)^{3/2}},\; t \gg C,\; \beta \gg N/J_S. \tag{3.3.104}$$

One cross-check it that the expressions (3.3.103) and (3.3.104) coincide when $t \sim N/J_S$.

The last step before the actual calculation of the evaporation rate is the expression for G_B. As we mentioned before, the number of bath fermions M must be much bigger than N. Here we assume M is big enough to keep the bath classical even at large times t, so the Green's function is

$$G_B^3 \sim \frac{1}{J_B^{3/2}(t-i\epsilon)^{3/2}}. \tag{3.3.105}$$

All these pieces can now be assembled to compute the energy flux. Integrating by parts in Eq. (3.3.61), we need to compute:

$$-\int_{-\infty}^{+\infty} dt\; \partial_t G_B^3 G_S \sim \frac{V_0^2}{N J_B^{3/2}} \int_{-\infty}^{+\infty} dt\; \frac{1}{(t-i\epsilon)^{5/2}} G_S(t). \tag{3.3.106}$$

First of all, if we put $\beta = \infty$, the system's Green's function (3.3.104) does not have singularities in the lower half-plane, so we can close the contour and get zero. This is expected: if both the system and the bath have zero temperature, then flux is zero.

To compute the integral at finite beta we consider the full integral representation (3.3.99). Notice that we can move the integral over t in Eq. (3.3.106) into the lower half-plane such that t acquires constant imaginary part of order β. In this case we can use the asymptotic formula in (3.3.104) for G_S. Hence, the flux is of order

$$\sim \frac{V_0^2}{(J_S J_B)^{3/2}} \frac{1}{\beta^3}. \tag{3.3.107}$$

Equating this to the loss of energy (3.3.97), we find only $\sqrt{t}$ behavior for β instead of exponential growth:

$$\beta' \sim \frac{V_0^2 N}{(J_S J_B)^{3/2}} \frac{1}{\beta}, \ \beta \gg N/J_S, \tag{3.3.108}$$

$$\beta(t) \sim \sqrt{\frac{V_0^2 N t}{(J_S J_B)^{3/2}}}. \tag{3.3.109}$$

As a check, note that for $\beta \ll N/J_S$ we had

$$\beta' \sim \frac{V_0^2}{N} \frac{\sqrt{J_S}\beta}{J_B^{3/2}}, \ \beta \ll N/J_S \tag{3.3.110}$$

from Eq. (3.3.85). Equations (3.3.108) and (3.3.85) agree for $\beta \sim N/J_S$.

Thus, in the quantum regime there is a cross-over from exponential behavior, $\beta \sim e^t$, to power-law behavior, $\beta \sim t^{1/2}$.

3.3.8 Checking the bound numerically

Having described all the parts of the curve analytically, let us discuss its precise form and check the proposed bound numerically. Our numerical setup is described in Appendix B.1. The main limitation comes from the fact that we cannot go to very low temperatures, because the Green's functions spread a lot. So we will limit ourselves to finite bath temperature. Also, we will study two kinds of interactions: marginal $f_S = 1, f_B = 3; f_S = 2, f_B = 2$ and irrelevant $f_S = 1, f_B = 5; f_S = 5, f_B = 1$.

V^2	F_{2/β_0}	$F_{2/\beta(t)}$
0.0	$\pm 10^{-7}$	$\pm 10^{-7}$
0.005	$(2.05 \pm 0.01) \times 10^{-4}$	$(2.06 \pm 0.01) \times 10^{-4}$
0.012	$(4.68 \pm 0.01) \times 10^{-4}$	$(4.73 \pm 0.01) \times 10^{-4}$
0.02	$(7.47 \pm 0.02) \times 10^{-4}$	$(7.70 \pm 0.01) \times 10^{-4}$

Table 3.1: Results for $F_{2/\beta}$ for the marginal deformation $(f_S, f_B) = (3, 1)$ with $J_S = J_B = 0.5, \beta_{\text{init}} = 20, \beta_{\text{bath}} = 100$. The errors were estimated by comparing the results of $dt = 0.1$ and $dt = 0.05$.

V^2	F_{2/β_0}	$F_{2/\beta(t)}$
0.01	$(5.13 \pm 0.03) \times 10^{-5}$	$(5.17 \pm 0.03) \times 10^{-5}$
0.05	$(2.48 \pm 0.02) \times 10^{-4}$	$(2.51 \pm 0.02) \times 10^{-4}$
0.1	$(4.79 \pm 0.04) \times 10^{-4}$	$(4.89 \pm 0.03) \times 10^{-4}$

Table 3.2: Results for $F_{2/\beta}$ for the irrelevant deformation $(f_S, f_B) = (5, 1)$ with $J_S = J_B = 0.5, \beta_{\text{init}} = 20, \beta_{\text{bath}} = 100$. The errors were estimated by comparing the results of $dt = 0.1$ and $dt = 0.05$.

At weak system-bath coupling, we do not expect a violation of the bound since we have a perturbative proof. However, at very strong coupling the final energy of the system is higher than the initial energy, because the interaction increases the ground state energy. Hence, something interesting might happen as we scan from weak coupling to strong coupling.

Our numerical results suggest that the integral in the bound is always bigger than zero. This is true even if we take $\beta(t)$ instead of the initial β. Our result are presented on Figures 3.8, 3.9 and Tables 3.1, 3.2. The main source of error is the fact that the energy not conserved even for $V = 0$ because of the discretization scheme, so we include the $V = 0$ case for reference.

3.3.9 Comparison to exact finite N calculations

Finally, we verify that the qualitative features of the energy curve persist at small N via direct numerical integration of the Schrodinger equation. Because it enables us to access larger system sizes, we work with pure states instead of mixed states and integrate the full system-bath Schrodinger equation using a Krylov approach.

As above, the system is a q_S-SYK model with N fermions while the bath is q_B-SYK model with M fermions. The fermions are represented in terms of spins using a standard Jordan-Wigner

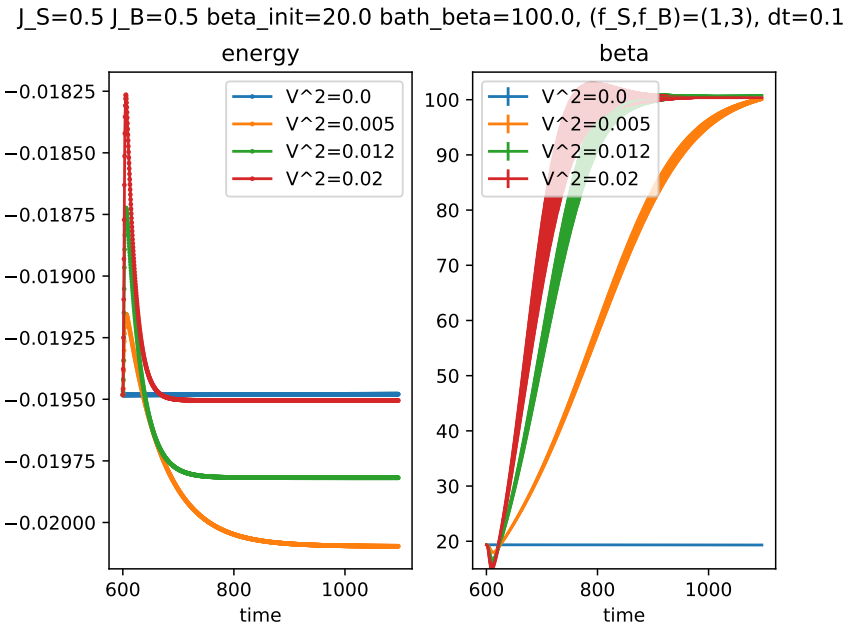

Figure 3.8: Energy and beta as functions of time for the marginal deformation $(f_S, f_B) = (3, 1)$ with $J_S = J_B = 0.5, \beta_{\text{init}} = 20, \beta_{\text{bath}} = 100$. The thickness of the beta curve indicates the uncertainty in beta.

construction. To prepare the inital state, we begin with a product state in the spin basis and evolve in imaginary time to produce:

$$|\psi_{\text{ini}}\rangle \propto e^{-\beta_S H_S/2 - \beta_B H_B/2} |\text{product}\rangle. \tag{3.3.111}$$

The coupling is then suddenly turned on at time $t = 0$ and the full system-bath composite is evolved forward in time. The energy of the system as well as the system-bath entanglement are measured as a function of time.

In Figure 3.10 we show an example of the energy curve for $N = 12$, $M = 20$, $q_S = 4$, $q_B = 4$, $f_S = 1$, $f_B = 3$, and $g = .2$. The initial temperatures were $\beta_{S0} = 1$ and $\beta_{B0} = 20$ in units where $J_S = J_B = 1$. One clearly sees the initial energy bump, the subsequent cross-over to energy loss, the slow draining of energy into the bath, and a final approach to true equilibrium. Note that the final equilibrium system energy is modulated by finite size fluctuations in the time domain.

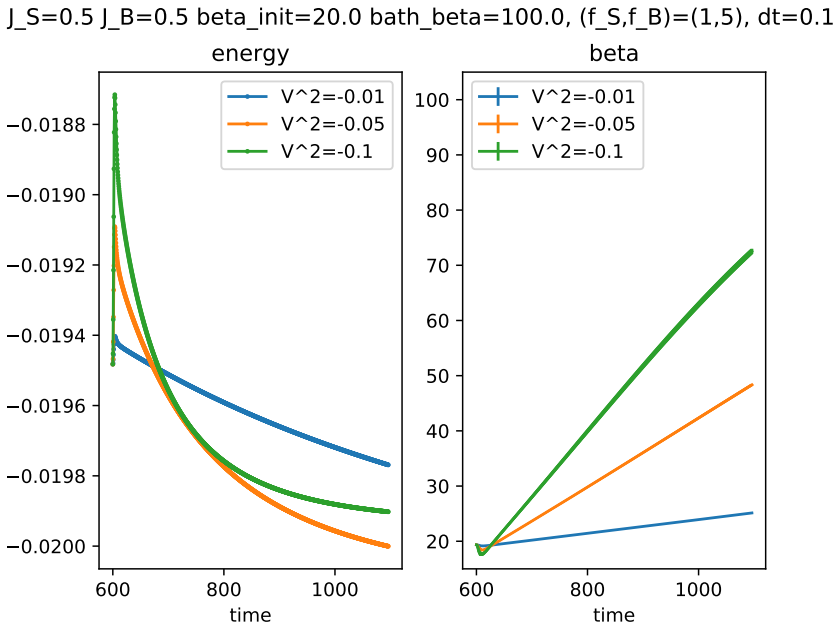

Figure 3.9: Energy and beta as functions of time for the irrelevant deformation $(f_S, f_B) = (5, 1)$ with $J_S = J_B = 0.5, \beta_{\text{init}} = 20, \beta_{\text{bath}} = 100$. The thickness of the beta curve indicates the uncertainty in beta.

The data shown constitute a single disorder sample with no disorder averaging. Also, the bound is satisfied for this example.

3.4 Discussion

Inspired by the problem of black hole evaporation, we studied in the detail the physics of thermalization for a system suddenly coupled to a bath. Our first key result is a positivity bound on the integrated energy flux. We proved it in general in perturbation theory and showed that it implied an instance of the ANEC. Our second key result is a detailed study of the thermalization dynamics for two coupled SYK clusters. In particular, at low energy we gave a thorough analytical discussion of the energy curve.

There are many directions for future work. One is to understand how far beyond perturbation theory our bound extends. In the SYK example, we found it to be quite robust. We suspect that quantum information ideas will be useful in this context, partly because the bulk interpretation

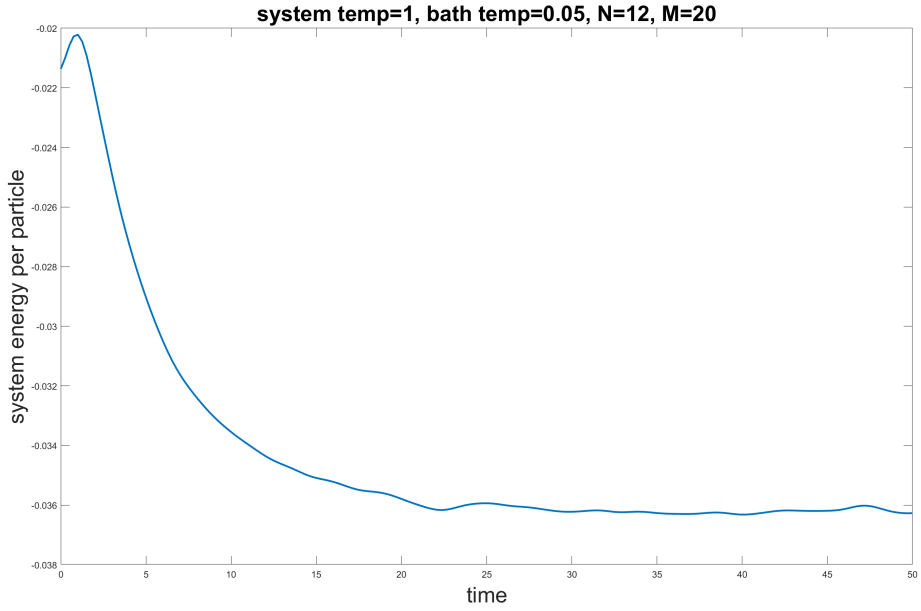

Figure 3.10: Energy curve for a finite size system-bath setup with $N = 12$ and $M = 20$. Other parameters are discussed in the main text.

of the bound in terms of the ANEC is associated with prohibiting unphysical communication between two entangled parties. There is also more to understand about the SYK case, for example, it may be possible to analytically solve the dynamical equations at large q.

More generally, it would be interesting to generalize our analysis to pure states, and to understand in detail the behavior of the entanglement entropy of various parts of the system. Finally, it is tempting to try to relate our rigorous Planckian bound on the energy curve to other more speculative Planckian bounds, for example, in transport physics. One idea for relating them is to the use the fact that dissipative transport generates heat, so perhaps this fact can be combined with some version of the setup we considered here?

Chapter 4

SYK wormhole formation in real time

4.1 Introduction and Summary

4.1.1 Motivation

The Sachdev–Ye–Kitaev (SYK) model [16, 17, 36, 120] is a strongly interacting but yet solvable model in the large N limit. At low energies, it displays an approximate conformal symmetry. In this region, the model has many features in common with nearly AdS_2 gravity, or Jackiw-Teitelboim (JT) gravity [112, 113, 121], coupled to matter fields. This is a simple two dimensional theory of gravity which describes some aspects of nearly extremal black holes in various dimensions.

An interesting variant is to consider a pair of identical SYK models coupled through a simple bilinear interaction [122], see also [123, 97, 124]. The ground state of this model has a gap, but its excitation spectrum also displays an approximate conformal symmetry. Furthermore, this ground state is close to the thermofield double state of two decoupled models. For reasons we explain below, we call the ground state of this coupled model "the SYK wormhole".

A conceptually similar state also arises when one considers two nearly extremal black holes that are relatively close, so that they are coupled. In this case, a traversable wormhole can connect

the near extremal throats [125]. This can be effectively modeled by a nearly AdS_2 gravity theory where we have direct interactions between the values of the bulk fields near the two boundaries [111, 122]. In other words, thinking of the Penrose diagram of AdS_2 as a strip, we put boundary conditions for the bulk fields that connect the two boundaries. The two boundaries are causally connected through the bulk, so that this spacetime describes a wormhole. This wormhole is the lowest energy configuration of the system and it also displays the approximate $SL(2, R)$ isometries of nearly AdS_2.

Given that this is a remarkable state, we are interested in knowing whether it is easy to get to it. In other words, if we start out from a general excited state of the coupled model, can we easily get to the ground state by cooling the system down? Or will the system get stuck in some other state? At first sight the answer seems straightforward, if it is the ground state, the system will surely find it if it can shed its excess energy to the bath. On the other hand, from the gravity perspective, the process involves a topology change. Such topology change might happen via a tunneling solution, but it would be exponentially suppressed in N (or the entropy of each separate black hole).

4.1.2 Wormhole formation in SYK

With this motivation in mind, we study this problem for the two coupled SYK models. We start with a relatively high temperature state of the coupled model which looks like two thermal density matrices, one for each SYK factor. Then we couple the system to a bath and study the evolution in real time by solving the large N Schwinger-Dyson equations. We find that the system indeed finds the "SYK wormhole" ground state in a time that is independent of N. In particular, there is no exponential suppression. Notice that the ability to efficiently find this ground state also makes it possible to prepare the thermofield double (TFD) state of the decoupled model, by simply switching off the interaction between the two sides [122], after we have found the ground state.

The approach we used is the following. The large N Dyson–Schwinger equations form a closed system for the two-point function [16, 17, 36, 120]. In the out-of-equilibrium situation that we are

considering, these equations are commonly referred to as the Kadanoff–Baym (KB) equations. We couple the system of two interacting SYK models to a large bath and find the real time dynamics using KB equations. The problem of coupling SYK to a bath was recently studied in [2] and we borrow some results from there. Also, the KB equations for a single SYK was recently studied numerically in [37, 106]. Here we study this problem solving the dynamical equations at $q = 4$. The problem has many time scales and due to numerical limitations we could not separate them all by large amounts. However, our numerical results seem to confirm the picture where the system follows the microcanonical equilibrium curve. We now briefly review this equilibrium thermodynamics.

4.1.3 Equilibrium thermodynamics

In the canonical ensemble the system has two phases: the low temperature one corresponding to the ground state, the SYK wormhole, and its excitations; and a higher temperature phase which is closer to two separate thermal SYK systems. The two phases are separated by a first order phase transition. In the large q limit, the black hole phase and the wormhole phase are smoothly connected by a canonically unstable phase with negative specific heat [122]. However, in the microcanonical ensemble, we expect that the system smoothly interpolates between these two phases. In other words, in the microcanonical ensemble we expect no phase transition as we lower the energy.

Figure 4.1 shows energy vs inverse temperature β for $q = 4$. We use energy instead of free energy or entropy because we will be dealing mostly with Lorentzian non-equilibrium correlators numerically and it is easier to find the temperature and the energy from them. There are three different regions. At high temperatures $T > T_{\rm 2BH}$ we have the phase we name the "two black holes phase". At low temperatures $T < T_{\rm WH}$ we have the phase we call "cold wormhole" phase, which can be viewed a as a wormhole with few thermal excitations. The two phases overlap, since $T_{\rm 2BH} < T_{\rm WH}$. In the intermediate temperatures regime $T_{\rm 2BH} < T < T_{\rm WH}$ we also expect a canonically unstable, but microcanonically stable, phase that we call "the hot wormhole phase". As we mentioned above, this phase can be found analytically in the large q limit. It has positive

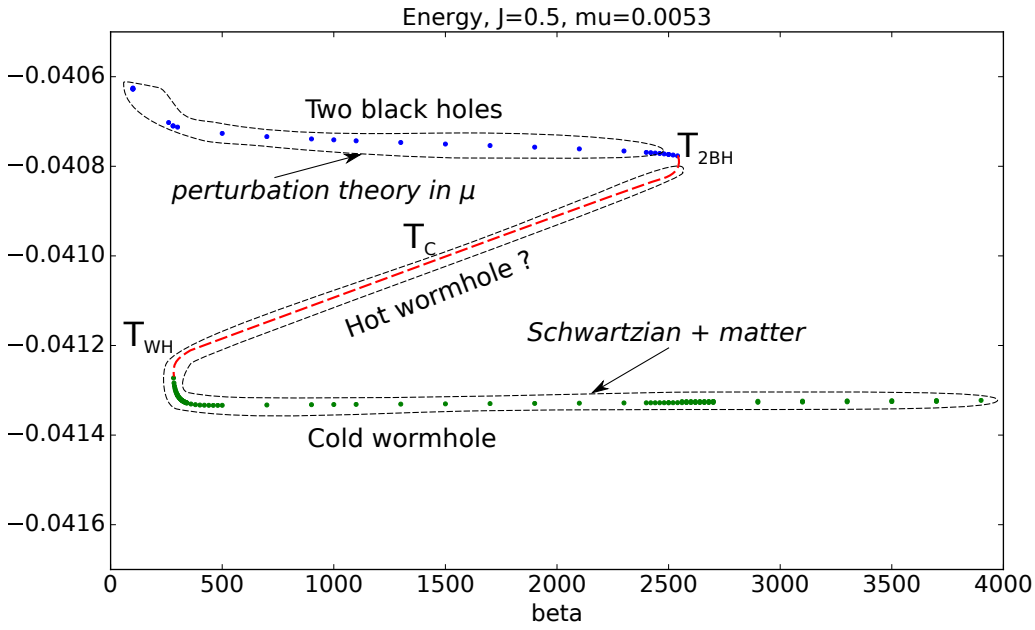

Figure 4.1: Dots: energy vs beta obtained by numerically solving DS equations for two coupled SYK models with $J = 0.5, \mu = 0.0053$. Blue dots correspond to the "two black holes phase", whereas green dots correspond to the "cold wormhole phase". Red dashed line: curve for the "hot wormhole" phase expected from a low energy analytic analysis. The question mark "?" reminds us that we were not able to find it as a solution of the euclidean DS equations.

entropy but negative specific heat. However, at finite q we do not known much about this phase, since we have been unable to find it by solving the Euclidean Schwinger Dyson equations. We interpret this failure as resulting from its canonical instability. This is why we put a question mark in Figure 4.1. We will find evidence for this phase through the real time evolution, since we will find that the temperature goes up as the energy monotonically goes down. There is also analytic evidence from a low energy analysis, as we will review later. The names "hot" or "cold" wormhole refer to how these would feel to an observer who is inside the wormhole, at its center, in a gravity picture for these configurations. As is clear from Figure 4.1, there are outside temperatures where we can have both a "cold" and "hot" wormhole. When we talk about temperatures in this chapter, we are always referring to the physical temperature as seen from the outside.

Figure 4.1 also displays the critical temperature, T_c, when two stable phases switch dominance in the canonical ensemble. For $T_{\rm 2BH} < T < T_c$ two black hole phase is thermodynamically metastable but is not a global minimum for the free energy. Similarly for $T_c < T < T_{\rm WH}$ and the cold wormhole phase. For our problem the microcanonical ensemble is more relevant. Notice that the different "phases" are continuously connected in the microcanonical ensemble, so they are not really sharply separated phases.

For small values of μ, the coupling between the two SYK models, we can make different analytic approximations for the different parts of the curve. For the two black hole region we can start with two separate thermal SYK models and use perturbation theory in μ. In this regime, the left-right correlator G_{LR} is small and of order μ. The gravity picture is that we have two separate hyperbolic disks with a boundary perturbation that connects the bulk fields on the two disks. We find that $T_{\rm 2BH}$ is in the region where this perturbation theory breaks down. For low temperatures the left-right correlator is of order one. We can access this regime by assuming that the system is close to the thermofield double state. The relevant part of the dynamics is captured by the Schwarzian mode. This aspect of the dynamics is the same for the SYK model and the nearly-AdS_2 gravity theory [116, 115, 103]. This describes both the cold wormhole and hot wormhole phases. In particular, we can see the existence of the hot wormhole phase in this approximation [122]. In particular, the temperature $T_{\rm WH}$ can be found within this approximation. We review this description in Section 4.2.3.

4.1.4 Gravity picture

One of our motivations was to understand whether a similar wormhole formation process occurs in more general theories of nearly-AdS_2 gravity with matter.

With this goal in mind we will present a gravity picture for the transition we have in the SYK model. We do not know the precise gravity dual of the SYK model. But we consider a nearly-AdS_2 gravity theory that has some of the same features. For questions that mainly involve the Schwarzian mode, the SYK and nearly-AdS_2 answers match precisely [116, 115, 103]. However, wormhole formation goes slightly beyond this approximation, and we need to incorporate one

important feature that is related to the origin of the ground state entropy, or "zero temperature" entropy, S_0, of the SYK model. If we start from a phase consisting of two thermal states, then the entropy will have a large contribution of size $2S_0$ (plus thermal corrections). As the wormhole forms, the system should be able to shed this large entropy into the bath. In gravity this involves topology change, which would naively be exponentially suppressed. On the other hand, as we discussed above, this happens without any such suppression in SYK.

We can reproduce this from a gravity picture as follows. First we view the two coupled systems as a nearly-AdS_2 gravity theory with N bulk fermion fields with Neumann boundary conditions. The two black hole phase consists of two hyperbolic disks with an interaction between the boundary values of the bulk fields. As we lower the temperature, this interaction effectively becomes strong and the theory flows to a new IR fixed point. The new fixed point is simply a theory with different boundary conditions, namely Dirichlet boundary conditions. This change in boundary conditions is similar to the one discussed in [126]. The two disks decouple again but the boundary conditions are effectively changed from Neumann to Dirichlet. Now we use the observation in [127], that e^{S_0} is equal to the ratio of the Neumann vs Dirichlet disk partition functions for N fermions. This means that the effective theory in the IR, with Dirichlet boundary condition has now $S_0^{eff} = 0$. This means that topology change "costs us nothing", and we can easily transition into the wormhole phase. In fact, by a similar argument we can say that the end of the hot wormhole phase also corresponds to the region where the interactions between the two sides of the global AdS_2 strip produce a flow that change the boundary conditions of the fermions from Neumann to Dirichlet.

In summary, we provide a qualitative gravity mechanism for the formation of the SYK wormhole. The purpose of this explanation was to contrast SYK with what we expect in a generic gravity theory. A generic gravity theory can have a number of fields much smaller than S_0. In this case, the change in boundary conditions would not significantly change S_0 and it would still be difficult to change the topology. For this reason we could not answer the question of whether there is an "easy way" of forming the wormhole for more general gravity theories, such as the case of four dimensional magnetically charged wormholes in the Standard Model [125].

The chaper is organized as follows. In Section 4.2 we review the two coupled SYK model [122]. We describe the perturbative approach at high temperatures, for the "two black hole phase". We also review the Schwarzian description of the low energy dynamics that describes the hot and cold wormhole phases. Section 4.3 contains our real time analysis of the formation of the wormhole. We set up the coupling to the bath, we write the Kadanoff-Baym equations (the real time Schwinger Dyson equations), and we present the result of a numerical analysis for some particular values of the parameters. In section 4.4, we discuss differences and similarities between SYK and nearly-AdS_2 (or JT) gravity and also provide the qualitative picture of the transition. Various computational details are discussed in the appendices.

4.2 The two coupled SYK model and its thermodynamics

4.2.1 Definition and properties of the ground state

Here we review properties of the two coupled SYK models introduced in [122]. The Hamiltonian of the model consists of two SYK terms coupled by an interaction

$$H = H^L_{\rm SYK} + H^R_{\rm SYK} + H_{\rm int} \tag{4.2.1}$$

where

$$H^L_{\rm SYK} + H^R_{\rm SYK} = \sum_{1\leq i<j<k<l\leq N} J_{ijkl}\left(\psi^L_i\psi^L_j\psi^L_k\psi^L_l + \psi^R_i\psi^R_j\psi^R_k\psi^R_l\right) \tag{4.2.2}$$

where the couplings are the same for both factors. They are Gaussian random variables with variance

$$\langle J^2_{ijkl}\rangle = \frac{3!J^2}{N^3}, \quad \text{no sum} \tag{4.2.3}$$

There is also a generalization where we consider a q fermion interaction term, instead of four. The interaction term has the form

$$H_{\rm int} = i\mu\sum_{j=1}^{N}\psi^L_j\psi^R_j \tag{4.2.4}$$

In the large N limit, μ and J stay fixed. We will mostly consider the case $\mu/J \ll 1$ and also consider temperatures $T/J \ll 1$. This will be true even for what we call "high" temperatures.

As an aside, let us mention that we can couple the two systems by an operator of dimension Δ

$$H_{\text{int}}^{\Delta} = i^F \mu (\mathcal{O}_\Delta)_L (\mathcal{O}_\Delta)_R \tag{4.2.5}$$

where F is the fermion number of $\mathcal{O}_\Delta$. We will mostly consider the case of (4.2.4) which corresponds to $\Delta = 1/4$ at low energies. However, we will give certain estimates for generic Δ.

Like a single SYK, this model, (4.2.1), is solvable in the large N limit. We have four types of correlators: $G_{LL}, G_{RR}, G_{LR}, G_{RL}$, each defined in Euclidean space as

$$G_{ab}(\tau) = \langle T\psi_a(\tau)\psi_b(0)\rangle \ , \quad \text{with} \quad a,\, b = L,\, R \tag{4.2.6}$$

Since we are dealing with Majorana fermions we have

$$G_{LL}(0^+) = G_{RR}(0^+) = \frac{1}{2} \tag{4.2.7}$$

We have a closed system of Dyson–Schwinger equations for the two point functions [122]

$$\partial_\tau G_{ab}(\tau) = \sum_c \Sigma_{ac} * G_{cb}(\tau) + \delta_{ab}\delta(\tau) \tag{4.2.8}$$

$$\Sigma_{ab}(\tau) = J^2 G_{ab}(\tau)^3 - i\mu_{ab}\delta(\tau) \ , \qquad \text{no sum} \tag{4.2.9}$$

where the convolution $*$ is taken along the Euclidean circle, $a, b = L, R$, and μ_{ab} is given by

$$\mu_{ab} = \begin{pmatrix} 0 & \mu \\ -\mu & 0 \end{pmatrix} \tag{4.2.10}$$

The system has a $\mathbb{Z}_4$ symmetry $\psi_L \to -\psi_R$, $\psi_R \to \psi_L$. Throughout our numerical computation we do not assume that this symmetry in unbroken. We find that it is unbroken, since the

(Euclidean) correlators we obtained obey the following relations:

$$G_{LL} = G_{RR} \text{ pure real} , \qquad G_{LR} = -G_{RL} \text{ pure imaginary} \tag{4.2.11}$$

A convenient expression for the energy is

$$\frac{E}{N} = \frac{J^2}{4} \int_0^\beta d\tau \ \left(-G_{LL}^4 - G_{RR}^4 - 2G_{LR}^4 \right) + i\mu G_{LR}(0) \tag{4.2.12}$$

The interaction term (4.2.4) is a relevant perturbation, since for a single SYK model the fermion ψ has dimension $\Delta = 1/4$. Therefore at relatively high temperatures we expect that we have two weakly coupled SYK models, whereas at low temperatures the system flows into a gapped phase with a gap that scales as [122]

$$E_{\text{gap}} \propto \mu^{2/3} J^{1/3} , \qquad \text{for} \quad \frac{\mu}{J} \ll 1, \text{ and } q = 4, \ \Delta = \frac{1}{4} \tag{4.2.13}$$

Moreover the ground state is close to the TFD of the two models with effective (inverse) temperature $\tilde{\beta}$:

$$|\text{TFD}\rangle = \sum_n e^{-\tilde{\beta} E_n/2} |\bar{E}_n\rangle_L \times |E_n\rangle_R , \qquad \tilde{\beta} J \propto \left(\frac{J}{\mu} \right)^{\frac{1}{2(1-\Delta)}} , \quad \Delta = \frac{1}{q} \tag{4.2.14}$$

The energy of the ground state, relative to the energy of the two decoupled SYK models, scales as

$$E_{\text{G}} - 2E_{0,\text{SYK}} \propto -N \frac{\mu^{4/3}}{J^{1/3}} \tag{4.2.15}$$

And for general Δ, $E_G - 2E_{0,\text{SYK}} \propto -\mu^{\frac{1}{1-\Delta}}$

Since there is a gap and the ground state is unique, the entropy is small in the "cold wormhole phase". Whereas in the two black hole phase, we have a big entropy $2S_0$, where $S_0 \approx N \times 0.23$ is the "zero temperature" entropy of a single SYK model. The transition temperature T_c is estimated by

$$T_c \sim -\frac{E_{\text{G}}}{2S_0} \propto \frac{\mu^{\frac{4}{3}}}{J^{\frac{1}{3}}}, \qquad \text{for} \ \ q = 4 \tag{4.2.16}$$

For arbitrary temperatures the Dyson-Schwinger equations can be solved numerically by starting from $G_{LR} = G_{RL} = 0, G_{LL} = G_{RR} = \frac{1}{2}$ and then using an iteration procedure similar to one described in [36]. After obtaining the solution for some value of temperature, we can use it as a seed for the iteration procedure at higher/lower temperature. Figure 4.1 shows energy as a function of beta for particular values of parameters $J = 0.5, \mu = 0.0053$.

4.2.2 Perturbation theory at high temperature

Here we use the term "high" temperatures for temperatures for the two black hole branch of the diagram $T \gg T_{2\text{BH}}$, but still $T/J \ll 1$.

For $\mu = 0$ we have two copies of the conventional SYK correlators [16, 17]

$$G(\tau)_{LL} = G(\tau)_{RR} = b\,\text{sgn}(\tau)\frac{1}{\sqrt{J\beta}}\left(\frac{\pi^2}{\sin^2\frac{\pi\tau}{\beta}}\right)^{1/4}, \qquad G_{LR} = 0 \tag{4.2.17}$$

with $b^4 = 1/(4\pi)$.

Now we turn on a small value of μ (4.2.4). If we are at sufficiently high temperature then the coupled system is still in the phase with two separate black holes [122]. Nonetheless, the correlation between left- and right- SYK is not zero. We can try to use the conformal perturbation theory to study the system.

To linear order in μ, only G_{LR} Green functions receive a correction:

$$\Delta G_{LR}(\tau_1 - \tau_2) = i\mu \int_0^\beta d\tau\; G_{LL}(\tau_1 - \tau) G_{RR}(\tau - \tau_2) \tag{4.2.18}$$

This integral is computed analytically in Appendix B.6. We can compare this leading order approximation against exact numerical solution of the Dyson–Schwinger equation for $J = 0.5, \mu = 0.05$ and different βs, see Figure 4.2.

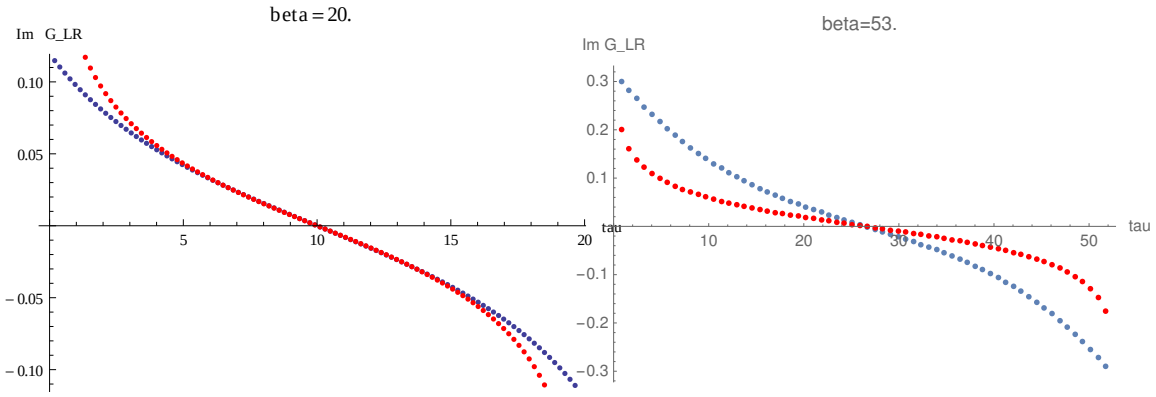

Figure 4.2: Euclidean Green function G_{LR}. The blue points correspond to the exact solution, and the red ones to the conformal answer (B.6.87). Left: $\beta = 20$. Right: $\beta = 53$. For this values of parameters the transition to the wormhole phase happens around $\beta_{2\text{BH}} \sim 61$. The approximation is better for higher temperatures.

Also in Appendix B.6 we computed the μ^2 correction to the energy. So that at low temperatures we have the following expression for the energy:

$$
\begin{aligned}
E &= 2E_{\text{SYK}} + \Delta E && (4.2.19)\\
E_{\text{SYK}} &= E_{0,\text{SYK}} + \frac{2\pi^2\alpha_S\sqrt{2}}{J\beta^2} && (4.2.20)\\
E_{0,\text{SYK}} &= -J \times 0.04063(1), \qquad \alpha_S = 0.0071 \pm 0.0004 && (4.2.21)\\
\Delta E &= \frac{1}{2\sqrt{4\pi}}\frac{\mu^2}{J}\left(2\log\frac{\pi}{\beta J} - 2 - c_1\right), \qquad c_1 = 1.66(1)
\end{aligned}
$$

where E_{SYK} is the low-temperature result for a single SYK [36] and ΔE is the leading μ^2 correction derived in Appendix B.6. The comparison between (4.2.19) and the numerics is presented on Figure 4.6(b).

This approximation works better for high temperatures and then deteriorates close to $T_{2\text{BH}}$, where the phase is supposed to connect with the hot wormhole phase.

Let us find out until what temperature we can trust the perturbation series in μ, (4.2.4). The first point is that only even terms are non-zero. The term of order μ^{2n} contains a $2n$-point function on the left and $2n$-point function on the right, each of these now computed in a single SYK model. We are only interested in connected correlators for computing the corrections to

the free energy. Higher point functions in SYK have two contributions: a purely conformal piece which is independent of β, up to an overall factor of $\left(1/\sqrt{J\beta}\right)^{4n}$ as in (4.2.17), plus contributions from the Schwarzian which are enhanced by an extra factor of βJ. We claim that the Schwarzian contributions are in fact zero, see Appendix B.7. The reason behind this cancellation is the following. When we work at large N we are solving the classical equations. The reparametrization mode has a solution that is time translation invariant. The two sides are coupled by convolutions of Green's functions but this translation symmetry remains unbroken. This means that there is no source for higher Fourier components of the reparametrization mode, so that the standard thermal solution continues to be a solution.

The integrals over time give β^{2n}. In total, we have $\frac{\mu^{2n}\beta^{2n}}{(J\beta)^n}$. So the expansion parameter is

$$\frac{\mu\beta}{\sqrt{J\beta}}\ , \qquad \text{for } \ q=4\ , \qquad \text{or} \qquad \frac{\mu\beta}{(J\beta)^{2\Delta}}\ , \qquad \text{for general } q \tag{4.2.22}$$

So we can trust the above perturbative answer until temperature

$$T_{\text{pert}} \propto J\left(\frac{\mu}{J}\right)^{\frac{1}{1-2\Delta}} \tag{4.2.23}$$

For $\Delta = 1/4$ this scales as μ^2, whereas $T_c \propto \mu^{4/3}$ is much larger.

We conjecture that the transition temperature T_{2BH}, when the two black holes phase cease to exist, in fact coincides with T_{pert}, when the perturbation theory in μ breaks down

$$T_{\text{2BH}} \sim T_{\text{pert}} \propto J\left(\frac{\mu}{J}\right)^{\frac{1}{1-2\Delta}} \tag{4.2.24}$$

We check this prediction for $\Delta = 1/4$ against the numerical phase diagram obtained in [122]. See Figures 4.3, 4.5.

One last comment on the leading result (4.2.18). In Appendix B.7, we studied the gravitational dressing of this term, searched for instabilities that would spontaneously break the $U(1)$ time translation symmetry, but did not find any.

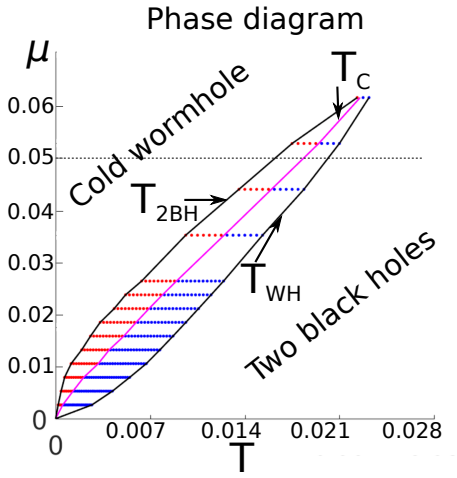

Figure 4.3: A reprint of the phase diagram obtained numerically in [122] for $J = 0.5$. The right solid black curve indicates $T_{\rm WH}$, purple line T_c and left solid black line $T_{\rm 2BH}$. The dashed horizontal line is at $\mu = 0.05$, the value of μ we will use in our real time numerical simulation. In this case $\beta_{\rm 2BH} \sim 61,\ \beta_c \sim 54,\ \beta_{\rm WH} \sim 49$.

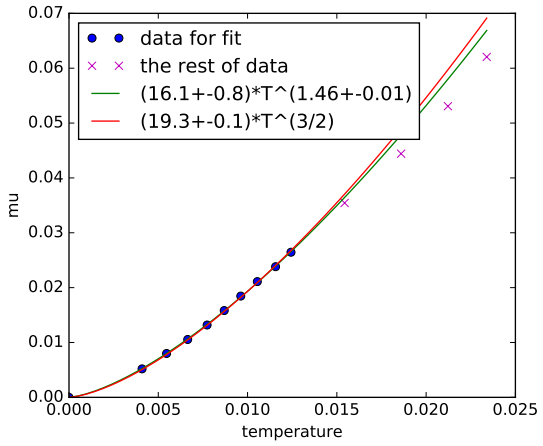

Figure 4.4: The fit for $T_{\rm WH}$ using the numerical data from [122] in Figure 4.3, using only data points with $\mu < 0.03$. The fit is consistent with the analytical prediction $\mu \sim T^{3/2}$.

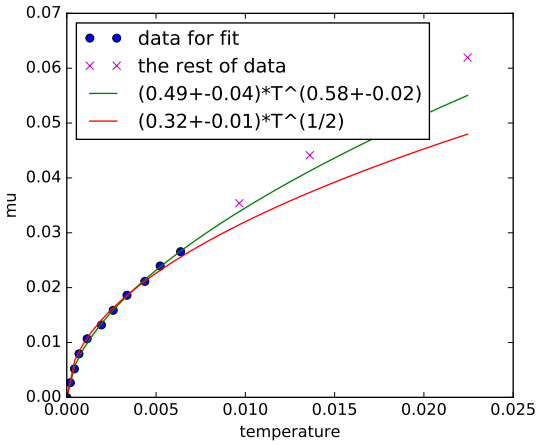

Figure 4.5: The fit for $T_{\rm 2BH}$ using the numerical data from [122] in Figure 4.3, using only data points with $\mu < 0.03$. The fit is consistent with the analytical prediction $\mu \sim \sqrt{T}$.

4.2.3 Low temperature thermodynamics using the Schwarzian

In this section we review the results of [122] on the Schwarzian description of the wormhole. We will see that the Schwarzian indeed admits a wormhole solution at low temperatures. Moreover, by including the matter contribution to the partition function one is able to see two phases

which join at (inverse) temperature $\beta_{\rm WH}$. One phase has positive heat capacity and almost zero entropy. This is a cold and mostly empty wormhole. The second phase has higher energy longer throat and negative heat capacity. This is wormhole with extra matter excitations inside. We will see shortly that at small enough μ this approximation predicts $\beta_{\rm WH}$ with good accuracy.

As we have mentioned before, the ground state of the system is close to the TFD state. Since we have global AdS_2 we have the following G_{LR} correlator in Euclidean signature:

$$G_{LR} = \frac{ib}{\sqrt{2J\cosh\left(\frac{t_L - t_R}{2}\right)}} \tag{4.2.25}$$

where t_L, t_R are times on left/right.

The action in the Schwarzian approximation now includes two kinetic terms[1] and an interaction

$$\begin{aligned} S &= S_{\rm kin} + S_{\rm int} && (4.2.26)\\ S_{\rm kin} &= -\frac{N\sqrt{2}\alpha_S}{J}\int du\ \left(\{\tanh\left(\frac{t_L(u)}{2}\right), u\} + \{\tanh\left(\frac{t_R(u)}{2}\right), u\}\right) && (4.2.27)\\ S_{\rm int} &= -Ni\mu\int du G_{LR}(u) = \frac{N\mu b}{\sqrt{2J}}\int du \frac{(\mathbf{t}_L'(u)\mathbf{t}_R'(u))^{1/4}}{\sqrt{\cosh\left(\frac{\mathbf{t}_L(u)-\mathbf{t}_R(u)}{2}\right)}} && (4.2.28)\end{aligned}$$

with α_S in (4.2.21). The wormhole solution is simply $\mathbf{t}_L = \mathbf{t}_R = \mathbf{t}'u$, where $\mathbf{t}'$ is a constant. The effective temperature, $\tilde{\beta}$ of the TFD state is given by

$$\tilde{\beta} = \mathbf{t}'\beta \tag{4.2.29}$$

Inserting into the action we get the free energy

$$F/N = \frac{\alpha_S\sqrt{2}}{J}\mathbf{t}'^2 - \frac{\mu b}{\sqrt{2J}}\mathbf{t}'^{1/2} \tag{4.2.30}$$

[1]For $q = 4$, $J = \sqrt{2}\mathcal{J}$ hence the extra $\sqrt{2}$.

We should also include the contribution from matter fields in the wormhole throat. If the temperature is low enough we excite only the lightest excitation in the bulk, which is the elementary fermion with mass 1/4. Its contribution to the free energy is:

$$\Delta F/N = -\frac{1}{\beta}\log\left(1+e^{-\tilde{\beta}/4}\right) \approx -\frac{1}{\beta}e^{-\mathbf{t}'\beta/4} \tag{4.2.31}$$

Extremizing the free energy with respect to $\mathbf{t}'$, which is the same as extremizing the full effective action, we have the following equation to determine $\mathbf{t}'$ and correspondingly $\tilde{\beta}$:

$$0 = \frac{\partial F_{\text{tot}}}{\partial \mathbf{t}'} = \frac{2\alpha_S\sqrt{2}}{J}\mathbf{t}' - \frac{\mu b}{2\sqrt{2J}}\mathbf{t}'^{-1/2} + \frac{1}{4}e^{-\mathbf{t}'\beta/4} \tag{4.2.32}$$

This equation has a solution with very small $\mathbf{t}'$ which we can not trust, because we were assuming that the temperatures are low. For large enough β two additional solutions emerge. One of them correspond to what we call the cold wormhole and the other to the hot wormhole. The latter has negative heat capacity and can be viewed as a wormhole with more excitations in the throat. Figure 4.6 shows the two branches for two different values of μ/J and their comparison to the numerical solution to the DS equations.

We can calculate T_{WH} from this equation. We simply need to find when these two solutions merge. To keep the discussion general, we consider general Δ, which corresponds to the case when the two sides are coupled through the product of two operators of dimension Δ. The equation for $\mathbf{t}'$ now reads as:

$$\frac{2\alpha_S\sqrt{2}}{J}\mathbf{t}' - \frac{\mu b_\Delta}{2(2J)^{2\Delta}}\mathbf{t}'^{2\Delta-1} + \Delta e^{-\mathbf{t}'\beta\Delta} = 0 \tag{4.2.33}$$

The cold wormhole branch can be approximately found [122] by neglecting the thermal excitations exponent in the above equation, so that $\mathbf{t}'$ is equal

$$\mathbf{t}' \propto \frac{\mu}{J^{2\Delta-1}} \tag{4.2.34}$$

Whereas the unstable branch with excitations can be approximated by neglecting the Schwarzian kinetic term $\sim \alpha_S \mathbf{t}'$:

$$\frac{\mu}{J^{2\Delta}} \mathbf{t}'^{2\Delta-1} \propto e^{-\mathbf{t}'\beta\Delta} \tag{4.2.35}$$

Plugging the $\mathbf{t}'$ from the first solution (4.2.34) into the above equation we find the T_{WH}:

$$T_{\text{WH}} \propto \frac{\mu^{\frac{1}{2-2\Delta}}}{\log J/\mu} \sim \frac{\mu^{2/3}}{\log J/\mu}, \text{ for } \Delta = 1/4 \tag{4.2.36}$$

Of course, both (4.2.34) and (4.2.35) are good for $T \ll T_{\text{WH}}$. Here we presented just estimates, but it is straightforward to solve (4.2.33) numerically, see Figure 4.6.

We can also compute the energy using[2]

$$E = F + TS = F + \beta \frac{\partial F}{\partial \beta} + \beta \frac{\partial F}{\partial \mathbf{t}'} \frac{d\mathbf{t}'}{d\beta} = 2E_{0,\text{SYK}} + \frac{\alpha_S \sqrt{2}}{J} \mathbf{t}'^2 - \frac{\mu b}{\sqrt{2J}} \mathbf{t}'^{1/2} + \frac{\mathbf{t}'}{4} e^{-\mathbf{t}'\beta/4} \tag{4.2.37}$$

where $E_{0,\text{SYK}}$ is the ground state energy of a single SYK, see (4.2.21).

In Figure 4.6 we have compared the results computed using eq. (4.2.37) with the numerical solution of the DS equation. For the value $\mu = 0.05$, which is the one we will use for the real time numerical computation, the agreement is not very good, but the qualitative form of the curve is similar, see Figure 4.6(a). This means that that μ is not low enough for an accurate Schwarzian description. Indeed if we lower μ we get very good agreement. See Figure 4.6(b) for $\mu = 0.0053$.

To summarize, for small μ, we have a hierarchy of temperatures

$$\begin{aligned} T_{\text{WH}} &\propto \frac{\mu^{\frac{1}{2-2\Delta}}}{\log J/\mu} \sim \frac{\mu^{2/3}}{\log J/\mu}, \qquad \text{for } \Delta = 1/4 \\ T_c &\propto \mu^{\frac{1}{1-\Delta}} \sim \mu^{4/3} \\ T_{\text{2BH}} &\propto \mu^{\frac{1}{1-2\Delta}} \sim \mu^2 \end{aligned} \tag{4.2.38}$$

where the rightmost term corresponds to $\Delta = 1/4$.

[2]When computing the derivatives one has to keep in mind that $\mathbf{t}'$ is a function of β. And use (4.2.32).

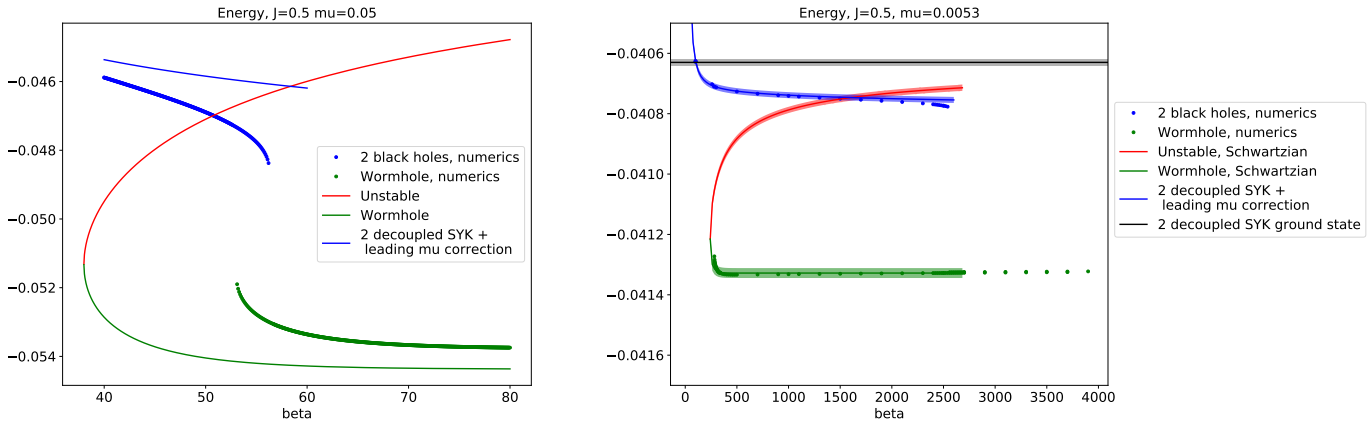

(a) (b)

Figure 4.6: Thermodynamics of the model for two different values of μ/J. In both $J = 0.5$ and in (a) $\mu = 0.05$ and in (b) $\mu = 0.0053$. The dots correspond to numerical solutions of the DS equation. The blue ones for the two black hole phase and the green ones for the cold wormhole phase. The black line is the ground state energy of two decoupled SYK, $2E_{0,SYK}$ (on the left plot it lies above the visible area). Blue curve: the perturbative result (4.2.19) for the energy. Green curve: wormhole branch of eq. (4.2.32). Red curve: unstable branch of eq. (4.2.32). The uncertainties, represented as shaded regions, come from the uncertainties in $E_{0,\text{SYK}}$ and α_S. We see that in (b) the agreement is very good. However, in (a) the agreement is not so good, but the qualitative form of the curve is similar, if we joint the two end points of the dotted lines.

4.3 Real time results

4.3.1 Coupling to a bath

In order to study the real-time formation of the wormhole, we need to cool down the system. Before considering real-time dynamics, first we need to understand how to couple our system to a thermal bath. Ideally we want the bath to be a large system in order to avoid back-reaction.

Generally, we can couple a system's operator $\mathcal{O}_S$ to a bath operator $\mathcal{O}_B$:

$$\Delta S = i^F V \int d\tau \; \mathcal{O}_S \mathcal{O}_B \tag{4.3.39}$$

where F is the fermionic number of $\mathcal{O}_S$.

If V is small and the bath is large we can study this interaction in the Lindblandian approximation by considering the 1-loop result and assuming that there is no back reaction on the bath, such that we can substitute the product $\mathcal{O}_B(t_1)\mathcal{O}_B(t_2)$ by VEV $\langle \mathcal{O}_B(t_1)\mathcal{O}_B(t_2)\rangle_B$:

$$\Delta S = -V^2 \int d\tau_1 d\tau_2 \; \mathcal{O}_S(\tau_1)\mathcal{O}_S(\tau_2)\langle \mathcal{O}_B(\tau_1)\mathcal{O}_B(\tau_2)\rangle_B \tag{4.3.40}$$

For our problem we have a varying temperature that sets an energy scale for the model. Specially for our numerical analysis, it is convenient to choose an interaction that is scale invariant (at least approximately), so that the effects of coupling to the bath are independent of the temperature. Otherwise the bath might be effectively decoupling in some temperature range and the system would take long to cool down.

A natural model for the bath is another SYK, possibly with larger number of fermions. We can consider the bath to be another single-SYK model with $q = q_B$ with large number of fermions M, much larger than the number of fermions in our system N. Recently this problem was studied in [2], we refer to this paper for details. If we denote the bath fermions by χ_α, then the coupling can involve an arbitrary number s of system fermions and p bath fermions.

Again, to warm-up, let us first consider the case when the system consists of a single-SYK model. The coupling between the bath and the system has the form:

$$\mathcal{L}_{\text{bath-system}} = V^{\alpha_1 \dots \alpha_p}_{i_1 \dots i_s} \psi_{i_1} \dots \psi_{i_s} \chi_{\alpha_1} \dots \chi_{\alpha_p} \tag{4.3.41}$$

where V is a random Gaussian-distibuted coupling. By choosing its variance appropriatly, the back reaction can be made of order $N/M \ll 1$. The Euclidean Dyson–Schwinger equations for the system stay the same except for a correction to the self-energy: the self-energy acquires an additional term,

$$\Delta\Sigma = \Sigma_B = \eta G_B^p G^{s-1} \tag{4.3.42}$$

where G_B is bath two-point function and η is proportional to the variance of V.

We can get a marginal interaction with $s = 1, p = 3$, when the bath consists of $q = 4$ SYK models (with, say $J_B = J_S$). This is the bath we will use. More precisely, we introduce two separate baths, one for each SYK factor

$$\mathcal{L}_{\text{bath-system}} = V_i^{\alpha_1\alpha_2\alpha_3}\psi_{L,i}\chi_{\alpha_1}\chi_{\alpha_2}\chi_{\alpha_3} + \tilde{V}_i^{\alpha_1\alpha_2\alpha_3}\psi_{R,i}\tilde{\chi}_{\alpha_1}\tilde{\chi}_{\alpha_2}\tilde{\chi}_{\alpha_3} \tag{4.3.43}$$

where V and $\tilde{V}$ are independent Gaussian-distributed variables. This interaction leaves Σ_{LR} unperturbed, but the other two self-energies have additional terms now:

$$\Delta\Sigma_{LL} = \Delta\Sigma_{RR} = \Sigma_B = \eta G_B^3 \tag{4.3.44}$$

The above equations are written in Euclidean signature. We now turn to Lorentzian equations.

4.3.2 Kadanoff–Baym equations

We now write down the Lorentzian time version of the DS equations. For details see Appendix B.8.

Here we will discuss the non-equilibrum situation following [36] and [37]. It is convenient to work right away on the Keldysh time contour, see [118] for a comprehensive introduction. We will need Lorentzian time correlators which are not time ordered. This can be achieved by introducing a Keldysh time contour which runs from $-\infty$ to $+\infty$ and then back from $+\infty$ to $+\infty$. First, one introduces a Wightman function

$$G_{ab}^{>}(t_1^-, t_2^+) = -i\langle\psi_a(t_1^-)\psi_b(t_2^+)\rangle, \tag{4.3.45}$$

where t_1, t_2 lie on different sides of the contour. This simply means that $\psi_b(t_2)$ is always located to the right of $\psi_a(t_1)$ in the correlator, regardless of time-ordering. This is why the Keldysh contour consists of two parts. Note the overall i in front of the correlator. Since we are dealing

with simple Majorana fermions the "lesser" function $G^<_{ab}$ is given by:

$$G^<_{ab}(t_1,t_2) = -G^>_{ba}(t_2,t_1) \tag{4.3.46}$$

Also we will need retarded and advanced Green functions:

$$\begin{aligned} G^R_{ab}(t_1,t_2) &= \theta(t_1-t_2)\left(G^>_{ab}(t_1,t_2) - G^<_{ab}(t_1,t_2)\right) \\ G^A_{ab}(t_1,t_2) &= \theta(t_2-t_1)\left(G^<_{ab}(t_1,t_2) - G^>_{ab}(t_1,t_2)\right) \end{aligned} \tag{4.3.47}$$

Dyson–Schwinger equations written on the Keldysh contour are known as Kadanoff–Baym equations, and are useful for non-equilibrium situations. Let us write them down explicitly for a single SYK:

$$\begin{aligned} i\partial_{t_1} G^>(t_1,t_2) = \Sigma * G &= \int_{-\infty}^{+\infty} dt \;\; \left(\Sigma^R(t_1,t)G^>(t,t_2) + \Sigma^>(t_1,t)G^A(t,t_2)\right) \\ -i\partial_{t_2} G^>(t_1,t_2) = G * \Sigma &= \int_{-\infty}^{+\infty} dt \;\; \left(G^R(t_1,t)\Sigma^>(t,t_2) + G^>(t_1,t)\Sigma^A(t,t_2)\right) \end{aligned} \tag{4.3.48}$$

where the self-energy $\Sigma^>$ is given by

$$\Sigma^>(t_1,t_2) = -J^2\left(G^>(t_1,t_2)\right)^3 \tag{4.3.49}$$

These equations for the complete system of two interacting SYKs and a bath are derived using the path integral in Appendix B.9.

Remember that the "greater" Green function $G^>(t_1^-,t_2^+)$ has time arguments lying on different sides of the Keldysh contour, this is why we do not have a delta-function on the right hand side of (4.3.48). The integral in the right hand side of (4.3.48), which involves different Green functions, is just a simple convolution $\Sigma * G$ along the Keldysh contour [38]. We can show it by writing the anti-time ordered $\Sigma = \Sigma^> - \Sigma^R$ and the time ordered $G = G^A + G^>$. One can easily see that equations (4.3.48) are casual.

Let us mention one subtlety. Strictly speaking, if one starts from a thermal state, then the precise Keldysh contour involves imaginary time stip at the end of the lower branch, at $t = 0$. This time strip has length β and prepares the thermal state. One can bypass this as follows. First we set the coupling to the bath to zero. Then we find the real time correlators at thermal equilibrium by solving the real time equations imposing the appropriate relations between the Green's functions, see e.g. (B.8.109). We then evolve the system for some time $t \gg \beta$ and then we turn on the coupling to the bath. For more details see Appendix B.10.

For two coupled SYK models one has to be very careful with the μ term. To understand its form on the Keldysh contour we can go back to G, Σ effective action derived in Appendix B.9

$$i\frac{S}{N} = \frac{1}{2}\operatorname{Tr}\log\left(\omega - \Sigma_{ab}(\omega)\right) - \sum_{ab}\int_{\mathcal{C}} dt_1 dt_2 \left(\frac{J^2}{8}G_{ab}(t_1,t_2)^4 + \frac{1}{2}\Sigma_{ab}(t_1,t_2)G_{ab}(t_1,t_2)\right) + \\ + \frac{i\mu}{2}\int_{\mathcal{C}} dt \ \left(G_{LR}(t,t) - G_{RL}(t,t)\right) - \frac{\eta}{2}\int_{\mathcal{C}} dt_1 dt_2 \left(G_{LL}(t_1,t_2) + G_{RR}(t_1,t_2)\right) G_B^3(t_1,t_2) \tag{4.3.50}$$

We see that the μ contribution to $\Sigma(t_1, t_2)$ is

$$\Delta\Sigma_{ab}(t_1,t_2) = i\mu_{ab}\delta_{\mathcal{C}}(t_1 - t_2) \tag{4.3.51}$$

In this expression t_1, t_2 can be on either side of the Keldysh contour, this is why Σ does not have an additional index, like $>, R, A$. Notice that the delta-function $\delta_{\mathcal{C}}$ is defined on the Keldysh contour as well. It yields non-zero answer if and only if $t_1 = t_2$ and t_1, t_2 are on the same side of the contour. Let us compute the contribitution of this term to the convolution $\Sigma * G$ along the Keldysh contour:

$$\Delta(\Sigma * G)(t_1^-, t_2^+)_{ab} = i\mu_{ac}\int_{\mathcal{C}} dt \ \delta_{\mathcal{C}}(t_1^- - t)G_{cb}(t - t_2^+) = i\mu_{ac}G^{>}_{cb}(t_1^-, t_2^+) \tag{4.3.52}$$

The final form of the Kadanoff–Baym equations, including the bath, is:

$$\begin{aligned} i\partial_{t_1} G^{>}_{ab}(t_1,t_2) &= i\mu_{ac} G^{>}_{cb}(t_1,t_2) + \int_{-\infty}^{+\infty} dt \ \left(\Sigma^{R}_{ac}(t_1,t) G^{>}_{cb}(t,t_2) + \Sigma^{>}_{ac}(t_1,t) G^{A}_{cb}(t,t_2)\right) \\ -i\partial_{t_2} G^{>}_{ab}(t_1,t_2) &= -i\mu_{ac} G^{>}_{cb}(t_1,t_2) + \int_{-\infty}^{+\infty} dt \ \left(G^{R}_{ac}(t_1,t) \Sigma^{>}_{cb}(t,t_2) + G^{>}_{ac}(t_1,t) \Sigma^{A}_{cb}(t,t_2)\right) \end{aligned} \tag{4.3.53}$$

where μ_{ab} is defined in eq. (4.2.10) and the self-energy is

$$\Sigma^{>}_{ab}(t_1,t_2) = -J^2 \left(G^{>}_{ab}(t_1,t_2)\right)^3 - \eta \delta_{ab} \left(G^{>}_{B}(t_1,t_2)\right)^3 \tag{4.3.54}$$

4.3.3 Forming the wormhole

Our numerical setup for solving KB equation (4.3.53),(4.3.54) is presented in Appendix B.10. We prepare initial Lorentz Green's functions using Lorentz-time Dyson–Schwinger equations described in Appendix B.8. Our initial Green's functions correspond to two interacting SYK models with non-zero μ at thermal equilibrium. In order to save computational time, the initial temperature is chosen close to (and slightly higher than) the transition temperature T_{2BH}.

We extract the temperature using the Fluctuation-Dissipation Theorem(FDT) for the two-point functions. Precisely, our numerical setup gives us the $G^{>}$ and $G^{<}$ Green's functions. At thermal equilibrium a certain combination of these Green's functions (eq. (B.10.128)) must be equal to $\tanh(\beta\omega/2)$ in the frequency domain. So we take the numerically obtained $G^{>}$ and $G^{<}$, make a discrete Fourier transform and fit eq. (B.10.128) with the tanh. We refer to Appendix B.10 for details about the precise choice of the Green's functions and the frequency domain for fit.

Our benchmark parameters are $J = J_B = 0.5$ (the system and the bath have the same coupling strength), $\mu = 0.05$. In this case, from Figure 4.3 we expect $\beta_{\text{2BH}} \sim 61$, $\beta_c \sim 54$, $\beta_{\text{WH}} \sim 49$.

We considered a few values for the system-bath coupling, $\eta = 0.04,\ 0.02,\ 0.01$. Figure 4.7 shows the results for $\beta_{\text{bath}} = 80,\ \eta = 0.04,\ \beta_{\text{initial}} = 40$ for different time steps. The energy is computed using eq. (B.10.127).

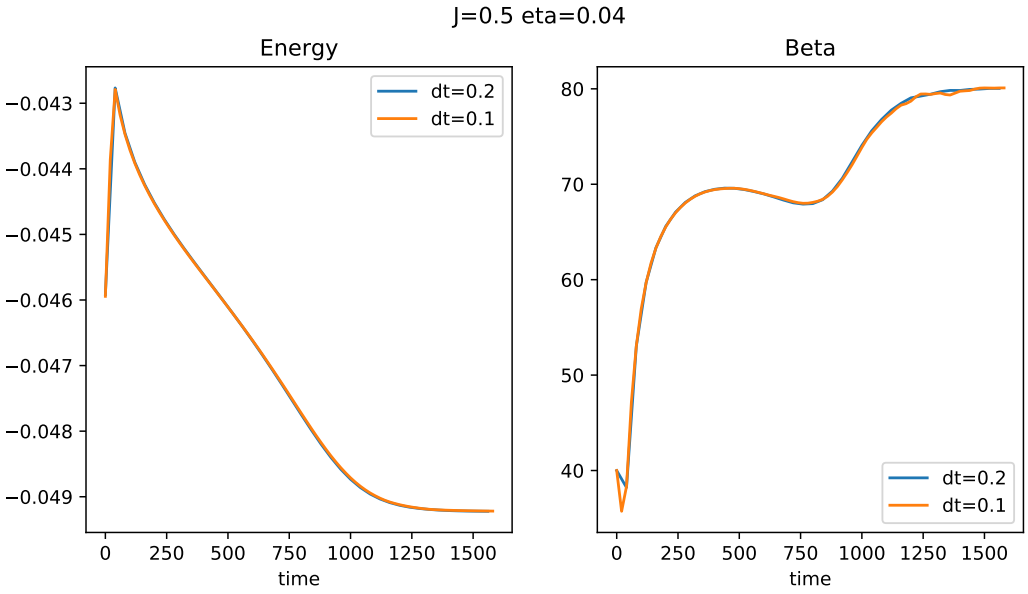

(a) (b)

Figure 4.7: Numerical results for $J = 0.5$ and $\mu = 0.05$, $\beta_B = 80$ and timesteps $dt = 0.2, 0.1$. (a) The energy as a function of time. The initial rise is due to the fact that we are coupling the bath to the system, and this changes the energy [2]. We then see the energy decreasing monotonicallly. (b) The inverse temperature as a function of time. We also see an initial sharp increase due to the coupling of the bath, then we see a decrease. Then a slight increase of the temperature that signals the phase with negative specific heat. Finally the temperature decreases again.

We can perform another check, this time taking η much smaller, namely $\eta = 0.01$. The result is shown on Figure 4.8. A few comments are in order. As is explained in detail in [2] the marginal system-bath interaction we will renormalize J, making it bigger. This is why expect that the actual transition will happen at higher β. This is indeed what we see. Moreover, the interaction with the bath will shift the ground state energy. To compensate for this we have shifted the energy vs beta curve in Figure 4.8 to match the final energy.

The red curve in Figure 4.8 has wild oscillations in temperature near the equilibrium for small η, see also Figures 4.7(b). The reason is the following. Because of the numerical error there is an additional flux of energy which pushes the system out of equilibrium. From the phase diagram

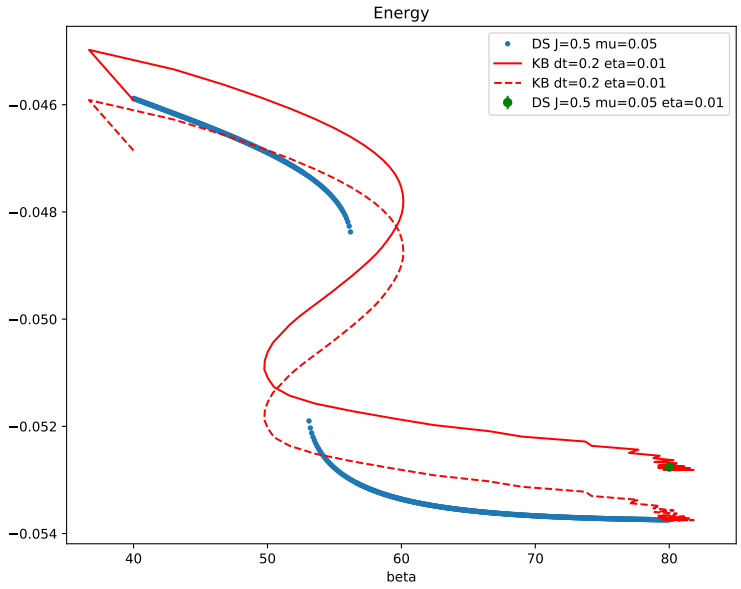

Figure 4.8: The comparison between $E(\beta)$ in equilibrium(blue points) and the real-time evolution of the system as it cools down (solid red line). The bath parameters are $\eta = 0.01$, $\beta_{\text{bath}} = 80$. The initial linear ramp of the red curve occurs because we switch on the coupling with the bath linearly in time. The dashed red line is the same as the solid line but shifted to match the final energy on the phase diagram. The green dot shows the equilibrium value of the system+bath energy.

(blue points) we see that the derivative $d\beta/dE$ is very large. If η is not big enough, the relaxation time is not small enough to smooth out these fluctuations.

The crucial question is whether we indeed have reached *the* wormhole phase or not. In principle, we might have ended up in some other phase. To verify that we have reached the wormhole we can make a precise check of the system's energy.

In the real-simulation the final value of the energy is(in units where $J = 0.5$):

$$E_{\text{KB}} = -0.05282(2) \tag{4.3.55}$$

where the uncertainty comes from changing the size of the diagonal strip and changing the timestep. Also we can ask ourselves how carefully is the initial state prepared. For an exact two-point function we know that $G_{aa}(0) = -0.5i$. However, the iterations of the real-time DS

equations have $G_{aa}(0) = -0.5002i$. The error coming from this is esentially the same as in the above number.

How do we compare this result with the equilibrium phase diagram? In fact, we can solve Euclidean Dyson–Schwinger equation for the coupled system+bath and compare the equilibrium energy. We start from the Euclidean correlators in the wormhole phase, add coupling to the bath and solve the DS equations again. The value of the energy we obtained this way is(again in units where $J = 0.5$):

$$E_{\mathrm{DS}} = -0.05276(3) \tag{4.3.56}$$

It is represented as green dot in Figure 4.8. The uncertainty is estimated by changing the number of discretization points and imposing different cutoffs for the iteration procedure. We see an agreement with (4.3.55) within one standard deviation. This suggests that we indeed reached the wormhole.

To understand what happens near the transition we can look at the maximum value of G_{LR}, see Figure 4.9 (lower part). We can notice that, during the transition through the unstable phase, the imaginary value of the correlator (which is proportional to the anticommutator) rapidly grows, indicating the growth in the information transmission rate.

Another thing we can see is that coupling to a bath generically thwarts the information transmission between the sides; for larger bath coupling η the ratio $\operatorname{Im} G_{LR}/\operatorname{Re} G_{LR}$ is smaller.

Figure 4.8 shows that the system is more or less following the thermodynamic curve. We see that the temperature and energy are smooth everywhere and the transition goes through a phase with negative heat capacity, where the energy decreases and the temperature increases.

To check whether the system remains thermal at all times we performed an additional check. Using the fluctuation dissipation theorem (FDT) we can find the temperature two ways: from LL correlator and the LR correlator, using (B.10.128). The result is shown on Figure 4.9 (upper part). We see that LL correlator is very close to thermal and the curve shows a clear period of temperature increase. In contrast, the temperature extracted from the LR correlator has big errorbars. This means that the LR correlator has larger deviations from precise thermality, and

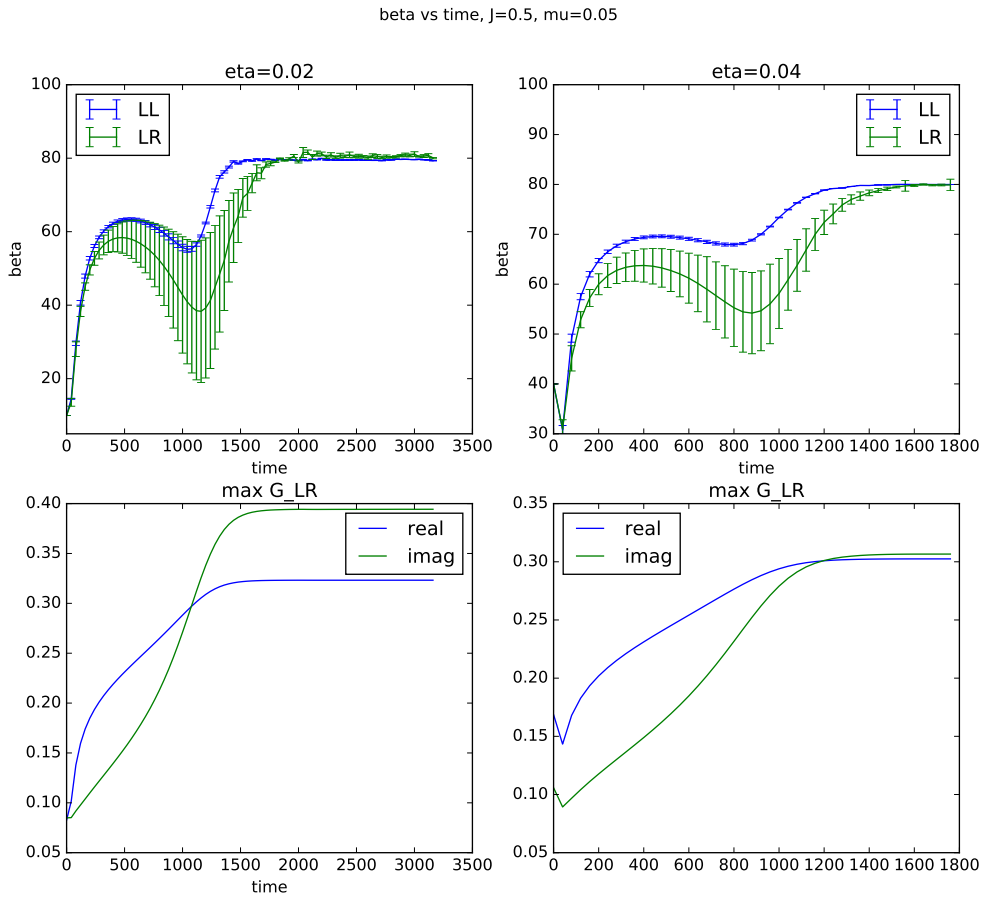

Figure 4.9: (Upper part) β as a function of time for $\eta = 0.02$ and 0.04. The error bars are taken from the covariance matrix, so the meaningful quantity is the relative size between them. (Lower part) the maximum of value of G_{LR} for the same values of η.

larger violations to the relation (B.10.128). We think that this happens for the following reason. We couple each SYK system to its own bath, so we have two uncorrelated baths. This introduces incoherence to the system, which can be seen on Figure 4.9: G_{LR} is decreases when we increase η. Moreover we are in the regime of small μ, which means that the two sides interact weakly, so the equilibration time for G_{LR} is much bigger than for G_{LL}. Therefore we expect that the error bars for LR temperature are big because our system-bath coupling is too big. And, if we managed to cool the system down more slowly, then the LR correlators would remain thermal.

Unfortunately, with our limited computer resources we could not go below $\eta = 0.01$. So we do not have a clear evidence for this interpretation.

4.3.4 Time to form the wormhole

In this subsection we provide analytic estimates for the time it takes to form the wormhole. We will first estimate the time it takes to reach $T_{\rm 2BH}$ and then the time it takes to reach from there to $T_{\rm WH}$. At this point we basically have a cold wormhole, so we will consider it to be already formed. We could also consider it formed once we reach $T_{\rm 2BH}$ and we start moving on the hot wormhole region.

In order to estimate these times we need an expression for the rate of energy emission into the bath. For a general coupling between a system and a large bath the energy loss rate can be written as (see [2] for more discussion)

$$\frac{dE}{dt} = 2i\eta \int_{-\infty}^{+\infty} d\tilde{t}\ \partial_{\tilde{t}} G_{LL}\left(\frac{t+\tilde{t}}{2}, \frac{t-\tilde{t}}{2}\right) G_B(\tilde{t})^3 \tag{4.3.57}$$

where factor of 2 comes from having both sides of coupled to a bath. In the above integral, we can replace the system two point function by the thermal one at the instantaneous temperature, assuming that the temperature varies slowly. Moreover, for SYK at low temperatures we can simply use conformal approximations for two-point functions.

If the bath temperature is much lower, than the system's temperature we can approximate bath Green's function by the zero temperature one

$$G_B = b\frac{1}{\sqrt{J_B i\,(t - i\epsilon)}} \tag{4.3.58}$$

Reaching $T_{\rm 2BH}$

In the two black hole holes phase we assume that G_{LL} is approximated by a single SYK thermal two-point function

$$G_{LL}(t) = b\frac{\sqrt{\pi}}{\sqrt{J\beta i \sinh\frac{\pi(t-i\epsilon)}{\beta}}} \tag{4.3.59}$$

Plugging these into (4.3.57) we see that the answer is determined by dimensional analysis up to an irrelevant numerical coefficient[3]:

$$\frac{dE}{dt} = -\,\text{const}\,\frac{\eta}{J_B^{3/2}\sqrt{J}\beta^2} \tag{4.3.60}$$

Differentiating the energy expression (4.2.20) with respect to the time, and solving a simple differential equation for $\beta(t)$, we find that it grows exponentially

$$\beta(t) \sim \beta_{\text{init}} \exp\left(\text{const}\,\frac{\eta\sqrt{J}t}{J_B^{3/2}}\right) \tag{4.3.61}$$

So that the time $\Delta t_{2\text{BH}}$ needed to go through the two black hole phase and reach $T_{2\text{BH}} \sim \mu^2/J$ depends only logarithmically on μ:

$$\Delta t_{2\text{BH}} \sim \frac{J_B^{3/2}}{\sqrt{J}\eta}\log\frac{J}{\mu^2\beta_{\text{init}}} \tag{4.3.62}$$

Reaching T_{WH}

Now let us calculate time Δt_{WH} which is needed to go through the hot wormhole phase and reach T_{WH}. To this end we will employ some results from the end of Section 4.2.3 about Schwarzian. This Schwarzian approximation breaks for very hot wormholes with temperature of order $T_{2\text{BH}}$, but holds for lower temperatures.

Suppressing the numerical coefficients, G_{LL} in this regime is given by:

$$G_{LL}(t) \propto \frac{\sqrt{\mathbf{t}'}}{\sqrt{J\sin\left(\mathbf{t}'(t-i\epsilon)\right)}} \tag{4.3.63}$$

where $\mathbf{t}'(t)$ is determined by the solution of eq. (4.2.32). The hot wormhole(unstable branch) is characterized by having $\mathbf{t}' \ll 1$, so eq. (4.2.32) can be simplified by neglecting Schwarzian kinetic

[3]We refer to [2] for the numerical coefficient.

term (the first term in eq. (4.2.32))

$$\exp\left(-\mathbf{t}'\beta/4\right) \sim \frac{\mu}{\mathbf{t}'^{1/2}} \tag{4.3.64}$$

This approximation breaks down near $T \sim T_{\rm WH}$, so we further assume that we use this approximation for temperatures which are slightly below or of order $T_{\rm WH}$.

From this equation, up to a logarithmic term in μ, $\mathbf{t}'$ and β are related by $\mathbf{t}' \sim 1/\beta$. Using (4.3.64), the energy (4.2.37) can be written as

$$E - 2E_{0,\rm SYK} \propto -\frac{\mu}{\sqrt{J\beta}} \tag{4.3.65}$$

We see that the heat capacity is negative

$$C_{\text{hot wormhole}} = \frac{dE}{dT} = -\beta^2 \frac{dE}{d\beta} \propto \frac{\mu\sqrt{\beta}}{\sqrt{J}} \tag{4.3.66}$$

We can compare the absolute value of this expression with the heat capacity of a regular SYK $C_{\rm SYK} \sim \frac{1}{J\beta}$

$$\frac{|C_{\text{hot wormhole}}|}{C_{\rm SYK}} \propto \mu\sqrt{J}\beta^{3/2} \propto \left(\frac{T_{\rm WH}}{T}\right)^{3/2} \tag{4.3.67}$$

This ratio is much bigger than 1 for $\beta \gg 1/(J^{1/3}\mu^{2/3}) \sim \beta_{\rm WH}$. So apart from the region close to $T_{\rm WH}$ the hot wormhole has a large negative heat capacity, compared to a single SYK model at the same temperature.

The energy flux can be computed using the expression (4.3.63) for G_{LL}. The result is again determined by scale symmetry and it is again proportional to $\mathbf{t}'^2 \sim 1/\beta^2$ as in (4.3.60). However, because of the big negative heat capacity, the time it takes to go through this region is much longer than (4.3.62). Solving for $\beta(t)$ we get

$$\beta_0^{3/2} - \beta_1^{3/2} = \frac{\eta}{\mu J_B^{3/2}} \left(t_1 - t_0\right) \tag{4.3.68}$$

In our case we start from $\beta_0 \sim \beta_{\rm 2BH}$ and end with $\beta_1 \sim \beta_{\rm WH}$. Since $\beta_{\rm 2BH} \gg \beta_{\rm WH}$ the overall time length is mostly determined by the region near $T_{\rm 2BH}$:

$$\Delta t_{\rm WH} \sim \frac{J^{3/2} J_B^{3/2}}{\eta \mu^2} \tag{4.3.69}$$

This timescale is much larger than $\Delta t_{\rm WH}$, (4.3.62), which scaled only logarithmically in μ. Moreover, it is mostly determined by the region near $T_{\rm 2BH}$, which is where the approximation is breaking down. So (4.3.69) should only be viewed as an order of magnitude estimate.

Our numerical results for $\beta(t)$ on Figures 4.7 and 4.9 seem to qualitatively support these conclusions. Notice that, as expected, the times are inversely proportional to the coupling to the bath η.

4.4 Two coupled black holes in gravity

The low energy description of the SYK model has some features in common with certain two dimensional theories of gravity. In this section, we study a similar problem in a gravitational theory in order to compare to the answers we found above.

We consider a Jackiw-Teitelboim theory of gravity coupled to matter, see [116, 115, 103] for details. This gravity theory describes a two dimensional black hole with an AdS_2 geometry. The AdS_2 space has a boundary. We consider a system containing two such black hole exteriors and we introduce a coupling for the two dimensional matter fields propagating in the bulk. We assume that have N such matter fields. Let us say that χ is a matter field with a certain mass m in the bulk and quantized with Neumann boundary conditions so that its dimension is Δ, with $\Delta < 1/2$. We couple their boundary values through a term, for each field,

$$S = i\tilde{\mu} \int du \chi_L(u) \chi_R(u) \ , \qquad \tilde{\mu} = \frac{\mu}{J^{2\Delta}} \tag{4.4.70}$$

were we imagine that J^{-1} is related to a cutoff in the radial AdS_2 direction[4] and u is the physical boundary time.

4.4.1 High temperature phase

We now consider the high temperature phase where in Euclidean space we have two separate disks that are connected through the interaction (4.4.70). Concentrating on the matter system, this interaction is easy to analyze because the full matter theory is just quadratic. In principle, we also need to consider the effects of gravity, and we will discuss them later. This interaction, (4.4.70), leads to the Feynman diagrams in Figure 4.10(a), which can be easily summed, as we explain below. Since the interaction is relevant, it becomes important at low temperatures. For sufficiently low temperatures, the net effect is to change the boundary conditions for the bulk fermions χ from Neumann to Dirichlet. Namely, at low temperatures we get two decoupled disks with Dirichlet boundary conditions for bulk fermions. We now discuss this more explicitly.

When $\tilde{\mu} = 0$ we have two separate disks and the matter partition function is just given by Z_N^2, namely the square of the partition function of a fermion with Neumann boundary conditions. Starting from this state we can now sum the diagrams in Figure (4.10)(a). For each fermion field, we get

$$Z_\mu = Z_N^2 \exp\left\{\frac{1}{2} Tr[\log(1+i\tilde{\mu}G)(1-i\tilde{\mu}G)]\right\} = Z_N^2 \ \left[\det(1+\tilde{\mu}^2 G_\Delta^2)\right]^{\frac{1}{2}} \tag{4.4.71}$$

where we think of $G(u_1, u_2) \propto [\sin \frac{u_1-u_2}{2}]^{-2\Delta}$ as a matrix with indices u_1, u_2. We have set $\beta = 2\pi$ for simplicity and we will restore it later.

For large $\tilde{\mu}$ we find that the partition function gets an additional factor of the determinant of G_Δ. It turns out that this produces the Dirichlet partition function [127, 128]

$$Z_{\tilde{\mu}\gg 1} = Z_N^2 \det G_\Delta e^{-\epsilon(\tilde{\mu})\beta} \propto Z_D^2 \ , \qquad \epsilon(\tilde{\mu}) \propto -(\tilde{\mu})^{\frac{1}{1-2\Delta}} \tag{4.4.72}$$

[4]With the AdS metric $ds^2 = (dx^2 + dz^2)/z^2$, this is the cutoff at $z = \epsilon$, and we are defining $J = 1/\epsilon$.

In the last equality we neglected the energy contribution, since we will be focusing on the ground state entropy contributions.

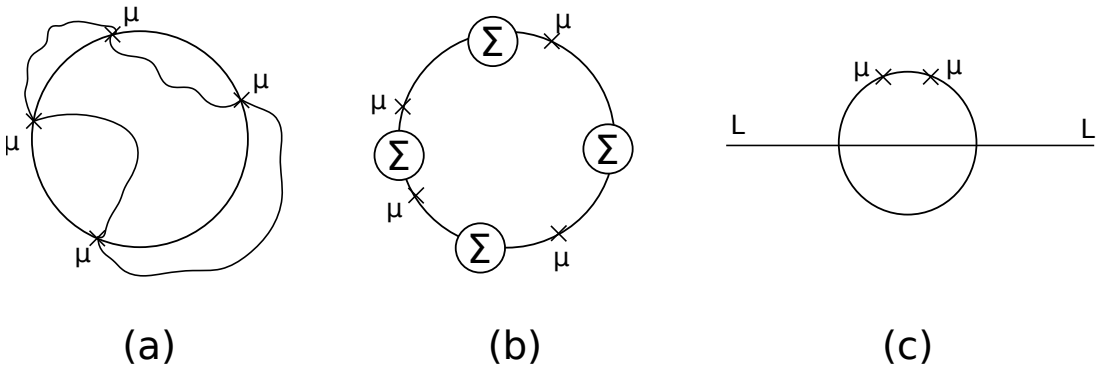

Figure 4.10: (a) Field theory diagrams when we add an interaction term $i\tilde{\mu}\chi_L\chi_R$ at the boundary of two disks. Here we picture one disk and the second as the outside. So $\chi^L\chi^L$ propagators are the ones inside the disk and $\chi^R\chi^R$ are outside the disk. (b) Diagrams in the two coupled SYK model that reproduce the field theory diagrams in (a). (c) An example of a diagram in the two coupled SYK model that is not present in field theory.

The conclusion is that if we start out with two disks with Neumann boundary conditions, after we turn on the relevant perturbation (4.4.70), for very low temperatures we get two decoupled disks again but with Dirichlet boundary conditions. This implies that for very low temperatures, the bulk fermion would be dual to an operator of dimension $1-\Delta$.

Restoring the factors of β, this transition happens at $\beta_{2\text{BH}}$ given by

$$1 \sim \tilde{\mu}\beta_{2\text{BH}}^{1-2\Delta} \ , \qquad \text{or} \qquad T_{2\text{BH}} \propto \left(\frac{\mu}{J^{2\Delta}}\right)^{\frac{1}{1-2\Delta}} \tag{4.4.73}$$

For $q = 4$ this reproduces (4.2.24). This is not surprising because we were summing the same type of diagrams. However, in the gravity case these are all the diagrams, so we can study the whole flow. The new IR fixed point simply corresponds to flipping the boundary conditions to Dirichlet. So nothing too dramatic happens in the gravity solution when we go to temperatures lower than the temperature $T_{2\text{BH}}$ in (4.4.73), except that the change in the boundary conditions will change the value of the ground state entropy.

In this discussion, we have ignored the dynamics of gravity. In principle, we could wonder whether we should consider non-trivial solutions of the Schwarzian theory. If we assume that the solution is invariant under translations for each disk, then, up to gauge symmetries of the Schwarzian theory, the only solution is the usual one. In Appendix B.7, we examine whether non-constant Schwarzian modes could lower the action. We find that they do not, at least in the approximation we considered. In our analysis we assumed that gravity is classical, which is correct if $\phi_r/\beta \gg 1$. Here ϕ_r is the JT gravity analog of the coefficient of the Schwarzian, the analog of $N\alpha_S/\mathcal{J}$. We have also assumed that we have a relatively low number of bulk quantum fields so that the effects of integrating them out does not significantly change the value of S_0, the ground state entropy. This is the regime where the gravity theory is simplest. As we will discuss below, the SYK model is different in this respect.

4.4.2 Low temperature phase

At very low temperatures the coupling (4.4.70) leads to the formation of a wormhole [122]. This is identical to the small μ coupled SYK model analysis of section 4.2.3, since the effects of gravity can also be described in terms of the Schwarzian mode.

When we decrease the temperature along the negative specific heat region (the hot wormhole phase), the wormhole is getting longer and longer. Or, more precisely, there is a larger redshift factor between the boundary and the center of the wormhole. Then, the interaction, which is a relevant deformation, becomes stronger. When we considered the problem for the disks, we found that for strong interactions we get an effective change in boundary conditions from Neumann to Dirichlet. Here we expect the same phenomenon when $\mathbf{t}'$ is becomes

$$\mathbf{t}' \propto T_{2\text{BH}} \propto \left(\frac{\mu}{J^{2\Delta}}\right)^{\frac{1}{1-2\Delta}} \tag{4.4.74}$$

where $\mathbf{t}'$ is the variable in (4.2.32), which is proportional to the value of the redshift factor at the center of the wormhole. In other words, $\mathbf{t}'$ becomes of the order of the temperature $T_{2\text{BH}}$ in (4.4.73). We refer to Appendix B.11 for details. At this value of $\mathbf{t}'$ the wormhole is so long that

the approximations used in deriving (4.2.33) are no longer valid. Interestingly, due to (4.2.35), this happens also at a temperature of the order of $T_{2\text{BH}}$, which is the temperature where the two disk solutions starts being corrected. This might appear as a coincidence, but it is not. In the hot wormhole phase we find that the temperature sets the value of $\mathbf{t}'$ and thus the amount of RG flow that the relevant left-right interaction undergoes. Therefore, this interaction becomes relevant at the same place.

This statement can be further verified by checking whether the hot wormhole thermodynamic curve (red curve in figure 4.6) will join with the two black hole phase (blue curve in figure 4.6) at $T = T_{2\text{BH}}$. In the hot wormhole phase the energy is given by (4.3.65) and in the two black hole phase by (4.2.19). Indeed, the two curves join at $T \sim T_{2\text{BH}}$.

In a gravity theory with a relatively low number of fields, we expect that after $T_{2\text{BH}}$ the wormhole phase might not exist any longer.

One conclusion is that, in a general JT gravity theory plus matter, we do *not* seem to be able to easily join the high temperature phase and the hot wormhole phase. This is mysterious in the gravity theory because it involves a topology change. Of course, the low temperature phase and the hot wormhole phase are connected smoothly at T_{WH} in a region where we can trust the wormhole analysis in the Schwarzian approximation, as discussed near (4.2.33).

4.4.3 Comparison with the SYK model

In the SYK model, the addition of the interaction corrects the original diagrams by inserting μ terms in the propagators. If we insert them outside the self energy correction (the Σ bubble), then we get diagrams which are identical to the ones we discussed in gravity, see Figure 4.10(b). However, in the SYK model we can also insert μ inside the self energy corrections, these are new diagrams that are not present in the gravity discussion, see Figure (4.10)(c).

As we mentioned above the region of the phase diagram near temperatures $T \sim T_{2\text{BH}}$ is different in a generic JT gravity theory plus matter than in SYK. However, we can consider the folloing gravitations model that would look more *qualitatively* similar to the SYK model.

First we note that the SYK ground state entropy is given by $S_0 = Ns_0$, where s_0 is given by [17, 127]

$$e^{s_0} = (\det G_\Delta)^{-\frac{1}{2}} = \frac{Z_N}{Z_D} , \qquad \text{for one Majorana fermion} \tag{4.4.75}$$

where the first equality follows from the usual G, Σ action at low energies. The second equality was mentioned in (4.4.72). This implies that if we want to describe the SYK model in terms of JT gravity, we should think that when the fermions have Dirichlet boundary conditions, the net entropy, or value of the topological terms in the action should be zero, $\phi_0 = 0$. Then the actual value of the ground state entropy of the usual, single boundary SYK model, (4.4.75), is simply given by the contribution of changing the boundary condition for the bulk fields from Dirichlet to Neumann [127].

Returning now to the coupled model and starting from the high temperature phase, we see that when we reach the temperature $T_{2\text{BH}}$ we are changing to a Dirichlet boundary condition. This means that the total S_0 now becomes zero, which implies that the topology change is easy. Similarly, if we start from the canonically unstable wormhole phase and approach $T_{2\text{BH}}$, we also see a change in the boundary conditions so that S_0 again becomes zero and topology change is easy. So we can join the two phases with a change in topology at $T_{2\text{BH}}$. In this way we can *qualitatively* understand the transition. We have given evidence that this is a smooth transition in the coupled SYK model. What we are discussing here is just a cartoon for a gravity picture of what is happening.

We also see why SYK is different than a generic JT gravity theory with a smaller number of fields. In such gravity theories the flow from Neuman to Dirichlet would not change S_0 by too much and the topology change remains suppressed. For this reason we have not been able to see a general mechanism for the transition that would also work in more general gravity theories, such as the Standard Model in the presence of magnetically charged black holes as discussed in [125].

4.5 Conclusion

In this chapter we studied the approach to the ground state of the two coupled SYK models [122]. We first discussed the equilibrium thermodynamics picture. In the microcannonical ensemble we expect a continuous picture with no phase transition. As the energy decreases, the temperature decreases up to a value $T_{\rm 2BH}$ where the system looks like two separate thermal SYK models with a small coupling. At $T_{\rm 2BH}$ this coupling becomes strong and the system transitions to a "hot wormhole" phase with negative specific heat. Now the temperature increases up to $T_{\rm WH}$ and then the wormhole becomes cooler and shorter, and the specific heat becomes positive again. This whole picture can be understood using simple analytic approximations, except for the transition region at $T \sim T_{\rm 2BH}$.

We found that the real time evolution looked as if the system is following the above equilibrium phase diagram. Unfortunately, for the parameters we could use in our numerical computation, we could not trust quantitatively the simple analytic approximations. However, these gave a qualitatively correct answer. The system remained near thermal equilibrium as it cooled down, except for some deviations in the G_{LR} correlator, which we think should disappear if we were to cool more slowly.

The conclusion is that, starting with a generic state of the two coupled SYK model, we can find the ground state by coupling the system to the bath and cooling it down. In particular, the system does not get stuck in a metastable state. This provides a feasible way to produce a state close to the TFD.

We also computed the time to form the wormhole. Most of the time is spent near the region with $T \sim T_{\rm 2BH}$.

One of our goals was to extract some general lessons for wormhole formation in gravity. Unfortunately, the SYK model seems to be special, and its special features becomes manifest in the ease by which we can connect the two black hole phase with the hot wormhole phase near $T \sim T_{\rm 2BH}$. These two phases do not seem to be so easy to connect in more general theories of

gravity. We qualitatively explained why topology is simpler in a gravity theory that is similar to the SYK model, but harder in a more general theory of gravity.

Nevertheless we cannot say how hard forming a wormhole would be in a more general theory of gravity, such as the one describing the wormholes in [125]. It seems hard, but maybe there is an "easy" pathway to form it. It would be interesting to answer this question.

We expect that this article would be relevant for efforts that try to do it using the SYK model, see the proposal in [129], for example.

Chapter 5

Spectra of Eigenstates in Fermionic Tensor Quantum Mechanics

5.1 Introduction and Summary

In recent literature there has been considerable interest in the quantum mechanical models where the degrees of freedom are fermionic tensors of rank 3 or higher [19, 20]. These models have solvable large N limits dominated by the so-called melonic diagrams. Such novel large N limits were discovered and developed in [39, 40, 41, 42, 43, 44, 45, 47, 48], mostly in the context of zero-dimensional tensor models with multiple $U(N)$ or $O(N)$ symmetries (for reviews, see [18, 46, 130]). The quantum mechanical tensor models are richer: they have interesting spectra of energy eigenstates and may have connections with physical systems like the quantum dots. More amibitiously, large N tensor quantum mechanics may provide a dual description of two-dimensional black holes [121, 116, 103, 115], in the sense of the gauge/gravity duality [5, 55, 56]. The original motivation [19] for introducing the tensor quantum mechanics is that they have a large N limit similar to the one in the Sachdev-Ye-Kitaev (SYK) model [16, 131, 88, 17], but without the necessity of the disorder. Indeed, as shown explicitly in [20], the 2- and 4-point functions in the large N tensor models are governed by the same Schwinger-Dyson equations as were derived earlier for the SYK-like models [17, 90, 36, 132, 133].

At the same time, there are significant differences between the tensor and SYK-like models. An early hint was the different scaling of the corrections to the large N limit [19] (see also the further work in [134, 135, 136, 137]); more recently, additional evidence for the differences is emerging in the operator spectra and Hagedorn transition [138, 139, 140]. The formal structure of the two types of models is indeed quite different: the SYK-like models containing a large number of fermions, $N_{\rm SYK}$, have no continuous symmetries (although an $O(N_{\rm SYK})$ symmetry appears in the replica formalism), while in the tensor models one typically encounters multiple symmetry groups. For example, in the Gurau-Witten (GW) model [19] containing 4 Majorana rank-3 tensors, the symmetry is $O(N)^6$; there is evidence [134, 138] that this model is the tensor counterpart of a 4-flavor generalization of the SYK model introduced in [133]. A simpler tensor quantum mechanics with a single rank-3 Majorana tensor has $O(N)^3$ symmetry [20] and is the tensor counterpart of the basic SYK model with real fermions. The quantum mechanics of complex rank-3 fermionic tensor, which has $SU(N)^2 \times O(N) \times U(1)$ symmetry [20], is the tensor counterpart of the variant of SYK model where real fermions are replaced by complex ones [141].

The absence of disorder and the presence of the continuous symmetry groups in the tensor models endows them with a number of theoretical advantages, but also makes them quite difficult to study. In the tensor models any invariant operator should be meaningful and be assigned a definite scaling dimension in the large N limit. While the simplest scaling dimensions coincide with those in the corresponding SYK-like models, the operator spectrum in tensor models is much richer: the number of $2k$-particle operators grows as $2^k k!$ [138, 139, 140].

Beyond the operator spectrum, it is interesting to investigate the spectrum of eigenstates of the Hamiltonian. While this spectrum is discrete and bounded for finite N, the low-lying states become dense for large N leading to the (nearly) conformal behavior where it makes sense to calculate the operator scaling dimensions. In the SYK model, the number of states is $2^{N_{\rm SYK}/2}$, and numerical calculations of spectra have been carried out for rather large values of $N_{\rm SYK}$ [92, 142]. They reveal a smooth distribution of energy eigenvalues, which is almost symmetric under $E \to -E$; it exhibits little sensitivity to the randomly chosen coupling constants J_{ijkl}.

Such numerical studies of the SYK model have revealed various interesting physical phenomena, including the quantum chaos.

The corresponding studies of spectra in the GW model [19] and the $O(N)^3$ model [20] have been carried out in [143, 50, 51, 144, 52, 145, 146], but in these cases the numerical limitations have been more severe – the number of states grows as $2^{N^3/2}$ in the $O(N)^3$ model and as 2^{2N^3} in the GW model. This is why only the $N = 2$ GW model and $N = 2, 3$ $O(N)^3$ models have been studied explicitly so far.[1] Furthermore, in the tensor models the states need to be decomposed into various representations of the symmetry groups. As a result, the details of the energy spectrum in the $O(N)^3$ tensor model are quite different from those in the corresponding SYK model with $N_{\rm SYK} = N^3$ fermion species.

The goal of this work is to improve our understanding of energy spectra in the tensor models. We will mostly focus on the simplest tensor model with $O(N)^3$ symmetry [20] and its generalization to $O(N_1) \times O(N_2) \times O(N_3)$, where the Majorana tensor degrees of freedom are ψ^{abc} with $a = 1, \ldots, N_1$; $b = 1, \ldots, N_2$; $c = 1, \ldots, N_3$, and anti-commutation relations

$$\{\psi^{abc}, \psi^{a'b'c'}\} = \delta^{aa'}\delta^{bb'}\delta^{cc'} \, . \tag{5.1.1}$$

The Hamiltonian is taken to be of the "tetrahedral" form [47, 20]

$$H = \frac{g}{4}\psi^{abc}\psi^{ab'c'}\psi^{a'bc'}\psi^{a'b'c} - \frac{g}{16}N_1N_2N_3(N_1 - N_2 + N_3) \, , \tag{5.1.2}$$

and we have added a shift to make the spectrum traceless. In section 5.2 we discuss some essential features of this model, including its discrete symmetries. In section 5.3 we will derive lower bounds on the energy in each representation of $SO(N_1) \times SO(N_2) \times SO(N_3)$. We will show that, in the melonic large N limit where $gN^{3/2} = J$ is kept constant, the most stringent bounds (5.3.38) scale as JN^3, in agreement with expectations for a system with N^3 degrees of freedom. On the other

[1] In [146] the exact values of the 140 singlet energies in the $O(2)^6$ GW model were found to square to integers. Due to the discrete symmetries of the GW model, there are only 5 distinct $E < 0$ eigenvalues (the singlet spectrum also contains 50 zero-energy states). For these reasons the singlet spectrum of the $O(2)^6$ GW model exhibits significant gaps.

hand, the splitting between lowest states in different representations is found to be of order J/N. Another derivation of this fact, based on effective action considerations, is presented in section 5.4. While this gap vanishes in the large N limit, we expect the splitting between states in the same representation to vanish much faster, i.e. as c^{-N^3}, where c is a positive constant. Such small singlet sector gaps are needed to account for the large low-temperature entropy, which is given by the sum over melonic graphs and, therefore, has to be of order N^3.

If the global symmetry of the quantum mechanical model is gauged, this simply truncates the spectrum to the $SO(N_1) \times SO(N_2) \times SO(N_3)$ invariant states. In section 5.5 we derive integral formulae for the number of singlets as functions of the ranks N_i. They lead to the conclusion that the singlets are present only when all N_i are even. The absence of singlets when some of N_i are odd can often be related to anomalies, which we discuss in section 5.5.2. For the $O(N)^3$ model, the number of singlet states is shown in Table 1; it exhibits rapid growth from 2 for $N = 2$, to 36 for $N = 4$, to 595354780 for $N = 6$. Thus, even though the $O(4)^3$ model is out of reach of complete numerical diagonalization because it has 64 Majorana fermions, in contrast to the SYK model with $N_{\text{SYK}} = 64$, it is far from the nearly conformal large N limit. Indeed, since the spectrum is symmetric under $E \to -E$ [138], the number of distinct singlet eigenvalues with $E < 0$ cannot exceed 18. Therefore, there are significant gaps in the singlet spectrum of the $O(4)^3$ model. On the other hand, the presence of the vast number of singlet states for the $O(6)^3$ model suggests that the low-lying singlet spectrum should be dense for $N = 6$ and higher. For large N the number of singlets grows as $\exp\left(N^3 \log 2/2 - 3N^2 \log N/2\right)$. Since all of these states must fit in an energy interval of order N^3, it is plausible that the gaps between low-lying singlet states vanish as c^{-N^3}.

The $O(N_1) \times O(N_2) \times O(N_3)$ tensor model (5.1.2) may be viewed as N_3 coupled Majorana $N_1 \times N_2$ matrices [49, 147]. As discussed in section 5.6.1, for $N_3 = 1$ we find a one-matrix model with $O(N_1) \times O(N_2)$ symmetry, which is exactly solvable because the Hamiltonian may be written in terms of a quadratic Casimir. When we set $N_3 = 2$ we find a complex $N_1 \times N_2$ matrix model with $O(N_1) \times O(N_2) \times U(1)$ symmetry. It may be studied numerically for values of N_1 and N_2 as large as 4 and reveals a spectrum which is integer in units of $g/4$. In section 5.6.3 we explain why

this fermionic matrix model is again exactly solvable and derive a concise expression (5.6.103) for its spectrum. When both N_1 and N_2 are even, so that the spectrum contains singlet states, we show that the ground state is a singlet. In section 5.6.2 we apply similar methods to another complex matrix model, which was introduced in [148] and has $SU(N_1) \times SU(N_2) \times U(1)$. It is the $N_3 = 1$ case of the complex tensor quantum mechanics with $SU(N_1) \times SU(N_2) \times O(N_3) \times U(1)$ symmetry [20]. We show that the Hamiltonian of this model may be expressed in terms of the symmetry charges. The solvable matrix models presented in section 5.6 have standard 't Hooft limits when $N_1 = N_2 = N$ is sent to infinity while $\lambda = gN$ is held fixed. Then the low-lying states have energies $\sim \lambda N^2$, while the splittings are of order λ. So, in contrast to the melonic large N limit, the energy levels don't become dense in the 't Hooft limit of the matrix models. Nevertheless, these fermionic matrix models are nice examples of exactly solvable 't Hooft limits.

5.2 The rank-3 tensor model and its symmetries

The $O(N_1) \times O(N_2) \times O(N_3)$ tensor model is specified by the action

$$S = \int dt \left(\frac{i}{2} \psi^{abc} \partial_t \psi^{abc} - H \right) , \tag{5.2.3}$$

where H is given in (5.1.2). Sometimes it will be convenient to use capital letters $A, B, \ldots$ to denote the multi-index, i.e. $A = (a, b, c)$. It is easy to see that the Hamiltonian (5.1.2) has a traceless spectrum: [2]

$$\sum_i d_i E_i = 0 , \qquad \sum_i d_i = 2^{[N_1 N_2 N_3/2]} , \tag{5.2.4}$$

where d_i is the degeneracy of eigenvalue E_i.

We can make some general restrictions on the possible values of the energies. Operators ψ obeying the anti-commutation relation (5.1.1) may be represented as the Majorana γ-matrices in $N_1 N_2 N_3$– dimensional Euclidean space. They have entries which, in our conventions, are integers divided by $\sqrt{2}$. As a result, the Hamiltonian is an integer matrix times $g/16$. It is a well-known

[2] One can easily compute $\mathrm{tr}(\psi^{abc}\psi^{ab'c'}\psi^{a'bc'}\psi^{a'b'c}) = \frac{1}{4} N_1 N_2 N_3 (N_1 - N_2 + N_3)$ working with ψ^{abc} as with a set of gamma matrices.

mathematical fact that such matrices cannot have rational eigenvalues. Therefore, in units of $g/16$, the energy eigenvalues have to be either integer or irrational numbers. The explicit results we will find are in agreement with this.

The discrete symmetries of the theory depend on whether some of the ranks are equal. In a $O(N_1) \times O(N)^2$ theory, $N_1 \neq N$, we may study interchange of the two $O(N)$ groups, which acts as $\psi^{abc} \to \psi^{acb}$. The invariant operators can be divided into even or odd under the interchange. The Hamiltonian (5.1.2) is odd [138], which implies that the energy spectrum is symmetric under $E \to -E$.

Let us construct the operator which implements the interchange $\psi^{abc} \to \psi^{acb}$:

$$P_{23} = 2^{N^2(N_1+1)/2} \prod_{a,b=c} \psi^{abc} \prod_{a,b>c} \left(\frac{\psi^{abc} + \psi^{acb}}{\sqrt{2}} \right). \tag{5.2.5}$$

This operator has the following properties

$$P_{23}^\dagger P_{23} = 1, \quad P_{23}^\dagger = \pm P_{23}, \quad P_{bc}^\dagger \psi^{abc} P_{bc} = (-1)^{N^2(N_1+1)/2+1} \psi^{acb}. \tag{5.2.6}$$

Due to the last relation one can check

$$\begin{aligned} P_{bc}^\dagger H P_{bc} &= P_{bc}^\dagger \left(\frac{g}{4} \psi^{abc} \psi^{ab'c'} \psi^{a'bc'} \psi^{a'b'c} - \frac{g}{16} N_1 N_2 N_3 (N_1 - N_2 + N_3) \right) P_{bc} = \\ &= \frac{g}{4} \psi^{acb} \psi^{ac'b'} \psi^{a'c'b} \psi^{a'cb'} - \frac{g}{16} N_1 N_2 N_3 (N_1 - N_2 + N_3) = \\ &= -\frac{g}{4} \psi^{abc} \psi^{ab'c'} \psi^{a'bc'} \psi^{a'b'c} + \frac{g}{16} N_1 N_2 N_3 (N_1 - N_2 + N_3) = -H \,, \end{aligned} \tag{5.2.7}$$

where we have renamed the repeated indices in the second line and used the anti-commutation relations (5.1.1) in the third line. Let us consider any state that is an eigenvector of the P_{23}, it exists because P_{23} is either hermitian or antihermitian

$$P_{23}|\lambda\rangle = \lambda|\lambda\rangle, \quad 1 = \langle\lambda|\lambda\rangle = \langle\lambda|P_{23}^\dagger P_{23}|\lambda\rangle = |\lambda|^2 \langle\lambda|\lambda\rangle = |\lambda|^2. \tag{5.2.8}$$

The energy of such state is equal to zero. Indeed,

$$E = \langle\lambda|H|\lambda\rangle = -\langle\lambda|P_{bc}^{\dagger} H P_{bc}|\lambda\rangle = -|\lambda|^2\langle\lambda|H|\lambda\rangle = -E, \quad E = 0 \tag{5.2.9}$$

Let us now discuss the case when all three ranks are equal and we have $O(N)^3$ symmetry. Then the invariant operators form irreducible representations of the group S_3 which interchanges the 3 $O(N)$ groups. The Hamiltonian is in the sign representation of degree 1: it is invariant under the even permutations and changes sign under the odd ones. Therefore, the symmetry of the Hamiltonian is the alternating group A_3, which is isomorphic to Z_3.

The $SO(N_i)$ symmetry charges are

$$Q_1^{aa'} = \frac{i}{2}[\psi^{abc}, \psi^{a'bc}] \ , \qquad Q_2^{bb'} = \frac{i}{2}[\psi^{abc}, \psi^{ab'c}] \ , \qquad Q_3^{cc'} = \frac{i}{2}[\psi^{abc}, \psi^{abc'}] \ . \tag{5.2.10}$$

In addition, each $O(N_i)$ group contains Z_2 parity symmetries which are axis reflections. Inside $O(N_1)$ there are parity symmetries $P^{a'}$: for a given a', $P^{a'}$ sends $\psi^{a'bc} \to -\psi^{a'bc}$ for all b, c and leaves all $\psi^{abc}, a \neq a'$ invariant. It is not hard to see that the corresponding charges are

$$P^{a'} = 2^{N_2 N_3} \prod_{bc} \psi^{a'bc} \tag{5.2.11}$$

One can indeed check that

$$\left(P^{a'}\right)^{\dagger} \psi^{abc} P^{a'} = (-1)^{\delta_{a,a'} + N_2 N_3} \psi^{abc} \ . \tag{5.2.12}$$

Similarly, there are Z_2 charges inside $O(N_2)$ and $O(N_3)$. A product of two different parity symmetries within the same $O(N_i)$ group is a $SO(N_i)$ rotation. Therefore, it is enough to consider one such Z_2 parity symmetry within each group and $O(N_i) \sim SO(N_i) \times Z_2$.

The anti-unitary time reversal symmetry $\mathcal{T}$ is a general feature of systems of Majorana fermions; it commutes with them and, therefore, with the Hamiltonian (5.1.2):

$$\mathcal{T}^{-1} \psi_{abc} \mathcal{T} = \psi_{abc} \ . \tag{5.2.13}$$

The action of $\mathcal{T}$ on the eigenstates depends on the total number of the Majorana fermions $N_1N_2N_3$ and is well-known in the theory of topological insulators and superconductors. If the total number of fermions is divisible by 8, the operator $\mathcal{T}$ acts trivially, so the ground state may be non-degenerate. Otherwise $\mathcal{T}$ acts non-trivially and one finds that the ground state must be degenerate.

5.3 Energy bounds for the $O(N_1) \times O(N_2) \times O(N_3)$ model

Since the Hilbert space of the model is finite dimensional, it is interesting to put an upper bound on the absolute value of the energy eigenvalues in each representation of the symmetry group. In this section we address this question in two different ways. We first derive a basic linear relation between the Hamiltonian, a quadratic Casimir operator, and a square of a Hermitian operator which is positive definite. This gives bounds which are useful for the representations where the quadratic Casimir of one of the orthogonal groups is near its maximum allowed value. We also find that the bounds are exactly saturated for $N_3 = 2$, but are not stringent when equal ranks become large. Then in section 5.3.2 we derive more refined bounds which are more stringent in the large N limit and give the expected scaling of the ground state energy. Furthermore, we derive a finite multiplicative factor which corrects the refined bound and allows us to deduce the ground state energy in the large N limit.

5.3.1 Basic bounds

To derive an energy bound we introduce the hermitian tensor

$$
\begin{aligned}
A^{bc,b'c'} &= \frac{i}{2}[\psi^{abc}, \psi^{ab'c'}] = i\psi^{abc}\psi^{ab'c'} - i\frac{N_1}{2}\delta^{bb'}\delta^{cc'} \\
(A^{bc,b'c'})^\dagger &= -i\psi^{ab'c'}\psi^{abc} + i\frac{N_1}{2}\delta^{bb'}\delta^{cc'} = i\psi^{abc}\psi^{ab'c'} - i\frac{N_1}{2}\delta^{bb'}\delta^{cc'} = A^{bc,b'c'} \,. \qquad (5.3.14)
\end{aligned}
$$

If we think of bc as a combined index which takes N_2N_3 values, then $A^{bc,b'c'}$ are the generators of the transformations in $O(N_2N_3) \supset O(N_2) \times O(N_3)$. The quadratic Casimir of $O(N_2N_3) \supset$

$O(N_2) \times O(N_3)$,

$$C_2^{O(N_2N_3)} = \frac{1}{2} A^{bc,b'c'} A^{bc,b'c'} \ , \tag{5.3.15}$$

and the quadratic Casimir of the $O(N_1)$ symmetry,

$$C_2^{O(N_1)} = \frac{1}{2} Q_1^{aa'} Q_1^{aa'} \tag{5.3.16}$$

are related by

$$C_2^{O(N_2N_3)} + C_2^{O(N_1)} = \frac{N_1 N_2 N_3}{8} \left(N_1 + N_2 N_3 - 2 \right) \ . \tag{5.3.17}$$

Therefore, for the states which appear in the model, we find the upper bound:

$$C_2^{O(N_1)} \leq \frac{1}{8} N_1 N_2 N_3 \left(N_1 + N_2 N_3 - 2 \right) \ . \tag{5.3.18}$$

This bound is saturated only if $C_2^{O(N_2N_3)} = 0$ so that the state is invariant under $SO(N_2N_3)$.

The Hamiltonian may be written as

$$H = -\frac{g}{4} A^{bc,b'c'} A^{bc',b'c} + \frac{g}{16} N_1 N_2 N_3 (N_2 - N_3) \ . \tag{5.3.19}$$

Now we note the inequality

$$C_2^{O(N_2N_3)} \pm \frac{1}{2} A^{bc,b'c'} A^{bc',b'c} = \frac{1}{4} (A^{bc,b'c'} \pm A^{bc',b'c})^2 \geq 0 \tag{5.3.20}$$

Combining this with (5.3.17) we get

$$\frac{2}{g} H \begin{cases} \leq \frac{1}{8} N_1 N_2 N_3 \left(N_1 + N_2 - N_3 + N_2 N_3 - 2 \right) - C_2^{O(N_1)} \, , \\ \geq C_2^{O(N_1)} - \frac{1}{8} N_1 N_2 N_3 \left(N_1 - N_2 + N_3 + N_2 N_3 - 2 \right) \, . \end{cases} \tag{5.3.21}$$

In an analogous fashion we can also derive the bounds in terms of C_2:

$$\frac{2}{g}H \begin{cases} \leq \frac{1}{8}N_1N_2N_3\left(N_2+N_3-N_1+N_1N_3-2\right)-C_2^{O(N_2)}\,, \\ \geq C_2^{O(N_2)}-\frac{1}{8}N_1N_2N_3\left(N_2-N_3+N_1+N_1N_3-2\right) \end{cases} \tag{5.3.22}$$

and similarly in terms of $C_2^{O(N_3)}$.

An interesting special case, which we will consider in section 5.6, is $N_3 = 2$ where we find a complex $N_1 \times N_2$ matrix model. For the singlet states where $C_2^{O(N_1)} = C_2^{O(N_2)} = 0$ the most stringent bound we get from (5.3.21) and (5.3.22) is

$$|H| \leq \frac{g}{8}N_1N_2(N_1+N_2)\ . \tag{5.3.23}$$

In section 5.6 we will show that these bounds are saturated by the exact solution for even N_1, N_2. For $N_1 = N_2 = N$ we have a $N \times N$ matrix quantum mechanics which possesses a 't Hooft large N limit where $gN = \lambda$ is held fixed. In this limit, the ground state energy is $E_0 = -\frac{\lambda}{4}N^2$, which has the expected scaling with N for a matrix model.

More generally, if at least one of the ranks is even (we will call it N_3), we may introduce the operators [52]

$$\begin{gathered} \bar{c}_{abk} = \frac{1}{\sqrt{2}}\left(\psi^{ab(2k-1)}+i\psi^{ab(2k)}\right), \quad c_{abk} = \frac{1}{\sqrt{2}}\left(\psi^{ab(2k-1)}-i\psi^{ab(2k)}\right), \\ \{c_{abk}, c_{a'b'k'}\} = \{\bar{c}_{abk}, \bar{c}_{a'b'k'}\} = 0, \quad \{\bar{c}_{abk}, c_{a'b'k'}\} = \delta_{aa'}\delta_{bb'}\delta_{kk'}\,, \end{gathered} \tag{5.3.24}$$

where $a = 1, 2, \ldots, N_1,\ b = 1, 2 \ldots, N_2$ and $k = 1, \ldots, \frac{N_3}{2}$. In this basis the $O(N_1) \times O(N_2) \times U(N_3/2)$ symmetry is manifest. The Hamiltonian becomes [52]

$$H = \frac{g}{2}\left(\bar{c}_{abk}\bar{c}_{ab'k'}c_{a'bk'}c_{a'b'k} - \bar{c}_{abk}\bar{c}_{a'bk'}c_{ab'k'}c_{a'b'k}\right) + \frac{g}{2}(N_2-N_1)Q + \frac{g}{16}N_1N_2N_3(N_2-N_1)\,, \tag{5.3.25}$$

where $Q = \frac{1}{2}[\bar{c}_{abk}, c_{abk}]$. The Hamiltonian is invariant under the charge conjugation symmetry which interchanges c_{abk} with $\bar{c}_{abk}$.

For any even N_3, using the basis (5.3.24) we define the oscillator vacuum state by the condition $c_{abk}\rangle 0 = 0$. Since this condition is invariant under $O(N_1 N_2)$, so is $\rangle 0$. Furthermore, all the states that are created by operators that are $O(N_1 N_2)$ invariant are also $O(N_1 N_2)$ invariant and have energy $\frac{g}{16} N_1 N_2 N_3 (N_2 - N_1)$. The number of such states is estimated to be the dimension of the maximal representation for the $O(N_3)$ group $\dim_{\max} \sim (N_1 N_2)^{N_3^2/8}$ (see apendix C.1 for details). The relation (5.3.17) also simplifies the search for the singlets. For example, we can first forget about the group nature of the third index in the approach of [52] and impose the vanishing of the Casimir of the third group afterwards. By studying the charges under $U(1) \in U(N_3/2)$ we find that the singlet states must have $N_1 N_2 N_3/4$ creation operators acting on $\rangle 0$.

Specifying the bound (5.3.21) to the equal ranks $N_1 = N_2 = N_3 = N$, we find

$$C_2^{O(N)_1} - \frac{1}{8} N^3 (N+2)(N-1) \leq \frac{2}{g} H \leq \frac{1}{8} N^3 (N+2)(N-1) - C_2^{O(N)_1} \,. \tag{5.3.26}$$

When the bound (5.3.18) is saturated, the corresponding state must have zero energy. This shows that all the states invariant under $O(N^2) \supset O(N)_2 \times O(N)_3$ have $E = 0$.

For the singlet states (5.3.26) gives

$$\frac{4}{g} |H| \leq \frac{1}{4} N^3 (N+2)(N-1) \,. \tag{5.3.27}$$

For $N = 2$, exact diagonalization gives that the ground states is a singlet with energy $E_0 = -2g$; this saturates the bound (5.3.27). For $N = 3$, exact diagonalization gives a ground state with energy $-\frac{5}{4}\sqrt{41} g \approx -8.0039 g$, which is in the $(2,2,2)$ representation of $O(3)^3$. Since for the 2 of $SO(3)$, $C_1 = 3/4$, the bound (5.3.26) is $E_0 \geq -\frac{33}{2} g$. This is satisfied and is far from being saturated.

In the large N limit, $J = g N^{3/2}$ is held fixed. Thus, we obtain a bound on the lowest singlet energy E_0, which is $E_0 \geq -c J N^{7/2}$, where c is a positive constant. Since we expect the ground

state energy to be of order N^3, this bound is not very informative at large N. A better bound at large N will be derived in the next section.

5.3.2 Refined bounds

In this section we present another approach to deriving energy bounds for the $O(N_1) \times O(N_2) \times O(N_3)$ invariant states, which gives a more stringent bound in the large N limit than the ones in the previous section.

Consider an arbitrary singlet density matrix ρ; this means a density matrix invariant under the $O(N_1) \times O(N_2) \times O(N_3)$ rotations. For example, it can be $\rho_s = \rangle s \langle s$, where $\rangle s$ is an singlet state, or if we have some representation $\mathcal{R}$ of the $O(N_1) \times O(N_2) \times O(N_3)$ with an orthonormal basis $\rangle e_i, i = 1..\dim \mathcal{R}$ we can define the projector on this subspace of the Hilbert space

$$\rho_{\mathcal{R}} = \frac{1}{\dim \mathcal{R}} \sum_{i=1}^{\dim \mathcal{R}} |e_i\rangle\langle e_i|, \quad \rho_R = 1, \quad \rho_{\mathcal{R}}^2 = \frac{1}{\dim \mathcal{R}} \rho_{\mathcal{R}} \,. \tag{5.3.28}$$

It is easy to see, that this density matrix is invariant under rotations $O^T \rho_{\mathcal{R}} O = \rho_{\mathcal{R}}$ for any $O \in O(N_1) \times O(N_2) \times O(N_3)$. We can calculate the mean value of the energy for this density matrix as

$$E = \operatorname{tr}[\rho_{\mathcal{R}} H] = \frac{g}{4} \operatorname{tr}\left[\rho \psi^{abc} \psi^{ab'c'} \psi^{a'bc'} \psi^{a'b'c}\right] - \frac{g}{16} N_1 N_2 N_3 (N_1 - N_2 + N_3) \,. \tag{5.3.29}$$

For a fixed a, b, c we can act by the rotation matrices (that act trivially on the singlet density matrix ρ_s) and make the interchange $a \leftrightarrow 1, b \leftrightarrow 1, c \leftrightarrow 1$. This argument gives us that

$$E = \frac{g}{4} N_1 N_2 N_3 \operatorname{tr}[\rho_{\mathcal{R}} h] - \frac{g}{16} N_1 N_2 N_3 (N_1 - N_2 + N_3), \quad h = \psi^{111} \psi^{1b'c'} \psi^{a'1c'} \psi^{a'b'1} \,, \tag{5.3.30}$$

where we sum over the repeated indexes. From now on we consider the density matrix to be of the form (5.3.28). Now we can estimate the trace in the formula (5.3.30). With the use of

Cauchy - Schwarz inequality, we have

$$\mathrm{tr}\left[\rho_{\mathcal{R}} h\right]^2 \leq \mathrm{tr}\left[\rho_{\mathcal{R}} h^\dagger h\right] = \frac{1}{2}\,\mathrm{tr}\left[\rho_{\mathcal{R}} \psi^{ab1}\psi^{a1c}\psi^{1bc}\psi^{1b'c'}\psi^{a'1c'}\psi^{a'b'1}\right]. \tag{5.3.31}$$

Because the density matrix $\rho_{\mathcal{R}}$ is a singlet we can rotate indices back to get

$$\mathrm{tr}\left[\rho_{\mathcal{R}} h\right]^2 \leq \frac{1}{2N_1N_2N_3}\,\mathrm{tr}\left[\rho_{\mathcal{R}} q^\dagger_{abc} q_{abc}\right], \quad q_{abc} = \psi^{ab'c'}\psi^{a'bc'}\psi^{a'b'c}. \tag{5.3.32}$$

We can express it is the following way

$$\left(\mathrm{tr}\left[\rho_{\mathcal{R}} h\right] - \frac{1}{4}\left(N_1 - N_2 + N_3\right)\right)^2 \leq \frac{1}{2N_1N_2N_3}\,\mathrm{tr}\left[\rho_{\mathcal{R}} q^2_{abc}\right] + \frac{1}{16}\left(N_1 - N_2 + N_3\right)^2 \tag{5.3.33}$$

The square of the operator q_{abc} can be expressed as a sum of Casimir operators due to the virtue of the anticommutation relations. That gives us the bound on the energies of states in representation $\mathcal{R}$:

$$|E_{\mathcal{R}}| \leq \frac{g}{16} N_1N_2N_3\Big(N_1N_2N_3 + N_1^2 + N_2^2 + N_3^2 - 4 - \frac{8}{N_1N_2N_3}\sum_{i=1}^{3}\left(N_i + 2\right)C_i^{\mathcal{R}}\Big)^{1/2}, \tag{5.3.34}$$

where $C_i^{\mathcal{R}}$ is the value of Casimir operator in the representation $\mathcal{R}$. For the singlet states this gives

$$|E| \leq \frac{g}{16} N_1N_2N_3(N_1N_2N_3 + N_1^2 + N_2^2 + N_3^2 - 4)^{1/2}. \tag{5.3.35}$$

Since $C_i \geq 0$ this bound applies to all energies. Let us note that for $N_3 = 2$ the square root may be taken explicitly:

$$|E|_{N_3=2} \leq \frac{g}{8} N_1N_2(N_1 + N_2), \tag{5.3.36}$$

which is identical to the earlier result (5.3.23). In section 5.6 we will show that this is saturated when N_1, N_2 are even and the ground state is a singlet.

For the case when $N_1 = N_2 = N_3 = N$ and $N > 2$ the bound (5.3.35) is more stringent than the earlier bound (5.3.27):

$$|E| \leq E_{bound} = \frac{g}{16} N^3 (N+2)\sqrt{N-1} \tag{5.3.37}$$

In the large N limit, $E_{bound} \to JN^3/16$, which is the expected behavior of the ground state energy; in the melonic limit it scales as N^3. We may expand (5.3.34) for large N to find

$$|E_{\mathcal{R}}| \leq \frac{g}{16} N^3 (N+2)\sqrt{N-1} \left(1 - \frac{4}{(N+2)(N-1)N^3} \sum_{i=1}^{3} C_i^{\mathcal{R}} + \dots\right) . \tag{5.3.38}$$

The discussion of the splittings between non-singlet and singlet states in section 5.4 will be in agreeement with the scaling of the second term.

We can try to estimate how close the singlet ground state $\rangle$vac comes to the bound (5.3.37) by using the exact propagator $G(t) = \langle T\psi^{abc}(t)\psi^{def}(0)\rangle$ in the large N limit. To do it let us consider the two states

$$|1\rangle = \psi^{111}|\text{vac}\rangle, \quad |2\rangle = \partial_t \psi^{111}|\text{vac}\rangle\,, \tag{5.3.39}$$

where we have introduced $\partial_t \psi_{abc} = i[H, \psi^{abc}]$. We can introduce the angle θ between these states

$$\cos^2\theta = \frac{|\langle 1|2\rangle|^2}{\langle 1|1\rangle\langle 2|2\rangle} = 2\frac{\left|\langle \text{vac}|\psi^{111}\partial_t\psi^{111}|\text{vac}\rangle\right|^2}{\langle \text{vac}|\left(\partial_t\psi^{111}\right)^2|\text{vac}\rangle} = 2\frac{\left|\langle \text{vac}|\psi^{abc}\partial_t\psi^{abc}|\text{vac}\rangle\right|^2}{N_1N_2N_3\langle \text{vac}|\left(\partial_t\psi^{abc}\right)^2|\text{vac}\rangle}, \tag{5.3.40}$$

where we have rotated back the indexes back by using the fact that the $\rangle$vac is a singlet state. One can notice $H = i\psi^{abc}\partial_t\psi^{abc}$, while $\langle \text{vac}|\left(\partial_t\psi^{abc}\right)^2|\text{vac}\rangle$ is just equal to the bound (5.3.35), then

$$\cos^2\theta = \frac{E_0^2}{E_{bound}^2}, \tag{5.3.41}$$

where E_{bound} is the bound on the singlet ground state energy (5.3.37). The other way to estimate this angle θ can be done in the following way. We shift the Hamiltonian, such that the ground state has the zero energy $(H - E_0)\rangle\text{vac} = 0$ and calculate the expectation value for the energy

for the state $|1\rangle$:

$$\langle E\rangle_1 = \frac{\langle 1|\,(H-E_0)\,|1\rangle}{\langle 1|1\rangle} = 2\langle \text{vac}|\psi^{111}(H-E_0)\psi^{111}|\text{vac}\rangle = 2i\langle \text{vac}|\psi^{111}\partial_t\psi^{111}|\text{vac}\rangle, \qquad (5.3.42)$$

at the same time the second moment of the energy is

$$\langle E^2\rangle_1 = \frac{\langle 1|(H-E_0)^2|1\rangle}{\langle 1|1\rangle} = 2\langle \text{vac}|\psi^{111}(H-E_0)^2\psi^{111}|\text{vac}\rangle = -2g^2\langle \text{vac}|\left(\partial_t\psi^{111}\right)^2|\text{vac}\rangle. \qquad (5.3.43)$$

Where we have used the fact that $\partial_t\psi_{abc} = i[H,\psi^{abc}]$. After that we can notice that (5.3.40) can be rewritten as

$$\cos^2\theta = \frac{\langle E\rangle_1^2}{\langle E^2\rangle_1}. \qquad (5.3.44)$$

If $\cos\theta = 1$, it means that $\langle E\rangle_1^2 = \langle E^2\rangle_1$ that can be true only if and if $\psi^{111}|\text{vac}\rangle$ is an eigenstate of the Hamiltonian. It would give that the propagator is

$$G(t) = \langle \psi^{abc}e^{-iHt}\psi^{a'b'c'}\rangle \propto \delta^{aa'}\delta^{bb'}\delta^{cc'}e^{-i\Delta E|t|}\,.$$

But as we know the solution for the propagator in the large N limit is a conformal propagator. From this we deduce that the bound can not be saturated. Nevertheless we can estimate the angle $\cos^2\theta$. Indeed, in the large N limit the propagator can be calculated numerically or approximated by a conformal one. From this we can calculate the $\langle E\rangle_1$ and $\langle E^2\rangle_1$. We assume $t > t' = 0$, $a = a', b = b', c = c'$ and insert the full basis $\rangle E_n$ of eigenstates of the Hamiltonian in the propagator to get

$$\langle \psi_{abc}(t)\psi_{abc}(0)\rangle = \sum_n |\langle \text{vac}|\psi_{abc}|E_n\rangle|^2\, e^{-i(E_n-E_0)t} = \int_0^\infty dE\rho(E)e^{-iEt},$$
$$\text{where} \quad \rho(E) = \sum_n |\langle \text{vac}|\psi_{abc}|E_n\rangle|^2\,\delta(E-E_n+E_0). \qquad (5.3.45)$$

The function $\rho(E)$ is known as a structure factor. From this we can calculate

$$\langle E\rangle_1 = \int_0^\infty dE\, E\, \rho(E), \quad \langle E^2\rangle_1 = \int_0^\infty dE\, E^2\, \rho(E), \quad \cos^2\theta = \frac{\langle E\rangle_1^2}{\langle E^2\rangle_1}. \tag{5.3.46}$$

One can use conformal propagator to estimate this angle, which gives $\cos\theta \approx 0.745$, while the numerical calculation [16] gives $\cos\theta = 0.6608$. From this and the formula (5.3.41) we get the ground state energy in the large N limit:

$$E_0 \to -\cos\theta\, E_{bound} = -\cos\theta\, \frac{JN^3}{16} \approx -0.041 JN^3\ . \tag{5.3.47}$$

This answer is close to the numerical result for the ground state energy in the SYK model [142]: $E_0 \approx -0.04 J N_{\rm SYK}$. One can make analogous calculations for the other representations. It gives us in the large N limit the following formula for the gap to the lowest state in a representation $\mathcal{R}$:

$$E - E_0 = \frac{J\cos\theta}{4N^2} \sum_{i=1}^{3} C_i^{\mathcal{R}} \tag{5.3.48}$$

5.4 Sigma model and energy gaps

In the large N limit the model 5.2.3 is dominated by melonic diagrams. This allows one to write down a closed system of Schwinger–Dyson equations for the Green function $G^{abc}_{a'b'c'}(t_1 - t_2) = \langle T\psi^{abc}(t_1)\psi^{a'b'c'}(t_2)\rangle$ and self-energy $\Sigma^{abc}_{a'b'c'}$ and the bare Green function $G^{abc}_{a'b'c',0}(\omega) = i\delta^a_{a'}\delta^b_{b'}\delta^c_{c'}/\omega$

For simplicity we shall introduce the multi-index $A = (a, b, c)$. We can look for a solution in the diagonal form $G^{AB} = G(t)\delta^{AB}$ and $\Sigma^{AB} = \Sigma(t)\delta^{AB}$. Then we have the following set of equations:

$$G^{-1}(\omega) = -i\omega - \Sigma(\omega)\,, \quad \Sigma(t) = J^2 G^3(t)\,. \tag{5.4.49}$$

These equations exactly coincide with the Schwinger–Dyson equations of the SYK model and have a conformal solution.

It was argued in [139] that the system of equations (5.4.49) can be obtained from the effective action [3]:

$$S_{\text{eff}} = -\log \text{Pf}\left(\delta_{AB}\partial_t + \Sigma_{AB}\right) + \int dt_1 dt_2 \left(-\Sigma_{AB}(t_1 - t_2)G^{AB}(t_2 - t_1) - \frac{g^2}{4}G^4(t_1 - t_2)\right) \tag{5.4.50}$$

This action was recently derived from two-particle irreducible diagrams in [137].

In the strong coupling limit $J \to \infty$ one can neglect the bare Green function. Then, as first noticed in [139], the *global* symmetry $O(N)^3$ is promoted to the gauged symmetry $O(N)^3$. Indeed, if we neglect $G_0^{AB}(\omega)$ in (5.4.49) then it is easy to see that we can generate a series of solutions by doing a gauge transformation:

$$\begin{aligned} G_{AB}(t_1 - t_2) &\to \left(O_{AA'}(t_1)\right)^T G_{A'B'}(t_1 - t_2) O_{BB'}(t_2) \\ \Sigma_{AB}(t_1 - t_2) &\to \left(O_{AA'}(t_1)\right)^T \Sigma_{A'B'}(t_1 - t_2) O_{BB'}(t_2) \end{aligned} \tag{5.4.51}$$

where we introduce matrix O in $O(N)^3$ which equals to $O_{AB} = O^1_{\alpha\alpha'} O^2_{\beta\beta'} O^3_{\gamma\gamma'}$.

The effective action (5.5.74) is also invariant under these transformations if one omits the term ∂_t in the Pfaffian. For finite J, the action ceases to be invariant. If we plug the gauge transformation (5.4.51) into the effective action (5.5.74), the potential does not change, while we will get a kinetic term for matrices O^i of order $1/J$. Indeed, for the conformal solution we have $\Sigma_{AB} = -\left(1/G\right)_{AB}$ and we can rewrite the kinetic part of the action as

$$-\log \text{Pf}\left(\delta_{AB}\partial_t + \Sigma_{AB}\right) = -\log \text{Pf}\left(\delta_{AB} - \partial_t G_{AB}\right) - \log \text{Pf}\left(\Sigma_{AB}\right) \tag{5.4.52}$$

The second term $\log \text{Pf}\left(\Sigma_{AB}\right)$ is invariant under gauge transformations. Then expanding the Pfaffian in the leading order in derivatives we get

$$\frac{1}{2}\int dt \ \text{Tr} \ \partial_t G_{AB}(t, t')\Big|_{t' \to t} \tag{5.4.53}$$

[3] For clarity, we have omitted the indices in the G^4 term. Explicitly, this term reads as $G^{a\beta\gamma}_{a'\beta'\gamma'} G^{\alpha b\gamma}_{\alpha' b'\gamma'} G^{\alpha\beta c}_{\alpha'\beta' c'} G^{abc}_{a'b'c'}$

Making the gauge transformation (5.4.51) of the conformal solution $G_{AB} = \delta_{AB} G$ and plugging into (5.4.53) we get:

$$\frac{1}{2}\int dt\ \mathrm{Tr}\left(N^3 \partial_t G + N^2 \sum_{i=1}^{3} O_i^T(t) G(t-t') \partial_t O_i(t') + \partial_t O_i^T(t) G(t-t') O_i(t')\right)\Big|_{t\to t'} \tag{5.4.54}$$

Factors N^2 come from $\mathrm{Tr}(O_1^T O_1) = N$. Now one has to regularize the limit $t_2 \to t_1$ but this does not going to affect N^2 factors. The details are worked out in [149, 137]. The upshot is that $G(t-t')O_i(t')$ becomes $\partial_t O_i(t)/J$ up to a normalization constant. This leads to the sigma model action

$$S_{SM} = \frac{\mathcal{A}N^2}{J}\int dt\, \mathrm{Tr}(\partial_t O_1^T \partial_t O_1 + \partial_t O_2^T \partial_t O_2 + \partial_t O_3^T \partial_t O_3)\,. \tag{5.4.55}$$

The spectrum of such a quantum mechanical sigma model is well-known: the Hamiltonian is proportional to the quadratic Casimir and the eigenstates are simply representations of $O(N)^3$. In our case:

$$H_{\text{gauge}} = \frac{J}{N^2\mathcal{A}}\left(C_2\left(O_1(N)\right) + C_2\left(O_2(N)\right) + C_2\left(O_3(N)\right)\right)\,. \tag{5.4.56}$$

We note that this has the same structure as the Casimir correction to the energy bound (5.3.38). Since for the lowest non-singlet representations $C_2 \sim N$, we find the energy gap between singlets and non-singlets to be of the order $\sim J/N$.

5.5 Counting singlet states

Suppose we have a free fermionic system of N Majorana fermions ψ^I, $I = 1, \ldots, M$ transforming under some representation $\mathcal{R}$ of the gauge group G. We want to compute the number of singlet states in such a system. In order to do it, we use the following method. The Lagrangian in the Euclidean space reads as:

$$L = \psi^I \partial_t \psi^I + \psi^I A_{IJ} \psi^J \tag{5.5.57}$$

where A_{IJ} is a real gauge field in the representation $\mathcal{R}$. Since Majorana fermions anticommute with each other, A_{IJ} must be anti-symmetric $A_{IJ} = -A_{JI}$. The partition function of the gauged

system at the temperature β is

$$Z_{\text{gauged}} = \mathcal{N} \int \mathcal{D}\psi\, \mathcal{D}A \;\; \exp\left(- \int_0^\beta dt\, L \right) , \tag{5.5.58}$$

where we have put the fermionic system on a circle with the circumference β with antiperiodic boundary conditions $\psi(t) = -\psi(t+\beta)$. The normalization factor $\mathcal{N}$ can be easily recovered if we study the ungauged model. The integration over $\mathcal{D}A$ gives the volume of the gauge group and the integral over the fermion variables will yield just the dimension of the Hilbert space because the Hamiltonian of the ungauged theory is equal to zero $H_{ungauge} = 0$. In this case the total number of states is simply $2^{M/2}$:

$$Z_{\text{ungauged}} = 2^{M/2} \int \mathcal{D}A = \mathcal{N} \int \mathcal{D}\psi\, \mathcal{D}A \;\; \exp\left(- \int_0^\beta dt \;\psi \partial_t \psi \right) . \tag{5.5.59}$$

From now on, we will put $\beta = 1$. If we fix Lorentz gauge $\partial_t A = 0$ with A in the Cartan subalgebra, the Faddeev-Popov determinant gives the Haar measure, while the path integral over Majoranna fermions gives the partition function of the system with Hamiltonian $H = -\psi^I A_{IJ} \psi^J$. Therefore the (5.5.58) can be rewritten as

$$Z_{\text{gauged}} = \int \mathcal{D}A \;\text{Tr}\, \left(\exp\left(-\psi^I A_{IJ} \psi^J \right) \right) , \tag{5.5.60}$$

The expression under the trace is an operator of rotations and can be interpreted as a character of the group acting in the Hilbert space of fermions. By the virtue of the representation theory we know that the integral of the character over a group is equal to the number of the trivial representations, i.e. the number of the singlet states. Therefore, Z_{gauged} equals the number of singlet states. If we insert in (5.5.58) a Wilson line in some representation $\mathcal{R}'$, it gives the character of this representation:

$$\left\langle \text{Tr}_{\mathcal{R}'} \exp\left(\oint A\, dt \right) \right\rangle = \#\text{states in the representation } \mathcal{R}'. \tag{5.5.61}$$

One can compute the partition function because the integral over ψ in both (5.5.58) and (5.5.59) is Gaussian; therefore, the problem boils down to computing the Pfaffian:

$$Z_{\text{gauged}} = 2^{M/2} \int \mathcal{D}A \frac{\text{Pf}(\partial_t + A)}{\text{Pf}(\partial_t)} \,. \tag{5.5.62}$$

As discussed above, we fix A to be a constant matrix in the Cartan subalgebra. The Faddeev–Popov determinant then yields the normalized Haar measure $d\lambda_G^N$ on the gauge group G [65]:

$$\int_G d\lambda_G^N = 1 \,. \tag{5.5.63}$$

Also, since A is anti-symmetric, the eigenvalues of A are pairs of pure-imaginary numbers $i\lambda_a, -i\lambda_a$, $a = 1, \ldots, \lfloor N/2 \rfloor$. The ratio of the Pfaffians is

$$\frac{\text{Pf}(\partial_t + A)}{\text{Pf}(\partial_t)} = \prod_{a=1}^{M/2} \cos(\lambda_a/2) \,. \tag{5.5.64}$$

There are different ways to derive this formula. One is to compute the ratio of determinants:

$$\frac{\text{Det}(\partial_t + A)}{\text{Det}(\partial_t)} = \prod_{a=1}^{M/2} \prod_{n=-\infty}^{\infty} \frac{\left(2\pi i \left(n + \frac{1}{2}\right) + i\lambda_a\right)\left(2\pi i \left(n + \frac{1}{2}\right) - i\lambda_a\right)}{\left(2\pi i \left(n + \frac{1}{2}\right)\right)^2} = \prod_{a=1}^{M/2} \cos(\lambda_a/2)^2 \,. \tag{5.5.65}$$

After that we note that if we go to the Fourier space, both ∂_t and A are real anti-symmetric matrices, so the ratio of Pfaffians must be a real smooth function of λ_a. Therefore, taking the square root of eq. (5.5.65) we get eq. (5.5.64). Alternatively, we can calculate the Pfaffian of $\partial_t + A$ in Fourier space. The result is the following formula:

$$\#\text{singlet states} = \int d\lambda_G^N \prod_{a=1}^{M/2} 2\cos(\lambda_a/2) \,, \tag{5.5.66}$$

where we have got the normalization by studying the ungauged theory (5.5.59).

Let us apply this approach to the case when Majorana fermions live in the fundamental representation of several orthogonal groups. It is important to distinguish between $SO(2n)$ and

$SO(2n+1)$. The Cartan subalgebra in the $SO(2n)$ algebra consists of the block diagonal matrices with 2×2 blocks

$$\begin{pmatrix} 0 & x_i \\ -x_i & 0 \end{pmatrix}, \tag{5.5.67}$$

where x_i is a rotation phase ranging from 0 to 2π. Geometrically it means that for a fixed $SO(2n)$ transformation, there is a basis in which this transformation looks like a set of rotations in independent two-planes. In the $SO(2n+1)$ case the last column/row is zero. It corresponds to a fixed one-dimensional subspace. *Non-normalized* Haar measure in these two cases reads as:

$$d\lambda_{SO(2n)} = \prod_{i<j}^{n} \sin\left(\frac{x_i - x_j}{2}\right)^2 \sin\left(\frac{x_i + x_j}{2}\right)^2 dx_1 \dots dx_n, \tag{5.5.68}$$

$$d\lambda_{SO(2n+1)} = \prod_{i<j}^{n} \sin\left(\frac{x_i - x_j}{2}\right)^2 \sin\left(\frac{x_i + x_j}{2}\right)^2 \prod_{j=1}^{n} \sin\left(\frac{x_j}{2}\right)^2 dx_1 \dots dx_n \,. \tag{5.5.69}$$

Now we discuss the case where the gauge group is the product of three orthogonal groups $SO(N_1) \times SO(N_2) \times SO(N_3)$, so that the gauge field decomposes as

$$A = A^1 \otimes \mathbb{1} \otimes \mathbb{1} + \mathbb{1} \otimes A^2 \otimes \mathbb{1} + \mathbb{1} \otimes \mathbb{1} \otimes A^3 \,. \tag{5.5.70}$$

For even N_i in eq. (5.5.66) eigenvalues λ_a are given by $x_i + y_j + z_k$, $-x_i + y_j + z_k$, $x_i - y_j + z_k$ and $x_i + y_j - z_k$, with $i = 1, \dots, \lfloor N_1/2 \rfloor$, $j = 1, \dots, \lfloor N_2/2 \rfloor$, $k = 1, \dots, \lfloor N_3/2 \rfloor$. Variables x_i, y_j, z_k are rotation phases for $SO(N_1)$, $SO(N_2)$ and $SO(N_3)$ respectively. In the case when one of the N_i is odd we have to add a zero eigenvalue to this list. With the use of the equation (5.5.66) we can write expicit form of the character of the representation and decompose it in terms of characters of the irreducible representations. For example, for the $O(2)^3$ model the number of singlets is given by the integral

$$\frac{16}{(2\pi)^3} \int_{-\pi}^{\pi} dx \int_{-\pi}^{\pi} dy \int_{-\pi}^{\pi} dz \cos\left(\frac{x+y+z}{2}\right) \cos\left(\frac{x+y-z}{2}\right) \cos\left(\frac{x-y+z}{2}\right) \cos\left(\frac{-x+y+z}{2}\right), \tag{5.5.71}$$

whose evaluation gives 2.

For the $O(N)^3$ model the number of singlets for various even N is given in Table 5.1. For odd N it is not hard to see that the integral which gives the number of singlets vanishes; this is related to the fact that each group exhibits an individual anomaly, which we discuss in the next section.[4] In the next section 5.5.1 we will show that the number of singlets grows as $\exp\left(N^3 \log 2/2 - 3N^2 \log N/2\right)$ for large even N.

N	# singlet states
2	2
4	36
6	595354780

Table 5.1: Number of singlet states in the $O(N)^3$ model

Using similar methods, the number of singlets can be calculated in the $O(N)^6$ GW model for low values of N, and the results are presented in Table 5.2. The fact that there are 140 states for $N = 2$ is in agreement with the direct construction of singlet states in [146].

N	# singlet states
2	140
3	63358
4	114876653804156708

Table 5.2: Number of singlet states in the $O(N)^6$ Gurau–Witten model

We may similarly calculate the number of singlets for the $O(N_1) \times O(N_2) \times O(N_3)$ models. When $N_2 = N_3 = 2$, while N_1 is even, there are 2 singlets. For the cases where $N_3 = 2$, while N_1 and N_2 are even, some answers are listed in Table 5.3. We note that the growth of the number of singlets for the $O(N)^2 \times O(2)$ model is much slower than for the $O(N)^3$ model. For low values of N it is not hard to write down explicit expressions for all the singlet states in the oscillator basis; see appendix C.2.3. For example, for the $O(4)^2 \times O(2)$ model we find that the 4 singlet energies are $\pm 16g$ and $\pm 4g$.

[4] Direct diagonalization of the Hamiltonian for $N = 3$ [50, 51] reveals that there are no non-degenerate eigenvalues, consistent with this. There are 8 ground states with energy $-\frac{5}{4}\sqrt{41}g \approx -8.00391g$; they transform in the spinorial $(2, 2, 2)$ representation. Substuting the value $C_i = 3/4$ into the bound (5.3.34) for the energy gives $-11.53g$, which is quite close to the actual value.

(N_1, N_2)	# singlet states
(4,4)	4
(6,4)	4
(6,6)	4
(8,4)	6
(8,6)	8
(8,8)	18
(10,4)	6
(10,6)	8
(10,8)	20
(10,10)	24

Table 5.3: Number of singlet states in the $O(N_1) \times O(N_2) \times O(2)$ model

5.5.1 Number of singlets for large N

In this section we will estimate the number of singlets in the $SO(N)^3$ model in the large N limit, assuming N to be odd $N = 2M$. For general N, the number of singlets is given by the following integral:

$$\text{singlet states} = \frac{1}{V^3}\int_{-\pi}^{\pi}[dx][dy][dz]\prod_{i,j,k=1}^{M} 16\cos\left(\frac{x_i+y_j+z_k}{2}\right)\cos\left(\frac{-x_i+y_j+z_k}{2}\right)\times$$
$$\cos\left(\frac{x_i-y_j+z_k}{2}\right)\cos\left(\frac{x_i+y_j-z_k}{2}\right)\times \tag{5.5.72}$$
$$\prod_{i<j}^{M}\sin^2\left(\frac{x_i-x_j}{2}\right)\sin^2\left(\frac{x_i+x_j}{2}\right)\sin^2\left(\frac{y_i-y_j}{2}\right)\sin^2\left(\frac{y_i+y_j}{2}\right)\sin^2\left(\frac{z_i-z_j}{2}\right)\sin^2\left(\frac{z_i+z_j}{2}\right)$$

Where V is the volume of $SO(N)$. When N is large, cosine functions oscillate very rapidly, so the integral localizes near $x_i = y_j = z_k = 0$. Near this point the integrand is positive, so we can exponentiate it:

$$\#\text{singlet states} = \int_{-\pi}^{\pi}[dx][dy][dz]\exp\left(4\sum_{n=1}^{\infty}\sum_{i,j,k=1}^{M}\frac{(-1)^{n+1}}{n}t^n\cos(nx_i)\cos(ny_j)\cos(nz_k)\right)\times$$
$$\prod_{i<j}^{M}\sin^2\left(\frac{x_i-x_j}{2}\right)\sin^2\left(\frac{x_i+x_j}{2}\right)\sin^2\left(\frac{y_i-y_j}{2}\right)\sin^2\left(\frac{y_i+y_j}{2}\right)\sin^2\left(\frac{z_i-z_j}{2}\right)\sin^2\left(\frac{z_i+z_j}{2}\right) \tag{5.5.73}$$

Notice that we have introduced a "regulator" t which we have to send to one: $t \to 1$. Similar integrals count operators in theories with tri-fundamental fields [140]. In such cases $t = e^{-1/T}$, where T is the temperature. So we are interested in the infinite temperature limit. This case has been studied in detail in [140]. Here we perform a similar analysis. As usual, we will encode the saddle-point configuration of the angles x, y, z using the density function $\rho(x)$ (obviously it is the same function for the three $SO(N)$ groups). Moreover this function is symmetric $\rho(x) = \rho(-x)$. It would be convenient to work with the normalized density $\int_{-\pi}^{\pi} dx\rho(x) = 1$. The effective action now reads as:

$$S[\rho] = \frac{1}{2}N^3 \int_{-\pi}^{\pi} dxdydz\ \rho(x)\rho(y)\rho(z) \sum_{n=1}^{\infty} \frac{(-1)^{n+1}t^n}{n} \cos(nx)\cos(ny)\cos(nz) + \\ + \frac{1}{4}N^2 \int_{-\pi}^{\pi} dxdx'\rho(x)\rho(x') \log\sin\left(\frac{x-x'}{2}\right)^4 + \frac{1}{4}N^2 \int_{-\pi}^{\pi} dydy'\rho(y)\rho(y') \log\sin\left(\frac{y-y'}{2}\right)^4 + \\ + \frac{1}{4}N^2 \int_{-\pi}^{\pi} dzdz'\ \rho(z)\rho(z') \log\sin\left(\frac{z-z'}{2}\right)^4 \tag{5.5.74}$$

In the infinite temperature limit the saddle-point density is non-zero only on a small interval $[-x_0, x_0]$ where $x_0 \sim \sqrt{\frac{2}{N}}$. The leading contribution is coming from the first term and it equals to $\frac{1}{2}N^3 \log 2$. But this yields simply the dimensions of the Hilbert space, which is $2^{\frac{1}{2}N^3}$. The subleading term is coming from the second term in (5.5.74). Fortunately, we will not need the exact value of x_0 because of the logarithmic behaviour:

$$\int_{-x_0}^{x_0} dxdx'\ \rho(x)\rho(x') \log\sin\left(\frac{x-x'}{2}\right)^4 \sim 4\int_{-x_0}^{x_0} dxdx'\ \rho(x)\rho(x') \log(x-x') \sim \\ \sim 4\int_{-x_0}^{x_0} dxdx'\ \rho(x)\rho(x') \log x_0 = 4\log x_0 \sim -2\log N \tag{5.5.75}$$

Therefore the subleading term is $-\frac{3}{4}N^2 \log N$. So, in total we have

$$\#\text{singlet states} \sim \exp\left(\frac{N^3}{2}\log 2 - \frac{3N^2}{2}\log N + O(N^2)\right) \tag{5.5.76}$$

5.5.2 Anomalies

Since we are studying fermions on a compact space S^1 there is a potential global anomaly associated with $\pi_1(G)$. And indeed it is well-known that $\pi_1(SO(N)) = \mathbb{Z}_2$. Corresponding "large" gauge transformation has a simple description: the gauge transformation matrix is the identity matrix, apart from one 2×2 block

$$\begin{pmatrix} \cos(2\pi t) & -\sin(2\pi t) \\ \sin(2\pi t) & \cos(2\pi t) \end{pmatrix} . \tag{5.5.77}$$

It is easy to see that after such transformation *one chosen* rotation phase x_i will be shifted by 2π: $x_i \to x_i + 2\pi$. It does not matter which x_i to pick up, since an even number of 2π-rotation blocks gives, in fact, a trivial element in $\pi_1(SO(N))$. It has been known for some time [54] that a theory of a single Majorana fermion in the fundamental representation of $SO(N)$ is suffering from this $\mathbb{Z}_2$ anomaly. It is instructive to see it using our machinery. The Pfaffian in this case reads as:

$$\prod_{i=1}^{N/2} \cos(x_i/2) \tag{5.5.78}$$

Under the shift $x_j \to x_j + 2\pi$ it changes sign. Therefore the theory is not invariant under large gauge transformations. In our case of $O(N_1) \times O(N_2) \times O(N_3)$ group it means that at least two out of three N_i should be even, otherwise we will have an odd number of anomalous multiplets. Since this anomaly is associated with only one group we will refer to it as "individual anomaly". It is easy to see that this anomaly is always $\mathbb{Z}_2$(in other words, it squares to one), even if we add more gauge groups.

If the gauge group is a product $SO(2n_1) \times SO(2n_2)$ there is a new anomaly mixing these two groups. For each group in the product, the large gauge transformation consists of identical 2×2 blocks:

$$\begin{pmatrix} \cos(\pi t) & -\sin(\pi t) \\ \sin(\pi t) & \cos(\pi t) \end{pmatrix} . \tag{5.5.79}$$

Since there are two gauge groups, at $t = 1$ overall -1 will cancel. Now *all* phases x_i and y_j are shifted by π: $x_i \to x_i + \pi,\ y_j \to y_j + \pi$. The Pfaffian reads as:

$$\prod_{i=1}^{n_1}\prod_{j=1}^{n_2} \cos\left(\frac{x_i + y_j}{2}\right) \cos\left(\frac{x_i - y_j}{2}\right) . \tag{5.5.80}$$

Under the large gauge transformation the Pfaffian acquires $(-1)^{n_1 n_2}$. This anomaly means that for $G = SO(2n_1) \times SO(2n_2) \times SO(N_3)$, N_3 can be odd only if the product $N_1 N_2$ is even. We will call this anomaly "mixed anomaly". This anomaly is not always $\mathbb{Z}_2$ as we will see shortly.

We do not find any more anomalies: using the long exact sequence in homotopy groups one can show that the fundamental group of $SO(2n_1) \times SO(2n_2)/\mathbb{Z}_2$[5] is equal to $\mathbb{Z}_2 \times \mathbb{Z}_2 \times \mathbb{Z}_2$ or $\mathbb{Z}_4 \times \mathbb{Z}_2$ depending on n_1 and n_2. Using the above explicit descriptions of the individual anomalies and the mixed anomaly we see that:

- If n_1 and n_2 are both even, then the square of the mixed anomaly gives a trivial gauge transformation. Indeed, for each gauge group the number N_i of 2π-rotation blocks (5.5.77) is even. Therefore, this is the case of $\mathbb{Z}_2 \times \mathbb{Z}_2 \times \mathbb{Z}_2$.

- If only one of n_i, say n_1, is odd, then the mixed anomaly squares to the individual anomaly of $SO(2n_1)$, since this group will have an odd number of 2π rotation blocks. Therefore, the anomalies form $\mathbb{Z}_4 \times \mathbb{Z}_2$.

- Finally, when both n_1 and n_2 are odd, then the mixed anomaly squares to the sum of the individual anomalies. This is again $\mathbb{Z}_4 \times \mathbb{Z}_2$.

5.6 Solution of some fermionic matrix models

When $N_3 = 1$ or $N_3 = 2$ the $O(N_1) \times O(N_2) \times O(N_3)$ symmetric tensor model (5.1.2) simplifies and becomes a fermionic $N_1 \times N_2$ matrix model. In this section we discuss the solution of these models. For the $O(N_1) \times O(N_2)$ real matrix model the Hamiltonian may be expressed

[5]One has to divide by $\mathbb{Z}_2$ because $g_1 \times g_2$ acts on ψ in the same way as $(-g_1) \times (-g_2)$

in terms of the quadratic Casimir operators, which shows that all the states within the same group representation have the same energy. This also applies to the $SU(N_1) \times SU(N_2) \times U(1)$ symmetric complex fermionic matrix model, which was considered in [148], [150] (see also [151]), and will be further discussed in section 5.6.2. However, the $O(N_1) \times O(N_2) \times U(1)$ complex fermionic matrix model is more complicated in that there are energy splittings within the same representation of the symmetry group. Nevertheless, as we show in section 5.6.3 this model is solvable.

5.6.1 The $O(N_1) \times O(N_2)$ model

Setting $N_3 = 1$ in the $O(N_1) \times O(N_2) \times O(N_3)$ symmetric tensor model (5.1.2) we find a real matrix model with $O(N_1) \times O(N_2)$ symmetry:

$$H = \frac{g}{4}\psi^{ab}\psi^{ab'}\psi^{a'b}\psi^{a'b'} - \frac{g}{16}N_1N_2(N_1 - N_2 + 1) \ . \tag{5.6.81}$$

Using the $SO(N_1)$ and $SO(N_2)$ charges

$$Q_1^{aa'} = \frac{i}{2}[\psi^{ab}, \psi^{a'b}] \ , \qquad Q_2^{bb'} = \frac{i}{2}[\psi^{ab}, \psi^{ab'}] \tag{5.6.82}$$

the Hamiltonian may be expressed in terms of the quadratic Casimirs:

$$H = -\frac{g}{2}C_2^{SO(N_2)} + \frac{g}{16}N_1N_2(N_2 - 1) = \frac{g}{2}C_2^{SO(N_1)} - \frac{g}{16}N_1N_2(N_1 - 1) \ . \tag{5.6.83}$$

This shows that, under the interchange of N_1 and N_2, $H \to -H$; therefore, for $N_1 = N_2$ the spectrum is symmetric around zero. The sum of this Casimir operators is fixed:

$$C_2^{SO(N_1)} + C_2^{SO(N_2)} = \frac{1}{2}Q_1^{aa'}Q_1^{aa'} + \frac{1}{2}Q_2^{bb'}Q_2^{bb'} = \frac{1}{8}N_1N_2(N_1 + N_2 - 2) \ . \tag{5.6.84}$$

This shows that there are no states which are singlets under both $SO(N_1)$ and $SO(N_2)$. The irreducible representations (r_1, r_2) which appear in the spectrum must satisfy the condition (5.6.84).

In appendix C.2.1 we list these representations for a few low values of N_1 and N_2. The complete lists of the energies and degeneracies are shown in Table 5.4.

For $O(N) \times O(N)$ with even N, we find that the ground state is a singlet under $O(N)_1$ and transforms in the $SO(N)_2$ representation whose Young diagram is a $\frac{N}{2} \times \frac{N}{2}$ square. The ground state has energy $E_0 = -gN^2(N-1)/16$, while the first excited state is in the fundamental of $O(N)_1$ which has quadratic Casimir $N-1$. Therefore, the energy gap

$$E_1 - E_0 = \frac{g}{2}(N-1) \ . \tag{5.6.85}$$

In the 't Hooft large N limit, $g \sim 1/N$ and the gap stays finite. Therefore, unlike the SYK and tensor models, the matrix model cannot exhibit quasi-conformal behavior.

(N_1, N_2)	(2,2)	(2,3)	(2,4)	(3,3)	(3,4)	(4,4)	(5,5)
$\frac{4}{g}E_{\text{degeneracy}}$	-1_2	-1_6	-2_6	-3_8	-6_8	-12_{10}	-20_{224}
	1_2	3_2	0_8	3_8	-2_{36}	-6_{64}	-10_{1024}
			6_2		6_{20}	-4_{54}	-4_{800}
						4_{54}	4_{800}
						6_{64}	10_{1024}
						12_{10}	20_{224}

Table 5.4: Spectra of the $O(N_1) \times O(N_2)$ models.

5.6.2 The $SU(N_1) \times SU(N_2) \times U(1)$ model

In [20] a class of complex tensor quantum mechanical models with $SU(N_1) \times SU(N_2) \times O(N_3) \times U(1)$ symmetry was introduced. We will use the Hamiltonian

$$H = g\bar{\psi}_{abc}\bar{\psi}_{a'b'c}\psi_{ab'c'}\psi_{a'bc'} + g(N_1 - N_2)Q + \frac{g}{4}N_1N_2N_3(N_1 - N_2)\,, \tag{5.6.86}$$

where ψ_{abc} with $a = 1, \ldots, N_1$, $b = 1, \ldots, N_2$ and $c = 1, \ldots, N_3$ are complex fermions with anti-commutation relations $\{\bar{\psi}_{abc}, \psi_{a'b'c'}\} = \delta_{aa'}\delta_{bb'}\delta_{cc'}$. The second and third terms were added to the Hamiltonian to make it traceless and invariant under the charge conjugation symmetry, which interchanges ψ_{abc} and $\bar{\psi}_{abc}$. This means it is invariant under $Q \to -Q$, where Q is the

$U(1)$ charge:

$$Q = \bar{\psi}_{abc}\psi_{abc} - \frac{1}{2}N_1N_2N_3 \ . \tag{5.6.87}$$

If we set $N_3 = 1$ we obtain a complex matrix model with $SU(N_1)\times SU(N_2)\times U(1)$ symmetry[6]

$$H = g\bar{\psi}_{ab}\bar{\psi}_{a'b'}\psi_{ab'}\psi_{a'b} + g(N_1 - N_2)Q + \frac{g}{4}N_1N_2(N_1 - N_2)\,, \tag{5.6.88}$$

which is the subject of this section. Note that the index contraction in the first term is different from those in (5.6.100); the $SU(N_1) \times SU(N_2) \times U(1)$ symmetry fixes it uniquely. This matrix model has some features in common with the $O(N_1) \times O(N_2)$ from the previous section. In both of them the energy is completely fixed by the quadratic Casimir operators of the symmetry group factors. Also, neither model contains states invariant under the entire symmetry group.

The $SU(N_i)$ charges with $i = 1, 2$ are

$$Q_1^\alpha = \bar{\psi}_{ab}(T_1^\alpha)_{aa'}\psi_{a'b}, \quad Q_2^\alpha = \bar{\psi}_{ab}(T_2^\alpha)_{bb'}\psi_{ab'} \ , \quad \alpha = 1, 2, \ldots, N_i^2 - 1 \ , \tag{5.6.89}$$

where we used the Hermitian $SU(N_i)$ generators $T_i^\alpha,\ i = 1, 2,\ \alpha = 1, \ldots, N_i^2 - 1$, normalized in the standard fashion:

$$\mathrm{Tr}(T_1^\alpha T_1^\beta) = \mathrm{Tr}(T_2^\alpha T_2^\beta) = \frac{1}{2}\delta^{\alpha\beta}\,. \tag{5.6.90}$$

Using the completeness relation (no sum over i):

$$(T_i^\alpha)_{aa'}(T_i^\alpha)_{bb'} = \frac{1}{2}\Big(\delta_{ab'}\delta_{a'b} - \frac{1}{N_i}\delta_{aa'}\delta_{bb'}\Big)\,. \tag{5.6.91}$$

[6] This Hamiltonian is related to that in section 4 of [148] by changing the coefficients of the second and third terms.

we find that the quadratic Casimirs of $SU(N_2)$ and $SU(N_2)$:

$$C_2^{SU(N_1)} = Q_1^\alpha Q_1^\alpha = \frac{1}{2}\bar\psi_{ab}\bar\psi_{a'b'}\psi_{ab'}\psi_{a'b} + \frac{1}{2}(N_1 - N_2)Q - \frac{1}{2N_1}Q^2 + \frac{1}{8}N_1N_2(2N_1 - N_2) \ ,$$
$$C_2^{SU(N_2)} = Q_2^\alpha Q_2^\alpha = -\frac{1}{2}\bar\psi_{ab}\bar\psi_{a'b'}\psi_{ab'}\psi_{a'b} + \frac{1}{2}(N_2 - N_1)Q - \frac{1}{2N_2}Q^2 + \frac{1}{8}N_1N_2(2N_2 - N_1) \ . \tag{5.6.92}$$

Adding them, we obtain the constraint

$$C_2^{SU(N_1)} + C_2^{SU(N_2)} = \frac{N_1 + N_2}{2N_1N_2}\left(\frac{(N_1N_2)^2}{4} - Q^2\right) \ . \tag{5.6.93}$$

To have the singlets of $SU(N_1)$ and $SU(N_2)$, we need the RHS to vanish. This means that there are only two $SU(N_1)\times SU(N_2)$ singlet states: the ones with $Q = \pm\frac{N_1N_2}{2}$. These are the oscillator vacuum $|0\rangle$, which is annihilated by all ψ_{ab}, and the state $|0'\rangle = \prod_{a,b}\bar\psi_{ab}|0\rangle$, which is annihilated by all $\bar\psi_{ab}$.

The absence of singlets for other values of Q may be seen explicitly as follows. The states with charge $-\frac{N_1N_2}{2} + m$ have the form

$$\bar\psi_{a_1b_1}\bar\psi_{a_2b_2}\dots\bar\psi_{a_mb_m}|0\rangle \ , \tag{5.6.94}$$

but there is no way to contract the indices of $SU(N_1)$ and of $SU(N_2)$; in contrast to the $O(N)$ case, the tensor $\delta_{a_1a_2}$ is not available. If $N_1 = N_2 = N$ there seems to be a state at level N obtained by contracting (5.6.94) with $\epsilon_{a_1\dots a_N}\epsilon_{b_1\dots b_N}$, but this state vanishes due to the Fermi statistics.

Using (5.6.92) we can express the Hamiltonian (5.6.88) in terms of the Casimirs:

$$H = g\Big(2C_2^{SU(N_1)} + \frac{1}{N_1}Q^2 - \frac{1}{4}N_1^2N_2\Big) . \tag{5.6.95}$$

Therefore, all the states in the same representation of $SU(N_1) \times SU(N_2) \times U(1)$ are degenerate, which makes this matrix model very simple. In table 5.5 we list the spectra of the the Hamiltonian (5.6.88) for a few different values of N_1 and N_2.

(N_1, N_2)	(1,2)	(1,3)	(2,2)	(2,3)
$\frac{2}{g}E_{\text{degeneracy}}$	-1_2	-1_6	-4_3	-5_{12}
	1_2	3_2	0_{10}	-3_{16}
			4_3	1_{12}
				3_{20}
				9_4

Table 5.5: Spectra of the $SU(N_1) \times SU(N_2) \times U(1)$ symmetric matrix models.

5.6.3 The $O(N_1) \times O(N_2) \times U(1)$ model

Setting $N_3 = 2$ in the $O(N_1) \times O(N_2) \times O(N_3)$ symmetric tensor model (5.1.2) we find a complex matrix model with $O(N_1) \times O(N_2) \times U(1)$ symmetry. This model has some features in common with the $SU(N_1) \times SU(N_2) \times U(1)$ model discussed in the previous section; they possess the same $2^{N_1 N_2}$ dimensional Hilbert space. However, in the present model the symmetry is broken to $O(N_1) \times O(N_2) \times U(1)$ by the Hamiltonian. Although the model is still exactly solvable, it is quite interesting in that the energy is not completely fixed by the quadratic Casimir operators of $O(N_1) \times O(N_2) \times U(1)$. Also, as we have seen in section 5.5, for even N_1 and N_2 the model contains singlet states.

To construct the Hilbert space, we define the operators [52]

$$\begin{aligned} &\bar{\psi}_{ab} = \frac{1}{\sqrt{2}}\left(\psi^{ab1} + i\psi^{ab2}\right), \quad \psi_{ab} = \frac{1}{\sqrt{2}}\left(\psi^{ab1} - i\psi^{ab2}\right), \\ &\{\bar{\psi}_{ab}, \bar{\psi}_{a'b'}\} = \{\psi_{ab}, \psi_{a'b'}\} = 0, \quad \{\bar{\psi}_{ab}, \psi_{a'b'}\} = \delta_{aa'}\delta_{bb'}, \end{aligned} \tag{5.6.96}$$

where $a = 1, 2, \ldots N_1$ and $b = 1, 2 \ldots N_2$. In this basis, the $O(2)$ charge is

$$\begin{aligned} &Q = \frac{1}{2}[\bar{\psi}_{ab}, \psi_{ab}] = \bar{\psi}_{ab}\psi_{ab} - \frac{1}{2}N_1 N_2, \\ &[Q, \bar{\psi}_{ab}] = \bar{\psi}_{ab}, \quad [Q, \psi_{ab}] = -\psi_{ab}, \end{aligned} \tag{5.6.97}$$

while the $SO(N_1)$ and $SO(N_2)$ charges are

$$Q_1^{aa'} = i\left(\bar{\psi}_{ab}\psi_{a'b} - \bar{\psi}_{a'b}\psi_{ab}\right) ,$$
$$Q_2^{bb'} = i\left(\bar{\psi}_{ab}\psi_{ab'} - \bar{\psi}_{ab'}\psi_{ab}\right) . \tag{5.6.98}$$

Squaring these charges, we find the following expressions for quadratic Casimirs:

$$C_2^{O(N_1)} = \frac{1}{2}Q_1^{aa'}Q_1^{aa'} = \bar{\psi}_{ab}\bar{\psi}_{ab'}\psi_{a'b}\psi_{a'b'} + \bar{\psi}_{ab}\bar{\psi}_{a'b'}\psi_{ab'}\psi_{a'b} + (N_1-1)\left(Q + \frac{1}{2}N_1N_2\right) ,$$
$$C_2^{O(N_2)} = \frac{1}{2}Q_2^{bb'}Q_2^{bb'} = \bar{\psi}_{ab}\bar{\psi}_{a'b}\psi_{ab'}\psi_{a'b'} - \bar{\psi}_{ab}\bar{\psi}_{a'b'}\psi_{ab'}\psi_{a'b} + (N_2-1)\left(Q + \frac{1}{2}N_1N_2\right) . \tag{5.6.99}$$

Setting $k = 1$ in (5.3.25), we find that the traceless form of the Hamiltonian is

$$H = \frac{g}{2}\left(\bar{\psi}_{ab}\bar{\psi}_{ab'}\psi_{a'b}\psi_{a'b'} - \bar{\psi}_{ab}\bar{\psi}_{a'b}\psi_{ab'}\psi_{a'b'}\right) + \frac{g}{2}(N_2-N_1)Q + \frac{g}{8}N_1N_2(N_2-N_1) . \tag{5.6.100}$$

This Hamiltonian exhibits the charge conjugation symmetry which acts as $\bar{\psi}_{ab} \leftrightarrow \psi_{ab}$. This means that states with opposite eigenvalues of Q have the same energy.

There is a "Clifford vacuum" state, which satisfies

$$\psi_{ab}|0\rangle = 0 , \qquad Q|0\rangle = -\frac{N_1N_2}{2}|0\rangle , \qquad H|0\rangle = \frac{g}{8}N_1N_2(N_2-N_1)|0\rangle . \tag{5.6.101}$$

There is also the conjugate vacuum $|0'\rangle = \prod_{ab}\bar{\psi}_{ab}|0\rangle$ which satisfies

$$\bar{\psi}_{ab}|0'\rangle = 0 , \qquad Q|0'\rangle = \frac{N_1N_2}{2}|0'\rangle , \qquad H|0'\rangle = \frac{g}{8}N_1N_2(N_2-N_1)|0'\rangle . \tag{5.6.102}$$

Both of these states are invariant not only under $O(N_1) \times O(N_2)$, but under the enhanced symmetry $O(N_1N_2)$. It is interesting to note that the states $|0\rangle$ and $|0'\rangle$ saturate the energy bound (5.3.34). Indeed, substituting $N_3 = 2$, $C_2^{O(N_3)} = Q^2 = (N_1N_2)^2/4$, $C_2^{O(N_1)} = C_2^{O(N_2)} = 0$ into that equation we find $|E| \leq \frac{g}{8}N_1N_2|N_2 - N_1|$. In fact, the bound obtained from (5.3.21)

completely fixes the energy to be $\frac{g}{8}N_1N_2(N_2-N_1)$ because the states are $O(N_1N_2)$ invariant and $C_2^{O(N_1N_2)}=0$.

The states with vanishing $O(2)$ charge Q are obtained by acting on $|0\rangle$ with $\frac{N_1N_2}{2}$ creation operators $\bar{\psi}_{ab}$. Then, to insure that the state is also a singlet under $SO(N_1)\times SO(N_2)$, we have to contract the indices using the invariant tensors $\epsilon_{a_1,\ldots a_{N_1}}$, $\delta_{a_1a_2}$ and $\epsilon_{b_1,\ldots b_{N_2}}$, $\delta_{b_1b_2}$. Some states invariant under $SO(N_1)\times SO(N_2)\times O(2)$ are listed in Appendix C.2.3.

For low values of N_1 and N_2 it is possible to construct the complete spectrum via direct numerical diagonalization. If $N_1 = N_2$ or if one or both N_i are equal to 2, the spectrum is symmetric under $E\to -E$ due to the fact that the interchange of two $O(N)$ groups send $H\to -H$. For all other values of N_i the spectrum is not symmetric under $E\to -E$. The results for some low values of N_1, N_2 are shown in table 5.6. For the $O(4)^2\times O(2)$ model the spectrum is plotted in figure 5.1.

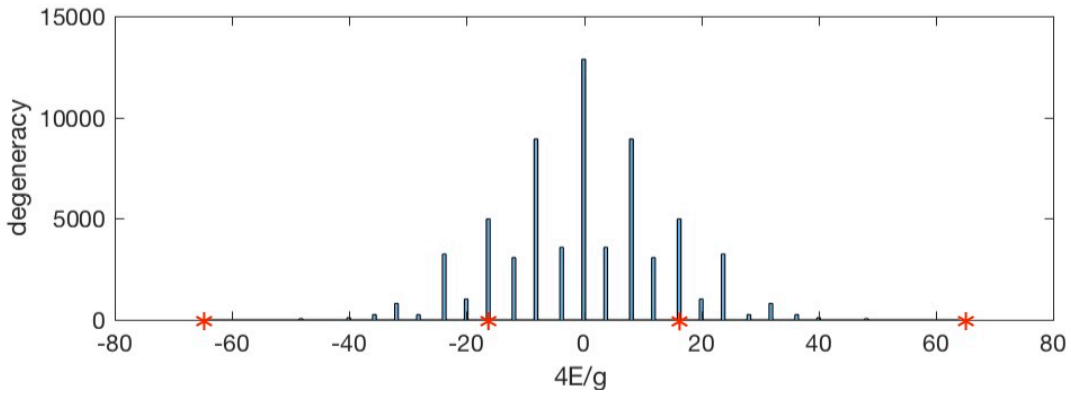

Figure 5.1: Spectrum of the $O(4)^2\times O(2)$ model. There are four singlet states, and the stars mark their energies.

A remarkable feature of the spectra is that all the eigenvalues of $4H/g$ are integers. This suggests that this fermionic matrix model is exactly solvable for any N_1 and N_2. This is indeed the case, as we now show. The Hilbert space can be constructed by repeatedly acting with $\bar{\psi}_{ab}$ on the vacuum state $|0\rangle$. One can group the a, b indices into a multi-index A, ranging from 1 to N_1N_2. The commutation relations are invariant under the action of $SU(N_1N_2)$ on the Hilbert space, which preserves the commutation relations. Let us notice that the first term of Hamiltonian

(N_1, N_2)	(2,2)	(2,3)	(3,3)	(2,4)	(4,3)	(4,4)
$\frac{4}{g}E_{\text{degeneracy}}$	-8_1	-13_2	-20_6	-24_1	-34_6	-64_1
	0_{14}	-7_6	-16_{18}	-16_2	-28_{24}	-48_{55}
	8_1	-3_2	-12_{16}	-12_{16}	-24_8	-40_{106}
		-1_{22}	-8_{60}	-8_{23}	-22_{76}	-36_{256}
		1_{22}	-4_{42}	-4_{16}	-20_{40}	-32_{810}
		3_2	0_{228}	0_{140}	-18_{14}	-28_{256}
		7_6	4_{42}	4_{16}	-16_{152}	-24_{3250}
		13_2	8_{60}	8_{23}	-14_{168}	-20_{1024}
			12_{16}	12_{16}	-12_{40}	-16_{4985}
			16_{18}	16_2	-10_{170}	-12_{3072}
			20_6	24_1	-8_{240}	-8_{8932}
					-6_{194}	-4_{3584}
					-4_{384}	0_{12874}
					-2_{270}	4_{3584}
					0_{248}	8_{8932}
					2_{640}	12_{3072}
					4_{384}	16_{4985}
					6_{76}	20_{1024}
					8_{312}	24_{3250}
					10_{216}	28_{256}
					14_{32}	32_{810}
					16_{128}	36_{256}
					18_{168}	40_{106}
					20_{64}	48_{55}
					26_{10}	64_1
					28_{24}	
					30_6	
					38_2	

Table 5.6: Spectra of the $O(N_1) \times O(N_2) \times O(2)$ models, which were obtained by a direct matrix diagonalization of the Hamiltonian (5.3.25) whose spectrum is traceless. If both N_1 and N_2 are even, the ground state is non-degenerate and is therefore a singlet.

(5.3.25) is invariant under $SU(N_1)\times O(N_2)\times U(1)$, while the second under $O(N_1)\times SU(N_2)\times U(1)$ groups. Therefore, the full Hamiltonian is invariant only under the action of $O(N_1) \times O(N_2)\times$ group. The complete Hilbert space is transformed under the $SU(N_1N_2)$ group that can be split into $SU(N_1) \times SU(N_2)$ representations. In each representation R under $SU(N_2)$, operators Q_2^α act by matrices $(T_2^\alpha)_R$ in the corresponding representation R. In turn, these representations can be split into $SO(N_1) \times SO(N_2)$ irreducible representations. Since the Hamiltonian has only

$SO(N_1) \times SO(N_2)$ symmetry, all the states in such a representation are degenerate (of course, not all the states in a given $SU(N_1) \times SU(N_2)$ representation are in general degenerate).

Now we take the difference between equations (5.6.99), and also use the difference of equations (5.6.92), to find the following nice expression for the Hamiltonian:

$$\begin{aligned} H &= -\frac{g}{2}\left(2C_2^{SU(N_1)} - 2C_2^{SU(N_2)} - C_2^{SO(N_1)} + C_2^{SO(N_2)} + \frac{N_2 - N_1}{N_1 N_2}Q^2\right) \\ &= -\frac{g}{2}\left(4C_2^{SU(N_1)} - C_2^{SO(N_1)} + C_2^{SO(N_2)} + \frac{2}{N_1}Q^2 - \frac{1}{4}N_1N_2(N_1+N_2)\right), \end{aligned} \tag{5.6.103}$$

where we used (5.6.93) to obtain the second line from the first. Due to the $C_2^{SO(N_i)}$ terms, the spectrum is not symmetric under $SU(N_1) \times SU(N_2)$.

Using (5.6.103) we can show that the lowest singlet saturates the energy bound (5.3.36), i.e. it is a ground state. For a singlet, Q and the quadratic Casimir operators of $SO(N_1)$ and $SO(N_2)$ vanish. To minimize the energy we should take a state which has the greatest possible value of $C_2^{SU(N_1)}$ allowed by (5.6.93). Thus, it has $C_2^{SU(N_1)} = \frac{(N_1+N_2)N_1N_2}{8}$ and $C_2^{SU(N_2)} = 0$, i.e. it is invariant under $SO(N_1) \times SU(N_2) \times O(2)$. Substituting this into (5.6.103) we see that this state has $E = -\frac{g}{8}(N_1+N_2)N_1N_2$, i.e. it saturates the bound (5.3.36). This value of Casimir corresponds to the rectangular Young diagram $\lfloor N_1/2 \rfloor \times N_2$ for $SU(N_1)$. Similarly, the singlet state with the highest possible energy, $E = \frac{g}{8}(N_1+N_2)N_1N_2$, has $C_2^{SU(N_2)} = \frac{(N_1+N_2)N_1N_2}{8}$ and $C_2^{SU(N_1)} = 0$, i.e. it is invariant under $SU(N_1) \times SO(N_2) \times O(2)$.

To calculate the energies of all states, we need to first decompose the Hilbert space into $SU(N_1)_L \times SU(N_2)_R$ representations and then, in turn, decompose these representations into $SO(N_1)_L \times SO(N_2)_R$ representations. To find which $SU(N_1)_L \times SU(N_2)_R$ representations (L, R) we have in the Hilbert space, we need to compute the following integral over $SU(N_1)_L \times SU(N_2)_R$:

$$\text{multiplicity}\,(L,R) = \int dU_1 dU_2 \;\; \exp\left(\sum_{n=1}^{\infty} \frac{(-1)^{n+1}}{n} \operatorname{Tr} U_1^n \;\; \operatorname{Tr} U_2^n\right) \operatorname{Tr}_L U_1 \;\; \operatorname{Tr}_R U_2 \tag{5.6.104}$$

We can always put U_1 and U_2 in a diagonal form: $U_1 = \mathrm{diag}(w_1, \ldots, w_{N_1})$, $U_2 = \mathrm{diag}(q_1, \ldots, q_{N_2})$. w_i and q_i are corresponding SU holonomies, i.e. $|w_i| = |q_i| = 1$ and $w_1 \ldots w_{N_1} = q_1 \ldots q_{N_2} = 1$.

Actually, it is not neccessary to compute the above integral for various representations. It is very well-known that characters of $SU(N_1)$ representations are Schur polynomials $\mathrm{Tr}_L\, U_1 = \chi_L(w)$ which form a basis in the space of symmetric functions of N_1 variables. This space also contains the so-called power series polynomials $\mathrm{Tr}\, U_1^n = p_n(w) = w_1^n + \cdots + w_{N_1}^n$. A conversion from power series p_n to χ_L can be easily done on a computer. For example,

$$p_1 = \chi_{\square}, \quad p_1^2 = \chi_{\square\square} + \chi_{\begin{smallmatrix}\square\\\square\end{smallmatrix}},$$
$$p_2 = \chi_{\square\square} - \chi_{\begin{smallmatrix}\square\\\square\end{smallmatrix}}, \quad p_1 p_2 = \chi_{\square\square\square} - \chi_{\begin{smallmatrix}\square\square\\\square\end{smallmatrix}}. \tag{5.6.105}$$

This suggests the following simple procedure yielding the list of all representations directly. One expands the exponent

$$\exp\left(\sum_{n=1}^{\infty} \frac{(-1)^{n+1}}{n} x^n\ \mathrm{Tr}\ U_1^n\ \mathrm{Tr}\ U_2^n\right) = \exp\left(\sum_{n=1}^{\infty} \frac{(-1)^{n+1}}{n} x^n p_n(w) p_n(q)\right) \tag{5.6.106}$$

in power series in x. Then at each level x^k we have a polynomial in $p_l(w)$ and $p_m(q)$. It can be re-expressed in terms of Schur polynomials. This gives the list of representations under $SU_L(N_1) \times SU_R(N_2)$ at level k, i.e. for states where there are k raising operators $\bar{\psi}$ acting on the vacuum.

After finding the representations under $SU(N_1)_L \times SU(N_2)_R$, we need to decompose then in terms of $SO(N_1)_L \times SO(N_2)_R$ representations. Recall that both SU and SO representations are classified by Young diagrams. The only difference is that for SO representations one has to subtract all the traces in each row, where indices are symmetric. It means that if we want to extract SO representations from a given SU representation λ, we need to consecutivly remove all possible pairs of boxes in each row. The resulting sequence of Young diagrams give SO representations.

Let us exhibit this method to find the spectrum of the $O(2)^3$ model. We have the following representations under $SU(2)_L \times SU(2)_R$ [7]:

$$2([1],[1]) + 2([2],[2]) + ([1],[3]) + ([3],[1]) \ . \tag{5.6.107}$$

The [2] of $SU(2)$ gives the spin 1 $SO(2)$ representation, whereas the [3] decomposes as $[3] = 2+0$. So we have the following $SO(2) \times SO(2)$ representations:

$$2(0,0) + 2(1,1) + 2(0,0) + (0,2) + (2,0) \ . \tag{5.6.108}$$

The two states $(0,0)$ coming from $([1],[3])$ and $([3],[1])$ have energies $\pm 2g$, while all the other states have energy zero. If we label the states by their $O(2)^3$ charges (Q_1, Q_2, Q_3), we find, in agreement with [144], that the states with $E = \pm 2g$ are $(0,0,0)$, while the 14 zero-energy states are

$$\begin{aligned}&(1,1,1),(0,0,2),(0,2,0),(2,0,0),(1,1,-1),(1,-1,1),(-1,1,1),\\ &(-1,-1,-1),(0,0,-2),(0,-2,0),(-2,0,0),(-1,-1,1),(-1,1,-1),(1,-1,-1) \ .\end{aligned} \tag{5.6.109}$$

These states may be decomposed into irreducible representations of the alternating group A_3. For example, the state with charges $(1,1,1)$ is invariant under A_3; the 3 states with charges $(0,0,2),(0,2,0),(2,0,0)$ can be combined into an invariant combination and a dimension 2 representation; etc.

As a further check, in appendix C.2.2 we calculate the spectrum of the $O(3) \times O(2) \times O(2)$ model using this method. The results for the energies and their degeneracies agree with the direct diagonalization of the Hamiltonian, whose results are assembled in Table 5.6. We also note that, due to the charge conjugation symmetry, the energies and representations at oscillator level n are the same as at level $N_1 N_2 - n$.

[7] Here we are using the notation multiplicity$([\text{dim}]_L, [\text{dim}]_R)$ for the $SU(2)_L \times SU(2)_R$ representations and multiplicity$(\text{spin}_L, \text{spin}_R)$ for $SO(2)_L \times SO(2)_R$ representations. For non-zero spin J, the $SO(2)$ representation is two-dimensional and includes the states with $SO(2)$ charge $Q = \pm J$.

Appendix A

Details of BFSS calculations

A.1 Details of the perturbative computations

A.1.1 Non singlets in the BMN matrix model

In this Appendix we will study the BMN matrix model. Lagrangian reads as follows:

$$\mathcal{L} = \frac{1}{g^2}\left(\frac{1}{2}\sum_{I=1}^{9}\left(\dot{X}^I\right)^2 - \frac{1}{2}\left(\frac{\mu}{3}\right)^2\sum_{a=1,2,3}(X^a)^2 - \frac{1}{2}\left(\frac{\mu}{6}\right)^2\sum_{i\geq 4}(X^i)^2 + \frac{1}{2}\psi\dot{\psi} - \frac{\mu}{8}\psi\gamma_{123}\psi + \right.$$
$$\left. -i\frac{1}{3}\mu g\sum_{a,b,c=1}^{3}\mathrm{Tr}\left(X^aX^bX^c\right)\epsilon_{abc} + \frac{1}{4}\mathrm{Tr}\left([X^I,X^J]^2\right) + i\frac{1}{2}\mathrm{Tr}\left(\psi\gamma^I[\psi,X^I]\right)\right) \tag{A.1.1}$$

And supersymmetry transformations are given by:

$$\begin{aligned}
\left[Q\epsilon, X^I\right] &= \psi\gamma^I\epsilon(t)\\
[Q\epsilon,\psi] &= \left(\gamma^I DX^I + c_I\mu X^I\gamma^I\gamma_{123} + i\frac{1}{2}[X^I,X^J]\gamma^{IJ}\right)\epsilon(t)\\
[Q\epsilon, A] &= \epsilon(t)\psi\\
\epsilon(t) &= e^{-\frac{1}{12}\mu\gamma_{123}t}\epsilon_0\\
c_a &= 1/3 \text{ for } a = 1,2,3 \text{ and } c_i = -1/6 \text{ for } i \geq 4
\end{aligned} \tag{A.1.2}$$

Note that supersymmetry transformations are time dependent. In the supercharge we have an additional term proportional to μ:

$$Q\epsilon = \mathrm{Tr}\left(-P^I\psi\gamma^I\epsilon - i\frac{1}{2g^2}[X^K, X^L]\psi\gamma_{KL}\epsilon - \frac{\mu}{g}c_I X^I\psi\gamma^I\gamma_{123}\epsilon\right) \tag{A.1.3}$$

Apart from the gauge transformation generator, supercharge anticommutator now also contains rotations generators $M_{\alpha\beta}$:

$$\{Q_\alpha, Q_\beta\} = 2H\delta_{\alpha\beta} + 2\,\mathrm{Tr}\left(GX^L\right)\gamma^L_{\alpha\beta} + M_{\alpha\beta} \tag{A.1.4}$$

$$\begin{aligned} M_{\alpha\beta} = &-(\mu/3)\sum_{i,j\geq 4}\mathrm{Tr}(X^jP^i)\left(\gamma_{ji}\gamma_{123}\right)_{\alpha\beta} + (2/3)\mu\sum_{a,b,c=1}^{3}\mathrm{Tr}(X^aP^b)\epsilon^{abc}\gamma^c_{\alpha\beta} \\ &-\frac{\mu}{6g^2}\sum_{i,j\geq 4}\mathrm{Tr}\left(\psi\gamma_{ij}\psi\right)\left(\gamma^{ij}\gamma^{123}\right)_{\alpha\beta} + \frac{\mu}{12g^2}\sum_{a,b\in 1,2,3}\mathrm{Tr}\left(\psi\gamma_{ab}\psi\right)\left(\gamma^{ab}\gamma^{123}\right)_{\alpha\beta} \end{aligned} \tag{A.1.5}$$

Also recall that the gauge transformation generator is given by:

$$G = \frac{i}{2g^2}\left(2[D_tX^I, X^I] + [\psi_\alpha, \psi_\alpha]\right) \tag{A.1.6}$$

Again, since the super charge gauge is invariant:

$$[Q_\alpha, G] = 0 \tag{A.1.7}$$

Hamiltonian is given by:

$$\begin{aligned} H = \frac{1}{g^2}\,\mathrm{Tr}\Bigg(&g^4\frac{P_I^2}{2} - \frac{1}{4}[X^I, X^J]^2 - i\frac{1}{2}\psi\gamma^I[\psi, X^I] + \frac{1}{2}\left(\frac{\mu}{3}\right)^2\sum_{a=1,2,3}(X^a)^2 + \\ &+\frac{1}{2}\left(\frac{\mu}{6}\right)^2\sum_{i\geq 4}(X^i)^2 + \frac{\mu}{8}\psi\gamma_{123}\psi + i\frac{\mu}{3}\sum_{a,b,c=1}^{3}\mathrm{Tr}\left(X^aX^bX^c\right)\epsilon_{abc}\Bigg) \end{aligned} \tag{A.1.8}$$

However since the supersymmetry transformations are time-dependent now, commutator of Hamiltonian with a supercharge is proportional to a supercharge:

$$[Q_\alpha, H] = -\operatorname{Tr}(\psi_\alpha G) - \frac{\mu}{12} Q_\beta \gamma^{123}_{\beta\alpha} \tag{A.1.9}$$

As in the BFSS case, we can remove the gauge transformation generators from the SUSY algebra by imposing (2.2.6) and redefining Hamiltonian:

$$H^{\text{new}} = H - \operatorname{Tr}\left(X^1 G\right) \tag{A.1.10}$$

Now lets discuss the perturbative spectrum of this model. It would be convenient to introduce indices from the beginning of the Latin alphabet $a, b, c, \ldots$ running from 1 to 3 whereas $i, j, k, \ldots$ run from 4 to 9. We can introduce creation-annihilation operators by:

$$\begin{aligned} a_b &= \sqrt{\frac{3}{\mu}} \left(\frac{g P_b}{\sqrt{2}} - i \frac{\mu}{3\sqrt{2} g} X_b \right) \\ a_i &= \sqrt{\frac{6}{\mu}} \left(\frac{g P_i}{\sqrt{2}} - i \frac{\mu}{6\sqrt{2} g} X_i \right) \end{aligned} \tag{A.1.11}$$

$SO(6)$ sector oscillators has mass $\mu/6$ and $SO(3)$ sector has mass $\mu/3$. Free Hamiltonian reads as:

$$H_0 = \frac{\mu}{3} \operatorname{Tr} a_b^\dagger a_b + \frac{\mu}{6} \operatorname{Tr} a_i^\dagger a_i \tag{A.1.12}$$

Let us concentrate on the lightest $SO(6)$ sector. The leading order correction to the energy was computed in [27] to be:

$$V^{(1)}_{\text{eff}} = g^2 \left(\frac{3}{\mu} \right)^2 \left(N : \operatorname{Tr} a_i^\dagger a_i : + \frac{1}{2} : \operatorname{Tr}[a_i^\dagger, a_i][a_j^\dagger, a_j] : - \frac{1}{2} : \operatorname{Tr}[a_i^\dagger, a_j][a_i^\dagger, a_j] : - : \operatorname{Tr}[a_i^\dagger, a_j^\dagger][a_i, a_j] : \right) \tag{A.1.13}$$

where one has to sum over all possible indices i, j ranging from 4 to 9.

Therefore for the simplest adjoint state $a_i^\dagger|0\rangle$ the first-order correction is positive. We can rewrite the effective potential in a bit different form [27]:

$$V_{\text{eff}}^{(1)} = g^2 \left(\frac{3}{\mu}\right)^2 \left(\frac{1}{2} \Big(: \mathrm{Tr}[a_i^\dagger, a^i] T^a : \Big) \Big(: \mathrm{Tr}[a_i^\dagger, a^i] T^a : \Big) - \frac{1}{2} : \mathrm{Tr}[a_i^\dagger, a_j][a_i^\dagger, a_j] : - : \mathrm{Tr}[a_i^\dagger, a_j^\dagger][a_i, a_j] : \right) \tag{A.1.14}$$

The last two terms are exactly the 1-loop dilatation operator in $\mathcal{N} = 4$ SYM. One can show that the first term is zero for singlet states. For non-singlet states build from $a_i^\dagger$ its value is proportional to the number of non-contracted indices. That is, this term is proportional to the quadratic Casimir of the corresponding representation. To sum up, at 1-loop level the energy of non-singlets in the representation R goes up:

$$\Delta \hat{H}_{\text{1-loop}} = \Delta \hat{H}_{\text{gauged, 1-loop}} + \frac{9g^2}{2\mu^2} C_2(R) \tag{A.1.15}$$

However, if we study the modified Hamiltonian (A.1.10), we have to take into account the correction coming from the operator $\mathrm{Tr}\left(X^1 G\right)$. Second-order perturbation theory for this additional correction yields:

$$-g^2 \left(\frac{3}{\mu}\right)^2 \left(: N \,\mathrm{Tr}\, a_i^\dagger a_i : + \frac{1}{2} : \mathrm{Tr}[a_i^\dagger, a_i][a_j^\dagger, a_j] : \right) \tag{A.1.16}$$

This contribution completely cancels the non-singlet contribution in (A.1.14). It means that the theory with supersymmetric Wilson loop has a protected $SO(6)$ sector, like the original theory. For example, the energy of the simplest adjoint state $a_i^\dagger|0\rangle$ is protected and is given by

$$E = \frac{\mu}{6} \tag{A.1.17}$$

A.1.2 BFSS model

In this Appendix we will discuss the perturbative spectrum of adjoints and derive the estimate (2.3.11). We consider a background with diagonal matrices $\langle X^I \rangle = B^I = \text{diag}(B^I_1, \ldots, B^I_N)$. These break the $SU(N)$ symmetry, so we will have a compact manifold of Goldstone bosons. In principle we need to study the quantum mechanics on this manifold. Since $SU(N)$ acts on this manifold this quantum mechanics gives rise to states charged under $SU(N)$. From the analysis of the gauged model we know that there is a single uncharged state. We now want to discussed the states with $SU(N)$ charges. One can obtain their spectrum as follows.

We want to study the angular motion around the diagonal background $\langle X^I \rangle = B^I$. Therefore we focus on X^I in the following form:

$$X^I(t) = U(t) B^I U^\dagger(t) \tag{A.1.18}$$

and plug this expression into the original Lagrangian to find the effective action for U:

$$S = \frac{1}{2g^2} \int dt \, \text{Tr} \left((U^\dagger \partial_t U)_r{}^s (\vec{B}_r - \vec{B}_s)^2 (U^\dagger \partial_t U)_s{}^r \right) \tag{A.1.19}$$

where we have used a shot-hand notation $\sum_{I=1}^9 (B^I_r - B^I_s)^2 = (\vec{B}_r - \vec{B}_s)^2$

Now we need to analyse the symmetries carefully. Under the original $SU(N)$ gauge transformation L, X^I transforms as in eq. (A.1.18): $X^I \to L X^I L^\dagger$. It is equivalent to multiplying U by L from the *left*:

$$U \to LU \tag{A.1.20}$$

In other words, the original gauge group $SU(N)$ acts by left rotations of U. Obviously, it is a symmetry of (A.1.19). So the states will come in $SU(N)$ multiplets. The corresponding charges are given by:

$$G_r{}^s = \frac{1}{g^2} \, \text{Tr} \left(U^\dagger \partial_t U [B^I, [B^I, U^\dagger T_r{}^s U]] \right) \tag{A.1.21}$$

It is straightforward to check that they coincide with the charges G in the Gauss law (1.2.2), as expected. Note that ${G_r}^s$ is not a matrix element, but a charge corresponding to $SU(N)$ algebra generator ${T_r}^s$ which has only one non-zero element on r-row and s-column.

However, we can also multiply U by a $SU(N)$ matrix R from the *right*:

$$U \to UR \tag{A.1.22}$$

This is not a symmetry of (A.1.19). So the corresponding current

$$\widetilde{G}_r{}^s = \frac{1}{g^2}\,\mathrm{Tr}\left(U^\dagger \partial_t U [B^I, [B^I, {T_r}^s]]\right) = \frac{1}{g^2}(U^\dagger \partial_t U)_r{}^s (\vec{B}_r - \vec{B}_s)^2 \tag{A.1.23}$$

does not commute with the Hamiltonian. Nonetheless, as was clarified in [59, 58] left and right multiplications of U are tightly related. To understant this, let us consider a wave function $\Psi^a_{\mathcal{R}}(X^I),\ a = 1, \ldots, \dim \mathcal{R}$ in some representation $\mathcal{R}$ under the gauge group. Since it lives in the representation $\mathcal{R}$ it has, by definition, the following decomposition:

$$\Psi^a_{\mathcal{R}}(X^I) = \sum_{b=1}^{\dim\ \mathcal{R}} U^{ab}_{\mathcal{R}} \psi_b\left(B^I\right) \tag{A.1.24}$$

where $U^{ab}_{\mathcal{R}}$ is the ab matrix element of U in the representation $\mathcal{R}$. We are interested solely in $\psi_b\left(B^I\right)$ which also lives in $\mathcal{R}$. Left $SU(N)$ rotations of U rotate $\Psi^a_{\mathcal{R}}(X^I)$ and U, leaving $\psi_b(B^I)$ invariant. Whereas right rotations transform U and $\psi_b(B^I)$, leaving $\Psi^a_{\mathcal{R}}(X^I)$ invariant. Note that in both cases the representation $\mathcal{R}$ *is the same*. It means that charges $\widetilde{G}_r{}^s$ act on states $\psi_b\left(B^I\right)$ by the corresponding generator $({T_r}^s)_{\mathcal{R}}$ in the representation $\mathcal{R}$.

What is the physical meaning of operators $\widetilde{G}_r{}^s$? One can think about X^I as a rigid body in a space acted on by the $SU(N)$ transformations. Since $\Psi^a_{\mathcal{R}}(X^I)$ stays invariant under $\widetilde{G}_r{}^s$, they have a meaning of angular momentum operators in the frame where the body is fixed. It is well-known from the classical mechanics, that such operators are very useful for studying the rigid body motion, despite the fact that they are not conserved.

As we have just mentioned, $\tilde{G}_r{}^s$ do not commute with the Hamiltonian. However, the Hamiltonian can be expressed in terms of them. Indeed, it is easy to see that

$$H = \frac{g^2}{2} \sum_{r,s=1}^{N} \frac{\widetilde{G}_s{}^r \widetilde{G}_r{}^s}{(\vec{B}_s - \vec{B}_r)^2} \tag{A.1.25}$$

When we focus on a particular representation $\mathcal{R}$, then $\widetilde{G}_r{}^s$ act by the $SU(N)$ generator $(T_r{}^s)_{\mathcal{R}}$ in this representation. The corresponding wave function depends only on B^I. This wave function is exactly what we previously called $\psi_b(B^I)$. Naively, H is a $\dim \mathcal{R} \times \dim \mathcal{R}$ matrix. However, the expression for the charges in (A.1.23) implies that the diagonal elements $\tilde{G}_s{}^s = 0$ vanish (no sum). This implies that we have much less components. As we will see shortly, in the simplest case of the adjoint representation instead of the naive $N^2 - 1$ we will have only $N - 1$ states. Generically all these states have different energies. However, we would like to emphasize that each of these $N - 1$ eigenstates has a degeneracy $N^2 - 1$(or $\dim \mathcal{R}$ in the generic case) because of the angular degree of freedom U which we have eliminated.

So far we have been using the canonical quantization of non-singlets. Below we will re-derive (A.1.25) using the path integral techniques. Moreover, the fact that we always have a degeneracy $\dim \mathcal{R}$ will become especially clear.

For the case of a single matrix model the result (A.1.25) was obtained in [59, 58, 60]. But unlike the one matrix case, we cannot diagonalize all the matrices simultaneously for generic matrix configurations. Therefore (A.1.25) will receive higher loop corrections from off-diagonal fluctuations of X^I and ψ_α.

There is another, more clean-cut way, how to derive eq. (A.1.25) which will illustrate the above points. As we have mentioned in section 2.2.4 if we are interested in excitations of the *ungauged* model in a representation $\bar{\mathcal{R}}$(conjugate to $\mathcal{R}$) under $SU(N)$ we can study the *gauged* model coupled to a Wilson line in representation $\mathcal{R}$:

$$\dim \mathcal{R}\, \mathrm{Tr}_{\mathcal{R}}\, P \exp\left(i \int dt\ A_t \right) = \dim \mathcal{R}\, \mathrm{Tr}\, P \exp\left(i \int dt\ (A_t)_r{}^s (T_s{}^r)_{\mathcal{R}} \right) \tag{A.1.26}$$

At this point it is by no means necessary to think about A_t as a gauge field. In the ungauged case one can think about it as an auxillary Lagrange multiplier which forces the states to live in a particular representation. Note, however, that in the ungauged model we have to multiply the Wilson loop by the dimension of the corresponding representation. This can be explained as follows. In the ungauged model we put A_t to be zero. We can achieve this by inserting the delta function into the path integral:

$$\delta\left(P\exp\left(i\int dt\ A_t\right)\right) \tag{A.1.27}$$

Now we can re-express the delta function in terms of characters [60]:

$$\delta\left(P\exp\left(i\int dt\ A_t\right)\right) = \sum_{\mathcal{R}} \dim\mathcal{R}\,\mathrm{Tr}_{\mathcal{R}}\,P\exp\left(i\int dt\ A_t\right) \tag{A.1.28}$$

We separate X^I into the constant background B^I and a fluctuation Y^I: $X^I = B^I + Y^I$. Then the part of the (bosonic) action containing A_t reads as:

$$\frac{1}{2g^2}\int dt\ \mathrm{Tr}\left(\partial_t Y^I + i[A_t, Y^I] + i[A_t, B^I]\right)^2 \tag{A.1.29}$$

At 1-loop level we can simply ignore Y^I and integrate out only A_t. However at higher loops one has to take Y^I into account. Without Y^I we have a simple quadratic action for A_t:

$$-\frac{1}{2g^2}\int dt\ (\vec{B}_r - \vec{B}_s)^2 (A_t)_r{}^s (A_t)_s{}^r \tag{A.1.30}$$

Overall, we have the following expression:

$$\dim\mathcal{R}\int DA_t\ \exp\left(-\frac{1}{2g^2}\int dt\ (\vec{B}_r - \vec{B}_s)^2 (A_t)_r{}^s (A_t)_s{}^r\right)\mathrm{Tr}\,P\exp\left(i\int dt\ (A_t)_r{}^s (T_s{}^r)_{\mathcal{R}}\right) \tag{A.1.31}$$

Integration over A_t yields the angular potential (A.1.25).

Note that because of the factor $\dim\mathcal{R}$, each eigenstate of the angular potential (A.1.25) will contribute to the partition function with degeneracy $\dim\mathcal{R}$.

In the adjoint case $(\widetilde{G}_r{}^s)_{\mathcal{R}}$ acts by a commutator with $T_r{}^s$ on the matrix w in the $SU(N)$ algebra. Moreover w has to be diagonal, since the diagonal charges $\widetilde{G}_s{}^s$ vanish: $w = \mathrm{diag}(w_1, \ldots, w_N)$. So we have the following eigenvalue problem[1]

$$Ew_r = \frac{g^2}{2} \sum_{s=1,\ s\neq r}^{N} \frac{w_r - w_s}{(\vec{B}_r - \vec{B}_s)^2} \ , \qquad \text{with} \quad \sum_{r=1}^{N} w_r = 0 \tag{A.1.32}$$

where the last constraint comes from the restriction that the diagonal matrix w is in the adjoint. This Eigenvalue problem will have $N-1$ eigenstates. We could identify the potential in figure 2.3 as the lowest energy state of this Hamiltonian, as a function of the $\vec{B}_s$. In general, the eigenvalues will depend on the particular pattern of the distances $(\vec{B}_r - \vec{B}_s)^2$. In the next subsection we solve it for the case when a large number of vectors $\vec{B}_s$ is uniformly distributed on S^8.

There is another very simple case when the energy can be obtained exactly. Suppose we are considering a configuration where the N vector $\vec{B}_s$ take only two values: N_1 are given by $\vec{B}_1$ and the rest, $N_2 = N - N_1$, by $\vec{B}_2$. Equation (A.1.32) will be well-defined if w_i obey the same property: there are N_1 coordinates w_1 and N_2 of w_2. Using the constraint $N_1 w_1 + N_2 w_2 = 0$ we easily obtain the energy:

$$E = \frac{\lambda}{2(\vec{B}_1 - \vec{B}_2)^2} \tag{A.1.33}$$

The result depends only on the sum $N_1 + N_2$ and not on the individual N_1,N_2. Also, the factor N in the numerator is important: we expect that the energy of adjoint excitations will scale as $\lambda^{1/3}$. Indeed, the expected size of the ground state wave function is $X \approx \lambda^{1/3}$. This is the value of X where this computation breaks down. We can then identify the energy at this value of X as the order of magnitude of the energy of the adjoint excitation

$$E_{\text{adj}} \approx \lambda / X^2 = \lambda^{1/3} \tag{A.1.34}$$

[1]This can be easily obtained using the following relations $[T_r{}^s, w] = (w_s - w_r) T_r{}^s$. and also $T_r{}^s T_r{}^s = 0,\ r \neq s$ and $(T_r{}^s T_s{}^r)_{vo} = \delta_{rv}\delta_{ro}$ (no sum over r, s)

Solving the potential for a uniform distribution

There is another case when we can solve (A.1.32) exactly. Namely, lets consider the large N limit with the N vectors $\vec{B}_s$ uniformly distributed on S^8 of radius X. We will show below that the lowest energy state has energy

$$E_1 = \frac{9\lambda}{28X^2} \tag{A.1.35}$$

and we will further compute spectrum around the ground state.

This is shown as follows. With a large number of vectors uniformly distributed on S^8 we can make a continuous approximation. Then eq. (A.1.32) becomes

$$Ew(\vec{n}) = \frac{\lambda}{2X^2 \mathrm{Vol}_{S^8}} \int d\Omega'_8 \ \frac{w(\vec{n}) - w(\vec{n}')}{|\vec{n} - \vec{n}'|^2}, \qquad \int d\Omega_8 \ w(\vec{n}) = 0 \tag{A.1.36}$$

where $\vec{n}$ and $\vec{n}'$ belong to a S^8 of unit radius. Now the adjoint problem (A.1.36) has $SO(9)$ rotation symmetry. It means that the eigenfunctions are basically given by the spherical harmonics in nine dimensions and the energy depends only on the total angular momentum l. It is the most convenient to evaluate the energy using the wave function which depends only on one polar angle θ (the angle between the unit vector and X^9 axis). For such functions the measure dy reads as $\mathrm{Vol}_{S^7} \ \sin^7\theta d\theta = \mathrm{Vol}_{S^7} \ (1-t^2)^3 dt$ In this case $w(\vec{n})$ is simply the Gegenbauer polynomial $C_l^{(7/2)}(t)$. Therefore,

$$E_l C_l^{(7/2)}(1) = \frac{35\lambda}{64X^2} \int_{-1}^{1} dt \ \frac{(1-t^2)^3}{2(1-t)} \left(C_l^{(7/2)}(1) - C_l^{(7/2)}(t) \right) \tag{A.1.37}$$

which leads to the following energies:

$$E_l = \frac{3\lambda}{8X^2} \left(1 - \frac{1}{C_l^{(7/2)}(1)} \right) \sim \frac{3\lambda}{4X^2} \left(1 - \frac{1}{7l^6} \right), \ l \gg 1 \tag{A.1.38}$$

This energy comes with a degeneracy

$$N_l = \frac{(2l+7)(l+6)!}{7!l!} \sim \frac{2l^7}{7!}, l \gg 7 \tag{A.1.39}$$

It is interesting that we get a finite range of energies, from a minimum one to a maximum. This pattern is similar to what we get by a simple WKB quantization of a toy model for the motion of a folded string in Appendix A.2. However, in the gravity case, we can also have the possibility of the string falling into the black hole which leads to a much larger number of states, a number proportional to N^2, one factor of N each for the separate string and anti-string ending on the black hole.

A.1.3 Goldstone modes and $SU(N)$ rotators for the BMN model vacua

Now let us discuss the spectrum around other vacua, where the matrices have non-zero expectation values of the form $X^a = \frac{\mu}{3} J^a$. This case can be analyzed as in the previous section. The only difference is that the initial action is

$$S = \frac{\mu^2}{18g^2} \int dt \ \sum_{a=1}^{3} \mathrm{Tr}[J^a, U^\dagger \partial_t U]^2 = \frac{\mu^2}{18g^2} \int dt \ \sum_{a=1}^{3} \mathrm{Tr}\, U^\dagger \partial_t U [J^a, [J^a, U^\dagger \partial_t U]] \tag{A.1.40}$$

And the right $SU(N)$ charge equals:

$$\widetilde{G}^p = \frac{\mu^2}{9g^2} \int dt \ \sum_{a=1}^{3} \mathrm{Tr}\left([J^a, [J^a, U^\dagger \partial_t U]] T^p \right) \tag{A.1.41}$$

with $T^p,\ p = 1, \ldots, N^2 - 1$ belonging to $SU(N)$ algebra.

As we have mentioned in the main text, J^a are not necessary in the irreducible representation. Generically, we need to decompose it into L irreducible representations of dimensions $N_k,\ k = 1, \ldots, L$ such that $N_1 + \ldots + N_L = N$. For simplicity we study the maximal representation $L = 1$ and $N_1 = N$, although the calculation below can be generalized to $L > 1$ case. Even for the maximal case, when we have only one representation it is quite difficult to obtain the exact spectrum. However, it is easy to find a sensible *lower bound*.

Since we have only the kinetic term the energy equals:

$$E = \frac{\mu^2}{18g^2}\,\mathrm{Tr}\int dt\ \sum_{a=1}^{3}[J^a, U^\dagger\partial_t U]^2 \tag{A.1.42}$$

Generically, there are many ways to select Lie algebra generators T^p. However, there is a very special choice of T^p, namely the fuzzy spherical harmonics $Y^j_m,\ j = 1,\dots,N-1,\ m = -j,\dots,j$. The nice thing about them is that they are eigenvalues of the fuzzy sphere Laplacian:

$$\sum_{a=1}^{3}[J^a,[J^a,Y^j_m]] = j(j+1)Y^j_m \tag{A.1.43}$$

Also they are orthogonal:

$$\mathrm{Tr}\left(Y^j_m Y^{j'}_{m'}\right) = \frac{1}{2}\delta_{jj'}\delta_{-mm'} \tag{A.1.44}$$

Because of that they also satisfy the completeness relation:

$$\sum_{jm}\left(Y^j_m\right)_r{}^s\left(Y^j_{-m}\right)_v{}^o = \frac{1}{2}\left(\delta^o_r\delta^s_v - \frac{1}{N}\delta^o_r\delta^s_v\right),\ r,s,v,o = 1,\dots,N \tag{A.1.45}$$

Correspondingly we have the non-conserved charges $\widetilde{G}^j_m$:

$$\widetilde{G}^j_m = j(j+1)\frac{\mu^2}{9g^2}\,\mathrm{Tr}\left(U^\dagger\partial_t U Y^j_m\right) \tag{A.1.46}$$

Finally, we can rewrite the Hamiltonian in terms of $\widetilde{G}^j_m$ using eq. (A.1.45):

$$\begin{aligned} H &= \frac{\mu^2}{9g^2}\sum_{a=1}^{3}\sum_{jm}\mathrm{Tr}\left(U^\dagger\partial_t U Y^j_m\right)\mathrm{Tr}\left(Y^j_{-m}[J^a,[J^a,U^\dagger\partial_t U]]\right) = \\ &= \frac{\mu^2}{9g^2}\sum_{jm} j(j+1)\,\mathrm{Tr}\left(U^\dagger\partial_t U Y^j_m\right)\mathrm{Tr}\left(Y^j_{-m}U^\dagger\partial_t U\right) = \\ &= \frac{9g^2}{\mu^2}\sum_{jm}\frac{\widetilde{G}^j_m\widetilde{G}^j_{-m}}{j(j+1)} \end{aligned} \tag{A.1.47}$$

As we have promised, we have re-expressed the Hamiltonian in terms of charges $\widetilde{G}$. If we focus on some particular representation $\mathcal{R}$, then $\widetilde{G}^j_m$ act as Lie algebra generators $(Y^j_m)_{\mathcal{R}}$ in this representation. For example, the sum $\sum_{jm} \widetilde{G}^j_m \widetilde{G}^j_{-m} = C_2(\mathcal{R})$ equals to the quadratic Casimir of the representation. Since $j \leq N-1$ we obtain the following lower bound for the energy:

$$H \geq \frac{9g^2}{\mu^2} \frac{1}{N(N-1)} C_2(\mathcal{R}). \tag{A.1.48}$$

The above derivation can be repeated when we have several fuzzy spheres with corresponding representations N_k. In this case one arrives at the following bound:

$$H \geq \frac{1}{\max\, N_k(N_k-1)} \frac{9g^2}{\mu^2} C_2\left(\mathcal{R}\right) \tag{A.1.49}$$

For the adjoint representation of $SU(N)$ the quadratic Casimir $C_2(adj)$ is simply N. The other representations that appear are those that can arise from products of adjoints. These are the representations that transform trivially under the Z_N center of $SU(N)$.

For "small" fuzzy spheres, when $N_k \sim \mathcal{O}(N^0)$ and $L \sim \mathcal{O}(N)$, $E_{\text{adj}} \gtrsim \lambda/\mu^2$. However, if we have a "big" sphere, when some $N_k \sim N$ and so $L \sim 1$, adjoints can have much smaller energy $E_{\text{adj}} \geq \frac{g^2}{N\mu^2}$. Note that both these bounds are consistent with

$$E \sim \frac{g^2 N}{R^2} C_2(\mathcal{R}) \tag{A.1.50}$$

with $R^2 = \frac{1}{3N} \operatorname{Tr}\left(J_1^2 + J_2^2 + J_3^2\right)$. Since for each irreducible representation N_k we have the following identity:

$$J_1^2 + J_2^2 + J_3^2 = \frac{N_k^2 - 1}{4}\, \mathbf{1} \tag{A.1.51}$$

where the right hand side is simply the quadratic Casimir of $SU(2)$ in the representation of dimension N_k.

(A.1.50) is what we would have naively guessed based on the similar formula for the case of diagonal matrices X that we derived in appendix (A.1.2), and was mentioned in (2.3.11).

A.2 Analyzing the motion of a folded string

In this appendix we consider the motion of a folded stretched string. This is just a one parameter family of solutions out of the whole space of possible string motions.

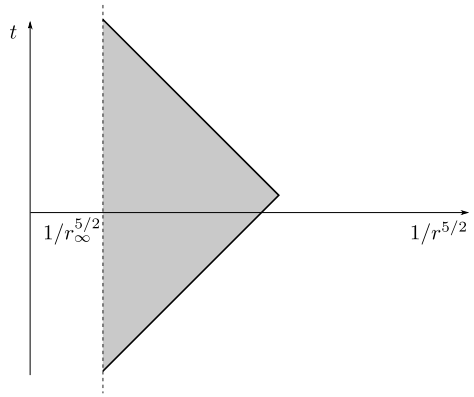

Figure A.1: Radial excitations of the adjoint string. The string tip moves close to a null-geodesic (bold line). $r_\infty \sim \lambda^{1/3}$ is the region where the high curvature region starts. We imagine that when the string reaches that point it bounces back with some reflection factor.

We can view the motion of the tip from the high curvature region to the low curvature and back as a kind of scattering problem. See Figure A.1. So we can calculate the total phase shift accumulated during the process via a WKB approximation.

We view the system as the tip of a string which is approximated as a particle with large momentum p and energy linear in the momentum. This tip is acted on by the rest of the string which provides a potential. The full Hamiltonian is

$$H = \sqrt{-\frac{g_{tt}}{g_{rr}}}|p| + \frac{r_\infty - r}{\pi} \tag{A.2.52}$$

where p is the momentum conjugate to r. The tip of the string starts from the large r region with very high ingoing radial momentum, the string pulls and slows it down until the tip bounces back to the large r region, see Figure A.1. The total phase shift then is

$$\delta_{\text{bulk}} = 2\int_{r_\infty - \pi E}^{r_\infty} dr\ p \tag{A.2.53}$$

Which can be re-written in terms of the total energy E given in (A.2.52). This gives for $E \to \frac{r_\infty}{\pi}$:

$$\delta_{\rm bulk} = \frac{8\sqrt{\lambda d_0}}{15\pi(\pi E_\infty - \pi E_n)^{3/2}} \tag{A.2.54}$$

Where $E_\infty \equiv \tilde{C}\lambda^{1/3}$ is the energy of a folded string that stretches all the way to $r = 0$. For this reason we expect that $\tilde{C} > C$ by an order one amount. A similar problem in the linear dilaton background that is dual to the double scaling limit of a single matrix model was analyzed in [62] and matched to the matrix model computation in [63].

In order to figure out the whole motion, we need to know how the tip bounces back from the high curvature region. This seems to be a difficult problem since the state that comes out could have more excitations on the string worldvolume. Solving this would involve connecting the motion in the weakly curved region to the motion in the perturbative matrix model region. We will not do this here. Instead we will simply assume that the problem is such that the string tip comes back out with an extra phase shift $\delta_{\rm high}$ from the high curvature region. Furthermore we will assume that it is basically a constant for $E \sim E_\infty$. This is a non-trivial assumption and it is likely wrong. The only reason we make it is to define a toy problem where we can now semiclassically quantize the motion by setting

$$\delta_{\rm bulk}(E) + \delta_{\rm high} = 2\pi n \tag{A.2.55}$$

Leading to

$$E_n \sim \lambda^{1/3}\left[\widetilde{C} - \frac{1}{\pi}\left(\frac{4\sqrt{d_0}}{15\pi^2(n-n_0)}\right)^{2/3}\right], \qquad n_0 \equiv \frac{\delta_{\rm high}}{2\pi} \tag{A.2.56}$$

Note that n_0 is not an integer.

We see that there is an infinite tower of excitations. For non-zero temperature, there is actually an $n_{max} - n_0 \propto T^{-3/5}$ where the states change behavior qualitatively, the folded string falls into the black hole horizon and stays there forever. (At finite N the string can break and

the fold can return to infinity). To describe this behavior we need to study the non-extremal metric (1.2.7). Now we have a non-extremal black hole with a horizon at $r = r_0$. If the string has enough energy to reach the horizon, then the tip will fall into the black hole and never come back. This sets an upper bound for the energy:

$$E_{\rm dec} - E_\infty = -\frac{r_0}{\pi} \tag{A.2.57}$$

Moreover now we have a finite number of excited states that do not fall into the black hole

$$n_{\rm max} - n_0 = \sqrt{\lambda d_0} \int_{r_0}^{r_\infty} dr \ \frac{r - r_0}{\pi^2 r^{7/2}(1 - r_0^7/r^7)} = \frac{4.06\sqrt{\lambda d_0}}{14\pi^2 r_0^{3/2}} \sim T^{-3/5}, \text{ for } r_\infty \gg r_0 \tag{A.2.58}$$

For states with $E > E_{\rm dec}$, the string tip falls into the black hole and the state becomes a string and an anti-string, both ending at the horizon as independent excitations.

A.3 Scaling properties of the solution and the action

In this Appendix we briefly discuss some scaling properties of the solution (1.2.7). We find that under the following rescaling of the coordinates the metric and the dilaton rescale as

$$\begin{aligned} t \to \eta t \ , \qquad & r \to \eta^{-2/5} r \\ ds^2 \to ds^2 \ \eta^{-3/5} \ , \qquad & e^{2\phi} \to e^{2\phi} \ \eta^{-21/5} \end{aligned} \tag{A.3.59}$$

The gravity action scales as

$$S_{\rm gravity} = \int d^{10}x \ e^{-2\phi}\sqrt{g}R \sim \eta^{-9/5} \sim T^{9/5} \tag{A.3.60}$$

Notice that β is rescaled when we rescale time. This is the correct behaviour of the Bekenstein–Hawking entropy (1.2.11). Notice that the action and entropy scale in the same way. Notice that

since the action changes (A.3.59) is not a symmetry of the action, but it helps determine the temperature dependence.

It turns out that the Dirac–Born–Infeld(DBI) action for a probe D0 brane in the *extremal* geometry (1.2.7) with $r_0 = 0$ has exactly the same scaling behaviour. This can be checked explicitly, but we can also derive it by the following observations. The action is

$$S_{\rm DBI} = -\int e^{-\phi} ds + \int A_t dt \tag{A.3.61}$$

We now observe

- The derivative of the free energy with respect to the charge yields the difference between the RR 1-form at the horizon and infinity[2]:

$$\frac{\partial F}{\partial N} = A_t\Big|_{\rm horizon} - A_t\Big|_{\rm infinity} \tag{A.3.62}$$

  this is why A_t scales as the free energy.

- Notice that the expression for A_t in (1.2.7) does not contain r_0. This is why it has exactly the same scaling for both extremal and non-extremal cases.

- Finally, both terms in (A.3.61) scale in the same way as in the extremal case because of the supersymmetry (there should be no force acting on a D0 brane at rest).

Now, this observation also explains why the following action has the same rescaling properties

$$S = \int dt \left[\vec{v}_i^{\,2} + ({\rm const})\frac{(\vec{v}_i - \vec{v}_j)^4}{|\vec{r}_i - r_j|^7}\right] \tag{A.3.63}$$

under (A.3.59). The reason is that the velocity expansion of (A.3.61) gives rise to a particular case of this action.

The point of these observations is to "explain" the observation in [152, 153] that (A.3.63) has the same scaling as the entropy. The arguments used in that paper were scaling arguments, and

[2]More precisely, one has to subtract the zero-temperature value in order to make this expression finite.

they have reproduced the entropy for simple scaling reasons. But it seems that the thermodynamics of (A.3.63) is really ill defined because it has a "fall to the center" instability.

Appendix B

SYK technicalities

B.1 Numerical setup for KB equations

This appendix describes our approach to the numerical solution of the Kadanoff–Baym equations. Our strategy is based on previous work on SYK reported in [37, 106].

We use a uniform two-dimensional grid to approximate the (t_1, t_2) plane. The grid spacing dt plays the role of a UV cutoff and should be much smaller than $1/J_S$ and $1/J_B$. To fix the units of energy and time, we set $J = 0.5$. In these units, we consider three grid spacings: $dt = 0.2$, $dt = 0.1$, and $dt = 0.05$. The primary numerical cost arises from the grid size, as the overall size must be large to study low temperature effects. Typically, the Green's functions decay exponentially, so the calculation can be streamlined by restricting attention to a strip $|t_1 - t_2| \lesssim c\beta_{\max}$ as shown in Figure B.5. All Green's functions are put to zero outside the strip. We take $\beta_{\max}$ to be the largest β in the problem, typically the inverse bath temperature. In practice, c is taken large enough to see converged results.

The initial Green's function is found by numerically solving the Lorentzian Schwinger–Dyson equation in equilibrium. To compute the integral in the KB equations we use the trapezoid method, and for the time propagation, we use a predictor-corrector scheme. Some care is needed when propagating along the diagonal. Fortunately, for Majorana fermions there is a simple

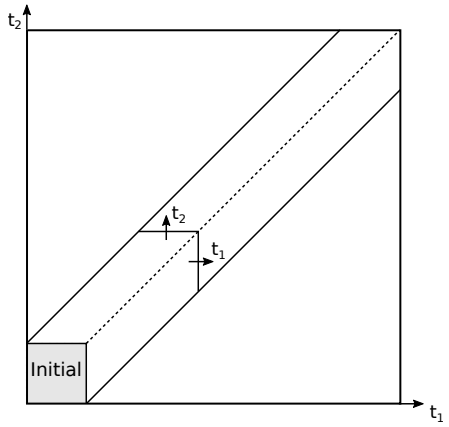

Figure B.1: Geometry of the (t_1, t_2) plane. The initial Green's functions are placed inside the gray box.

relation:

$$G_S^>(t,t) = -\frac{i}{2}. \tag{B.1.1}$$

However, for the Green's function obtained by numerically solving the DS equation the diagonal value is not exactly $-i/2$, so on a discrete lattice we just propagate this value:

$$G_S^>(j,j) = G_S^>(0,0). \tag{B.1.2}$$

The integral in the bound (3.1.5) is also computed using the trapezoid rule and the energy time derivative is discretized in a simple way: $(E_{j+1} - E_j)/dt$. To estimate the error the integral is computed for different time steps and without the coupling to the bath. Note also that we can not really integrate all the way to infinity. In order not to rely on any extrapolations, we use a crude upper-bound for the error obtained from integration over a finite interval. Obviously, since the flux is decreasing and beta in increasing to β_b we have the following inequality:

$$\int_{t_f}^{\infty} dt\ E_S' e^{-\kappa t/\beta(t)} \leq E_S'(t_f) \int_{t_f}^{+\infty}\ dt e^{-\kappa t/\beta_b} = \frac{1}{\kappa} E_S'(t_f)\beta_b e^{-\kappa t_f/\beta_b} = I_\kappa^{\mathrm{err}}. \tag{B.1.3}$$

Finally, there is a question of how to define the temperature at particular time t in non-equilibrium situation? There are two possibilities. We can consider the "diagonal slice" $G^{>}_{\text{eq}}(t;\delta)$:

$$G^{>}_{\text{eq},t}(\delta) = G^{>}_{S}(t-\delta, t+\delta), \tag{B.1.4}$$

treat it as a two-point function in the equilibrium, and find the temperature using the fluctuation-dissipation theorem (FDT):

$$\frac{\text{Im}(G^{>}_{\text{eq},t}(\omega) + G^{<}_{\text{eq},t}(\omega))}{(-2)\,\text{Im}\, G^{R}_{\text{eq},t}(\omega)} = -\tanh\frac{\beta(t)\omega}{2}. \tag{B.1.5}$$

However, this choice does not respect causality in time. Another choice is the "corner slice": $G^{>}_{\text{eq}}(t,\delta)$:

$$G^{>}_{\text{eq},t}(\delta) = \theta(\delta)G^{>}_{S}(t-\delta,t) + \theta(-\delta)G^{>}_{S}(t,t+\delta). \tag{B.1.6}$$

This choice respects causality and this corner Green's function enters in the definition of energy (1.3.30). Therefore we will adopt the corner definition. Unfortunately, the FDT holds for low frequencies only, since large frequencies are affected by the size of the discretization step. However in all our setups the relation (B.10.128) holds for low frequencies up to the frequencies of order of the discretization step $1/dt$. see Figure B.6 for a typical behavior.

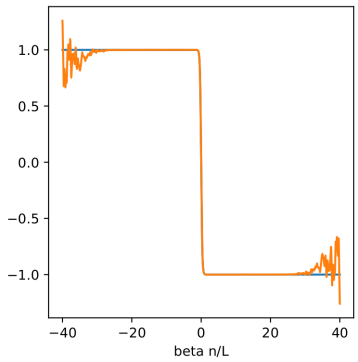

Figure B.2: (Orange) The left hand side of eq. (B.10.128) for $\beta = 80$, $dt = 0.2$. The Green function is localized on a strip of width $L = 1600$. (Blue) *tanh* function. They coincide up to frequencies corresponding to the timescale $\sim \beta/30 \sim 2.6$, which is comparable to the timestep 0.2.

B.2 Energy flux from KB equations

Consider the case $q = 4$ and one system fermion in the interaction ($f_S = 1$). The generalization to other cases is straightforward. For clarity, we denote the system's "greater" Green's function $G_>$ simply by G_S and bath's "greater" function as G_B. The energy is given by:

$$E_S(t_1) = -i\frac{J_S^2}{4}\int_{-\infty}^{t} dt_2 \ \left(G_S(t_1,t_2)^4 - G_S(t_2,t_1)^4\right). \tag{B.2.7}$$

Our approach is to differentiate it and use the KB equations. We will assume that the coupling to the bath is switched on at time $t = 0$:

$$\begin{aligned}\frac{dE_S(t_1)}{dt_1} = V^2 J_S^2 \int_{-\infty}^{t_1} dt_2 \int_0^{t_1} dt_3 \left(G_B(t_1,t_3)^{f_B} + G_B(t_3,t_1)^{f_B}\right)\Big(G_S(t_1,t_2)^3 G_S(t_3,t_2) - \\ G_S(t_2,t_1)^3 G_S(t_2,t_3)\Big) + \\ V^2 J_S^2 \int_{-\infty}^{t_1} dt_2 \int_0^{t_2} dt_3 \left(G_S(t_3,t_2) + G_S(t_2,t_3)\right)\Big(- G_S(t_1,t_2)^3 G_B(t_1,t_3)^{f_B} + \\ G_S(t_2,t_1)^3 G_B(t_3,t_1)^{f_B}\Big).\end{aligned} \tag{B.2.8}$$

This is the leading term in V. If we trust this expansion, then we can use the initial G_S to find the flux.

We can exchange the integration order in the second term:

$$\int_{-\infty}^{t_1} dt_2 \int_0^{t_2} dt_3 \to \int_0^{t_1} dt_3 \int_{t_3}^{t_1} dt_2 \to \int_0^{t_1} dt_3 \left(\int_{-\infty}^{t_1} dt_2 - \int_{-\infty}^{t_3} dt_2\right). \tag{B.2.9}$$

After that, we use the equilibrium Dyson–Schwinger equation for G_S to convert the convolution over t_2 into a time derivative, arriving at

$$E_S' = iV^2 \int_{-t}^{t} du G_B(u - i\epsilon)^{f_B} \partial_u G_S(u - i\epsilon). \tag{B.2.10}$$

B.3 Locating the peak

Suppose that the bath is "fast": $J_B\beta \ll 1$. If we assume that $t_{\text{peak}}J_B \ll 1$, then G_B varies slowly and we can Taylor expand it around $u = 0$ to greatly simplify the result. In the first part of Eq. (3.3.69) we can simply put $G_B^{f_B} = -i/2$, whereas in the integral we put $\partial_u G_B^{f_B} = -3J_B/2$. Up to an overall coefficient the flux is

$$\text{Im}\left(\frac{i\sqrt{i}}{\sqrt{\sinh\left(\frac{\pi u}{\beta}\right)}} + \frac{3\beta J_B}{\pi}\,\text{EllipticF}\left(\frac{\pi(\beta - 2iu)}{4\beta}, 2\right)\right) \tag{B.3.11}$$

Assuming $u/\beta \gg 1$ we can approximate the elliptic function by a constant:

$$\text{EllipticF}\left(\frac{\pi(\beta - 2iu)}{4\beta}, 2\right) \approx -i\,\text{EllipticK}(-1). \tag{B.3.12}$$

Now it is easy to balance the two terms to estimate

$$t_{\text{peak}} \sim \beta \log\left(\frac{1}{J_B\beta}\right), \quad J_B\beta \ll 1. \tag{B.3.13}$$

Note that both assumptions, $t_{\text{peak}}/\beta \gg 1$ and $t_{\text{peak}}J_B \ll 1$, are satisfied.

In the opposite regime, $J_B\beta \ll 1$, we assume that $t_{\text{peak}}/\beta \ll 1$. Then we can expand G_S:

$$G_S = \frac{b\sqrt{i\pi}}{\sqrt{J_S\beta}}\left(\frac{\sqrt{\beta}}{\sqrt{\pi u}} - \frac{1}{12}\left(\frac{\pi u}{\beta}\right)^{3/2}\right). \tag{B.3.14}$$

Now the integral in Eq. (3.3.69) can be computed analytically to give a lengthy expression with rational functions and a logarithm. However, if we assume that $t_{\text{peak}}J_B \gg 1$ and expand in large time u, then we find that the leading imaginary contributions are

$$2i\beta^2 J_B^2 - u^3 J_B^2 \pi^2 \log\left(4iJ_B(u - i\epsilon)\right). \tag{B.3.15}$$

Thus, we have the estimate:

$$t_{\text{peak}} \sim \frac{\beta}{(\beta J_B)^{1/3}}, \quad J_B\beta \gg 1. \tag{B.3.16}$$

Again, our two assumptions, $t_{\text{peak}} J_B \gg 1$ and $t_{\text{peak}}/\beta \ll 1$, are satisfied.

B.4 Equation of motion in Schwarzian

It is convenient to first compute the variation with respect to a general reparametrization $t(u)$, then later to plug in the thermal solution,

$$t[u] = \tanh\left(\frac{\pi u}{\beta}\right). \tag{B.4.17}$$

As is well-known, the variation of the Schwarzian is equal to minus the time derivative of the Schwarzian. After we vary with respect to $t_+ - t_-$ and put $t_+ = t_-$, the leading term is

$$\partial_t \left(\text{Sch}(t[u], u)\right) = \frac{\beta}{\pi}\cosh^2\frac{\pi u}{\beta}\partial_u \left(\text{Sch}(t[u], u)\right) = \frac{\beta}{\pi}\cosh^2\frac{\pi u}{\beta}\partial_u\left(\frac{2\pi^2}{\beta^2}\right). \tag{B.4.18}$$

Now we deal with the interaction term. One has to vary

$$\int_{\mathcal{C}} du_1 du_2 \; X_B(u_1 - u_2)\left(\frac{t_1' t_2'}{(t_1 - t_2)^2}\right)^{1/4}. \tag{B.4.19}$$

Since V^2 is already small, after taking the variation we can plug in the thermal solution. Another reason for this is that the integral is dominated by $u_{12} < \beta$, whereas $\beta[u]$ changes on scales much bigger than β.

Variation with respect to the t_1 yields

$$-\int_{\mathcal{C}} du_2 \; \left(X_B(u_1 - u_2)\frac{(t_1' t_2')^{1/4}}{2(t_1 - t_2)^{3/2}} + \partial_{u_1}\left(X_B(u_1 - u_2)\frac{(t_1' t_2')^{1/4}}{4t_1'(t_1 - t_2)^{1/2}}\right)\right). \tag{B.4.20}$$

Recall that the combination

$$\frac{(t_1' t_2')^{1/4}}{(t_1 - t_2)^{1/2}} = \left(\frac{\pi/\beta}{\sinh\left(\frac{\pi(u_1-u_2)}{\beta}\right)} \right)^{1/2} \tag{B.4.21}$$

is proportional to $G_S(u_1 - u_2)$, so it is a function only of the difference $u_1 - u_2$. Therefore, if ∂_{u_1} does not act on $1/t_1$ it can be transformed into ∂_{u_2} to give a total derivative.

After taking the derivative we will have

$$-\int_{\mathcal{C}} du_2 \; X_B(u_1 - u_2) \frac{\cosh\frac{\pi u_1}{\beta}}{2\sinh^{3/2}\left(\frac{\pi(u_1-u_2)}{\beta}\right)} \left(\cosh\frac{\pi u_1}{\beta} + \sinh\frac{\pi u_1}{\beta} \sinh\frac{\pi(u_1-u_2)}{\beta} \right), \tag{B.4.22}$$

which is equal to

$$-\int_{\mathcal{C}} du_2 \; X_B(u_1 - u_2) \frac{\cosh^2\frac{\pi u_1}{\beta}}{2\sinh^{3/2}\left(\frac{\pi(u_1-u_2)}{\beta}\right)}. \tag{B.4.23}$$

Hence, in the end we have:

$$-2 \times \cosh\left(\frac{\pi u_1}{\beta}\right)^2 \int_{\mathcal{C}} du_2 \; X_B(u_1 - u_2) \frac{\cosh\frac{\pi}{\beta}(u_1 - u_2)}{2\sinh^{3/2}\frac{\pi}{\beta}(u_1 - u_2)}, \tag{B.4.24}$$

where an extra factor of 2 came from a similar variation with respect to the t_2.

Now we need to remember that we are working on the Keldysh contour, and the variation is over $t_+ - t_-$. This gives four pieces:

- $u_{1,+}$, $u_{2,+}$,
- $u_{1,-}$, $u_{2,-}$,
- $u_{1,+}$, $u_{2,-}$,
- $u_{1,-}$, $u_{2,+}$.

These integrals combine into twice the integral over the Wightman functions:

$$2 \times \int_{-\infty}^{+\infty} du_2. \tag{B.4.25}$$

The last step is to change variables: $u_2 \to x\beta + u_1$ and combine this contribution with that of the kinetic term (B.4.18):

$$\frac{8\pi^2\alpha_S}{\mathcal{J}_S\beta^3}\beta' = \frac{i\sqrt{i}bV^2\pi^{3/2}}{(J_S)^{1/2}\beta^{1/2}} \int_{-\infty}^{+\infty} dx\ X_B(\beta(u-i\epsilon))\frac{\cosh\pi\,(x-i\epsilon)}{\sinh^{3/2}\pi\,(x-i\epsilon)}. \tag{B.4.26}$$

Note that the factor of $\cosh^2(\pi u_1/\beta)$ has cancelled out, meaning that the ansatz with slowly-varying beta is actually consistent with the equations of motion.

B.5 Bounds on energy flow

B.5.1 Perturbative energy flow calculation for bosonic coupling

Consider a system initially in a thermal state of the form

$$\rho_0 = \frac{e^{-\beta_S H_S - \beta H_B}}{Z_S Z_B} \tag{B.5.27}$$

where the initial system Hamiltonian is H_S and the bath Hamiltonian is H_B. At time zero, a system bath coupling gH_{SB} is turned on, at which point the full Hamiltonian is

$$H = H_0 + gH_{SB} \tag{B.5.28}$$

where $H_0 = H_S + H_B$.

The rate of the change of the system energy as a function of time is

$$E_S' = \mathrm{tr}\left(\rho_0 e^{iHt}[igH_{SB}, H_S]e^{-iHt}\right). \tag{B.5.29}$$

This equation follows from the fact that $[H, H_S] = g[H_{SB}, H_S]$. Let us assume that the system-bath coupling is of the form

$$H_{SB} = O_S O_B, \tag{B.5.30}$$

noting that the most general coupling is a sum of such terms. Then the rate of energy change is

$$E'_S = \langle e^{iHt} i g [O_S, H_S] O_B e^{-iHt} \rangle_0. \tag{B.5.31}$$

To work perturbatively in g, we move to the interaction picture, defining

$$e^{-iHt} = e^{-iH_0 t} U. \tag{B.5.32}$$

To zeroth order in g, U is simply the identity, in which case $E' = 0$ as follows form the thermality of the initial state.

To first order in g, U is given by

$$U = 1 - ig \int_0^t dt' H_{SB}(t') + \cdots \tag{B.5.33}$$

where $H_{SB}(t')$ denotes the Heisenberg operator with respect to H_0 at time t'. The rate of energy change to second order in g is

$$E'_S = (ig)^2 \int_0^t dt' \langle [O_S(t') O_B(t'), [O_S, H_S](t) O_B(t)] \rangle_0. \tag{B.5.34}$$

From the equation of motion

$$[O_S, H_S](t) = i \partial_t O_S(t), \tag{B.5.35}$$

it follows that

$$E'_S = i g^2 \int_0^t dt' \langle [\partial_t O_S(t) O_B(t), O_S(t') O_B(t')] \rangle_0. \tag{B.5.36}$$

Note that the commutator has also been reversed, hence the extra minus sign. There are two terms from the commutator,

$$[\partial_t O_S(t)O_B(t), O_S(t')O_B(t'),] = \partial_t O_S(t)O_S(t')[O_B(t), O_B(t')] + [\partial_t O_S(t), O_S(t')]O_B(t')O_B(t). \tag{B.5.37}$$

Since the initial state factorizes, it follows that the energy rate of change can be written as a sum of products of system and bath correlators; these are defined as

$$X_{S/B} = \langle O_{S/B}(t)O_{S/B}(t')\rangle_0 \tag{B.5.38}$$

and

$$X^R_{S/B} = -i\langle[O_{S/B}(t), O_{S/B}(t')]\rangle_0. \tag{B.5.39}$$

Since the O operators are Hermitian, it follows that $\langle O(t')O(t)\rangle = \langle O(t)O(t')\rangle^*$. Then the rate of energy change is

$$E'_S = -g^2 \int_0^t dt' \left\{\partial_t X_S(t-t')X^R_B(t-t') + \partial_t X^R_S(t-t')X^*_B(t-t')\right\}. \tag{B.5.40}$$

Note that technically the time derivative acts on both $\theta(t)$ and $O_S(t)$ in X^R_S, but this doesn't matter because O_S commutes with itself. We have used the fact that the initial state is thermal to conclude that the dependence on t, t' reduces to a dependence on $t - t'$ only.

It is useful to rewrite the two terms in E'_S using a spectral representation. The first term is

$$\partial_t X_S(t-t')X^R_B(t-t') = \int \frac{d\omega}{2\pi}\frac{d\omega'}{2\pi}\frac{d\nu}{2\pi} e^{-i(\omega+\omega')(t-t')} \frac{-i\omega A_{S+}(\omega)A_B(\nu)}{\omega' + i0^+ - \nu}. \tag{B.5.41}$$

The second term is

$$\partial_t X^R_S(t-t')X^*_B(t-t') = \int \frac{d\omega}{2\pi}\frac{d\omega'}{2\pi}\frac{d\nu}{2\pi} e^{-i(\omega-\omega')(t-t')} \frac{-i\omega A_S(\nu)A_{B+}(\omega')}{\omega + i0^+ - \nu}. \tag{B.5.42}$$

The integral over t' in the expression for E'_S can be done to yield

$$\int_0^t dt' e^{-i(\omega+\omega')(t-t')} = \frac{1-e^{-i(\omega+\omega')t}}{i(\omega+\omega')} \tag{B.5.43}$$

and

$$\int_0^t dt' e^{-i(\omega-\omega')(t-t')} = \frac{1-e^{-i(\omega-\omega')t}}{i(\omega-\omega')}. \tag{B.5.44}$$

With a view towards the desired inequality, one can integrate these expressions against $e^{-\kappa t}$ for arbitrary κ. The result is

$$\int_0^\infty dt e^{-\kappa t} \frac{1-e^{-i(\omega+\omega')t}}{i(\omega+\omega')} = \frac{1}{\kappa[\kappa+i(\omega+\omega')]} \tag{B.5.45}$$

and

$$\int_0^\infty dt e^{-\kappa t} \frac{1-e^{-i(\omega-\omega')t}}{i(\omega-\omega')} = \frac{1}{\kappa[\kappa+i(\omega-\omega')]}. \tag{B.5.46}$$

In the first term the ω' integral can be carried out by contour, similarly for the ω integral in the second term (because these frequencies do not appear in the spectral functions). Closing in the upper half plane gives

$$\int \frac{d\omega'}{2\pi} \frac{1}{\kappa[\kappa+i(\omega+\omega')]} \frac{1}{\omega'+i0^+-\nu} = -\frac{1}{\kappa(\nu+\omega-i\kappa)} \tag{B.5.47}$$

and

$$\int \frac{d\omega}{2\pi} \frac{1}{\kappa[\kappa+i(\omega-\omega')]} \frac{\omega}{\omega+i0^+-\nu} = \frac{-\omega'-\nu-i\kappa}{2\kappa(-\omega'+\nu-i\kappa)}. \tag{B.5.48}$$

Adding back all the factors, the first term becomes

$$-g^2 \int \frac{d\omega}{2\pi} \frac{d\nu}{2\pi} \frac{-i\omega A_{S+}(\omega) A_B(\nu)}{-\kappa[\omega+\nu-i\kappa]} \tag{B.5.49}$$

and the second term is

$$-g^2 \int \frac{d\omega'}{2\pi} \frac{d\nu}{2\pi} \frac{-i(-\omega'-\nu-i\kappa) A_S(\nu) A_{B+}(\omega')}{2\kappa(-\omega'+\nu-i\kappa)}. \tag{B.5.50}$$

To compare the two terms, we relabel variables in both terms so that ω appears in A_S and ω' appears in A_B. The full expression for the integrated energy rate of change is thus

$$F_\kappa = i\frac{g^2}{\kappa}\int \frac{d\omega}{2\pi}\frac{d\omega'}{2\pi}\left[-\frac{\omega A_{S+}(\omega)A_B(\omega')}{\omega+\omega'-i\kappa} - \frac{(\omega'+\omega+i\kappa)A_S(\omega)A_{B+}(\omega')}{2(-\omega'+\omega-i\kappa)}\right]. \tag{B.5.51}$$

The useful identity $A_+(-\omega) = A_-(\omega)$ gives

$$\int d\omega A(\omega)f(\omega) = \int d\omega A_+(\omega)[f(\omega)-f(-\omega)]. \tag{B.5.52}$$

Applied to the first term (ω' integral), an equivalent integrand is

$$A_{S+}A_{B+}\left(-\frac{\omega}{\omega+\omega'-i\kappa}+\frac{\omega}{\omega-\omega'-i\kappa}\right). \tag{B.5.53}$$

Applied to the second term (ω integral), an equivalent integrand is

$$-\frac{A_{S+}(\omega)A_{B+}(\omega')}{2}\left(\frac{\omega'+\omega+i\kappa}{-\omega'+\omega-i\kappa}-\frac{\omega'-\omega+i\kappa}{-\omega'-\omega-i\kappa}\right) \tag{B.5.54}$$

or

$$A_{S+}(\omega)A_{B+}(\omega')\left(\frac{\omega}{-\omega+\omega'+i\kappa}+\frac{\omega}{\omega+\omega'+i\kappa}\right). \tag{B.5.55}$$

The terms may be recombined to give

$$A_{S+}(\omega)A_{B+}(\omega')\left(-\frac{\omega}{\omega+\omega'-i\kappa}+\frac{\omega}{\omega+\omega'+i\kappa}\right), \tag{B.5.56}$$

thanks to a cancellation of two terms. The real part is then simply zero while the imaginary part is

$$\text{Im}: -\frac{2\omega\kappa}{(\omega+\omega')^2+\kappa^2}. \tag{B.5.57}$$

Combined the imaginary overall prefactor, it follows that the integrated rate of change is

$$F_\kappa = \int dt e^{-\kappa t}E_S' = 2g^2\int \frac{d\omega}{2\pi}\frac{d\omega'}{2\pi}\frac{\omega A_{S+}(\omega)A_{B+}(\omega')}{(\omega+\omega')^2+\kappa^2}. \tag{B.5.58}$$

The integrated flux simplifies in various limits. For example, $\kappa \to \infty$ corresponds to the short time limit. The integrated flux obeys

$$F_{\kappa\to\infty} \to 2\frac{g^2}{\kappa^2}\int \frac{d\omega}{2\pi}\frac{d\omega'}{2\pi}\omega A_{S+}(\omega)A_{B+}(\omega'). \tag{B.5.59}$$

Using

$$\int d\omega\omega A_+(\omega) = \frac{1}{2}\int d\omega\omega A(\omega) = \int_{\omega\geq 0} d\omega\omega A(\omega) \geq 0, \tag{B.5.60}$$

it follows that

$$F_{\kappa\to\infty} \geq 0 \tag{B.5.61}$$

in agreement with Almheiri's lemma.

The limit $\kappa \to 0$ corresponds to the long time limit in which case the flux is dominated by the late time value. The integral over ω can be done by replacing the denominator with a delta function of $\omega + \omega'$ times π/κ,

$$F_{\kappa\to 0} \to -\frac{g^2}{\kappa}\int \frac{d\omega'}{2\pi}\omega' A_{S+}(-\omega')A_{B+}(\omega'). \tag{B.5.62}$$

Relabeling ω' as ω, the integral can be written

$$F_{\kappa\to 0} \to -\frac{g^2}{\kappa}\int \frac{d\omega}{2\pi}\omega\frac{A_S(\omega)A_B(\omega)}{(e^{\beta_S\omega}-1)(1-e^{-\beta_B\omega})}. \tag{B.5.63}$$

This form is convenient since $A(\omega)$ is antisymmetric and so the product of two is symmetric. The integral can also be written

$$F_{\kappa\to 0} \to -\frac{g^2}{\kappa}\int \frac{d\omega}{2\pi}\omega\frac{e^{(\beta_B-\beta_S)\omega/2}A_S(\omega)A_B(\omega)}{4\sinh\frac{\beta_S\omega}{2}\sinh\frac{\beta_B\omega}{2}}. \tag{B.5.64}$$

Using the symmetry of the integrand, this can be written once more as

$$F_{\kappa\to 0} \to -\frac{g^2}{\kappa}\int_{\omega\geq 0} \frac{d\omega}{2\pi}\omega\frac{\sinh\frac{(\beta_B-\beta_S)\omega}{2}A_S(\omega)A_B(\omega)}{2\sinh\frac{\beta_S\omega}{2}\sinh\frac{\beta_B\omega}{2}}. \tag{B.5.65}$$

This form is nice because it makes it clear that the energy flow is negative or positive depending only on whether $\beta_B - \beta_S$ is positive or negative.

B.5.2 Review of spectral representation

Here we briefly review the spectral representation used above. Consider a Hermitian operator O in a system with Hamiltonian H in a thermal state at temperature $T = 1/\beta$. The two correlators of interest are

$$X = \langle O(t)O(0)\rangle \tag{B.5.66}$$

and

$$X^R(t) = -i\theta(t)\langle[O(t), O(0)]\rangle. \tag{B.5.67}$$

Both correlators have an expansion in terms of energy eigenstates. These are

$$X(t) = \sum_{n,m} p_n |\langle n|O|m\rangle|^2 e^{i(E_n - E_m)t} \tag{B.5.68}$$

and

$$X^R(t) = -i\theta(t) \sum_{n,m} p_n |\langle n|O|m\rangle|^2 \left[e^{i(E_n - E_m)t} - e^{-i(E_n - E_m)t}\right]. \tag{B.5.69}$$

The Fourier transforms are

$$X(\omega) = \int_{-\infty}^{\infty} dt e^{i\omega t} X(t) = \sum_{n,m} \sum_{n,m} p_n |\langle n|O|m\rangle|^2 2\pi\delta(\omega - (E_m - E_n)) \tag{B.5.70}$$

and

$$X^R(\omega) = \sum_{n,m} \sum_{n,m} p_n |\langle n|O|m\rangle|^2 \left(\frac{1}{\omega + i0^+ - (E_m - E_n)} - \frac{1}{\omega + i0^+ + (E_m - E_n)}\right). \tag{B.5.71}$$

The spectral function is defined by the equation

$$X^R(\omega) = \int \frac{d\nu}{2\pi} \frac{A(\nu)}{\omega + i0^+ - \nu}, \tag{B.5.72}$$

from which it follows that

$$A(\nu) = A_+(\nu) - A_-(\nu) \tag{B.5.73}$$

with

$$A_\pm(\nu) = \sum_{n,m} p_n |\langle n|O|m\rangle|^2 2\pi\delta(\nu \mp (E_m - E_n)). \tag{B.5.74}$$

Exchaning n and m in the definition of A_- shows that

$$A_- = \sum_{n,m} p_m |\langle n|O|m\rangle|^2 2\pi\delta(\nu - (E_m - E_n)), \tag{B.5.75}$$

and using $E_m = E_n + \nu$ plus the explicit form of p_m, it follows that

$$A_- = e^{-\beta\nu} A_+ \tag{B.5.76}$$

and that

$$A(\nu) = (1 - e^{-\beta\nu}) A_+(\nu). \tag{B.5.77}$$

We also see that $X(\omega)$ obeys

$$X(\omega) = A_+(\omega). \tag{B.5.78}$$

B.5.3 General argument for perturbative bound

Once again, the integrated flux is

$$F_\kappa = 2g^2 \int \frac{d\omega}{2\pi} \frac{d\omega'}{2\pi} \frac{\omega A_{S+}(\omega) A_{B+}(\omega')}{(\omega+\omega')^2 + \kappa^2}. \tag{B.5.79}$$

Convering to $A_S(\omega)$ gives

$$F_\kappa = 2g^2 \int \frac{d\omega}{2\pi} \frac{d\omega'}{2\pi} \frac{\omega A_S(\omega) A_{B+}(\omega')}{(\omega+\omega')^2 + \kappa^2} \frac{1}{1 - e^{-\beta_S \omega}}. \tag{B.5.80}$$

Using the fact that $\omega A_S(\omega)$ is symmetric in ω, we may symmetrize the remaing function of ω without changing the integral. The result is

$$F_\kappa = g^2 \int \frac{d\omega}{2\pi}\frac{d\omega'}{2\pi}\frac{\omega A_S(\omega)A_{B+}(\omega')[\omega^2+\omega'^2+\kappa^2-2\omega\omega'\coth\frac{\beta_S\omega}{2}]}{[(\omega+\omega')^2+\kappa^2][(\omega-\omega')^2+\kappa^2]}. \tag{B.5.81}$$

Now the only potentially negative part of this expression is the function

$$f = \omega^2+\omega'^2+\kappa^2-2\omega\omega'\coth\frac{\beta_S\omega}{2}. \tag{B.5.82}$$

It is interesting to ask under what conditions $f \geq 0$. It may be written as

$$f = \left(\omega' - \omega\coth\frac{\beta_S\omega}{2}\right)^2 + \kappa^2 + \omega^2\left(1-\coth^2\frac{\beta_S\omega}{2}\right). \tag{B.5.83}$$

The function $\omega^2(1-\coth^2(\omega/2))$ is symmetric and monotonically increasing for positive ω. Its value at $\omega = 0$ is $-\frac{4}{\beta_S^2}$. Hence it follows that if κ is large enough, the function $\kappa^2 + x^2(1-\coth^2(x/2))$ is non-negative. From this we conclude that $F_\kappa \geq 0$ provided

$$\kappa \geq \frac{2}{\beta_S}. \tag{B.5.84}$$

This constraint applies for any system and bath provided that: (1) the system-bath coupling is a product of two Hermitian operators and (2) we work perturbatively in the coupling.

B.6 Perturbation theory in μ

Let us start from computing μ correction to G_{LR}. We need to compute

$$\Delta G_{LR}(\tau_1-\tau_2) = i\mu\int_0^\beta d\tau\ G_{LL}(\tau_1-\tau)G_{RR}(\tau-\tau_2) =$$
$$= i\frac{\mu b^2\pi}{J\beta}\int_0^\beta d\tau\ \operatorname{sgn}(\tau_1-\tau)\operatorname{sgn}(\tau-\tau_2)\frac{1}{\sqrt{\sin\left(\frac{\pi|\tau_1-\tau|}{\beta}\right)}}\frac{1}{\sqrt{\sin\left(\frac{\pi|\tau-\tau_2|}{\beta}\right)}} \tag{B.6.85}$$

Because of the translational invariance along the thermal circle the answer depends on $\tau_1 - \tau_2$ only. So one can put $\tau_2 = 0$. After changing the variables to $x = \tan(\pi\tau/\beta)$ we have the following integral:

$$i(1+x_1^2)^{1/4} \times \frac{\mu b^2}{J} \int_{-\infty}^{\infty} dx \ \operatorname{sgn}(x_1 - x)\operatorname{sgn}(x) \frac{1}{\sqrt{|x|}\sqrt{|x_1 - x|}\sqrt{1+x^2}} \tag{B.6.86}$$

This integral can be computed analytically. Because of the sgn functions there are three integration domains. So the answer has three parts:

$$\Delta G_{LR}(x(\tau)) = i\frac{\mu b^2}{J}(I_1 - I_2 + I_3)(1+x^2)^{1/4} \tag{B.6.87}$$

where

$$\begin{aligned} I_1 &= \frac{2}{\sqrt{1-ix}}\left(\text{EllipticK}\left(1 - \frac{2x}{i+x}\right) - i\text{EllipticF}\left(\frac{\pi}{4}, \frac{2x}{i+x}\right)\right) \\ I_2 &= \frac{2}{(1+x^2)^{1/4}}\text{EllipticK}\left(\frac{1}{2} - \frac{1}{2\sqrt{1+x^2}}\right) \\ I_3 &= \frac{2}{x}\ {}_3F_2\left(\frac{1}{2}, \frac{1}{2}, 1; \frac{3}{4}, \frac{5}{4}; -\frac{1}{x^2}\right) \end{aligned} \tag{B.6.88}$$

Now, let us compute the correction to energy. From the path integral the leading correction to the free energy is

$$-\beta\Delta F = -\frac{\mu^2\beta}{2}\int_0^\beta d\tau \ G_{LL}(\tau)G_{RR}(\tau) \tag{B.6.89}$$

We can recover the integral by taking $\tau \to 0$ limit in the conformal answer (B.6.87) for G_{LR}. Unfortunatelt it produces a logarithmic UV divergence which we cut at $\tau = 1/J$:

$$\Delta F = \frac{1}{2\sqrt{4\pi}}\frac{\mu^2}{J}\left(2\log\frac{\pi}{J\beta} - c_1\right) \tag{B.6.90}$$

where c_1 is the cut-off dependent constant. We can not find it from the conformal perturbation theory, because it is an effective low-energy theory with a build-in UV cutoff of order J. From

the above expression we read off the energy correction:

$$\Delta E = \frac{1}{2\sqrt{4\pi}} \frac{\mu^2}{J} \left(2 \log \frac{\pi}{J\beta} - 2 - c_1 \right) \tag{B.6.91}$$

Also notice that the constant $-c_1 - 2$ is not simply a correction to the ground state energy. As we mentioned in the main text, perturbation theory in μ breaks down at large $\beta_{\rm 2BH} \sim J/\mu^2$, so we can not take the limit $\beta \to \infty$ in this expression. This is signalled by the presence of the logarithm. This divergence has IR nature, and it is not caused by using the conformal answer in the integral (B.6.89).

To extract c_1 we can compute integral (B.6.89) using the numerically obtained G_{LL}. We find that $c_1 = 1.66(1)$. This agrees very well with the actual numerical result for the energy - Figure 4.6.

B.7 Checking whether Schwarzian fluctuations are stable

Let us start from doing a 1-loop calculation for Schwarzian first. We again assume that we in the phase with two separate black holes. Then the action will involve two Schwarzian terms plus the interaction piece. For a moment we can imagine that instead of a simple interaction $\mu\psi_L\psi_R$ we have a term involving composite operators $i^F \mu \mathcal{O}_L \mathcal{O}_R$ with zero expectation values: $\langle \mathcal{O}_{L(R)} \rangle = 0$. F is the $\mathcal{O}_{L(R)}$ fermionic number. The Schwarzians interact because Schwarzians gravitationally dress $\mathcal{O}_{L(R)}$ by time reparametrizations.

In the perturbation theory the leading contribution is of order μ^2:

$$\int D\psi_L D\psi_R \ \exp\left(-S_L - S_R - i^F \mu \int du \ \mathcal{O}_L \mathcal{O}_R \right) = \tag{B.7.92}$$
$$= \int D\psi_L D\psi_R \ \exp\left(-S_L - S_R - \mu^2 \int du_1 du_2 \langle \mathcal{O}_L \mathcal{O}_L \rangle \langle \mathcal{O}_R \mathcal{O}_R \rangle \right)$$

Explicitly the action is:

$$S = -\int du\ \frac{N\alpha_S}{\mathcal{J}}\{f_L, u\} - \int du\ \frac{N\alpha_S}{\mathcal{J}}\{f_R, u\} - \tag{B.7.93}$$
$$N\frac{\mu^2 c_{\mathcal{O}}^2}{J^{4\Delta}}\int du_1 du_2 \left(\frac{f_L'(u_1)f_L'(u_2)}{(f_L(u_1)-f_L(u_2))^2}\right)^{\Delta}\left(\frac{f_R'(u_1)f_R'(u_2)}{(f_R(u_1)-f_R(u_2))^2}\right)^{\Delta}$$

where Δ is the dimension of $\mathcal{O}_{L(R)}$, for ψ_L it is $\Delta = \frac{1}{4}$ and $\{f, u\}$ denotes Schwarzian derivative:

$$\{f(u), u\} = \frac{f'''}{f'} - \frac{3}{2}\left(\frac{f''}{f'}\right)^2 \tag{B.7.94}$$

Finite temperature solution without interaction reads as:

$$f_L = f_R = \tan\frac{\pi u}{\beta} \tag{B.7.95}$$

We can perturb it by ϵ_L, ϵ_R:

$$f_L = \tan\left(\frac{\pi u}{\beta} + \epsilon^L(u)\right) \tag{B.7.96}$$

$$f_R = \tan\left(\frac{\pi u}{\beta} + \epsilon^R(u)\right) \tag{B.7.97}$$

$$\tag{B.7.98}$$

and to see whether the two black hole system has a perturbative instability at some temperature. For simplicity we can put $\beta = \pi$ and expand ϵ in Fourier modes:

$$\epsilon = \sum_{n=-\infty}^{+\infty} \epsilon_n e^{2inu} \tag{B.7.99}$$

Before doing an actual computation, let us stop and explain why Schwarzian does not contribute classicaly here and at higher loops. By classically we mean that its contribution is suppressed by $1/N$. Since we are in a thermal state (B.7.96) is the a translation symmetry along the Euclidean time u. This is why after expanding in Fourier modes (B.7.99) we will not have terms linear in ϵ_n. It means that the thermal solution (B.7.96) is still a classical solution of

Schwarzian equations of motion even with complicated non-local interaction induced by loops. Since we have an overall N in front of the action, integrating out ϵ_n will lead to a subleading correction.

Let us return to the actual 1-loop calculation. The only subtlety is that one has to be careful with the time ordering, since the denominator involves

$$\left(\sin^2\left(u_1-u_2+\epsilon^L(u_1)-\epsilon^L(u_2)\right)\right)^{\Delta}=\sin^{2\Delta}|u_1-u_2+\epsilon^L(u_1)-\epsilon^L(u_2)| \tag{B.7.100}$$

The result for the marginal deformation $\Delta=1/2$:

$$S/N=\frac{\alpha_S}{\mathcal{J}\beta}\sum_{n=2}^{+\infty}\epsilon^{l,r}_{-n}\left(n^4-n^2\right)\epsilon^{L,R}_n+\frac{c_\Delta^2\mu^2\beta^2}{(J\beta)^2}\left(8\pi^2|\epsilon_2^L-\epsilon_2^R|^2+32\pi^2|\epsilon_3^L-\epsilon_3^R|^2+80\pi^2|\epsilon_4^L-\epsilon_4^R|^2\right)+\ldots \tag{B.7.101}$$

and the coefficients tend to grow. One can also evaluate non-quadratic terms. Below are the first three. All of them have positive coefficients too:

$$+28\pi^2|\epsilon_2^L-\epsilon_2^R|^4+224\pi^2|\epsilon_3^L-\epsilon_3^R|^4+952\pi^2|\epsilon_3^L-\epsilon_3^R|^4+\ldots \tag{B.7.102}$$

$$+\frac{2860\pi^2}{9}|\epsilon_2^L-\epsilon_2^R|^6+\ldots$$

For the case of relevant deformation $\mu\psi_L\psi_R$ with $\Delta=1/4$ the results are similar. The interaction term has the expansion:

$$\frac{8}{3}|\epsilon_2^L+\epsilon_2^R|^2+8|\epsilon_2^L-\epsilon_2^R|^2+\frac{48}{5}|\epsilon_3^L+\epsilon_3^R|^2+\frac{80}{3}|\epsilon_3^L-\epsilon_3^R|^2+\ldots \tag{B.7.103}$$

$$+\frac{304}{15}|\epsilon_2^L+\epsilon_2^R|^4+\frac{4432}{105}|\epsilon_2^L-\epsilon_2^R|^4+\frac{7146}{55}|\epsilon_3^L+\epsilon_3^R|^4+\frac{137018}{495}|\epsilon_3^L-\epsilon_3^R|^4+\ldots$$

$$+\frac{135424}{693}|\epsilon_2^L+\epsilon_2^R|^6+\frac{1053952}{2835}|\epsilon_2^L-\epsilon_2^R|^6+\ldots \tag{B.7.104}$$

And the coefficient in front is $b^2\frac{\mu^2\beta^2}{J\beta}$.

In principle, we can go to higher orders in μ. Curiously, μ^4 correction is negative for ϵ_2.

B.8 Lorentz time Dyson–Schwinger equation

B.8.1 Single SYK

Let us first consider a single SYK in Euclidean time. Then the DS equations have the form:

$$\Sigma(\tau) = J^2 G(\tau)^3$$
$$(-i\omega - \Sigma(\omega))G(\omega) = 1 \tag{B.8.105}$$

Now we want to switch to Lorentzian time. We define the Wightman function with an extra $-i$:

$$-i\langle\psi_i(t)\psi_i(0)\rangle = G^{>}(t) \tag{B.8.106}$$

As is well-known, upon the analytical continuation in time domain, the time-ordered Euclidean two-point function becomes the Wightman function, therefore[1]:

$$\Sigma^{>}(t) = -J^2 \left(G^{>}(t)\right)^3 \tag{B.8.107}$$

The other DS equation is written in the frequency space, this is why after the analytic continuation it will involve the retarded components:

$$G^R(\omega)(\omega - \Sigma^R(\omega)) = 1 \tag{B.8.108}$$

So far we have not used any information about the state we are considering. This information is needed to connect $G^{>}$ and G^R. In thermal state we can use Fluctuation-Dissipation Theorem(FDT):

$$G^{>}(\omega) = \frac{2i\,\mathrm{Im}\,G^R(\omega)}{e^{-\beta\omega}+1} \tag{B.8.109}$$

An example of how the Wightman's function look is presented on Figure B.3.

[1]The minus sign is subtle: one can recover it either from the effective action (4.3.50) on the Keldysh contour or doing a careful analytic continuation through the frequency space as was done in [36]

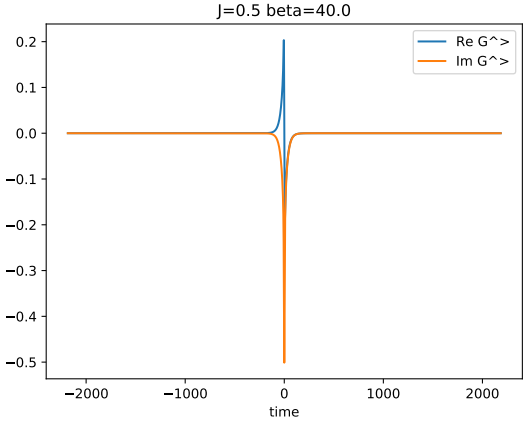

Figure B.3: Wightman's function $G^{>}$ for single $q = 4$ SYK with $J = 0.5,\ \beta = 40$

B.8.2 Two coupled SYK

Now we have 4 Green's functions. The self-energies have similar expressions:

$$\Sigma^{>}_{ab}(t) = -J^2 (G^{>}_{ab}(t))^3 + i\mu_{ab} \tag{B.8.110}$$

and the equation (B.8.108) should be understood as a matrix equation. For the diagonal Green's functions the FDT has the same form:

$$G^{>}(\omega)_{aa} = \frac{2i \operatorname{Im} G^R_{aa}(\omega)}{e^{-\beta\omega} + 1} \tag{B.8.111}$$

However the imaginary part of the off-diagonal components is skew-symmetric in time, so we have:

$$G^{>}(\omega)_{LR} = \frac{\operatorname{Re} G^R_{LR}(\omega)}{e^{-\beta\omega} + 1} \tag{B.8.112}$$

This system of equations can be solved numerically by the iteration procedure used for a single SYK model [36]. To ensure that the iteration procedure converges to an actual solution we monitor the discrepancies of eqs. (4.2.8):

$$d_{ab} = \frac{1}{N_{\text{points}}} \| \partial_\tau G_{ab}(\tau) - \Sigma_{ac} * G_{cb}(\tau) - \delta_{ab}\delta(\tau) \|^2 \tag{B.8.113}$$

and make sure that $d_{ab} < 10^{-10}$. The typical number of discretization points is $N_{\text{points}} \sim 2^{17}$.

Before the transition the diagonal Green's function look similar to single SYK ones - Figure B.4

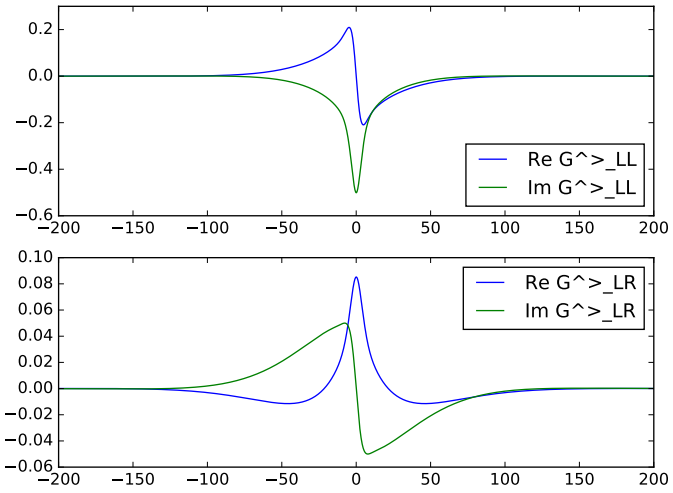

Figure B.4: Wightman's function $G^{>}$ for two coupled $q = 4$ SYK with $J = 0.5,\ \mu = 0.05,\ \beta = 40$

B.9 Derivation of the effective action

Let us write down explicitly the total action for the system on the Keldysh contour $\mathcal{C}$. We will suppress the bath action. Bath fermions χ_α and $\tilde{\chi}_\alpha$, $\alpha = 1, \ldots, M$ belong to independend $q = 4$ SYK systems with coupling J_B. We denote their two-point functions by G_B:

$$G_B^{>}(t_1^-, t_2^+) = -i\frac{1}{M}\sum_\alpha \langle \chi_\alpha(t_1^-)\chi_\alpha(t_2^+)\rangle = -i\frac{1}{M}\sum_\alpha \langle \tilde{\chi}_\alpha(t_1^-)\tilde{\chi}_\alpha(t_2^+)\rangle \tag{B.9.114}$$

The total action consists of four terms:

$$S_{\text{tot}} = S_{\text{kin}} + S_{\text{J}} + S_\mu + S_{\text{bath}} \tag{B.9.115}$$

- S_{kin} is a standard kinetic term for fermions:

$$iS_{\text{kin}} = i\int_{\mathcal{C}} dt\ \sum_j \left(\psi_j^L \partial_t \psi_j^L + \psi_j^R \partial_t \psi_j^R\right) \tag{B.9.116}$$

- S_{J} is SYK interaction:

$$iS_{\text{J}} = i\int_{\mathcal{C}} dt \sum_{i<j<k<l} J_{ijkl}\left(\psi_i^L \psi_j^L \psi_k^L \psi_l^L + \psi_i^R \psi_j^R \psi_k^R \psi_l^R\right) \tag{B.9.117}$$

- S_μ is Maldacena–Qi interaction term:

$$iS_\mu = \int_{\mathcal{C}} dt\ \mu \sum_j \psi_j^L \psi_j^R \tag{B.9.118}$$

- Finally S_{bath} is interaction with the bath:

$$iS_{\text{bath}} = i\int_{\mathcal{C}} dt \sum_{\alpha_1<\alpha_2<\alpha_3,i} \left(V_i^{\alpha_1\alpha_2\alpha_3}\psi_{L,i}\chi_{\alpha_1}\chi_{\alpha_2}\chi_{\alpha_3} + \tilde{V}_i^{\alpha_1\alpha_2\alpha_3}\psi_{R,i}\tilde{\chi}_{\alpha_1}\tilde{\chi}_{\alpha_2}\tilde{\chi}_{\alpha_3}\right) \tag{B.9.119}$$

As usual, we can integrate out the disorders leading to bi-local expression in terms of ψ, χ and $\tilde{\chi}$. Couplings V and $\tilde{V}$ are Gaussing with the variance [2]:

$$\langle (V_i^{\alpha_1\alpha_2\alpha_3})^2\rangle = \langle \left(\tilde{V}_i^{\alpha_1\alpha_2\alpha_3}\right)^2\rangle = \frac{3!\eta}{M^3},\ \text{no sum} \tag{B.9.120}$$

The action can be made quadratic in fermions by introducing the largrangian multiplier Σ, which is integrated over along the imaginary axis:

$$iS_{\text{lag}} = -\frac{N}{2}\int_{\mathcal{C}} dt_1 dt_2\ \sum_{ab}\Sigma_{ab}(t_1,t_2)\left(G_{ab}(t_1,t_2) - \frac{1}{N}\sum_j \psi_j^a(t_1)\psi_j^b(t_2)\right) \tag{B.9.121}$$

Note that we have an overall minus if front of the action. It is important for the equation connecting the self-energies Σ and Green's functions. Integrating out the fermions produces we

effective action (4.3.50):

$$i\frac{S_{\rm tot}}{N} = \frac{1}{2}\,\mathrm{Tr}\log\left(\omega - \Sigma_{ab}(\omega)\right) - \sum_{ab}\int_{\mathcal{C}} dt_1 dt_2 \left(\frac{J^2}{8}G_{ab}(t_1,t_2)^4 + \frac{1}{2}\Sigma_{ab}(t_1,t_2)G_{ab}(t_1,t_2)\right) + \\ + \frac{i\mu}{2}\int_{\mathcal{C}} dt\ \left(G_{LR}(t,t) - G_{RL}(t,t)\right) - \frac{\eta}{2}\int_{\mathcal{C}} dt_1 dt_2 \left(G_{LL}(t_1,t_2) + G_{RR}(t_1,t_2)\right) G_B^3(t_1,t_2) \tag{B.9.122}$$

Variation of this action with respect to Σ_{ab} and G_{ab} yield the KB equations (4.3.53) and (4.3.54)

B.10 Numerical methods for wormhole formation

Now let us describe the numerical method for solving Kadanoff–Baym equations. Numerical solution of Kadanoff–Baym equations for SYK model was described previously in [37, 106] and our approach is essentially the same.

We will use two-dimensional grid with uniform timestep to discretize (t_1, t_2) plane. The timestep dt should be much smaller than the characteristic time-scales in SYK $1/J, 1/\mu$. Since $\mu \ll J$, the $1/J$ constraint is much stricter. We will work with $J = 0.5$ this is just a choice to fix energy units. Our time steps will be $0.2, 0.1, 0.05$. The main numerical limitation comes from the fact that the Green functions have spread $\sim \beta$, so we can not go to very big β, since we will have to use a huge grid. At finite temperature the Green functions decay exponentially, so to greatly speed up the computation we will concentrate on the strip $|t_1 - t_2| \lesssim c\beta_{\max}$ on the (t_1, t_2) plane - Figure B.5. We will assume that outside this strip all the Green functions are zero. The constant $\beta_{\max}$ is the maximal β in the problem at hand. In our case $\beta_{\max} = \beta_B$ - bath's beta. One can verify that one c is big enough the result of the computation does not change.

With the computation power avaliable to us, in order to keep the computation time to be of order of dozens of hours, β should be less than 100. This limits us to $\mu \gtrsim 0.05$. For $\mu = 0.05$ the transition beta is ~ 61 - see Figure 4.6.

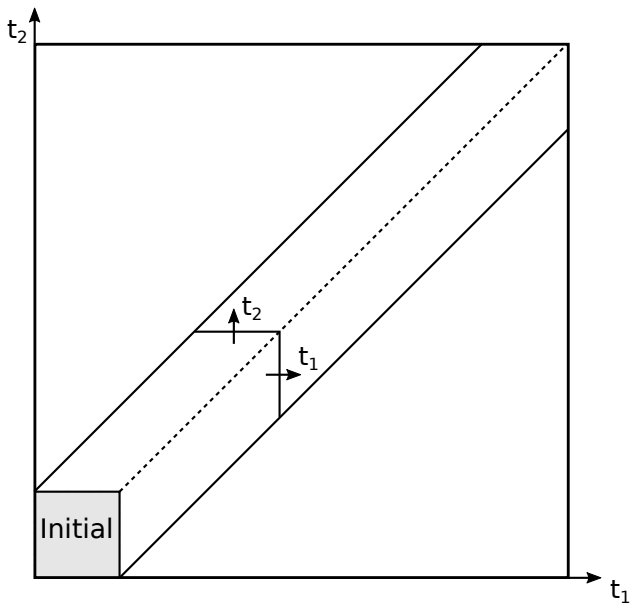

Figure B.5: Geometry of the (t_1, t_2) plane. The initial Green functions are placed inside the gray box.

The system-bath coupling η should be much smaller than $J^2 = 0.25$ so that the system remain thermal. We will use η in the range $0.01 - 0.04$. Moreover to avoid large gradients we will switch on the coupling linearly, with the switch-on time $T_{\text{switch}} = 20$.

Initial Green function is found by numerically solving Lorentz-time equilibrium Dyson–Schwinger equation as described in Appendix B.8. The bath Green function is obtained in a similar fashion. In order to avoid large speads in the bath's Green function, β_B will be in the range $70 - 100$.

To compute the integral in KB equations we will use trapezoid method and for the time propagation we use predictor-corrector scheme. The same techniques have been used in [37, 106]. For KB equations one has to be careful with propagating the Green function along the diagonal. Fortunately, for Majorana fermions there is a simple relation:

$$G^{>}_{aa}(t,t) = -\frac{i}{2} \tag{B.10.123}$$

However, for the Green function obtained by numerically solving the DS equation the diagonal value is not exactly $-i/2$, so on a discrete lattice we will just propagate this value:

$$G^{>}_{aa}(j,j) = G^{>}_{aa}(0,0) \tag{B.10.124}$$

For the mixed G_{LR} we do not have a simple relation like that. So we will use again the predictor-corrector scheme. The value on the diagonal can be found by either propagating along t_1 or t_2. We will take the avarge of these results.

Let us define the "corner slice" Green functions as $G^{>}_{T,ab}(x)$:

$$G^{>}_{T,ab}(x) = \theta(x)G^{>}_{ab}(T-x,T) + \theta(-x)G^{>}_{ab}(T,T+x) \tag{B.10.125}$$

Then the energy at time $t = T$ can be computed analogously to eq. (4.2.12):

$$\frac{E}{N} = \frac{i}{4}\left(\partial_x G^{>}_{T,LL} + \partial_x G^{>}_{T,RR} + \frac{i\mu}{2} G^{>}_{T,LR}\right), \qquad \text{at } x = 0 \tag{B.10.126}$$

Computing the time derivatives using the KB eqution one arrives at the following integral form:

$$\frac{E}{N} = -i\frac{J^2}{4}\int_{-\infty}^{\infty} dx\, \mathrm{sgn}(x)\left(G^{>}_{T,LL}(x)^4 + G^{>}_{T,RR}(x)^4 + 2G^{>}_{T,LR}(x)^4\right) + i\mu G^{>}_{T,LR}(0) \tag{B.10.127}$$

Along the time evolution the system cools down, so formally the temperature is not well defined. However, if the cooling process is slow we might expect that at each point in time the short-time correlators will be thermal. In order to extract the temperature we need to choose the 1D slice of the Green function $G^{>}_{S,ab}$ to use the Fluctuation-Dissipation theorem(FDT). For the same side correlators and different side correlators it looks slightly different. For the same side case we have:

$$\frac{\mathrm{Im}\left(G^{>}_{T,aa}(\omega) + G^{<}_{T,aa}(\omega)\right)}{(-2)\,\mathrm{Im}\, G^{R}_{T,aa}(\omega)} = -\tanh\frac{\beta(T)\omega}{2} \tag{B.10.128}$$

where for different sides it reads as:

$$\frac{\mathrm{Re}\left(G^{>}_{T,ab}(\omega)+G^{<}_{T,ab}(\omega)\right)}{(-2)\,\mathrm{Re}\,G^{R}_{T,ab}(\omega)}=-\tanh\frac{\beta(T)\omega}{2},\ a\neq b \tag{B.10.129}$$

To the extent that the system is in thermal equilibrium, it is time translation invariant and it does not matter what the value of t_1+t_2 is. We will actually choose the corner slice Green function $G^{>}_{T,ab}$ in (B.10.125). This choice is motivated by the fact that exactly these Greens function enter in the definition of energy (B.10.127).

Then one can fit it the left hand side of (B.10.128) with the tanh function to extract the temperature. We need to select a frequency range of at least a couple of temperatures in order to really probe the thermalization. On the other hand, for very large frequencies the numerical data has a lot of noise coming from discrete timestep, see Figure B.6. Typically we will fit eq. (B.10.128) up to frequencies of order 10 temperatures, i.e. $\beta n/L\sim 10$. Although the results do not depend much of this choice.

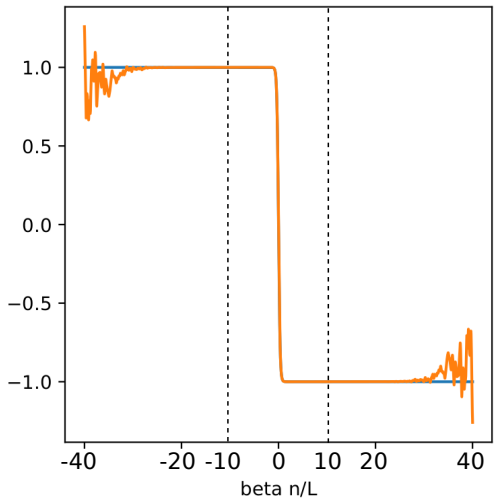

Figure B.6: (Orange) The left hand side of eq. (B.10.128) for $\beta=80$, $dt=0.2$. The Green function is defined on a strip of width $L=1600$. (Blue) *tanh* function. We expect that they should match for frequencies much less than the inverse discretization timestep: $n/L\ll 1/dt$. In on this graph this UV cutoff is at $\beta n_{\max}/L\sim 400$. The region used for the fit, $\beta|n|/L\leq 10$, is within the dashed lines.

B.11 Change of boundary conditions

First we need derive an analogue of (4.4.72) for the case of global AdS_2. We start from fermions having Dirichlet boundary conditions on both boundaries and add an extra fermion $\chi_{L,R}$ on the boundary to initiate the flow from Dirichlet to Neumann boundary conditions. Essentially this way we perform a Legendre transformation [126]. This way we obtain the relation:

$$Z_N = Z_D \sqrt{\det \hat{G}_{1-\Delta}} \tag{B.11.130}$$

where $\hat{G}_{1-\Delta}$ is the matrix

$$\begin{pmatrix} G^{LL}_{1-\Delta} & G^{LR}_{1-\Delta} \\ G^{RL}_{1-\Delta} & G^{RR}_{1-\Delta} \end{pmatrix} \tag{B.11.131}$$

with with standard conformal correlators

$$G^{LL}_{1-\Delta} \propto \left(\sinh\left(\frac{t}{2}\right)\right)^{2\Delta-2} \tag{B.11.132}$$

$$G^{LR}_{1-\Delta} \propto \left(\cosh\left(\frac{t}{2}\right)\right)^{2\Delta-2} \tag{B.11.133}$$

Now let us return to our problem with the μ term. So now we have Neumann fermions plus the interaction term $\mu\psi_L\psi_R$ coupling the two boundaries. The partition function can be easily found:

$$Z_\mu = Z_{\mu=0}\sqrt{\det\left(1+\hat{\mu}\hat{G}_\Delta\right)} \tag{B.11.134}$$

where the matrix $\hat{\mu}$ is given by eq. (4.2.10). For large μ we have

$$Z_{\mu\gg 1} \propto Z_N \sqrt{\det \hat{G}_\Delta} \tag{B.11.135}$$

To conclude that $Z_{\mu\gg 1} \propto Z_D$ we need the matrix relation

$$\hat{G}_{1-\Delta}(\omega)\hat{G}_\Delta(\omega) = \mathrm{id} \tag{B.11.136}$$

In fact this relation coincides with the conformal(i.e. neglecting the time derivative) Dyson–Schwinger equation (4.2.8).

Appendix C

Casimirs and matrix models

C.1 The eigenvalues of the quadratic Casimir operator

In this appendix we describe the value of quadratic Casimir operator for the representations of $O(N)$ and $SU(N)$ groups in terms of Young diagrams. To extract the irreducible representation corresponding to a Young diagram from a generic tensor, we first fill in the boxes with this tensor indices, then we symmetrize over the indexes in the rows and after that antisymmetrize the indexes in the columns. In the case of the orthogonal group we additionally subtract all possible traces from the tensor.

For the representation of the group $O(N)$ that is described by the Young diagram Y with row lengths λ_i, the quadratic Casimir operator is equal to

$$C_2^{O(N),Y} = \sum_{i=1}^{\lfloor N/2 \rfloor} \lambda_i \left(\lambda_i + N - 2i\right) \tag{C.1.1}$$

The dimension of this representation reads as:

$$\dim_\lambda = \frac{1}{h_\lambda} \prod_{i=1}^{k} \frac{(\lambda_i + N - k - i - 1)!}{(N-i)!} \prod_{j=1}^{i} (\lambda_i + \lambda_j + N - i - j) \tag{C.1.2}$$

where h_λ is the product of all hook lengths. For each box the hook length is defined as:

$$\text{(hook length)} = \text{(number of boxes to the right)} + \text{(number of boxes below)} + 1 \qquad \text{(C.1.3)}$$

The following lemma will be useful for studying the matrix models. Let us consider two groups $O(2n)$ and $O(2m)$ and Young diagram Y_n for group $O(2n)$ such that the length of the rows is less then m. There is a maximal Young diagram – a rectangular $n \times m$, that we shall denote as $Y_{n\times m}$. We would like to consider a specific Young diagram $Y_m = (Y_{n\times m}/Y_n)^T$ for a group $O(2m)$, where T stands for transposition. Then

$$C_2^{Y_n} + C_2^{Y_m} = n^2 m + n m^2 - nm \ . \qquad \text{(C.1.4)}$$

The proof goes as following. Let λ_i be the length of rows of the diagram Y_n, we introduce $\lambda_0 = m, \lambda_{n+1} = 0$. Then

$$C_2^{Y_n} = \sum_{i=1}^{n} \lambda_i \left(\lambda_i + 2(n-i)\right) \qquad \text{(C.1.5)}$$

The value of Casimir operator of $C_2^{Y_m}$ can be expressed as the following. The difference $\lambda_i - \lambda_{i+1}$ is just equal to the number of the rows that has length $n - i$. Then

$$C_2^{Y_m} = \sum_{i=0}^{n} \left[(\lambda_i - \lambda_{i+1})\,(n-i)^2 + (n-i)\left(\lambda_i^2 - \lambda_{i+1}^2 - \lambda_i + \lambda_{i+1}\right)\right] \qquad \text{(C.1.6)}$$

After that it is easy to see

$$C_2^{Y_m} = mn^2 + nm^2 - nm - \sum_{i=0}^{n} \lambda_i \left(\lambda_i + 2(n-i)\right) \qquad \text{(C.1.7)}$$

So eventually it gives us

$$C_2^{Y_m} + C_2^{Y_n} = mn^2 + nm^2 - nm \ . \qquad \text{(C.1.8)}$$

We will call the representation with Young diagram $Y_{n\times m}$ to be maximal and for $O(N)$ group the dimension is $\dim_{\max} \sim n^{m^2/2}$.

We will also need an explicit expression for the quadratic Casimir of $SU(N)$. For a Young diagram Y with row lengths λ_i, column lengths μ_j and total number of boxes b it is given by:

$$C_2^{SU(N),Y} = \frac{1}{2}\left(bN + \sum \lambda_i^2 - \sum \mu_j^2 - \frac{b^2}{N}\right) . \tag{C.1.9}$$

C.2 Examples of energy spectra in the matrix models

C.2.1 The $O(N_1) \times O(N_2)$ model for small N_1, N_2

Let us list the allowed representations for some low values of N_1 and N_2. For $O(2)$ we label the representations by the integer charge Q so that the quadratic Casimir $C_2^{O(2)} = Q^2$; for $O(3)$ by spin j so that $C_2^{O(3)} = j(j+1)$; for $O(4) \sim SU(2) \times SU(2)$ by spins (j_1, j_2) so that $C_2^{O(4)} = 2j_1(j_1+1) + 2j_2(j_2+1)$.

For the $O(2) \times O(2)$ model we find 2 states with $4E/g = -1$ with charges $(\pm 1, 0)$ and 2 states with $4E/g = 1$ with charges $(0, \pm 1)$.

For the $O(2) \times O(3)$ model we find 6 states with $4E/g = -1$ which have $SO(3)$ spin 1 and $SO(2)$ charges $\pm 1/2$; and 2 states with $4E/g = 3$ which have $SO(3)$ spin 0 and $SO(2)$ charges $\pm 3/2$.

For the $O(3) \times O(3)$ model we find 8 states with $4E/g = -3$ which have spins $(1/2, 3/2)$; and 8 states with $4E/g = 3$ which have spins $(3/2, 1/2)$ (note the appearance of half-integral spins which correspond to spinorial representations).

For the $O(2) \times O(4)$ model we find 6 states with $4E/g = -2$ which have $SO(2)$ charge zero and are in the $SO(4)$ representation $(1,0)+(0,1)$; 8 states with $E = 0$ which have $SO(2)$ charges ± 1 and are in the $SO(4)$ representation $(1/2, 1/2)$; and 2 states with $4E/g = 6$ which have $SO(2)$ charges ± 2 and are $SO(4)$ singlets.

For the $O(3) \times O(4)$ model we find 8 states with $4E/g = -6$ which have $SO(3)$ spin zero and are in the $SO(4)$ representation $(3/2, 0) + (0, 3/2)$; 36 states with $4E/g = -2$ which have $SO(3)$

spin 1 and are in the $SO(4)$ representation $(1/2,1)+(1,1/2)$; and 20 states with $4E/g=6$ which have $SO(3)$ spin 2 and are in the $SO(4)$ representation $(1/2,0)+(0,1/2)$.

For the $O(4)\times O(4)$ model we find 10 ground states with $4E/g=-12$ which are $SO(4)_1$ singlets and are in the $SO(4)_2$ representation $(2,0)+(0,2)$; 64 states with $4E/g=-6$ which are in $SO(4)_1$ representation $(1/2,1/2)$ and in the $SO(4)_2$ representation $(1/2,3/2)+(3/2,1/2)$; etc.

For the $O(6)\times O(6)$ model we find 84 ground states with $4E/g=-45$ which are $SO(6)_1$ singlets and are in the $SO(6)_2$ representation whose Young diagram is a 3×3 square. The first excited state has $4E/g=-35$; it transforms as a vector of $SO(6)_1$ and in the representation of $SO(6)_2$ whose Young diagram has 3 boxes in the first row, 3 in the second row, and 2 in the third row.

Due to the relation (C.1.4) we can state the general correspondence between the representations of $O(N_1)\times O(N_2)$ if N_1 and N_2 are even. If the state is described by representation Y_1 for the group $O(N_1)$, then it has the representation $\left(Y_{N_1/2\times N_2/2}/Y_1\right)^T$ for the second group $O(N_2)$.

C.2.2 The $O(2)\times O(3)\times U(1)$ model

As was described in the main text, first we have to find $SU(2)\times SU(3)$ representations and then decompose into $SO(2)\times SO(3)$ irreducible representations. After that we can directly apply the exact formula (5.6.103) for the energy.

Let us list the explicit form of quadratic Casimirs. For $SO(2)$ the quadratic Casimir is simply Q^2, where Q is the charge. For $SU(2)$ and $SO(3)$ it equals $j(j+1)$ where j is spin(an integer for $SO(3)$ and half-integer for $SU(2)$). For $SU(3)$ the quadratic Casimir in our normalization reads as:

$$C_2^{SU(3)}(=\frac{1}{2}\left(l_1^2+l_2^2-\frac{1}{3}(l_1+l_2)^2+2l_1\right), \tag{C.2.10}$$

where $l_1>l_2>\ldots$ are the row lengths of the Young diagram λ defining the representation λ. For example, $C_2^{SU(3)}(\square)=\frac{4}{3}$, $C_2^{SU(3)}(\square\square)=\frac{10}{3}$ and $C_2^{SU(3)}(\begin{smallmatrix}\square\square\\\square\end{smallmatrix})=3$ (the last one is the adjoint representation).

The spectrum can be found in Table C.1; it coincides with the one in Table 5.6.

Level	$SU(2) \times SU(3)$ irrep	$SO(2) \times SO(3)$ irrep	$\frac{4}{g}$ Energy
0	$\varnothing \times \varnothing$	$\varnothing \times \varnothing$	-3
1	$\square \times \square$	$\square \times \square$	-1
2	$\square\square \times \square$	$\square\square \times \square$	1
2		$\varnothing \times \square$	-7
2	$\varnothing \times \square\square$	$\varnothing \times \square\square$	1
2		$\varnothing \times \varnothing$	13
3	$\square \times \begin{smallmatrix}\square\square\\\square\end{smallmatrix}$	$\square \times \square\square$	-1
3		$\square \times \square$	7
3	$\square\square\square \times \varnothing$	$\square\square\square \times \varnothing$	3
3		$\square \times \varnothing$	-13
4	$\varnothing \times \square\square$	$\varnothing \times \varnothing$	13
4		$\varnothing \times \square\square$	1
4	$\square\square \times \square$	$\varnothing \times \square$	-7
4		$\square\square \times \square$	1
5	$\square \times \square$	$\square \times \square$	-1
6	$\varnothing \times \varnothing$	$\varnothing \times \varnothing$	-3

Table C.1: Energy spectrum of the $O(2) \times O(3) \times O(2)$ model. Due to the charge conjugation symmetry for the last $O(2)$ charge, the energies and representations are invariant under transformation level $\to 6 -$ level.

C.2.3 Explicit form of some singlet states

The construction of singlet states for the $O(N_1) \times O(N_2) \times O(N_3)$ tensor quantum mechanics is in general a difficult problem, but it simplifies when one of the groups is $O(2)$. The singlet states, which exist only when N_1 and N_2 are even, may sometimes be written down by inspection in the oscillator basis. In this basis, in addition to the manifest $SO(N_1) \times SO(N_2)$ symmetry, there is manifest discrete $Z_2 \times Z_2$ parity symmetry contained inside $O(N_1) \times O(N_2)$.

For example, for the $O(2)^3$ model there are only two singlet states

$$\epsilon_{a_1a_2}\delta_{b_1b_2}\bar{\psi}_{a_1b_1}\bar{\psi}_{a_2b_2}|0\rangle \ , \quad \epsilon_{b_1b_2}\delta_{a_1a_2}\bar{\psi}_{a_1b_1}\bar{\psi}_{a_2b_2}|0\rangle \ , \tag{C.2.11}$$

since due to the Fermi statistics the other two invariant contractions vanish. Under the $Z_2 \times Z_2$ symmetry these states are $(-,+)$ and $(+,-)$, respectively. In agreement with section 5.6.3, one of these states is invariant under $SU(2) \times SO(2) \times SO(2)$, while the other under $SO(2) \times SU(2) \times SO(2)$.

Generalizing to any $O(N_1)\times O(2)^2$ model with even N_1, we again find only two singlet states. They may be written as

$$\epsilon_{a_1,\ldots a_{N_1}}\delta_{b_1b_2}\ldots\delta_{b_{N_1-1}b_{N_1}}\bar\psi_{a_1b_1}\ldots\bar\psi_{a_{N_1}b_{N_1}}|0\rangle\ ,\quad \left(\epsilon_{b_1b_2}\delta_{a_1a_2}\bar\psi_{a_1b_1}\bar\psi_{a_2b_2}\right)^{N_1/2}|0\rangle\ . \tag{C.2.12}$$

One of these states is invariant under $SU(N_1)\times SO(2)\times SO(2)$, while the other under $SO(N_1)\times SU(2)\times SO(2)$.

For the $O(4)^2\times O(2)$ model there are 4 singlet states

$$\begin{gathered}\epsilon_{a_1a_2a_3a_4}\epsilon_{a_5a_6a_7a_8}\delta_{b_1b_5}\ldots\delta_{b_4b_8}\bar\psi_{a_1b_1}\ldots\bar\psi_{a_8b_8}|0\rangle\ ,\quad \epsilon_{b_1b_2b_3b_4}\epsilon_{b_5b_6b_7b_8}\delta_{a_1a_5}\ldots\delta_{a_4a_8}\bar\psi_{a_1b_1}\ldots\bar\psi_{a_8b_8}|0\rangle\ ,\\ \left(\epsilon_{a_1a_2a_3a_4}\delta_{b_1b_2}\delta_{b_3b_4}\bar\psi_{a_1b_1}\ldots\bar\psi_{a_4b_4}\right)\left(\delta_{a_5a_6}\delta_{a_7a_8}\delta_{b_5b_7}\delta_{b_6b_8}\bar\psi_{a_5b_5}\ldots\bar\psi_{a_8b_8}\right)|0\rangle\ ,\\ \left(\epsilon_{b_1b_2b_3b_4}\delta_{a_1a_2}\delta_{a_3a_4}\bar\psi_{a_1b_1}\ldots\bar\psi_{a_4b_4}\right)\left(\delta_{b_5b_6}\delta_{b_7b_8}\delta_{a_5a_7}\delta_{a_6a_8}\bar\psi_{a_5b_5}\ldots\bar\psi_{a_8b_8}\right)|0\rangle\ .\end{gathered} \tag{C.2.13}$$

The first pair of states have energies $E=\pm 16g$, saturating the energy bound (5.3.23). One of these states is invariant under $SU(4)\times O(4)\times O(2)$, while the other under $O(4)\times SU(4)\times O(2)$. The second pair of states have energies $E=\pm 4g$.

Defining the antisymmetric matrix $M_{b_1b_2}=\bar\psi_{ab_1}\bar\psi_{ab_2}$, we can write the first two states as

$$\left(\mathrm{tr}\, M^4\pm\frac{1}{2}(\mathrm{tr}\, M^2)^2\right)|0\rangle \tag{C.2.14}$$

By analogy with (C.2.14), for N a multiple of 4 we may build a set of states by acting on $|0\rangle$ with traces of powers of M. For example, for $N=8$ we can act with $\mathrm{tr}\, M^{16}$, $\mathrm{tr}\, M^2\,\mathrm{tr}\, M^{14}$, etc. The number of such terms is $P(8)$, i.e. the number of partitions of 8 into positive integers, and $P(8)=22$. For $O(12)^2\times O(2)$ the number of such terms is $P(18)=385$. However, these terms are not linearly independent, so this should be regarded as an upper bound on the number of invariant states.

More generally, for $O(N)^2 \times O(2)$ with N a multiple of 4, this upper bound is $P(N^2/8)$, which grows exponentially with N:

$$P(N^2/8) \to \frac{2}{N^2\sqrt{3}} \exp\left(\frac{\pi N}{2\sqrt{3}}\right) \ . \tag{C.2.15}$$

Bibliography

[1] J. Maldacena and A. Milekhin, "To gauge or not to gauge?," *JHEP* **04** (2018) 084, arXiv:1802.00428 [hep-th].

[2] A. Almheiri, A. Milekhin, and B. Swingle, "Universal Constraints on Energy Flow and SYK Thermalization," arXiv:1912.04912 [hep-th].

[3] J. Maldacena and A. Milekhin, "SYK wormhole formation in real time," arXiv:1912.03276 [hep-th].

[4] I. R. Klebanov, A. Milekhin, F. Popov, and G. Tarnopolsky, "Spectra of eigenstates in fermionic tensor quantum mechanics," *Phys. Rev. D* **97** no. 10, (2018) 106023, arXiv:1802.10263 [hep-th].

[5] J. M. Maldacena, "The Large N limit of superconformal field theories and supergravity," *Int. J. Theor. Phys.* **38** (1999) 1113–1133, arXiv:hep-th/9711200 [hep-th]. [Adv. Theor. Math. Phys.2,231(1998)].

[6] N. Beisert, C. Ahn, L. F. Alday, Z. Bajnok, J. M. Drummond, L. Freyhult, N. Gromov, R. A. Janik, V. Kazakov, T. Klose, and et al., "Review of ads/cft integrability: An overview," *Letters in Mathematical Physics* **99** no. 1-3, (Oct, 2011) 332. http://dx.doi.org/10.1007/s11005-011-0529-2.

[7] P. K. Kovtun, D. T. Son, and A. O. Starinets, "Viscosity in strongly interacting quantum field theories from black hole physics," *Physical Review Letters* **94** no. 11, (Mar., 2005) . http://dx.doi.org/10.1103/PhysRevLett.94.111601.

[8] J. Maldacena, S. H. Shenker, and D. Stanford, "A bound on chaos," arXiv:1503.01409 [hep-th].

[9] G. Penington, "Entanglement Wedge Reconstruction and the Information Paradox," arXiv:1905.08255 [hep-th].

[10] A. Almheiri, T. Hartman, J. Maldacena, E. Shaghoulian, and A. Tajdini, "Replica Wormholes and the Entropy of Hawking Radiation," *JHEP* **05** (2020) 013, arXiv:1911.12333 [hep-th].

[11] G. Penington, S. H. Shenker, D. Stanford, and Z. Yang, "Replica wormholes and the black hole interior," arXiv:1911.11977 [hep-th].

[12] N. Itzhaki, J. M. Maldacena, J. Sonnenschein, and S. Yankielowicz, "Supergravity and the large N limit of theories with sixteen supercharges," *Phys. Rev.* **D58** (1998) 046004, arXiv:hep-th/9802042 [hep-th].

[13] K. N. Anagnostopoulos, M. Hanada, J. Nishimura, and S. Takeuchi, "Monte Carlo studies of supersymmetric matrix quantum mechanics with sixteen supercharges at finite temperature," *Phys. Rev. Lett.* **100** (2008) 021601, arXiv:0707.4454 [hep-th].

[14] M. Hanada, Y. Hyakutake, J. Nishimura, and S. Takeuchi, "Higher derivative corrections to black hole thermodynamics from supersymmetric matrix quantum mechanics," *Phys. Rev. Lett.* **102** (2009) 191602, arXiv:0811.3102 [hep-th].

[15] E. Berkowitz, E. Rinaldi, M. Hanada, G. Ishiki, S. Shimasaki, and P. Vranas, "Precision lattice test of the gauge/gravity duality at large-N," *Phys. Rev.* **D94** no. 9, (2016) 094501, arXiv:1606.04951 [hep-lat].

[16] S. Sachdev and J. Ye, "Gapless spin fluid ground state in a random, quantum Heisenberg magnet," *Phys. Rev. Lett.* **70** (1993) 3339, arXiv:cond-mat/9212030 [cond-mat].

[17] A. Kitaev, "A simple model of quantum holography." http://online.kitp.ucsb.edu/online/entangled15/kitaev/,http://online.kitp.ucsb.edu/online/entangled15/kitaev2/. Talks at KITP, April 7, 2015 and May 27, 2015.

[18] R. Gurau and J. P. Ryan, "Colored Tensor Models - a review," *SIGMA* **8** (2012) 020, arXiv:1109.4812 [hep-th].

[19] E. Witten, "An SYK-Like Model Without Disorder," arXiv:1610.09758 [hep-th].

[20] I. R. Klebanov and G. Tarnopolsky, "Uncolored random tensors, melon diagrams, and the Sachdev-Ye-Kitaev models," *Phys. Rev.* **D95** no. 4, (2017) 046004, arXiv:1611.08915 [hep-th].

[21] B. de Wit, J. Hoppe, and H. Nicolai, "On the Quantum Mechanics of Supermembranes," *Nucl. Phys.* **B305** (1988) 545.

[22] T. Banks, W. Fischler, S. H. Shenker, and L. Susskind, "M theory as a matrix model: A Conjecture," *Phys. Rev.* **D55** (1997) 5112–5128, arXiv:hep-th/9610043 [hep-th]. [,435(1996)].

[23] J. Polchinski, "M theory and the light cone," *Prog. Theor. Phys. Suppl.* **134** (1999) 158–170, arXiv:hep-th/9903165 [hep-th].

[24] D. E. Berenstein, J. M. Maldacena, and H. S. Nastase, "Strings in flat space and pp waves from N=4 superYang-Mills," *JHEP* **04** (2002) 013, arXiv:hep-th/0202021 [hep-th].

[25] K. Dasgupta, M. M. Sheikh-Jabbari, and M. Van Raamsdonk, "Matrix perturbation theory for M theory on a PP wave," *JHEP* **05** (2002) 056, arXiv:hep-th/0205185 [hep-th].

[26] J. M. Maldacena, M. M. Sheikh-Jabbari, and M. Van Raamsdonk, "Transverse five-branes in matrix theory," *JHEP* **01** (2003) 038, arXiv:hep-th/0211139 [hep-th].

[27] N. Kim, T. Klose, and J. Plefka, "Plane wave matrix theory from N=4 superYang-Mills on R x S**3," *Nucl. Phys.* **B671** (2003) 359–382, arXiv:hep-th/0306054 [hep-th].

[28] G. T. Horowitz and A. Strominger, "Black strings and P-branes," *Nucl. Phys.* **B360** (1991) 197–209.

[29] A. W. Peet and J. Polchinski, "UV / IR relations in AdS dynamics," *Phys. Rev.* **D59** (1999) 065011, arXiv:hep-th/9809022 [hep-th].

[30] D. N. Kabat, G. Lifschytz, and D. A. Lowe, "Black hole thermodynamics from calculations in strongly coupled gauge theory," *Int. J. Mod. Phys.* **A16** (2001) 856–865, arXiv:hep-th/0007051 [hep-th]. [,216(2000)].

[31] D. Kadoh and S. Kamata, "Gauge/gravity duality and lattice simulations of one dimensional SYM with sixteen supercharges," arXiv:1503.08499 [hep-lat].

[32] S. Catterall and T. Wiseman, "Black hole thermodynamics from simulations of lattice Yang-Mills theory," *Phys. Rev.* **D78** (2008) 041502, arXiv:0803.4273 [hep-th].

[33] V. G. Filev and D. O'Connor, "The BFSS model on the lattice," *JHEP* **05** (2016) 167, arXiv:1506.01366 [hep-th].

[34] H. Lin and J. M. Maldacena, "Fivebranes from gauge theory," *Phys. Rev.* **D74** (2006) 084014, arXiv:hep-th/0509235 [hep-th].

[35] M. S. Costa, L. Greenspan, J. Penedones, and J. Santos, "Thermodynamics of the BMN matrix model at strong coupling," *JHEP* **03** (2015) 069, arXiv:1411.5541 [hep-th].

[36] J. Maldacena and D. Stanford, "Remarks on the Sachdev-Ye-Kitaev model," *Phys. Rev.* **D94** no. 10, (2016) 106002, arXiv:1604.07818 [hep-th].

[37] A. Eberlein, V. Kasper, S. Sachdev, and J. Steinberg, "Quantum quench of the Sachdev-Ye-Kitaev Model," *Phys. Rev.* **B96** no. 20, (2017) 205123, arXiv:1706.07803 [cond-mat.str-el].

[38] G. Stefanucci and R. Van Leeuwen, *Nonequilibrium many-body theory of quantum systems: a modern introduction*. Cambridge University Press, 2013.

[39] R. Gurau, "Colored Group Field Theory," *Commun. Math. Phys.* **304** (2011) 69–93, arXiv:0907.2582 [hep-th].

[40] R. Gurau and V. Rivasseau, "The 1/N expansion of colored tensor models in arbitrary dimension," *Europhys. Lett.* **95** (2011) 50004, arXiv:1101.4182 [gr-qc].

[41] R. Gurau, "The complete 1/N expansion of colored tensor models in arbitrary dimension," *Annales Henri Poincare* **13** (2012) 399–423, arXiv:1102.5759 [gr-qc].

[42] V. Bonzom, R. Gurau, A. Riello, and V. Rivasseau, "Critical behavior of colored tensor models in the large N limit," *Nucl. Phys.* **B853** (2011) 174–195, arXiv:1105.3122 [hep-th].

[43] A. Tanasa, "Multi-orientable Group Field Theory," *J. Phys.* **A45** (2012) 165401, arXiv:1109.0694 [math.CO].

[44] V. Bonzom, R. Gurau, and V. Rivasseau, "Random tensor models in the large N limit: Uncoloring the colored tensor models," *Phys. Rev.* **D85** (2012) 084037, arXiv:1202.3637 [hep-th].

[45] S. Dartois, V. Rivasseau, and A. Tanasa, "The $1/N$ expansion of multi-orientable random tensor models," *Annales Henri Poincare* **15** (2014) 965–984, arXiv:1301.1535 [hep-th].

[46] A. Tanasa, "The Multi-Orientable Random Tensor Model, a Review," *SIGMA* **12** (2016) 056, arXiv:1512.02087 [hep-th].

[47] S. Carrozza and A. Tanasa, "$O(N)$ Random Tensor Models," *Lett. Math. Phys.* **106** no. 11, (2016) 1531–1559, arXiv:1512.06718 [math-ph].

[48] R. Gurau, "The complete $1/N$ expansion of a SYK–like tensor model," arXiv:1611.04032 [hep-th].

[49] F. Ferrari, "The Large D Limit of Planar Diagrams," arXiv:1701.01171 [hep-th].

[50] I. Klebanov, D. Roberts, D. Stanford, and G. Tarnopolsky, "unpublished (December 2017),".

[51] C. Krishnan, K. V. P. Kumar, and S. Sanyal, "Random Matrices and Holographic Tensor Models," *JHEP* **06** (2017) 036, arXiv:1703.08155 [hep-th].

[52] C. Krishnan and K. V. P. Kumar, "Towards a Finite-N Hologram," *JHEP* **10** (2017) 099, arXiv:1706.05364 [hep-th].

[53] E. Witten, "Global Anomalies in String Theory," in *Symposium on Anomalies, Geometry, Topology Argonne, Illinois, March 28-30, 1985*. 1985. https://www.sns.ias.edu/witten/symp-global-anomalies-stringtheory-1985.

[54] S. Elitzur, Y. Frishman, E. Rabinovici, and A. Schwimmer, "Origins of Global Anomalies in Quantum Mechanics," *Nucl. Phys.* **B273** (1986) 93–108.

[55] S. S. Gubser, I. R. Klebanov, and A. M. Polyakov, "Gauge theory correlators from noncritical string theory," *Phys. Lett.* **B428** (1998) 105–114, arXiv:hep-th/9802109 [hep-th].

[56] E. Witten, "Anti-de Sitter space and holography," *Adv. Theor. Math. Phys.* **2** (1998) 253–291, arXiv:hep-th/9802150 [hep-th].

[57] E. Berkowitz, M. Hanada, E. Rinaldi, and P. Vranas, "Gauged And Ungauged: A Nonperturbative Test," *JHEP* **06** (2018) 124, arXiv:1802.02985 [hep-th].

[58] D. J. Gross and I. R. Klebanov, "Vortices and the nonsinglet sector of the c = 1 matrix model," *Nucl. Phys.* **B354** (1991) 459–474.

[59] G. Marchesini and E. Onofri, "Planar Limit for SU(N) Symmetric Quantum Dynamical Systems," *J. Math. Phys.* **21** (1980) 1103.

[60] D. Boulatov and V. Kazakov, "One-dimensional string theory with vortices as the upside down matrix oscillator," *Int. J. Mod. Phys.* **A8** (1993) 809–852, arXiv:hep-th/0012228 [hep-th].

[61] V. Kazakov, I. K. Kostov, and D. Kutasov, "A Matrix model for the two-dimensional black hole," *Nucl. Phys.* **B622** (2002) 141–188, arXiv:hep-th/0101011 [hep-th].

[62] J. M. Maldacena, "Long strings in two dimensional string theory and non-singlets in the matrix model," *JHEP* **09** (2005) 078, arXiv:hep-th/0503112 [hep-th]. [Int. J. Geom. Meth. Mod. Phys.3,1(2006)].

[63] L. Fidkowski, "Solving the eigenvalue problem arising from the adjoint sector of the c=1 matrix model," arXiv:hep-th/0506132 [hep-th].

[64] E. Witten, "Anti-de Sitter space, thermal phase transition, and confinement in gauge theories," *Adv. Theor. Math. Phys.* **2** (1998) 505–532, arXiv:hep-th/9803131 [hep-th].

[65] O. Aharony, J. Marsano, S. Minwalla, K. Papadodimas, and M. Van Raamsdonk, "The Hagedorn - deconfinement phase transition in weakly coupled large N gauge theories," *Adv. Theor. Math. Phys.* **8** (2004) 603–696, arXiv:hep-th/0310285 [hep-th]. [,161(2003)].

[66] Y. Asano, G. Ishiki, T. Okada, and S. Shimasaki, "Emergent bubbling geometries in the plane wave matrix model," *JHEP* **05** (2014) 075, arXiv:1401.5079 [hep-th].

[67] Y. Asano, G. Ishiki, S. Shimasaki, and S. Terashima, "On the transverse M5-branes in matrix theory," arXiv:1701.07140 [hep-th].

[68] S.-J. Rey and J.-T. Yee, "Macroscopic strings as heavy quarks in large N gauge theory and anti-de Sitter supergravity," *Eur. Phys. J.* **C22** (2001) 379–394, arXiv:hep-th/9803001 [hep-th].

[69] J. M. Maldacena, "Wilson loops in large N field theories," *Phys. Rev. Lett.* **80** (1998) 4859–4862, arXiv:hep-th/9803002 [hep-th].

[70] L. F. Alday and J. Maldacena, "Comments on gluon scattering amplitudes via AdS/CFT," *JHEP* **11** (2007) 068, arXiv:0710.1060 [hep-th].

[71] J. Polchinski and J. Sully, "Wilson Loop Renormalization Group Flows," *JHEP* **10** (2011) 059, arXiv:1104.5077 [hep-th].

[72] G. T. Horowitz and E. J. Martinec, "Comments on black holes in matrix theory," *Phys. Rev.* **D57** (1998) 4935–4941, arXiv:hep-th/9710217 [hep-th].

[73] R. Gregory and R. Laflamme, "Black strings and p-branes are unstable," *Phys. Rev. Lett.* **70** (1993) 2837–2840, arXiv:hep-th/9301052 [hep-th].

[74] A. Karch and E. Katz, "Adding flavor to AdS / CFT," *JHEP* **06** (2002) 043, arXiv:hep-th/0205236 [hep-th].

[75] A. M. Kaufman, M. E. Tai, A. Lukin, M. Rispoli, R. Schittko, P. M. Preiss, and M. Greiner, "Quantum thermalization through entanglement in an isolated many-body system," *Science* **353** no. 6301, (Aug., 2016) 794800. http://dx.doi.org/10.1126/science.aaf6725.

[76] H. Bernien, S. Schwartz, A. Keesling, H. Levine, A. Omran, H. Pichler, S. Choi, A. S. Zibrov, M. Endres, M. Greiner, V. Vuletic, and M. D. Lukin, "Probing many-body dynamics on a 51-atom quantum simulator," *Nature* **551** no. 7682, (Nov., 2017) 579–584. http://dx.doi.org/10.1038/nature24622.

[77] J. Zhang, G. Pagano, P. W. Hess, A. Kyprianidis, P. Becker, H. Kaplan, A. V. Gorshkov, Z.-X. Gong, and C. Monroe, "Observation of a many-body dynamical phase transition with a 53-qubit quantum simulator," *Nature* **551** no. 7682, (Nov., 2017) 601604. http://dx.doi.org/10.1038/nature24654.

[78] P. Hayden and J. Preskill, "Black holes as mirrors: Quantum information in random subsystems," *JHEP* **09** (2007) 120, arXiv:0708.4025 [hep-th].

[79] Y. Sekino and L. Susskind, "Fast Scramblers," *JHEP* **10** (2008) 065, arXiv:0808.2096 [hep-th].

[80] W. Brown and O. Fawzi, "Scrambling speed of random quantum circuits," 2012.

[81] S. Sachdev, *Quantum Phase Transitions*. Cambridge University Press, 2001. https://books.google.com/books?id=Ih_E05N5TZQC.

[82] S. A. Hartnoll, "Theory of universal incoherent metallic transport," *Nature Physics* **11** no. 1, (Dec., 2014) 5461. http://dx.doi.org/10.1038/nphys3174.

[83] J. A. N. Bruin, H. Sakai, R. S. Perry, and A. P. Mackenzie, "Similarity of scattering rates in metals showing t-linear resistivity," *Science* **339** no. 6121, (2013) 804–807, https://science.sciencemag.org/content/339/6121/804.full.pdf. https://science.sciencemag.org/content/339/6121/804.

[84] N. Hussey, K. Takenaka, and H. Takagi, "Universality of the mott–ioffe–regel limit in metals," *Philosophical Magazine* **84** no. 27, (2004) 2847–2864.

[85] A. Lucas, "Operator size at finite temperature and planckian bounds on quantum dynamics," *Phys. Rev. Lett.* **122** (May, 2019) 216601. https://link.aps.org/doi/10.1103/PhysRevLett.122.216601.

[86] A. Legros, S. Benhabib, W. Tabis, F. Laliberte, M. Dion, M. Lizaire, B. Vignolle, D. Vignolles, H. Raffy, Z. Z. Li, and et al., "Universal t-linear resistivity and planckian dissipation in overdoped cuprates," *Nature Physics* **15** no. 2, (Nov., 2018) 142147. http://dx.doi.org/10.1038/s41567-018-0334-2.

[87] J. Zaanen, "Planckian dissipation, minimal viscosity and the transport in cuprate strange metals," *SciPost Physics* **6** no. 5, (May, 2019) . http://dx.doi.org/10.21468/SciPostPhys.6.5.061.

[88] A. Georges, O. Parcollet, and S. Sachdev, "Mean Field Theory of a Quantum Heisenberg Spin Glass," *Physical Review Letters* **85** (July, 2000) 840–843, cond-mat/9909239.

[89] A. Georges, O. Parcollet, and S. Sachdev, "Quantum fluctuations of a nearly critical heisenberg spin glass," *Phys. Rev. B* **63** (Mar., 2001) 134406. http://link.aps.org/doi/10.1103/PhysRevB.63.134406.

[90] J. Polchinski and V. Rosenhaus, "The Spectrum in the Sachdev-Ye-Kitaev Model," *JHEP* **04** (2016) 001, arXiv:1601.06768 [hep-th].

[91] D. Bagrets, A. Altland, and A. Kamenev, "Power-law out of time order correlation functions in the SYK model," *Nucl. Phys.* **B921** (2017) 727–752, arXiv:1702.08902 [cond-mat.str-el].

[92] A. M. Garca-Garca and J. J. M. Verbaarschot, "Spectral and thermodynamic properties of the Sachdev-Ye-Kitaev model," *Phys. Rev.* **D94** no. 12, (2016) 126010, arXiv:1610.03816 [hep-th].

[93] Y. Gu, X.-L. Qi, and D. Stanford, "Local criticality, diffusion and chaos in generalized sachdev-ye-kitaev models," *Journal of High Energy Physics* **2017** no. 5, (May, 2017) 125.

[94] A. Altland, D. Bagrets, and A. Kamenev, "Syk non fermi liquid correlations in nanoscopic quantum transport," 2019.

[95] H. Guo, Y. Gu, and S. Sachdev, "Transport and chaos in lattice sachdev-ye-kitaev models," *Physical Review B* **100** no. 4, (July, 2019) . http://dx.doi.org/10.1103/PhysRevB.100.045140.

[96] O. Can and M. Franz, "Solvable model for quantum criticality between the sachdev-ye-kitaev liquid and a disordered fermi liquid," *Physical Review B* **100** no. 4, (July, 2019) . http://dx.doi.org/10.1103/PhysRevB.100.045124.

[97] J. Kim, I. R. Klebanov, G. Tarnopolsky, and W. Zhao, "Symmetry Breaking in Coupled SYK or Tensor Models," *Phys. Rev.* **X9** no. 2, (2019) 021043, arXiv:1902.02287 [hep-th].

[98] O. Can, E. M. Nica, and M. Franz, "Charge transport in graphene-based mesoscopic realizations of sachdev-ye-kitaev models," *Physical Review B* **99** no. 4, (Jan., 2019) . http://dx.doi.org/10.1103/PhysRevB.99.045419.

[99] X. Dai, S.-K. Jian, and H. Yao, "The global phase diagram of the one-dimensional syk model at finite n," 2018.

[100] D. Chowdhury, Y. Werman, E. Berg, and T. Senthil, "Translationally invariant non-fermi-liquid metals with critical fermi surfaces: Solvable models," *Physical Review X* **8** no. 3, (July, 2018) . http://dx.doi.org/10.1103/PhysRevX.8.031024.

[101] D. Ben-Zion and J. McGreevy, "Strange metal from local quantum chaos," *Physical Review B* **97** no. 15, (Apr., 2018) . http://dx.doi.org/10.1103/PhysRevB.97.155117.

[102] J. V. Rocha, "Evaporation of large black holes in AdS," *J. Phys. Conf. Ser.* **222** (2010) 012005.

[103] J. Engelsy, T. G. Mertens, and H. Verlinde, "An investigation of AdS_2 backreaction and holography," *JHEP* **07** (2016) 139, arXiv:1606.03438 [hep-th].

[104] A. Almheiri, "Holographic Quantum Error Correction and the Projected Black Hole Interior," arXiv:1810.02055 [hep-th].

[105] Y. Chen, H. Zhai, and P. Zhang, "Tunable Quantum Chaos in the Sachdev-Ye-Kitaev Model Coupled to a Thermal Bath," *JHEP* **07** (2017) 150, arXiv:1705.09818 [hep-th].

[106] R. Bhattacharya, D. P. Jatkar, and N. Sorokhaibam, "Quantum Quenches and Thermalization in SYK models," arXiv:1811.06006 [hep-th].

[107] M. S. Morris, K. S. Thorne, and U. Yurtsever, "Wormholes, Time Machines, and the Weak Energy Condition," *Phys. Rev. Lett.* **61** (1988) 1446–1449.

[108] D. Hochberg and M. Visser, "The Null energy condition in dynamic wormholes," *Phys. Rev. Lett.* **81** (1998) 746–749, arXiv:gr-qc/9802048 [gr-qc].

[109] M. Visser, S. Kar, and N. Dadhich, "Traversable wormholes with arbitrarily small energy condition violations," *Phys. Rev. Lett.* **90** (2003) 201102, arXiv:gr-qc/0301003 [gr-qc].

[110] M. Visser, "Lorentzian wormholes. From Einstein to Hawking," (1996) 412 pp. AIP Press.

[111] P. Gao, D. L. Jafferis, and A. C. Wall, "Traversable Wormholes via a Double Trace Deformation," *JHEP* **12** (2017) 151, arXiv:1608.05687 [hep-th].

[112] R. Jackiw, "Lower Dimensional Gravity," *Nucl. Phys.* **B252** (1985) 343–356.

[113] C. Teitelboim, "Gravitation and Hamiltonian Structure in Two Space-Time Dimensions," *Phys. Lett.* **126B** (1983) 41–45.

[114] J. D. Brown, *LOWER DIMENSIONAL GRAVITY*. 1988.

[115] K. Jensen, "Chaos in AdS_2 Holography," *Phys. Rev. Lett.* **117** no. 11, (2016) 111601, arXiv:1605.06098 [hep-th].

[116] J. Maldacena, D. Stanford, and Z. Yang, "Conformal symmetry and its breaking in two dimensional Nearly Anti-de-Sitter space," *PTEP* **2016** no. 12, (2016) 12C104, arXiv:1606.01857 [hep-th].

[117] P. Zhang, "Evaporation dynamics of the sachdev-ye-kitaev model," 2019.

[118] A. Kamenev, *Field theory of non-equilibrium systems*. Cambridge University Press, 2011.

[119] T. G. Mertens, G. J. Turiaci, and H. L. Verlinde, "Solving the Schwarzian via the Conformal Bootstrap," *JHEP* **08** (2017) 136, arXiv:1705.08408 [hep-th].

[120] A. Kitaev and S. J. Suh, "The soft mode in the Sachdev-Ye-Kitaev model and its gravity dual," *JHEP* **05** (2018) 183, arXiv:1711.08467 [hep-th].

[121] A. Almheiri and J. Polchinski, "Models of AdS_2 backreaction and holography," *JHEP* **11** (2015) 014, arXiv:1402.6334 [hep-th].

[122] J. Maldacena and X.-L. Qi, "Eternal traversable wormhole," arXiv:1804.00491 [hep-th].

[123] A. M. García-García, T. Nosaka, D. Rosa, and J. J. M. Verbaarschot, "Quantum chaos transition in a two-site Sachdev-Ye-Kitaev model dual to an eternal traversable wormhole," *Phys. Rev.* **D100** no. 2, (2019) 026002, arXiv:1901.06031 [hep-th].

[124] P. Gao and D. L. Jafferis, "A Traversable Wormhole Teleportation Protocol in the SYK Model," arXiv:1911.07416 [hep-th].

[125] J. Maldacena, A. Milekhin, and F. Popov, "Traversable wormholes in four dimensions," arXiv:1807.04726 [hep-th].

[126] I. R. Klebanov and E. Witten, "AdS / CFT correspondence and symmetry breaking," *Nucl. Phys.* **B556** (1999) 89–114, arXiv:hep-th/9905104 [hep-th].

[127] Y. Gu, A. Kitaev, S. Sachdev, and G. Tarnopolsky, "Notes on the complex Sachdev-Ye-Kitaev model," arXiv:1910.14099 [hep-th].

[128] J. Maldacena, G. J. Turiaci, and Z. Yang, "Two dimensional Nearly de Sitter gravity," arXiv:1904.01911 [hep-th].

[129] A. Chen, R. Ilan, F. de Juan, D. Pikulin, and M. Franz, "Quantum holography in a graphene flake with an irregular boundary," *Physical review letters* **121** no. 3, (2018) 036403.

[130] R. Gurau, "Invitation to Random Tensors," *SIGMA* **12** (2016) 094, arXiv:1609.06439 [hep-th].

[131] O. Parcollet and A. Georges, "Non-Fermi-liquid regime of a doped Mott insulator," *Physical Review B* **59** (Feb., 1999) 5341–5360, cond-mat/9806119.

[132] A. Jevicki, K. Suzuki, and J. Yoon, "Bi-Local Holography in the SYK Model," *JHEP* **07** (2016) 007, arXiv:1603.06246 [hep-th].

[133] D. J. Gross and V. Rosenhaus, "A Generalization of Sachdev-Ye-Kitaev," arXiv:1610.01569 [hep-th].

[134] V. Bonzom, L. Lionni, and A. Tanasa, "Diagrammatics of a colored SYK model and of an SYK-like tensor model, leading and next-to-leading orders," *J. Math. Phys.* **58** no. 5, (2017) 052301, arXiv:1702.06944 [hep-th].

[135] I. R. Klebanov and G. Tarnopolsky, "On Large N Limit of Symmetric Traceless Tensor Models," *JHEP* **10** (2017) 037, arXiv:1706.00839 [hep-th].

[136] F. Ferrari, V. Rivasseau, and G. Valette, "A New Large N Expansion for General Matrix-Tensor Models," arXiv:1709.07366 [hep-th].

[137] D. Benedetti and R. Gurau, "2PI effective action for the SYK model and tensor field theories," arXiv:1802.05500 [hep-th].

[138] K. Bulycheva, I. R. Klebanov, A. Milekhin, and G. Tarnopolsky, "Spectra of Operators in Large N Tensor Models," arXiv:1707.09347 [hep-th].

[139] S. Choudhury, A. Dey, I. Halder, L. Janagal, S. Minwalla, and R. Poojary, "Notes on Melonic $O(N)^{q-1}$ Tensor Models," arXiv:1707.09352 [hep-th].

[140] M. Beccaria and A. A. Tseytlin, "Partition function of free conformal fields in 3-plet representation," *JHEP* **05** (2017) 053, arXiv:1703.04460 [hep-th].

[141] S. Sachdev, "Bekenstein-Hawking Entropy and Strange Metals," *Phys. Rev.* **X5** no. 4, (2015) 041025, arXiv:1506.05111 [hep-th].

[142] J. S. Cotler, G. Gur-Ari, M. Hanada, J. Polchinski, P. Saad, S. H. Shenker, D. Stanford, A. Streicher, and M. Tezuka, "Black holes and random matrices," *Journal of High Energy Physics* **2017** no. 5, (2017) 118.

[143] C. Krishnan, S. Sanyal, and P. N. Bala Subramanian, "Quantum Chaos and Holographic Tensor Models," *JHEP* **03** (2017) 056, arXiv:1612.06330 [hep-th].

[144] S. Chaudhuri, V. I. Giraldo-Rivera, A. Joseph, R. Loganayagam, and J. Yoon, "Abelian Tensor Models on the Lattice," arXiv:1705.01930 [hep-th].

[145] C. Krishnan, K. V. Pavan Kumar, and D. Rosa, "Contrasting SYK-like Models," *JHEP* **01** (2018) 064, arXiv:1709.06498 [hep-th].

[146] C. Krishnan and K. V. Pavan Kumar, "Exact Solution of a Strongly Coupled Gauge Theory in 0+1 Dimensions," arXiv:1802.02502 [hep-th].

[147] T. Azeyanagi, F. Ferrari, P. Gregori, L. Leduc, and G. Valette, "More on the New Large D Limit of Matrix Models," arXiv:1710.07263 [hep-th].

[148] D. Anninos and G. A. Silva, "Solvable Quantum Grassmann Matrices," *J. Stat. Mech.* **1704** no. 4, (2017) 043102, arXiv:1612.03795 [hep-th].

[149] J. Yoon, "SYK Models and SYK-like Tensor Models with Global Symmetry," arXiv:1707.01740 [hep-th].

[150] M. Tierz, "Polynomial solution of quantum Grassmann matrices," *J. Stat. Mech.* **1705** no. 5, (2017) 053203, arXiv:1703.02454 [hep-th].

[151] D. Anninos, F. Denef, and R. Monten, "Grassmann Matrix Quantum Mechanics," *JHEP* **04** (2016) 138, arXiv:1512.03803 [hep-th].

[152] A. V. Smilga, "Comments on thermodynamics of supersymmetric matrix models," *Nucl. Phys.* **B818** (2009) 101–114, arXiv:0812.4753 [hep-th].

[153] T. Morita, S. Shiba, T. Wiseman, and B. Withers, "Warm p-soup and near extremal black holes," *Class. Quant. Grav.* **31** (2014) 085001, arXiv:1311.6540 [hep-th].